The Relationship Between Precipitation and Electromagnetic Signals in Schumann Resonances

by

Daniel S. Castro

Submitted to the Department of Electrical Engineering and Computer Science

in partial fulfillment of the requirements for the degrees of

Bachelor of Science in Electrical Engineering and Computer Science

and

Master of Engineering in Electrical Engineering and Computer Science

at the

MASSACHUSETTS INSTITUTE OF TECHNOLOGY

February 2000

Author.....
Department of Electrical Engineering and Computer Science
February 11, 2000

Certified by.....
Earle R. Williams
Principal Research Scientist
Thesis Supervisor

Accepted by.....
Arthur C. Smith
Chairman, Department Committee on Graduate Theses

The Relationship Between Precipitation and Electromagnetic Signals in Schumann Resonances

by

Daniel S. Castro

Submitted to the Department of Electrical Engineering and Computer Science

February 11, 2000

in partial fulfillment of the requirements for the degrees of

Bachelor of Science in Electrical Engineering and Computer Science
and
Master of Engineering in Electrical Engineering and Computer Science

Abstract

Electromagnetic background and transient signals caused by global lightning activity are continuously recorded in the Schumann resonance band (3-120 Hz) from the MIT Schumann resonance site in West Greenwich, Rhode Island. These measurements are compared with precipitation estimates provided by the National Aeronautics and Space Administration (NASA) and the National Oceanic Atmospherics Administration (NOAA). Spatial and quantitative analyses reveal a rough proportionality between pairs of these three quantities as well as the existence of an apparent planetary wave with approximate 5-day periodicity. Schumann resonance analyses have detected this wave in several regions of the world, suggesting that the physical origin of the wave is global. Regional analyses show a significant correlation between transients and rainfall in Africa, with substantially less significant correlations in South America and the Maritime Continent. Physical features of these extraordinary lightning events also provide new insight regarding the electrical and meteorological criteria for sprites. In particular, this thesis provides preliminary evidence for the possibility of oceanic, negative-stroke lightning events associated with sprites.

Thesis Supervisor: Earle R. Williams
Title: Principal Research Scientist

Contents

List of Figures

Acknowledgements

The compilation of this thesis would have not been possible without the knowledgeable guidance of my thesis advisor Earle Williams. His patience and understanding will be remembered long after this thesis is submitted. I would also like to thank Bob Boldi and Everest Huang for their considerable help in maintaining our Schumann resonance data set and for their selfless desire to always provide me with a helping hand. Special thank to George Huffman from the National Aeronautics and Space Administration (NASA) and John Janowiak from the National Oceanic Atmospherics Administration (NOAA) for providing me with their respective precipitation estimates and to Dr. Vadim Mushtak for providing the source strength conversion plots included in this thesis.

Gracias a mi familia por el apoyo que me han dado en este semejante camino. Quiero que sepan que, aunque estemos fisicamente separados, yo siempre les he llevado en mi corazon. En cada paso que tomo, siento el espiritu de los tres. Efrain, a ti te quiero como si fueras mi padre. Siempre nos has cuidado con ternura y sin capricho. Para mi, eres el ejemplo tipico de lo que debe ser un hombre; padre y trabajador. Alva y Mami, los sacrificios de ustedes dos me han hecho el hombre que ahora soy. Y por eso es que dedidico este tesis a las dos mujeres mas importantes de mi vida; mi hermana y mi mama.

Chapter 1

Introduction

In this thesis, a multivariable analysis between precipitation and the two distinct measures of the Earth's Schumann resonances--the background and the transients--is performed for Africa, South America, and the Maritime Continent (which includes Indonesia, The Phillipines, Malaysia, and Australia). Analysis of individual days reveals a rough proportionality between pairs of these three variables. Furthermore, these observations reveal an approximate 5-day periodicity, which is consistent with previous studies on planetary waves (Wallace, 1971, Reed et al., 1977, Madden and Julian, 1972). Also included in this thesis is a study of how these factors influence the production of sprites/elves. Daily global precipitation data provided by the National Aeronautics and Space Administration (NASA) are compared with Schumann resonance data collected from a single station in West Greenwich, Rhode Island for selected days when local weather is not appreciably affecting the electromagnetic measurements. Additional gridded daily rainfall estimates are provided by the National Oceanic and Atmospheric Administration (NOAA) for the African continent and also compared. The background intensity is assumed to be the total integration of "ordinary" global lightning. Due to the favorable geographic location of Africa with respect to West Greenwich, the North-South magnetic component of the background intensity can be used to

represent Africa, whereas South America and the Maritime Continent are represented in the East-West magnetic signal. Schumann resonance transients are detected, processed and mapped in latitude/longitude whenever the signal from a high-energy lightning event lies well above a pre-defined background threshold.

1.1 Schumann Resonances and their Excitation by Lightning

Resonant electromagnetic waves called Schumann resonances (SR) propagate through the giant waveguide formed by the Earth-ionosphere cavity. These resonances are created by global lightning activity and have a fundamental mode of 8 Hz (approximately one EM wavelength around the world). Through continental scale SR comparisons, two distinct measurements are produced; the background and the transients. The background resonances are maintained by ordinary lightning (both positive and negative) from severe and non-severe thunderstorms while transient resonances are created by high-energy lightning events that 'ring' the Earth-ionosphere cavity. These high-energy transient events produce vertical electric and horizontal magnetic fields that can be measured above the background level of all the smaller amplitude lightning events.

1.2 Background on 5-Day Wave

Previous investigations regarding the 5-day wave phenomenon have had difficulty determining whether their analyses revealed global or regional waves (Burpee, 1976). Evidence of such a planetary wave has been presented by Madden and Julian (1972), which describe it as being

a 5-day global-scale, wave number 1 pressure wave. Madden and Julian showed that these oscillations were relatively small (0.5-mb) and that they were associated with a westward propagating disturbance. Furthermore, they suggest that these waves are to be distinguished from the 4-5 day African Easterly waves discussed by Wallace (1971) and Reed et al. (1977). Later work by Burpee (1976) showed that, since small perturbations in pressure often have a significant impact on meteorology, the amplitude of the 5-day wave becomes somewhat more discernible through meteorological measurements such as precipitation. Although the amplitude variation in precipitation found by Burpee (1976) was also relatively small (approximately 10 %), evidence in this thesis suggest that rainfall can indeed be used to detect the 5-day wave. Recent studies by Price et al. (1999) and Sentman et al. (1996) as well as work presented in this thesis show that, SR techniques can also be used to identify the 5-day wave and that the relative amplitude variations of these waves are substantially larger, compared to pressure and precipitation.

1.3 History of Schumann Resonances

Theoretical investigations of the electromagnetic resonances produced by lightning were first conducted by Schumann (1952). Schumann's initial calculations found the resonant frequencies of these electromagnetic waves under the assumption that the Earth-ionosphere cavity contained perfectly conducting boundaries. These resonant frequency calculations were later improved when Schumann replaced his infinite conductivity model between the earth and its ionosphere with a more accurate finite conductivity profile (Schumann, 1957). The existence of Schumann resonance modes was confirmed by Balser and Wagner (1960) with their presentation of the first spectrum. Similar to Schumann's infinite conductivity resonant frequency calculations, this spectrum revealed peak resonances of 8, 14, 20, and 26 Hz. Diurnal variations and the

inhomogeneous ionosphere were later taken into account by Wait (1962) marking the beginning of extensive Schumann resonance calculations within the scientific community (Polk and Fitchen, 1962; Balser and Wagner, 1962; Chapman and Jones, 1964; Rycroft, 1965; Madden, 1965; and Nelson, 1967). During this period, numerical experiments to evaluate the effects of the conductivity profile of the ionosphere were also being conducted (Jones, 1967). Also published during this period was the work of Ogawa et al. (1967) which confirmed the global phenomenon of Schumann resonances and documented Q-type and N-type bursts.

The normal mode theory of Schumann resonances proposed by Wait (1962) was first used by Jones and Kemp (1970) to determine the source location of single stroke lightning events. Source location estimates were calculated by comparing theory with individual spectra of the electric and magnetic fields. The wave impedance method was later developed by Kemp and Jones (1971) which determines the source-observer distance through the unique electric to magnetic field ratio of a particular event. An asymptotic approximation to the theory was first introduced by Ishaq and Jones (1977) and was later modified with new approaches by Nickolaenko (1994).

The implementation of monitoring the vertical electric component of global lightning activity via SR methods from a single station was first demonstrated by Clayton and Polk (1977). In 1980, Bliokh et al. published a disquisition on Schumann resonances and, in 1987, Sentman published a paper on the effects of magnetic elliptical polarization on Schumann resonance. The study conducted by Clayton and Polk (1977) was extended by Heckman et al. (1998) to include the monitoring of the East-West and North-South magnetic field components in addition to the vertical electric component.

1.4 Methods for Background and Transient Analysis

1.4.1 Normal Mode Equations

The theoretical frequency spectra for the electric and magnetic field components resulting from transient events are calculated using frequency-dependent normal mode equations obtained from the Wait and Jones model (Wait, 1996; Jones, 1967; Ishaq and Jones, 1977). This model assumes a spherically symmetric ionosphere about the Earth's center that can radially vary. The equations are given by

$$E_z(f) = i\frac{I(f)ds\,\nu(f)(\nu(f)+1)P^0_{\nu(f)}(-\cos\theta)}{4a^2\varepsilon_0 2\pi f h\sin(\pi\nu(f))}\frac{[volt]}{[meter][Hz]}$$

and

$$H_\phi(f) = \left(-\frac{I(f)dsP^1_{\nu(f)}(-\cos\theta)}{4ah\sin(\pi\nu(f))}\right)\frac{[ampere]}{[meter][Hz]}$$

In the equations above, the current moment is defined as $I(f)ds$, where $I(f)$ is the current in amperes and ds is the vertical distance that this current flows. The propagation and dissipative

characteristics of the atmosphere are both frequency dependent and are described by the complex eigenvalue ν. $P^{0,1}_{\nu(f)}(x)$ are Legendre functions with complex subscripts and θ is the great circle distance between the source and receiver. The radius of the Earth and the height of the ionosphere are described by a and h respectively.

Present methods for calculating the frequency spectrum of the source current moment $I(f)ds$ require dividing the recorded complex electromagnetic spectra by the theoretical spectra. This method is somewhat problematic though because it neglects the fact that the transient signal is actually contaminated by the background signal in the respective spectra. Therefore, the influence of the constant background Schumann resonance on the source current moment is never taken into account causing transients with power comparable to the background to be undetected as opposed to the larger, more conspicuous transients. This problem may be resolved in the future by coupling the background machine with the transient machine. This way, the background signal associated with each recorded transient can be taken into account.

1.4.2 Data Acquisition from Rhode Island Site

This study makes use of an extensive automated digital archive from West Greenwich, Rhode Island first developed by Wong (1996) which includes the application and development of signal processing algorithms for locating and characterizing large lightning transients (Huang, 1997). This site continuously records two perpendicular components of the magnetic field and the vertical electric field in a band pass from 3-120 Hz. All signals are time-tagged with an on-site global positioning system (GPS) clock. Fast Fourier Transforms (FFT's) of the time series are computed and displayed in real time before being recorded on a 486 personal computer.

Chapter 2

The Relationship Between Background and Transient Schumann Resonances

2.1 Previous Work

Despite the availability of a common mathematical framework, the global scale analysis of the background and transient signals (from global lightning activity) has historically been researched separately (C. Polk and D. Sentman for the background; D.L. Jones and A.P. Nickolaenko for the transients). The first dual studies of these signals were conducted by Ogawa et al. (1966), Fellman (1973) and Lazebnyy and Nickolaenko (1975), but without the benefit of either meteorological information or interest. However, conclusions drawn from these respective studies were different. According to Ogawa et al. (1966), the transient signals are generally unrelated to the background signal. Furthermore, this study concluded that the background had a universal time diurnal variation whereas the transients appeared to be controlled by local time. The findings in Fellman (1973) on the other hand were that the transients are highly correlated with the background signals, each with a substantial global diurnal variation. Finally, Lazebnyy and Nickolaenko (1975) argued that there existed a negligible diurnal variation in transient activity and that these transients were largely of oceanic origin. Findings in this thesis reveal a rough proportionality between peak

magnetic background intensity and total number of lightning transients. This thesis also reveals a systematic diurnal variation in transient activity that lags the peak background intensity of that particular day. This finding is consistent with the diurnal variation of lightning in regional studies (Williams et al., 1999).

2.2 Background Resonances

The overlapping effects of total global lightning activity maintain a quasi-steady electromagnetic signal in the extremely low frequency (ELF) range of 3—120 Hz. This ELF signal is continuously recorded in Rhode Island and defined to be the SR background signal. Individual background spectra are produced by performing numerical Lorentzian fits on all recorded SR power spectra. Figure 2-1 below shows a sample power spectrum for the electric field from approximately 1 day of background data, with clearly defined Schumann resonant mode peaks at 8 Hz, 14 Hz, 20 Hz, and 26 Hz.

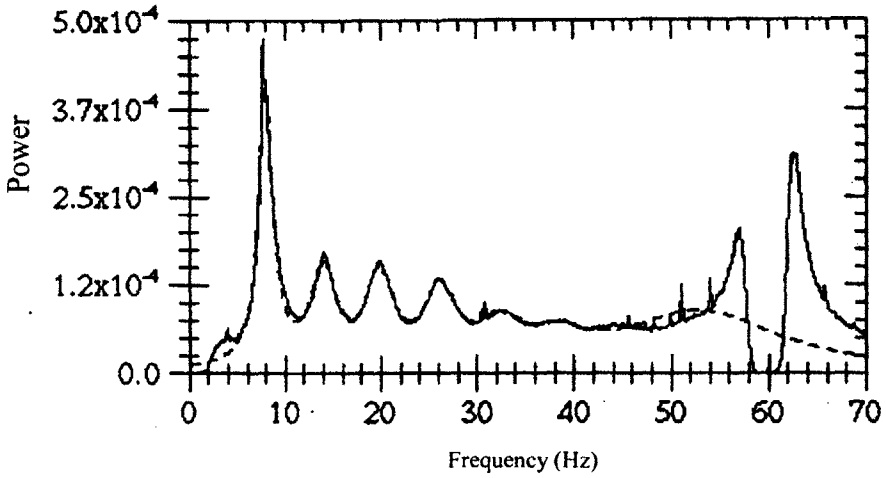

Figure 2-1: Sample ELF Background Spectrum

2.2.1 Diurnal Variation in H_{ew} and H_{ns} Signals

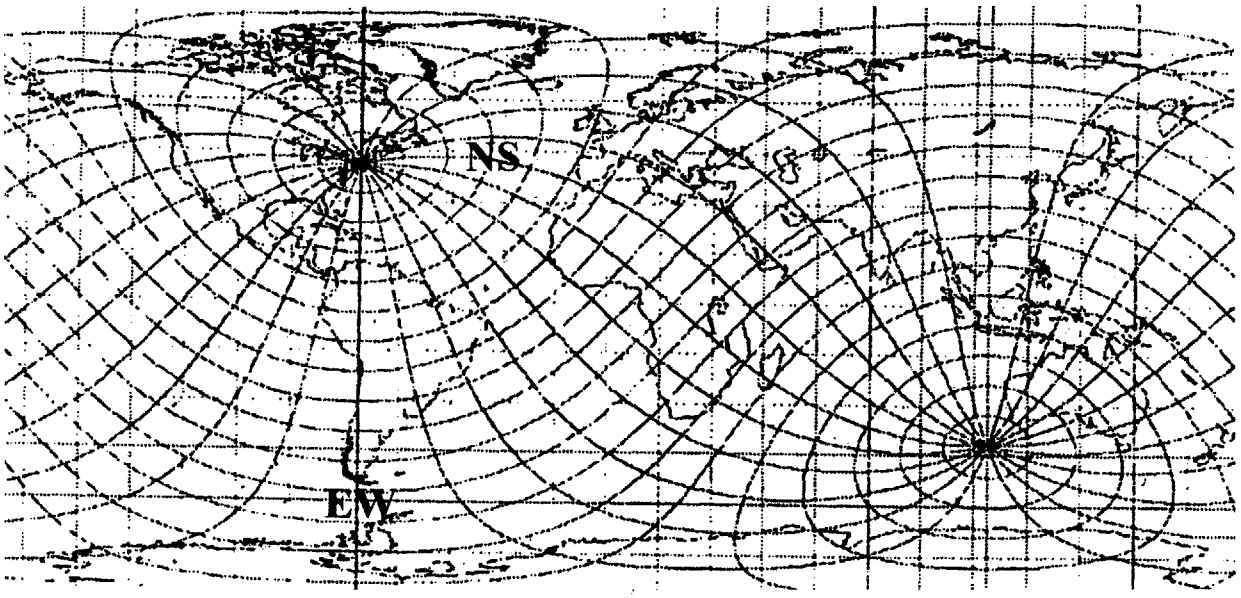

Figure 2-2: Great Circle Paths from West Greenwich, RI

Because of their geographical locations relative to the Rhode Island site, Africa and South America have different dominant magnetic field components. Vertical lightning current in Africa, which lies nearly due east on a great circle path from Rhode Island, produces a North-South dominated magnetic response. South America on the other hand, has a predominant East-West magnetic component. Figure 2-2 demonstrates the orientation of the East-West / North-South great circle paths with respect to the Rhode Island site.

A systematic peak in lightning activity occurring in the late local afternoon (Whipple, 1929) causes consistent diurnal peaks in background intensity for Africa and South America as is shown in Figure 2-3. The signature magnetic diurnal variations for Africa and South America therefore peak respectively at 14 and 20 Universal Time (UT). The abundance of afternoon lightning activity in these regions evolves into large mesoscale charge reservoirs needed to produce high-energy CG's that occur later in the diurnal cycle (Williams, 1998). (See Figure 2-3)

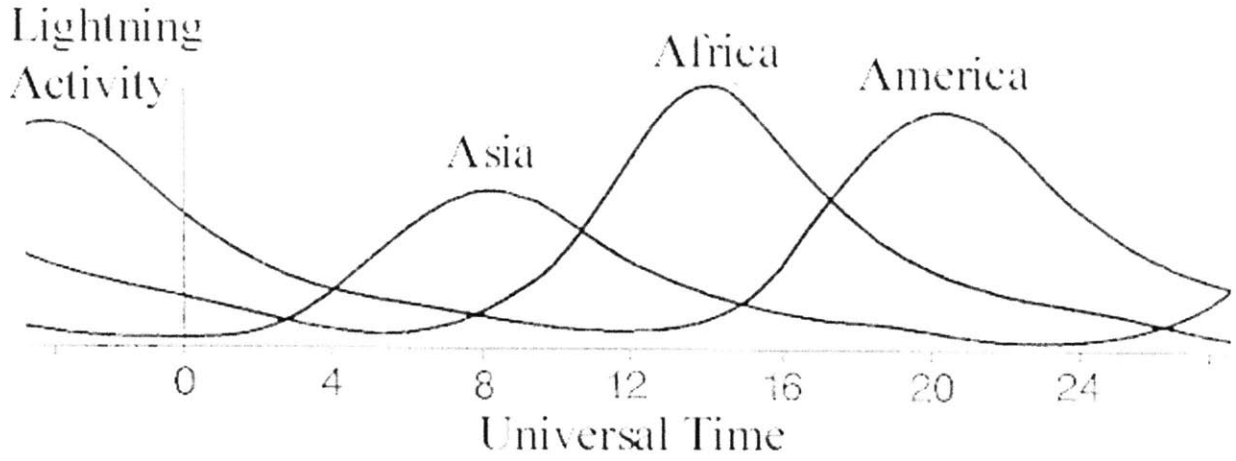

Figure 2-3: Whipple Curve

2.3 Transient Excitations

A transient is essentially a point source excitation of the Earth-ionospheric cavity--a single lightning discharge that for several hundred milliseconds dominates the power in the cavity over all other lightning flashes on the planet. The large signal-to-noise ratio in the measurement and the normal mode theory for EM waves in the cavity enable the location of that event from single station records of vertical electric and horizontal magnetic fields in Rhode Island. The margin of error in locating events (0.5 – 1.0 Mm) is relatively large (Boccippio et al., 1998). However, the level of uncertainty still permits the distinction of the African, South American and Maritime Continent 'chimneys'. Approximately 1 in 10000 lightnings on the planet can be located in this manner. All the others are buried in their own noise--that is the 'background' Schumann resonances. Figure 2-4 illustrates a sample ELF transient detection, superimposed on the background signal.

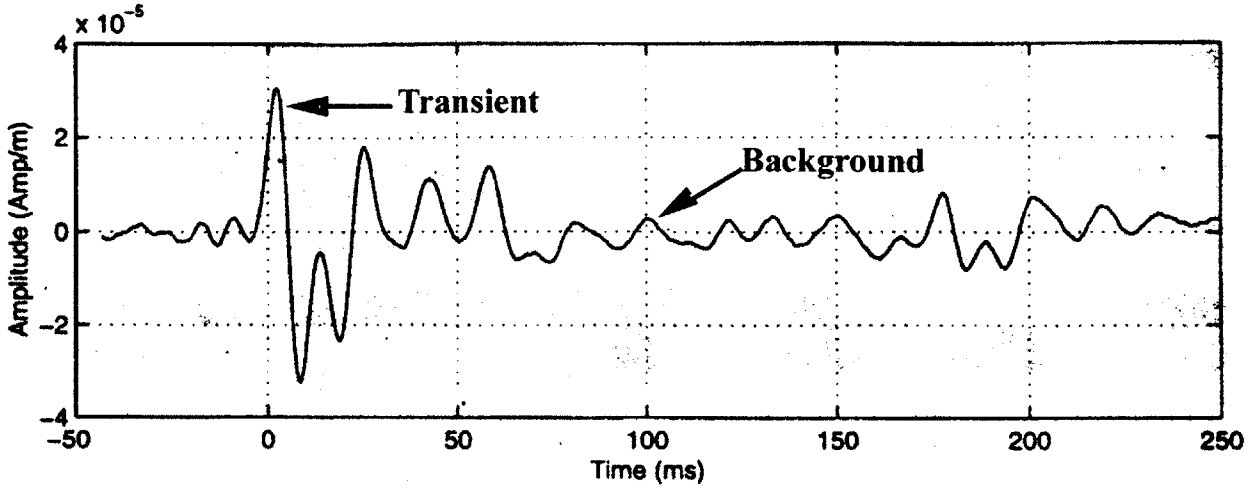

Figure 2-4: Sample Electric ELF Transient

2.3.1 Data Collection and Triggering of Events

Digital data are collected from the Rhode Island site approximately once every 2 weeks on 1 gigabyte Iomega jaz cartridges. Between visits, the data collection apparatus is prone to occasional failure. Factors such as wind, rain, snow, animals, local power failures, and nearby lightning events can (and often do) cause instabilities in the system. As a result from these instabilities, time gaps in transient detection will occur.

The large accumulation of data, resulting from continuous transient detection, makes the current data storage capacity of the Rhode Island site a limiting factor. A triggering mechanism that records only transient events rising above a certain threshold has been implemented in order to address this issue. The trigger threshold is directly determined from the magnetic power (amplitude) using the following formula,

$$A = \sqrt{\frac{1}{2}(H_{ns}^2 + H_{ew}^2)}$$

When the quantity A rises above a certain threshold (currently set at 11.6μA/m), data is recorded 100 milliseconds before and 400 milliseconds after the trigger point of a particular transient event, resulting in a half second data window (the actual data window currently used is 100 milliseconds of pre-trigger and 400 milliseconds of post-trigger). As a result of using this trigger threshold mechanism, all events falling below the trigger threshold will not be recorded, thus saving data storage space.

2.4 Background/Transient Plots

Previous studies describing the relationship between 'background' Schumann resonances and transient activity (Williams et al., 1999) are supported in this thesis. Daily plots, for all days between 12/13/96-12/27/96, superimposing the background intensity and transient count vs. time have been produced in order to visualize better the background/transient relationship. Because of their geographical location with respect to Rhode Island, the African contribution to the background intensity is most prevalent in the North-South magnetic component while the South American contribution is most prevalent in the East-West component (See Figure 2-2). Days are chosen according to the stability of the transient detection machine at the Rhode Island site and the relative "cleanness" of the recorded background data in this interval. In general, the background signals are of higher quality in the winter because locally interfering storms are not present. Figure

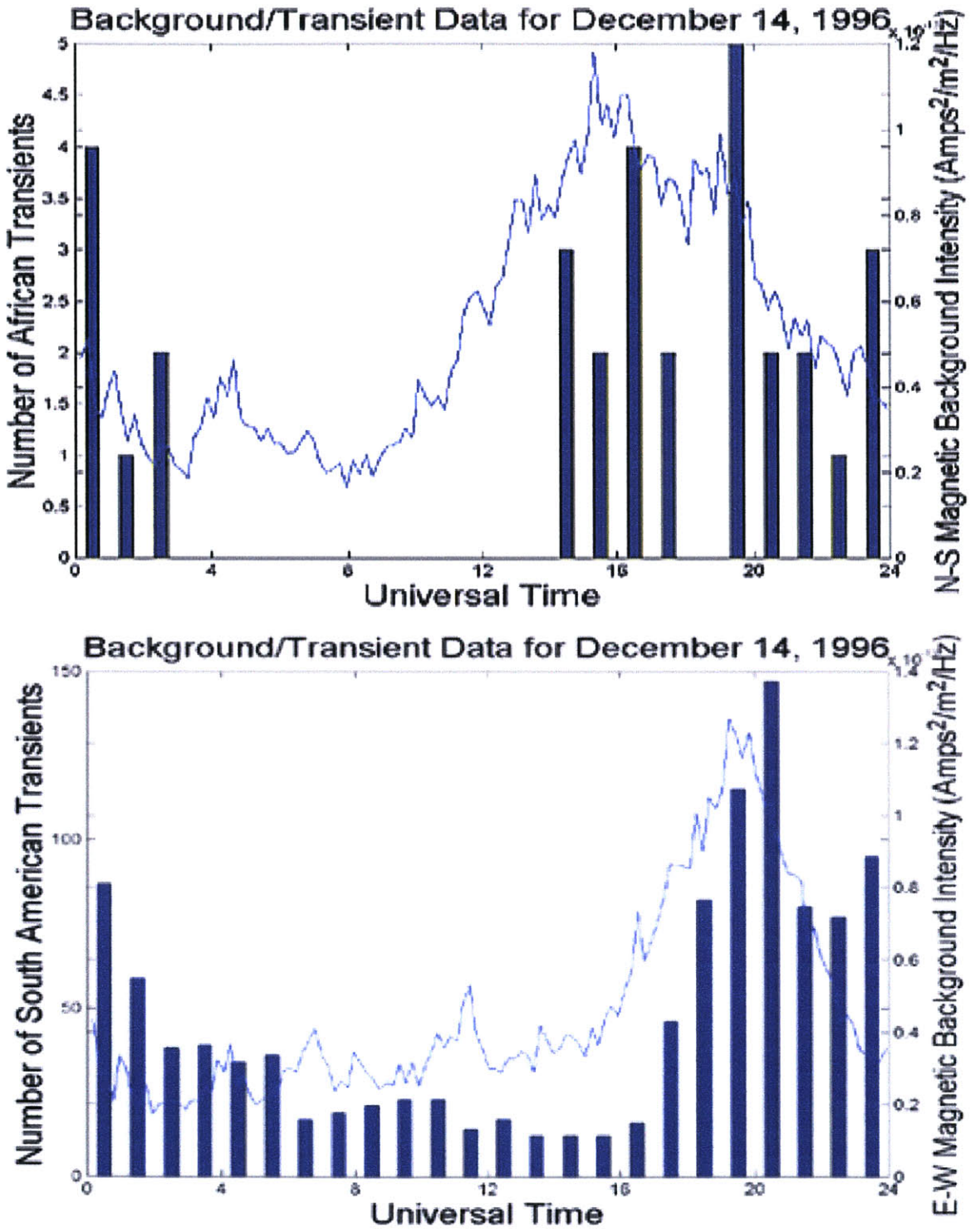

Figure 2-5: Background/Transient Plots for Africa and South America

2-5 respectively illustrates the relationship between African and South American transient events and their predominant magnetic background intensity for a typical day within this time. (See Appendix A for a complete set of plots)

Several other days systematically show that the background/transient relationship is the same; with the majority of African transients tending to occur during the 14UT-24UT interval and that the majority of South American transients occurring in the 19UT-4UT interval, closely following their respective N-S and E-W background magnetic intensities. Since peak transient activity continues several hours after the background has peaked, it can be inferred that a strong background signal is a necessary prerequisite for large transient activity. Further research will of course be needed to substantiate this claim.

Scatter plots are also useful in visualizing this relationship. The two scatter plots shown in Figure 2-6 graph the total daily number of transients in Africa and South America vs. their corresponding peak background intensity for that day. Points on these plots correspond to observations on several days between December 1996 and February 1997 (12/13/96-12/27/96, 1/5/97-1/13/97, and 2/1/97-2/13/97). A regression line is included on both of these plots providing strong evidence for a positive correlation ($R^2 = 0.0952$ for South America/EW magnetic component; $R^2 = 0.2069$ for Africa/NS magnetic component).

The scatter in both of these plots, however, is significantly reduced when only positive-stroke transient events are taken into account, as is shown in Figure 2-7 ($R^2 = 0.2313$ for South America and peak EW magnetic intensity; $R^2 = 0.4234$ for Africa and NS peak magnetic intensity). Reasons for such behavior are still unclear, although a possible explanation might have to do with the formation of large mesoscale convective systems (MCS's) and their subsequent relation to positive cloud-to-ground lightning (Williams, 1998). If valid, this explanation would suggest the

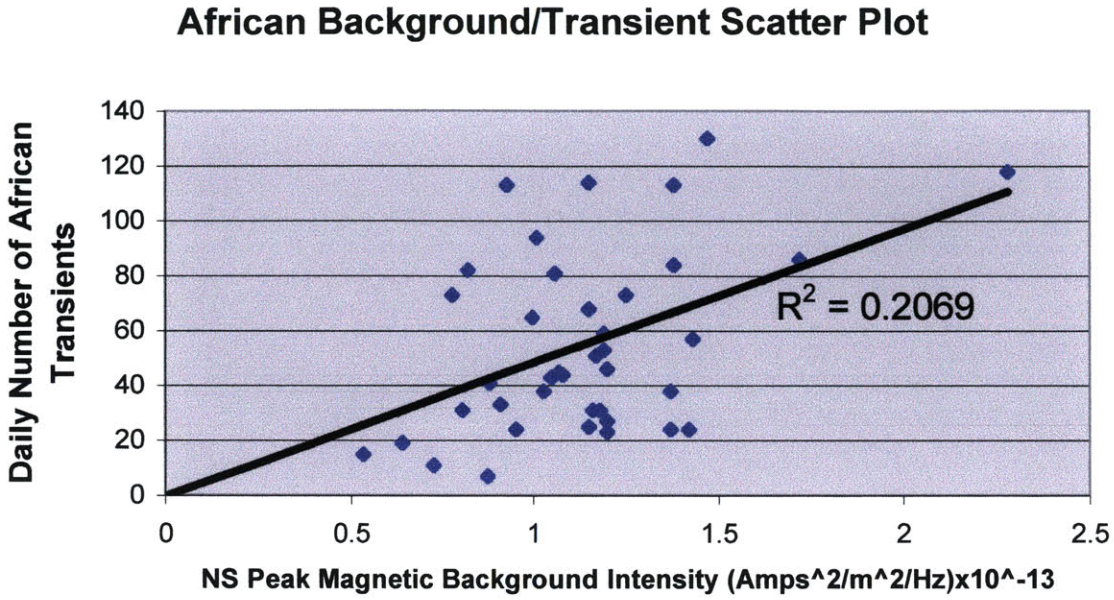

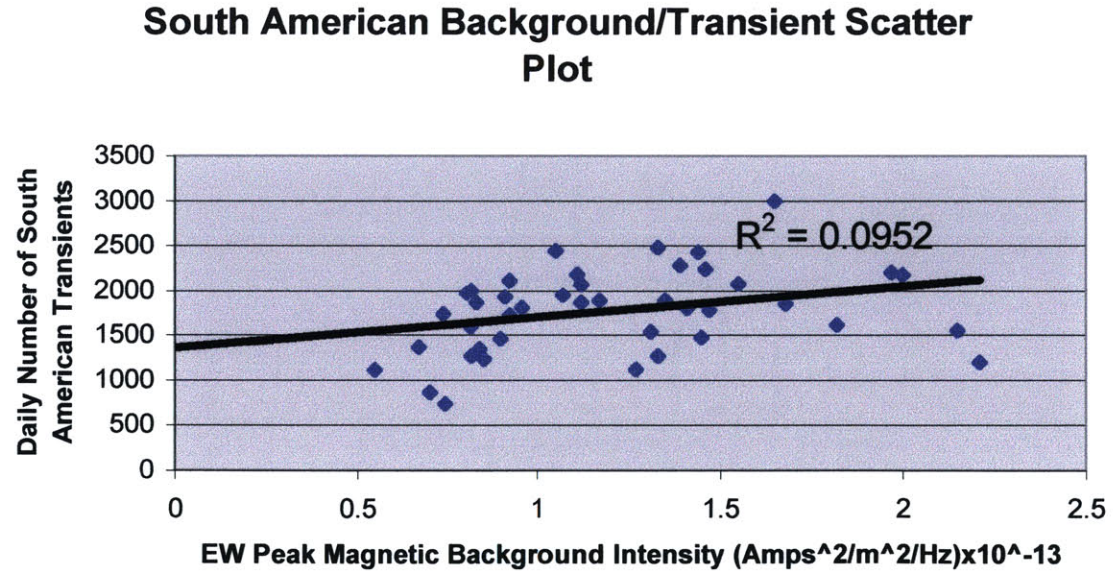

Figure 2-6: Background/Transient Scatter Plots for Individual Days in Africa and South America

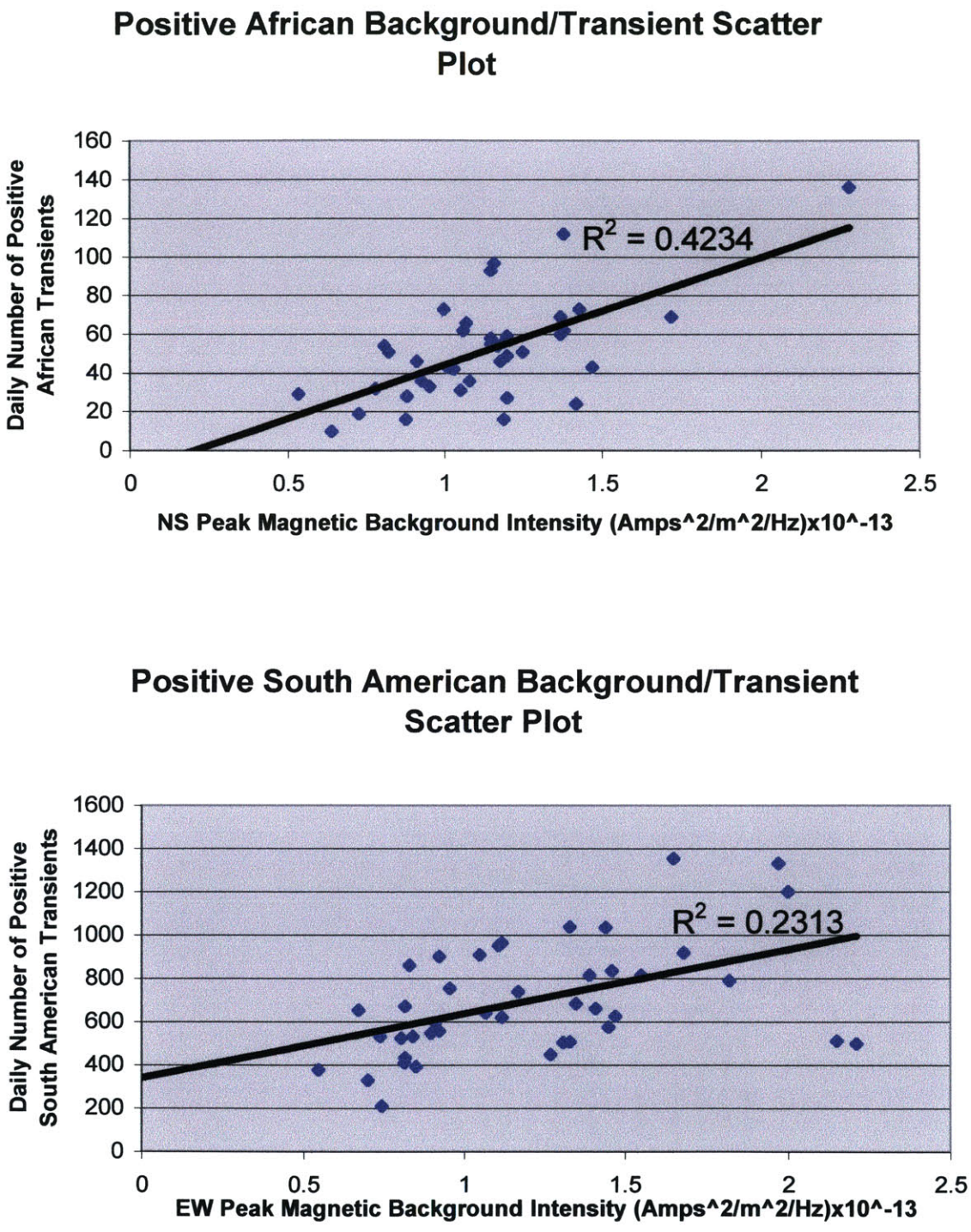

Figure 2-7: Background/Transient Scatter Plots for Individual Days in Africa and South America (Positive Transient Events Only)

possibility of using the total number of positive transients as a rough indicator of a particular region's 'chimney' strength because of the relative certainty that these events did indeed occur in that region (as opposed to simply using EW/NS components of the background magnetic intensity, which have contributions from other regions that are sometimes not negligible). Positive cloud-to-ground lightning activity has also been shown to be directly proportional to number of sprite observations (Huang et al., 1999, Williams et al., 1999), which will be discussed later in Chapter 4.

Chapter 3

The Relationship Between Lightning Transient Counts and Precipitation on a Regional Basis

Regional precipitation estimates for Africa, South America, and the Maritime Continent are calculated from the NASA data set for all days between 5/7/98 – 6/20/98 and compared with Schumann resonance transient activity for each respective region (the criteria for choosing this particular interval, was determined by the availability of continuous SR transient data from Rhode Island). Regional precipitation estimates for Africa, South America, and the Maritime Continent are obtained from NASA, with an additional African precipitation estimate provided by NOAA. Latitude/Longitude coordinates defining each of the three regions are indicated below

Africa→	20W < Longitude < 50E	20S < Latitude < 20N
Maritime Continent→	70E < Longitude < 170E	30S < Latitude < 30N
South America→	30W < Longitude < 90W	45S < Latitude < 15N

3.1 NASA Rainfall Data Set

Global precipitation data were obtained from the "Global Precipitation Climatology Project (GPCP) One-Degree Daily Precipitation Data Set" (Huffman et al., 2000). The data are provided, via anonymous file transfer protocol (ftp://rsd.gsfc.nasa.gov/pub/1dd/), by the NASA Goddard Space Flight Center in the form of a 360 x 180 array, with X (longitude) incrementing most rapidly West to East from the Prime Meridian, and then Y (latitude) incrementing North to South. With a resolution of 1-degree-latitude x 1-degree-longitude (Cylindrical Equal Distance Projection), this data set creates a complete global array of points. Figure 3-1 illustrates the proper orientation of this map.

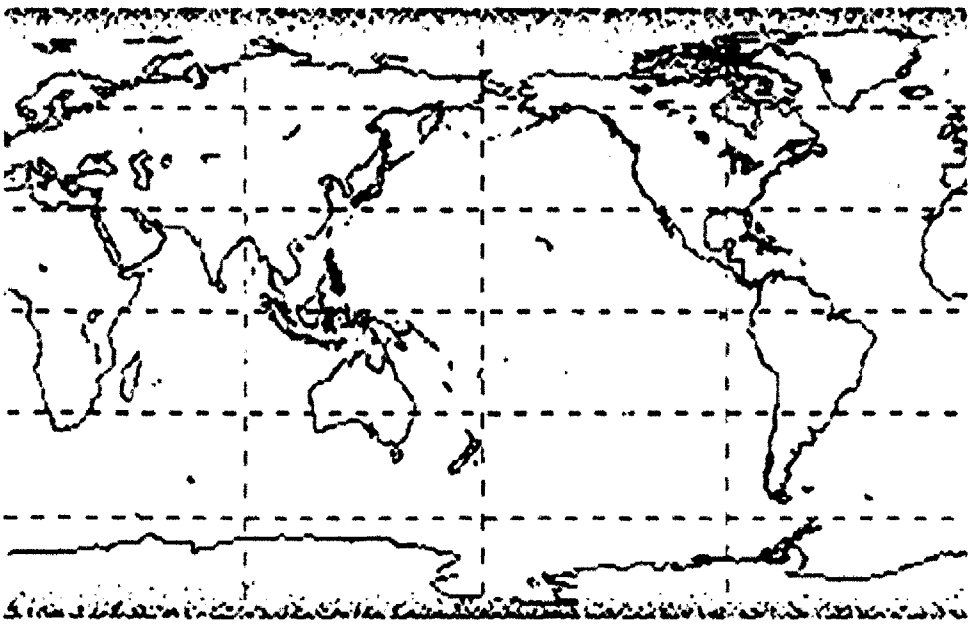

Figure 3-1: Properly oriented NASA map

3.1.1. Description of Methods for NASA Data Set

The NASA data set is unique in that it is the only data set with the attributes of being global, daily, and formed by combining multiple data sources. In particular, this data set combines information from three sources: the GPCP Geostationary Satellite Precipitation Data Centre (Infrared Temperature brightness (Tb) histograms), the GPCP Merge Development Centre (GPCP SG Merged Precipitation estimate and GPROF fractional occurrence), and the GSFC Satellite Data Utilization Office (TOVS precipitation estimates).

The estimate produced by the GPCP Geostationary Satellite Precipitation Data Centre (GSPDC) is the accumulation of several infrared (IR) images gathered via satellite. Each cooperating geostationary (geo) satellite operator (the Geosynchronous Operational Environmental Satellites, or GOES, United States; the Geosynchronous Meteorological Satellite, or GMS, Japan; and the Meteorological Satellite, or Meteosat, European Community) accumulates three-hourly infrared IR imagery. These are forwarded to GSPDC as 24-class histograms of Tb on a 1x1-deg lat/lon grid. The global geo-IR data are then merged on a global grid. In parallel, the NOAA-series low-earth-orbit (leo) satellite operator (United States) provides GOES Precipitation Index (GPI) values on a 1x1-deg lat/lon grid accumulated to the nearest 3-hourly time.

The GPCP satellite-gauge precipitation product (SG) is produced as part of the GPCP Version 2x79 Combined Precipitation Data Set by the GPCP Merge Development Centre (GMDC). Data from various satellites are combined to form a multi-satellite (MS) product. Depending on data availability, this product may be computed differently. For the period analyzed in this thesis, data from the geo-IR, leo-IR, TOVS, and SSM/I satellites are combined. TOVS is merged with

SSM/I where the SSM/I data are suspect (outside about 45N-S) or missing. Then SSM/I and geo-IR are approximately time-matched to compute local coefficients to adjust the full geo-IR GPI to the bias of the SSM/I in the 40N-S band. As well, leo-IR GPI is approximately scaled to the SSM/I.

The Goddard Profiling Algorithm (GPROF) Version 4.0 is described in Kummerow et al. (1996). In summary, GPROF is a multichannel physical approach for retrieving information on rainfall and vertical cloud structure from satellite-based passive microwave observations (here, SSM/I). Version 4.0 applies a Bayesian inversion method to the observed microwave brightness temperatures using an extensive library of cloud-model-based relations between hydrometeor profiles and microwave brightness temperatures. Each hydrometeor profile is associated with a surface precipitation rate. GPROF includes a procedure that accounts for inhomogeneities of the rainfall within the satellite field of view. Over land and coastal surface areas the algorithm reduces to a scattering-type procedure using only the higher-frequency channels. This loss of information arises from the physics of the emission signal in the lower frequencies when the underlying surface is other than all water.

The TOVS precipitation estimate (Susskind and Pfanendtner, 1989 and Susskind et al., 1997) is computed from a regression relationship between collocated rain gauge measurements and several TOVS-based parameters that relate to cloud volume: clout-top pressure, fractional cloud cover, and relative humidity profile. The relationship is allowed to vary seasonally and latitudinally. The data are delivered for daily nodes (ascending/descending) on a 1x1-deg grid.

3.1.2 Regional Precipitation Comparison

The long wave structure of Schumann resonances provides information on regional lightning activity in three major tropical zones (America, Africa, and the Maritime Continent). Integrated precipitation estimates for these same regions are calculated by, first taking each pixel estimate within a particular region and multiplying it by its corresponding pixel area. Pixel areas are determined by taking into account the latitudinal dependence of pixel zonal extent. After multiplying each pixel by its corresponding area, the estimate of an entire region is determined by simply summing all products within each respective region. Figure 3-2 below demonstrates the precipitation variations for these three regions, where the rainfall estimates for the ocean-dominated Maritime Continent are larger than estimates for the other two regions by more than a factor of two, on average.

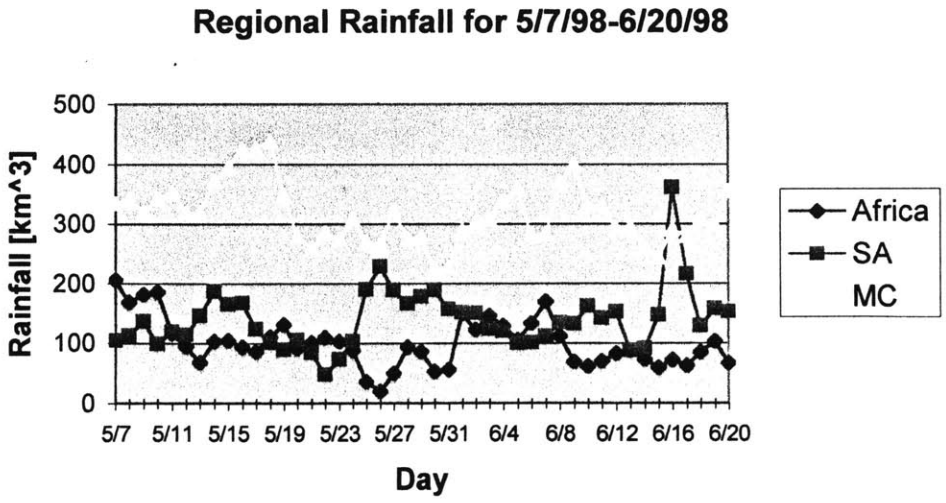

Figure 3-2: Time Series for Regional Rainfall

As we can see from Figure 3-2, there is much day-to-day variability in each of the three convective regions with comparatively greater variability over the tropical continental zones of Africa and South America than over the ocean-dominated Maritime Continent. For example, the African rainfall estimate for 6/1/98 (150 km^3) is approximately three times larger than the African estimate for 5/31/98 (57 km^3). Although three-fold changes in daily precipitation do not occur in the Maritime Continent and South America within this interval, significant day-to-day variability can still be found (e.g. difference in rainfall estimate for Maritime Continent from 5/18/98 to 5/19/98 = -90 km^3; difference in rainfall estimate for South America from 6/15/98 to 6/16/98 = +213 km^3). The three regions seem to have a negligible inter-dependence, with the exception of Africa and South America. Figure 3-3 summarizes this inter-dependence with scatter plots for each pair of regions.

As we can see from Figure 3-3, the African rainfall estimate is inversely proportional to the South American rainfall estimate. The distance between Africa and South America (approximately one quarter of the total circumference of the Earth) suggests that this inverse relationship may in fact be a wave number 2 planetary wave (i.e. one region is maximum when the other is a minimum and vice-versa) similar to the one described by Burpee (1976). In contrast, random scatter in both the MC/African and MC/South American scatter plots demonstrate little correlations between these pairs of regions. It is difficult however to determine whether this behavior is truly indicative of the Maritime chimney due to large amount of oceanic convection included as part of the Maritime Continent region for this study. Future studies might consider including a land-only mask in their analyses in order to better quantify the continental behavior of these three chimneys.

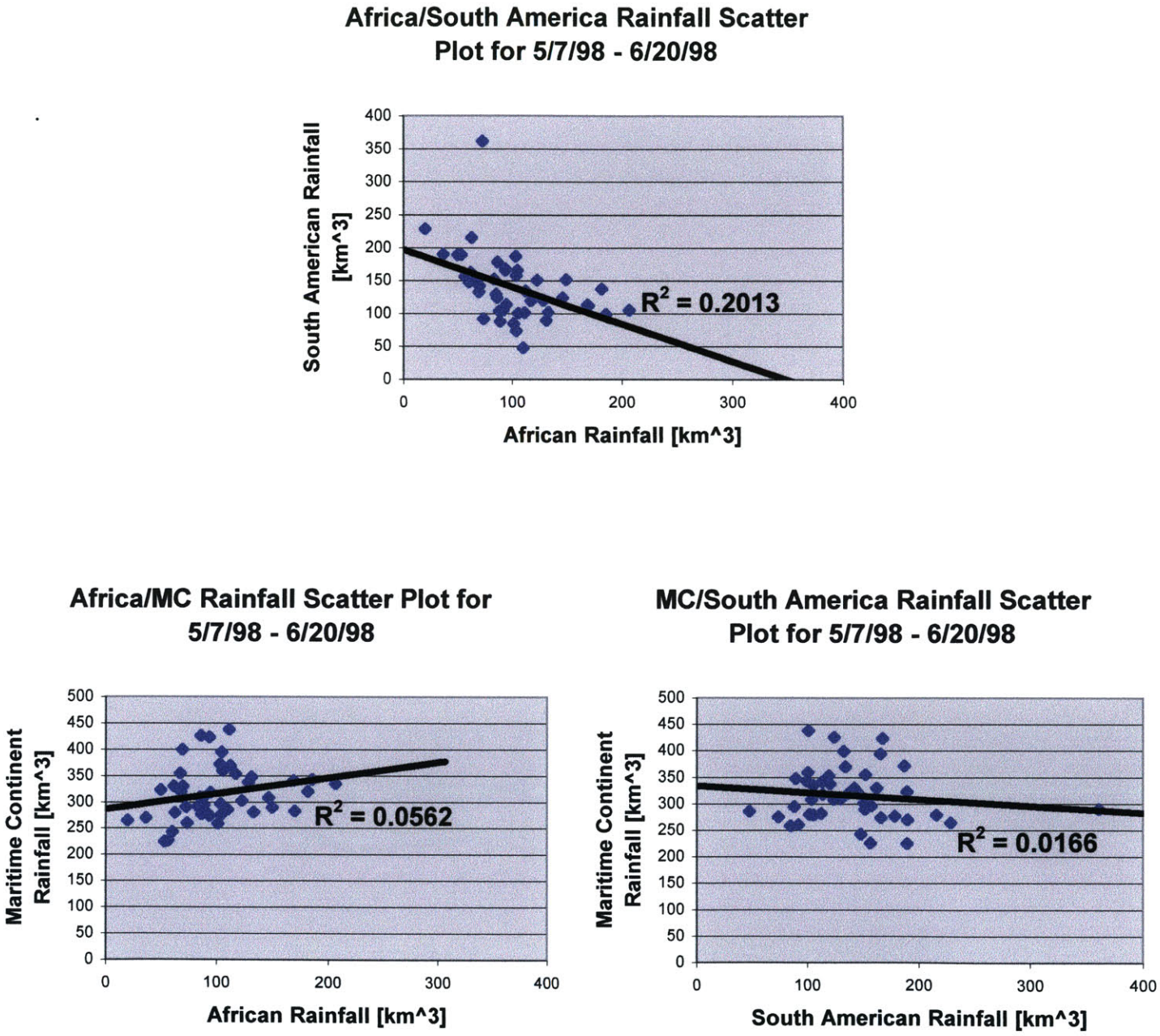

Figure 3-3: Scatter Plots for Regional Rainfall

3.2 NOAA Rainfall Data Set

Additional African precipitation estimates are provided, via anonymous file transfer protocol (ftp://ftp.ncep.noaa.gov/pub/cpc/kouskyj/daily_estimates/), by the National Center for Environmental Prediction (NCEP) of the NOAA (Herman et al., 1997). These data are archived daily in the form of a 751 x 801 array, beginning at (20W, 40S) and ending at (55E, 40N). With a resolution of 0.1-degrees-latitude x 0.1-degrees-longitude (Cylindrical Equal Distance Projection), this data set encompasses the entire continent of Africa including the adjacent ocean. Figure 3-4, demonstrates the spatial coverage of the NOAA data set.

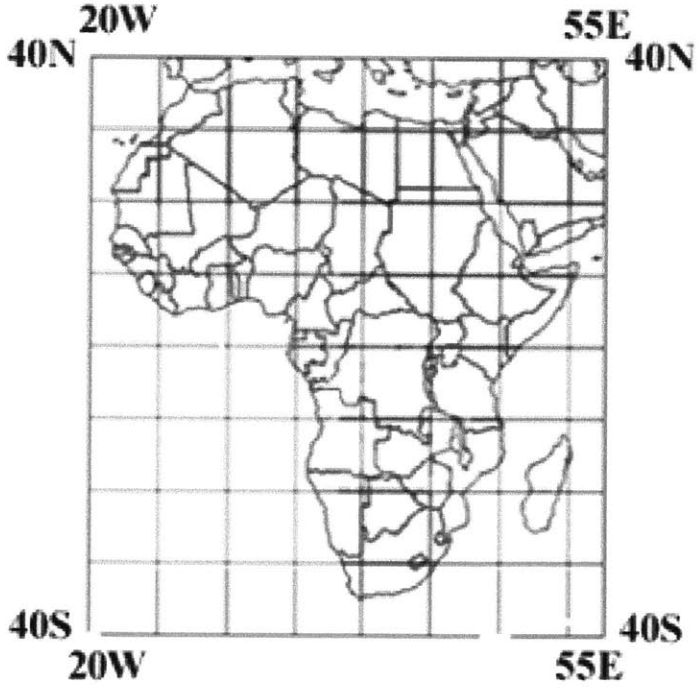

Figure 3-4: Spatial Coverage of NOAA Data Set

3.2.1 Description of Methods for NOAA Data Set

Observations used for calculating precipitation estimates for the NOAA data set include Meteostat satellite data, Global Telecommunications (GTS) rain-gauge reports, model analyses of wind and relative humidity, and orography for the computation of estimates of accumulated rainfall. Preliminary estimates of accumulated precipitation are made based on the GOES Precipitation Index (GPI), and later corrected using a bias field determined by the GTS observational data. These biases are then fitted to a grid using optimal interpolation to produce a convective rainfall estimate. In regions where precipitation is due to orographic lifting and the low cloud tops are relatively warm, local terrain features with numerical model analyses of meteorological parameters are incorporated. Rainfall from both convective and stratiform cloud types is finally incorporated into the total accumulated precipitation estimate by combining the techniques described above.

Similar to the NASA dataset, the NOAA data set utilizes data collected from the Meteostat satellite. Cloud top temperatures are determined from IR digital data at 5 km pixel resolution. These data are accessed every 30 minutes and then reformatted and converted to a geographic grid with 0.1-degree resolution.

A total of approximately 760 GTS stations report rain gauge estimates every 6 hours. These reports are first utilized in the CPC (Climate Prediction Center) Climate Assessment Data Base (CADB), for monitoring of climate anomalies (Finger et al., 1985). All quality control is done prior to the processing of precipitation estimates within the CADB (Thomas and Patterson, 1983). For each 24-hour period, these values are then accumulated to provide a daily rain gauge estimate.

Model analyses of surface wind and surface relative humidity are provided daily at 00, 06, 12, and 18 Universal Time (UT) from the 1-degree horizontal resolution Environmental Modeling Center (EMC) Global Data Assimilation System (GDAS). After acquiring the data, it is interpolated to a 0.1-degree horizontal resolution grid.

3.3 Comparison Between NOAA and NASA Data Sets

Despite the difficulty of quantifying continental-scale rainfall, the NOAA and NASA data sets compare relatively well with each other. The average daily African rainfall estimate for the 5/7/98 – 6/20/98 interval is 120km^3 and 91 km^3 respectively for the NASA and NOAA data sets. Both the time series and scatter plot shown in Figure 3-5 demonstrate the relative agreement between these data sets for this particular interval. In particular, the time series demonstrates relatively good phase agreement while the scatter plot shows a rough 1-to-1 relationship.

Discrepancies between these two data sets are most likely due to their respective biasing algorithms for interpreting satellite data. The NASA data set, for example, is collected entirely via satellite and determines its estimates with GPI techniques. However, it has been shown that the GPI technique generally overestimates precipitation falling over land as compared to rain-gauge reports (Arkin and Ardanuy, 1989), while over tropical oceans the bias is near zero (Xie and Arkin, 1995). The GPI technique is also notorious for underestimating rainfall over the coastal and mountainous regions of Africa (Herman et al., 1997). In creating the NOAA data set, the NCEP developed a procedure that removes biases from the GPI estimate by computing differences from the accumulated precipitation determined from rain-gauge reports and the GPI estimate. It should

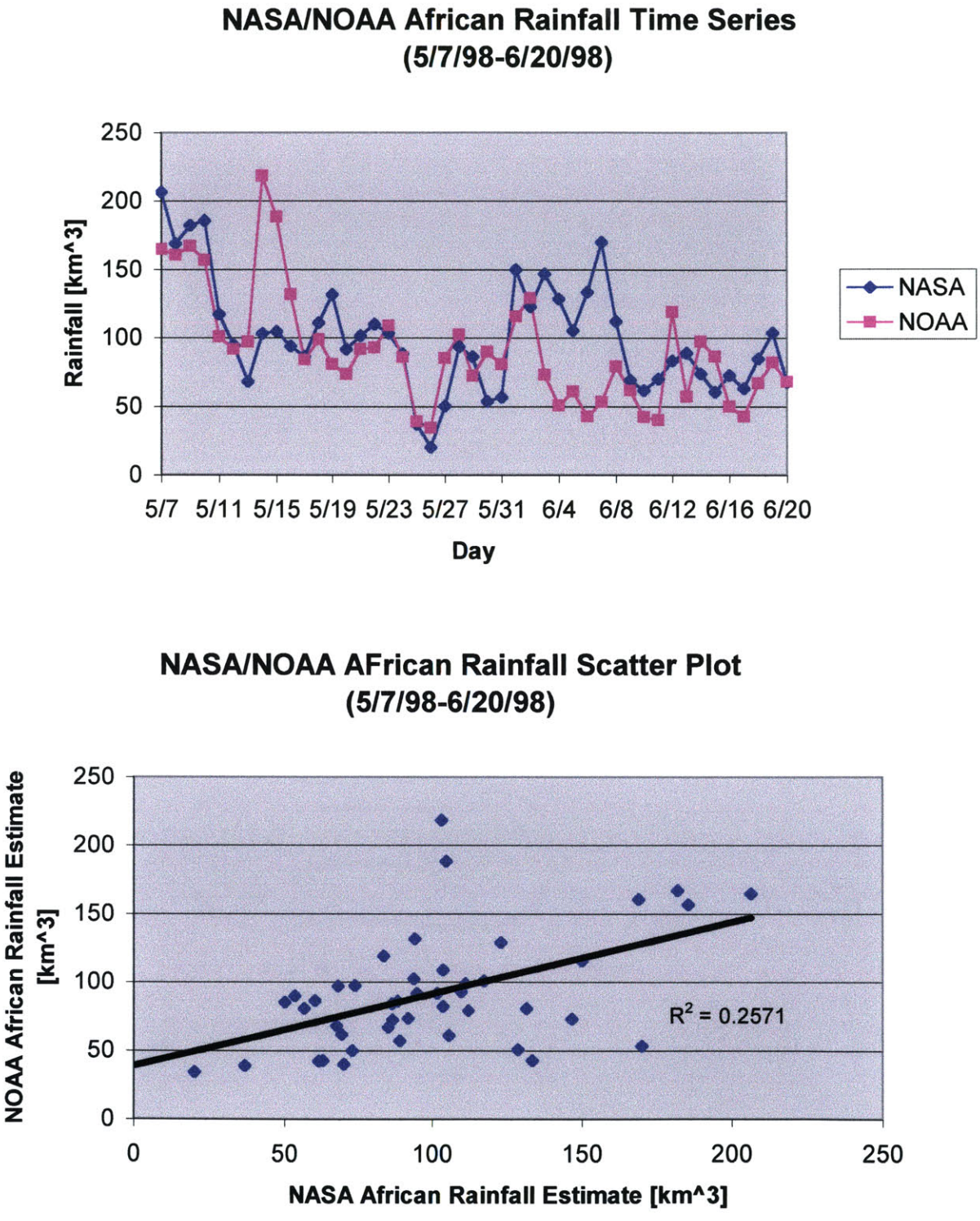

Figure 3-5: NASA/NOAA Time Series and Scatter Plot

also be noted that the NOAA estimates are occasionally much larger than the NASA estimates (e.g. 5/14/98). In such cases it is possible that large rain gauge estimates taken from a single station create overestimates in the NOAA data set (see maps for 5/14/98 in Appendices B and C). Whether such anomalies are taken into account by the NOAA algorithm however is unconfirmed. Figure 3-6 illustrates the spatial agreement between the NOAA and NASA data sets on June 1, 1998. Maps illustrating this relationship for all other days within the 5/7/98 – 6/20/98 interval are included in Appendices B and C.

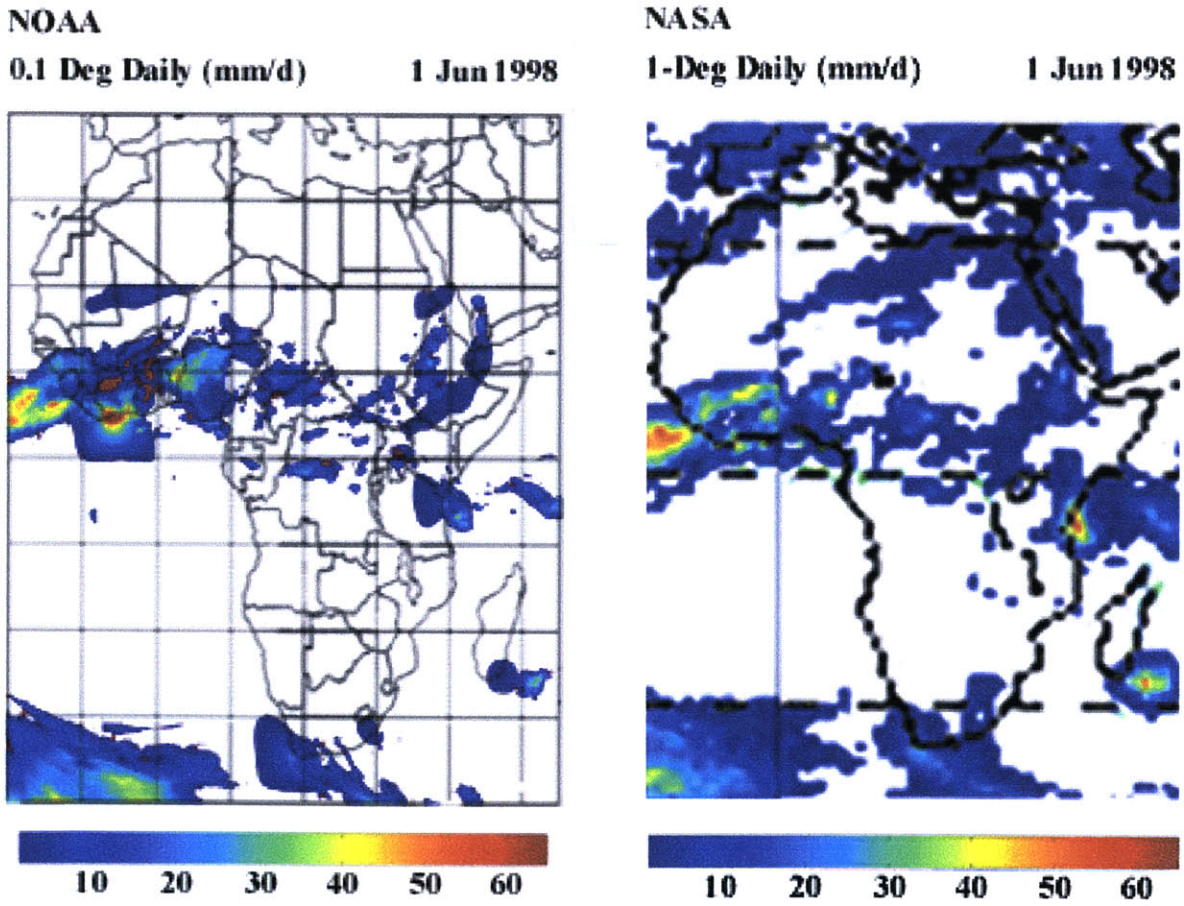

Figure 3-6: NOAA/NASA African Rainfall Maps for June 1, 1998

3.4 Comparison between Precipitation and Lightning Transients

Regional transient activity for Africa, South America, and the Maritime Continent is monitored for all days between 5/7/98 and 6/20/98. Coordinates for these three regions are assigned consistent with those described in the analysis for the NASA dataset. Figures 3-7 and 3-8 illustrate the results of this analysis by superimposing the daily time series of transient activity and precipitation for each of the three regions. Scatter plots are included in these figures as well to demonstrate how well these two quantities relate on a regional basis.

As we can see from these figures, regional transient activity has varying degrees of correlation with precipitation. Africa and South America both show a rough positive correlation between these two quantities, whereas the Maritime Continent demonstrates a slightly negative correlation. The R^2 values in the Maritime Continent and South American transient/rainfall relationships ($R^2 = 0.016$ for the Maritime Continent; $R^2 = 0.0074$ for South America) however suggest that these correlations are statistically insignificant as opposed to the two African R^2 values ($R^2 = 0.3185$ for the NOAA data set; $R^2 = 0.2137$ for the NASA data set). A comparison of several daily precipitation maps with daily global transient maps, show that these two quantities have a strong spatial relationship, despite having relatively low R^2 values. For Africa and the globe, Figures 3-9 and 3-10 respectively illustrate the spatial relationship between transient activity and

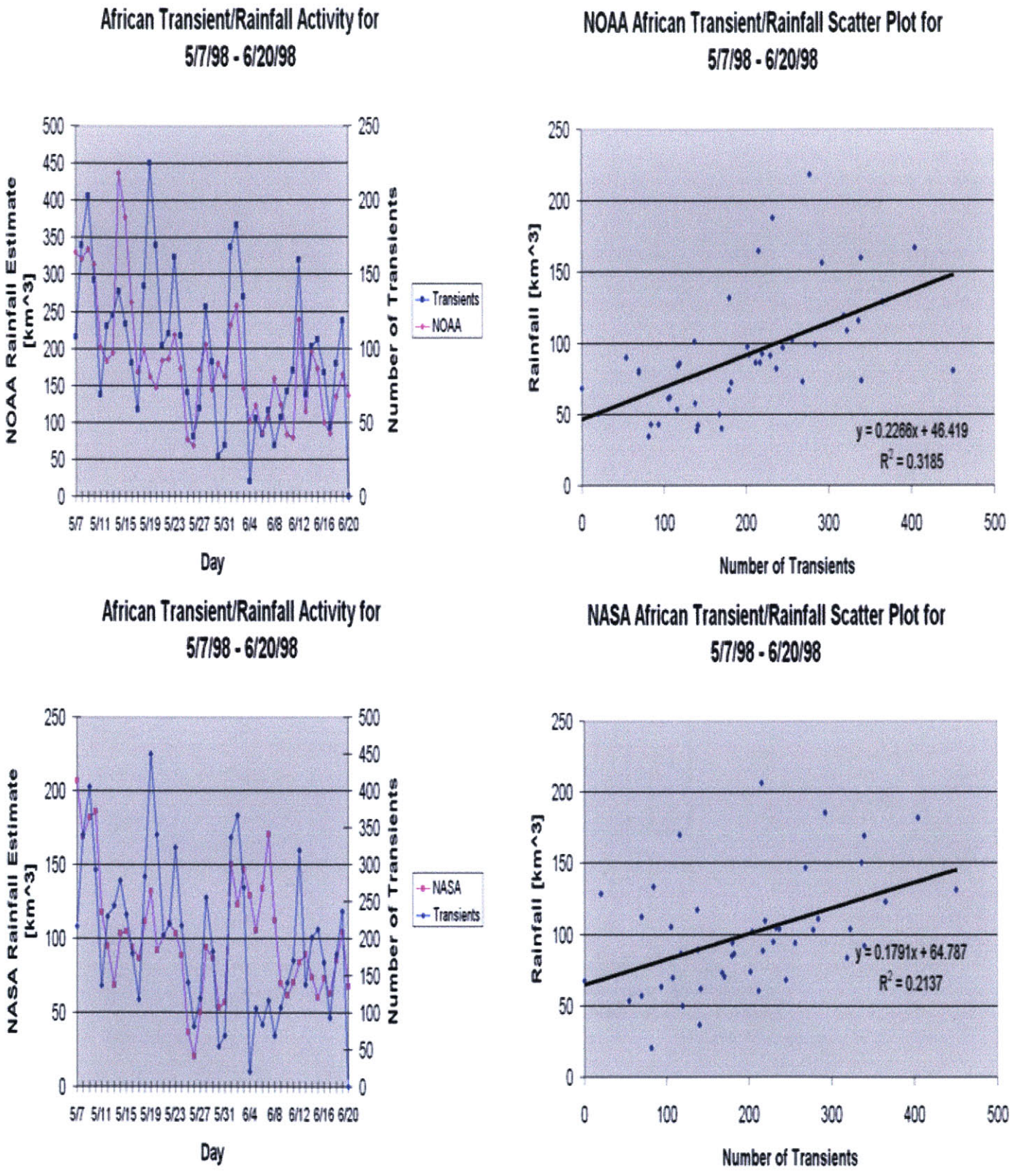

Figure 3-7: African Transient/Rainfall Relationship

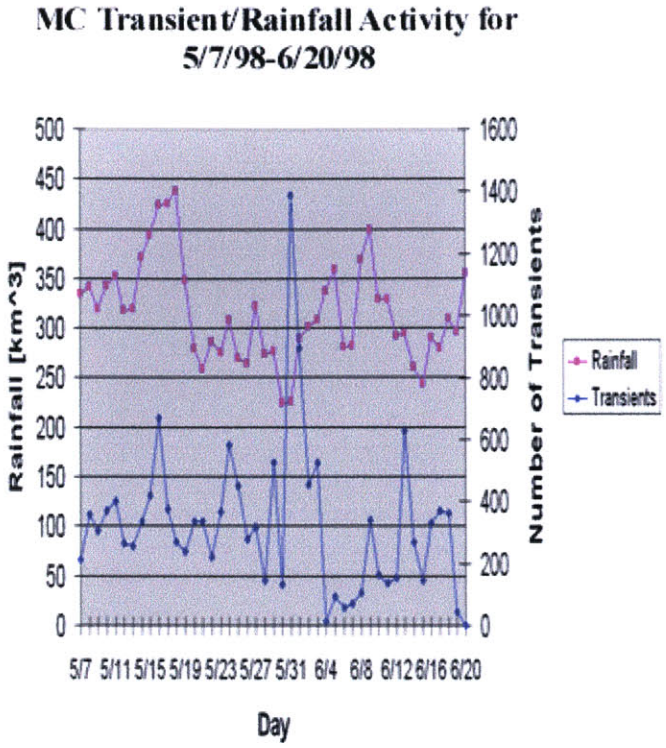

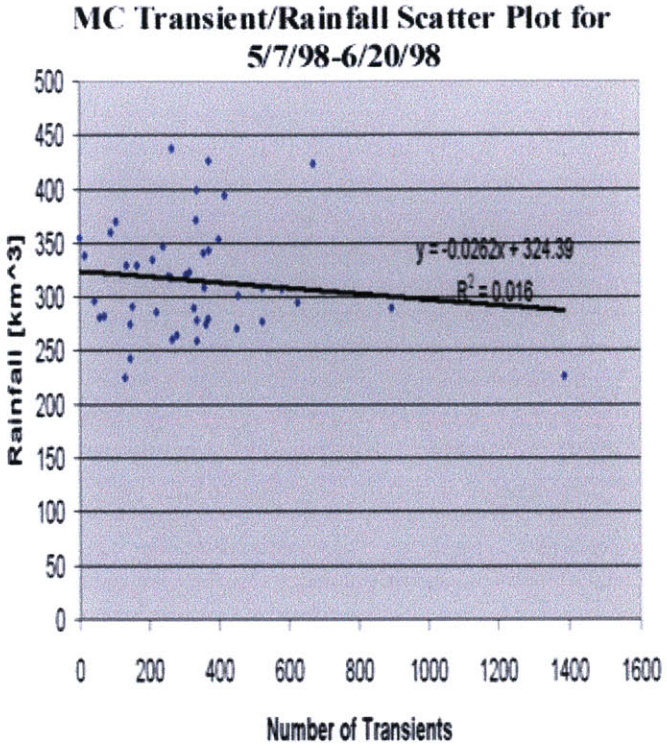

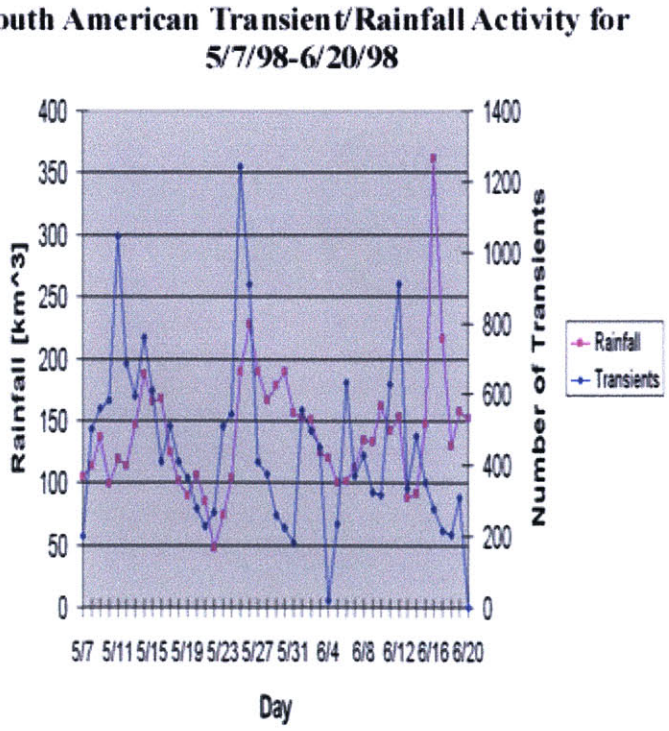

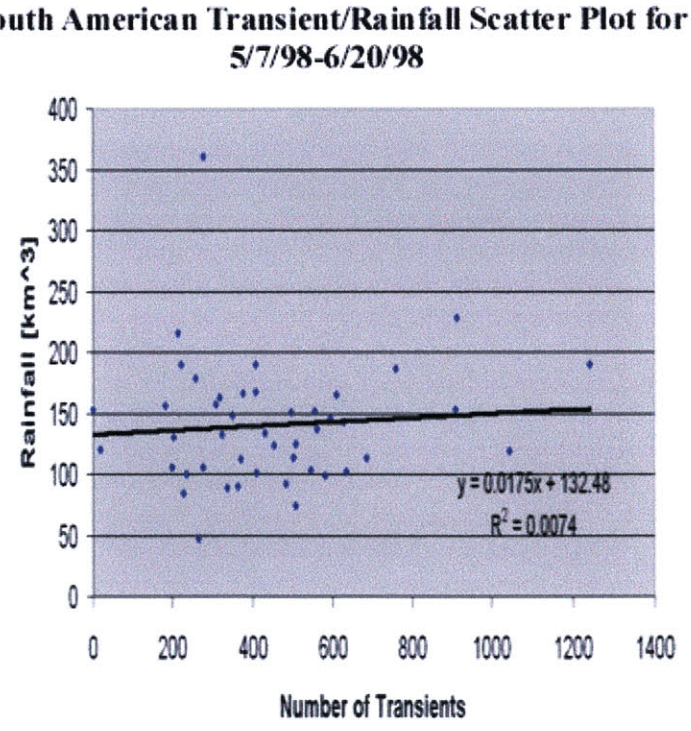

Figure 3-8: Transient/Rainfall Relationship in Maritime Continent and South America

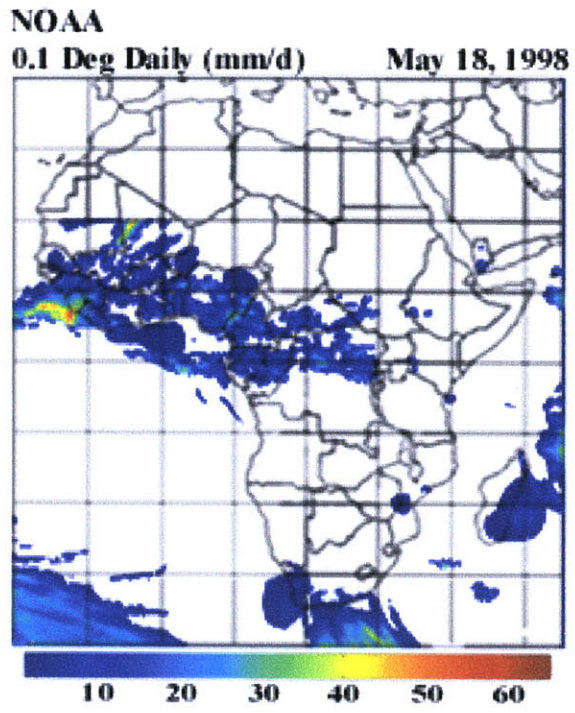

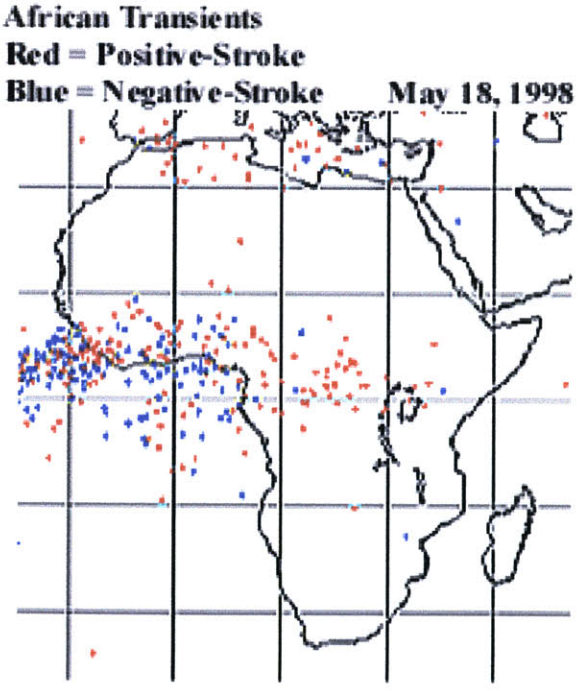

Figure 3-9: NOAA Transient/Rainfall Spatial Comparison

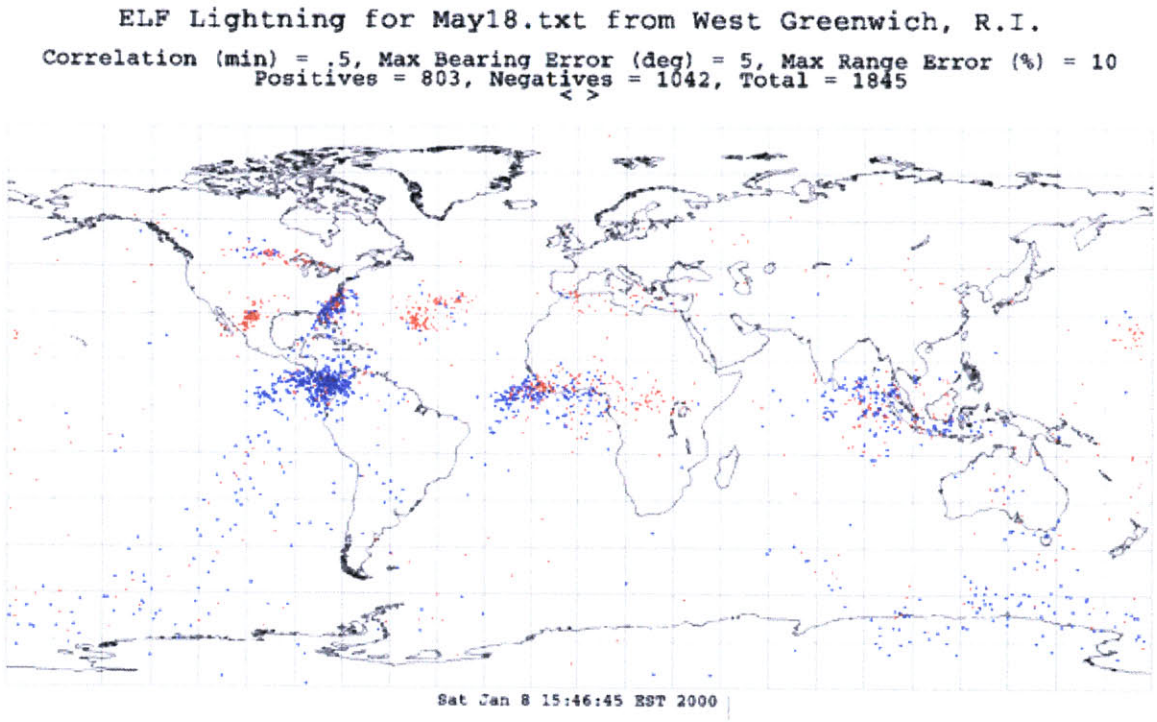

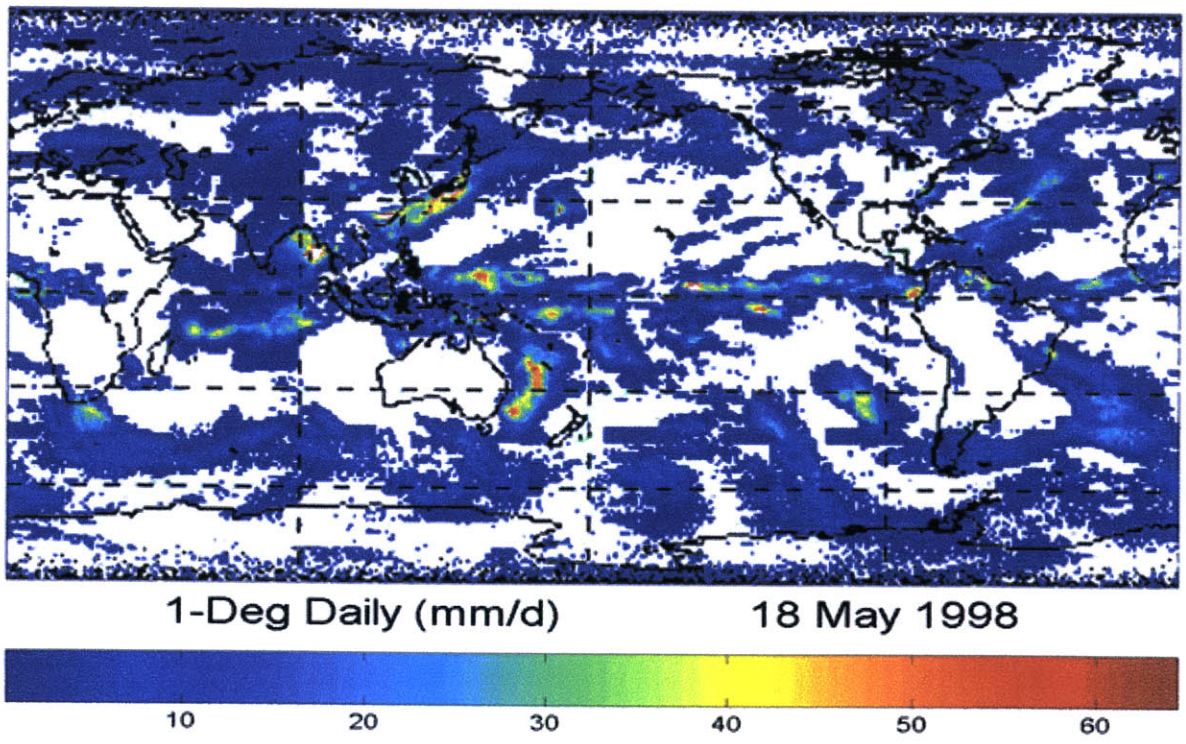

Figure 3-10: NASA Transient/Rainfall Spatial Comparison

precipitation in the NOAA and NASA data sets for May 18, 1998. It should be noted that, in both figures, oceanic transients tend to be negative-stroke events while land-based transients tend to be positive-stroke events. Nevertheless, transient events of both polarity, spatially agree with the two precipitation maps. It should also be noted that the small 'ringed' area immediately southwest of Australia in Figure 3-10, corresponds to the antipode of our recording site in Rhode Island. In this region, transient events are not processed. Please refer to Appendices B and C for maps of other days between 5/7/98 – 6/20/98.

3.5 Global Wave Discussion

Whether the 5-6 day periodicity described above are local or global in nature is an interesting question. With respect to Africa, this wave could simply be an 'easterly' wave similar to the one described by Reed et al. (1977). However, there is much more evidence suggesting that the periodicity shown above is actually the result of a planetary wave which propagates around the world from east to west at much higher speeds (Madden and Julian, 1972).

Arguments against an 'easterly' wave, begin with the fact that they are seasonal in nature and are not very common during the chosen interval. In Figure 3-11, a complete time series summarizing African rainfall throughout an entire year has been constructed in order to demonstrate that this 5-day periodicity is not season-dependant and is therefore not an 'easterly' wave. Also, since the African transient count is integrated over the entire African region, maximum contributions to this integral will come from the central part of Africa and will cause any contributions from an 'easterly' propagating wave to be negligible.

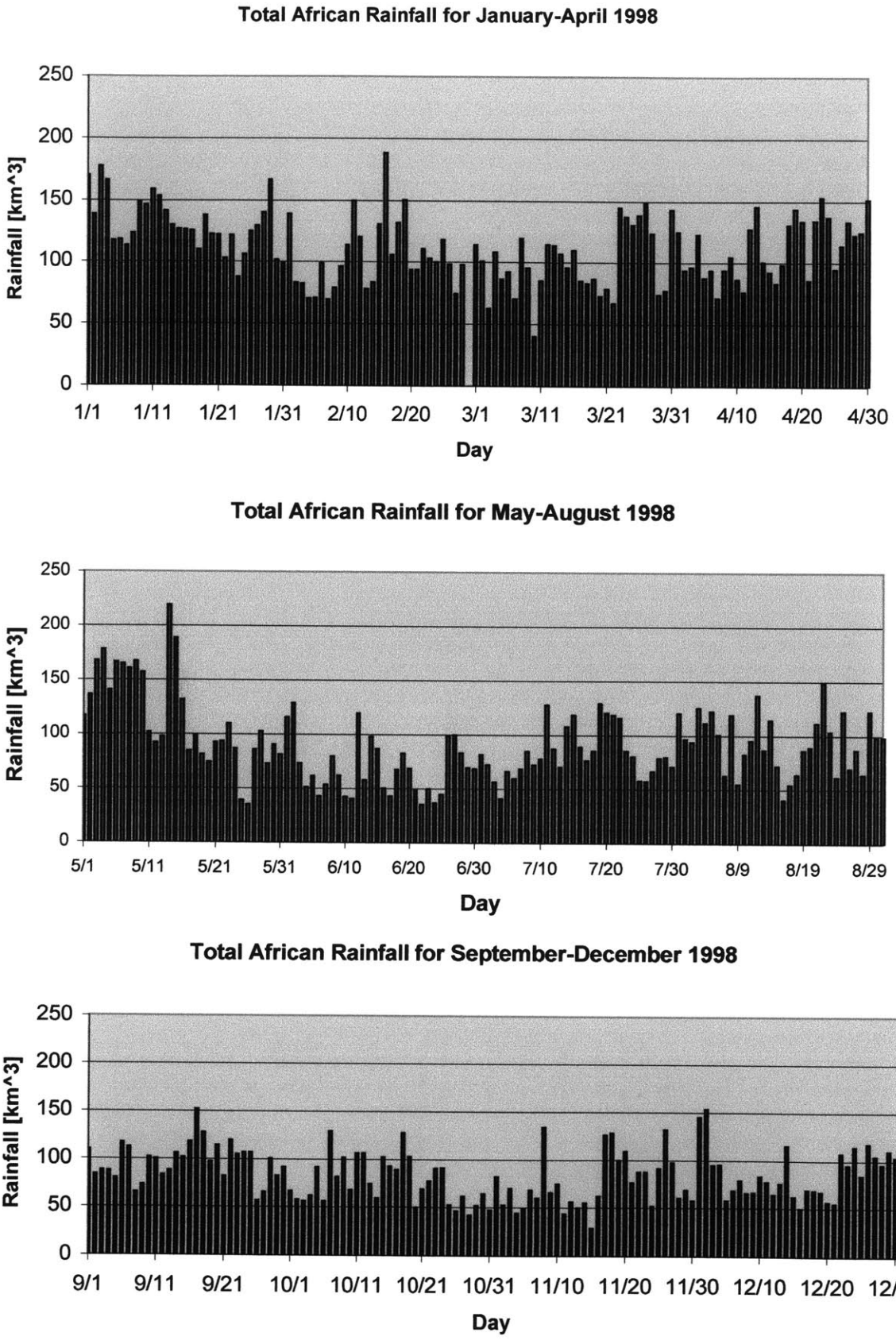

Figure 3-11: NOAA African Annual Rainfall Estimate for 1998

Spectral analyses of transient activity are made for each region during the 5/7/98 – 6/20/98 interval. These analyses are conducted by taking the FFT of the transient count time series for each region (each time series is sampled at a nyquist rate of 1/2T Days^{-1}, where T = 44 Days, representing the 44 days within this interval). The resultant frequency spectra are shown in Figure 3-12, revealing an approximate 4-6 day periodicity in Africa and the Maritime Continent (no clear periodicity in South America).

Since this 5-day wave is apparently absent in South America during this analysis (see Figure 3-12), the case for a planetary wave is weakened. Previous studies by Harth et al. (1982) however have shown the existence of a weak 5-day signal in South America. From this study, it is suggested that the South American 5-day signal is most apparent during the months of October, November, and December when tropical South America is most conditionally unstable. Continuous SR data from Rhode Island were unavailable for these months in 1998 and 1997, but were available for 1996. Figure 3-13, illustrates a South American time series for this period and its corresponding frequency spectrum which does indeed posses a strong component near 5 days, thereby supporting the global wave contention.

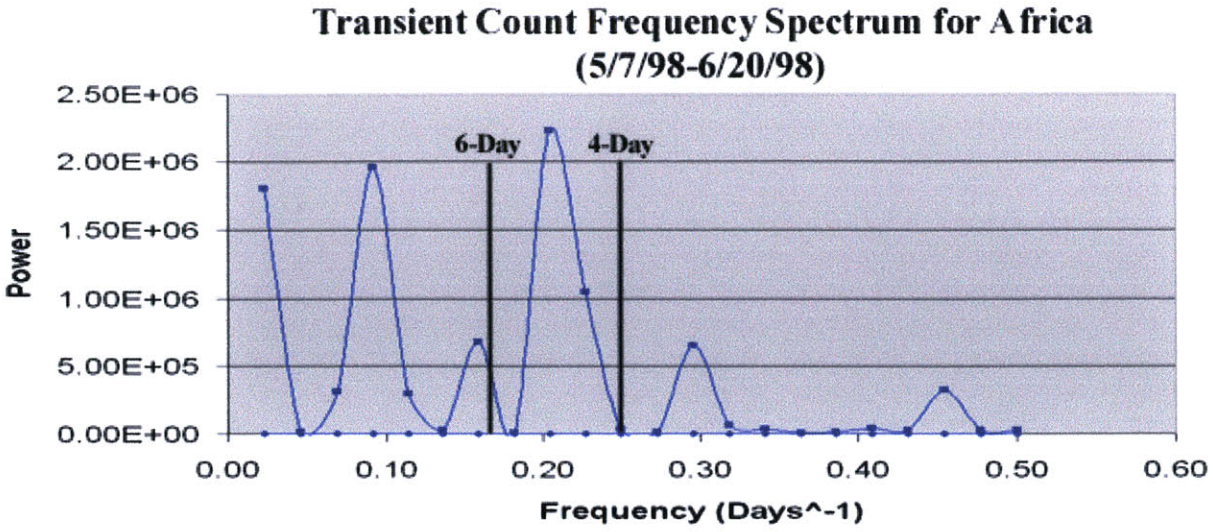

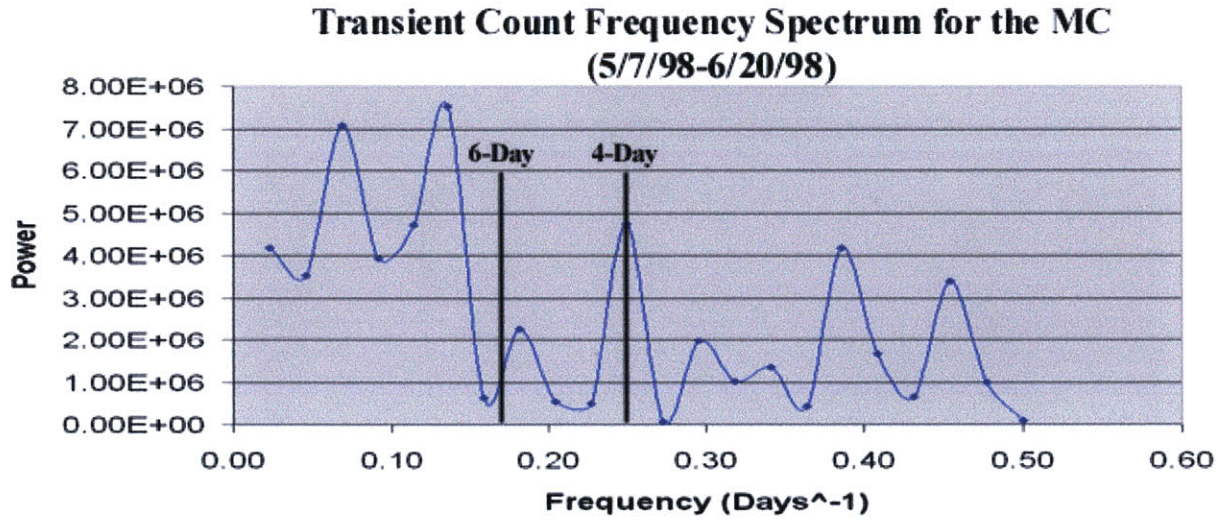

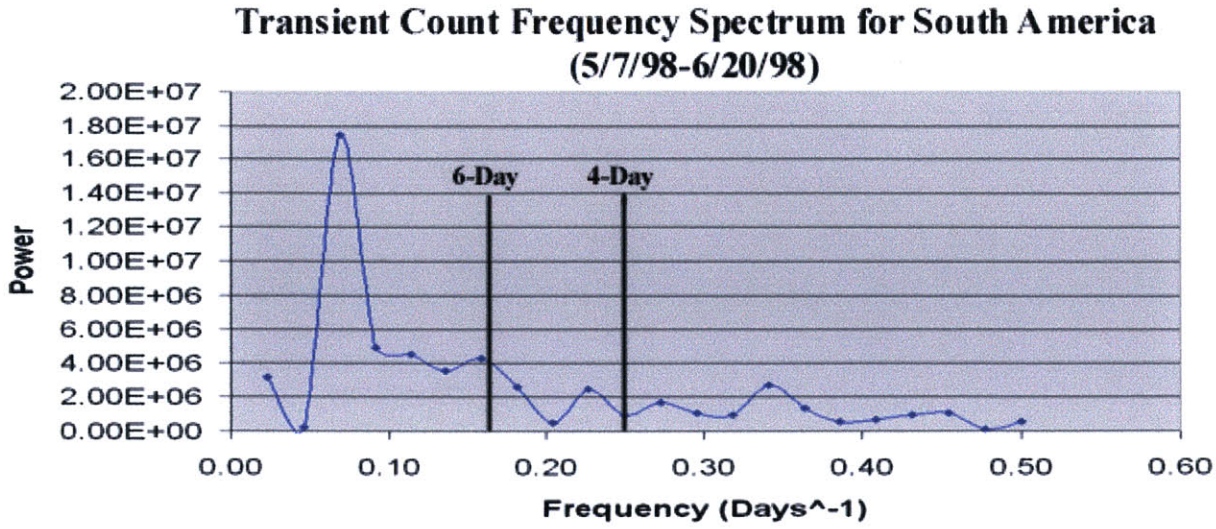

Figure 3-12: Frequency Spectra of Regional Transient Count

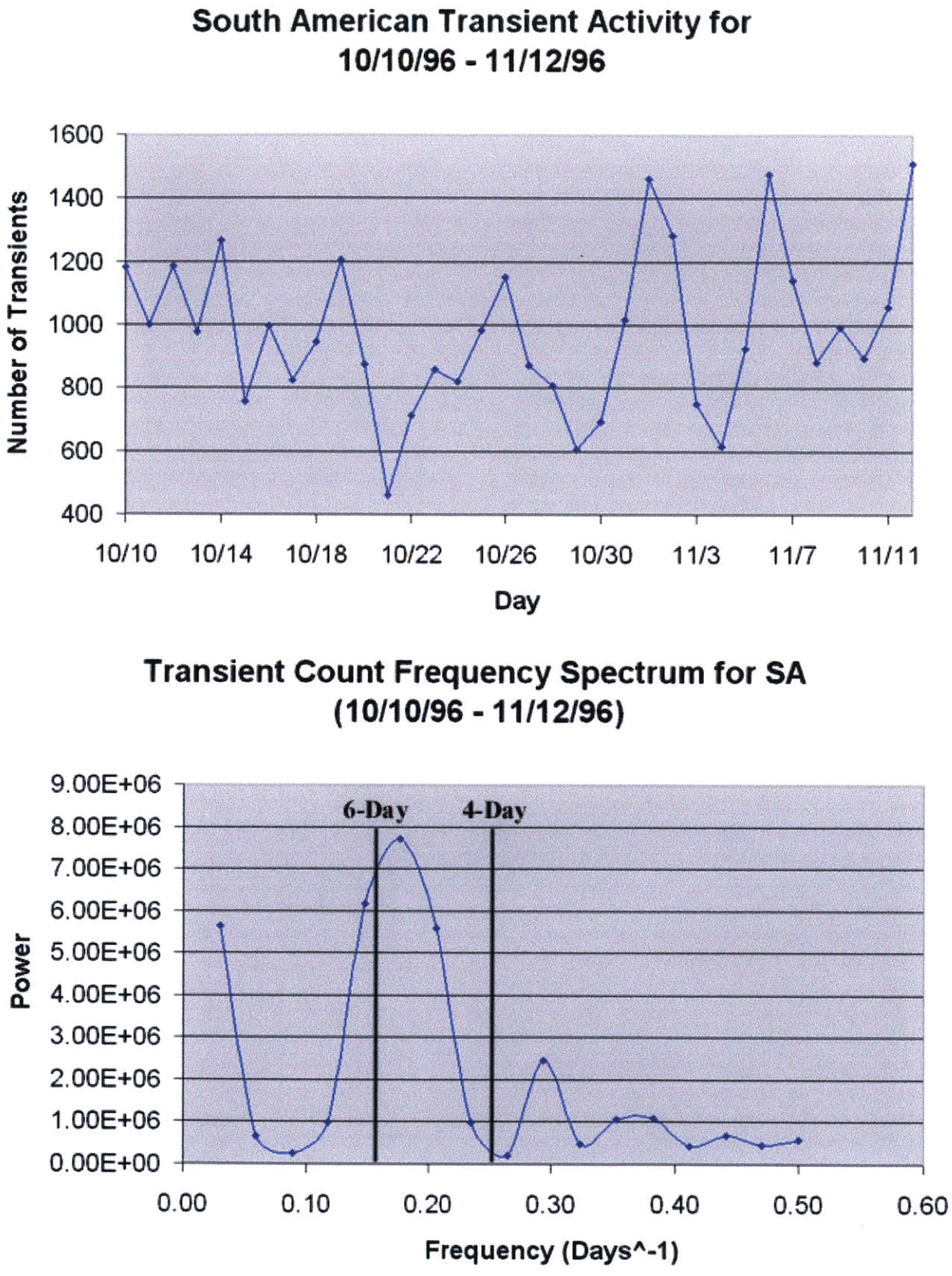

Figure 3-13: Time Series of Transients for South America and Associated Frequency Spectrum for 10/10/96-11/12/96

Chapter 4

Sprites and the Behavior of Vertical Charge Moments

The vertical charge moment QdS of the lightning transients discussed in previous chapters has recently become an important quantity associated with mesosphere optical phenomenon known as sprites. Moreover, studies have shown that the magnitude of a vertical charge moment can be useful in predicting the occurrence of this phenomenon (Huang et al., 1999). By determining its location and measured fields, via SR methods, the vertical charge moment of a lightning transient event is calculated. SR methods are also utilized to determine the polarity of individual transients according to the initial excursion of their respective electric field. Figure 4-1 illustrates the distribution of charge moments for thousands of positive and negative transients for both Africa and South America. The distribution summarized in Figure 4-1 shows a dominance of negative flashes for $QdS < 400$ C-km and a dominance of positive flashes for $QdS > 400$ C-km. In the latter interval, positives outnumber negatives by about 5 to 1. For comparison, the charge moment in the troposphere needed for conventional dielectric breakdown at 75 km altitude is 750 C-km. These results when taken together are qualitatively consistent with earlier work on charge moments with more conventional electrostatic methods and with the association of sprites with positive ground flashes. Quantitatively, however, too few 'negative' sprites have been observed (this issue is discussed further in section 4.1.3).

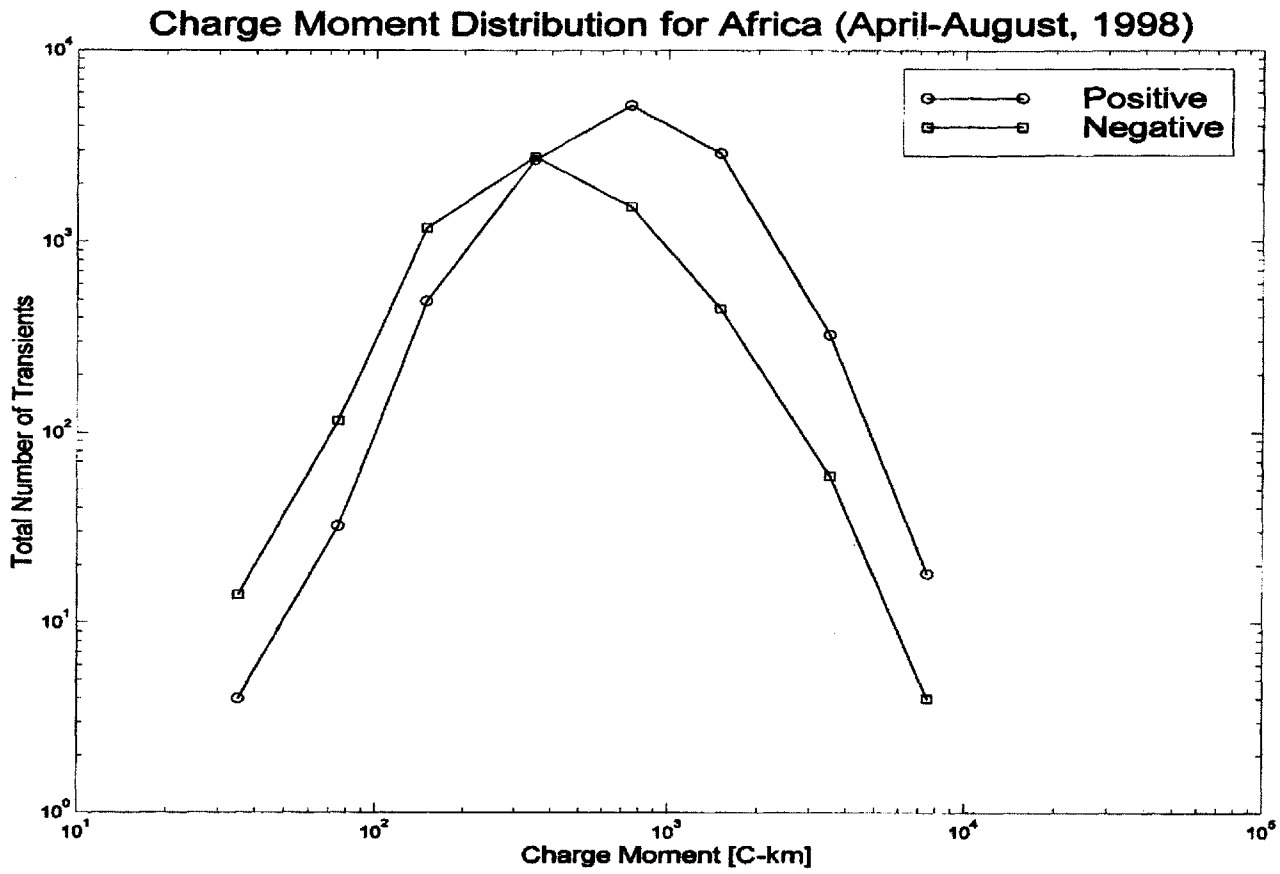

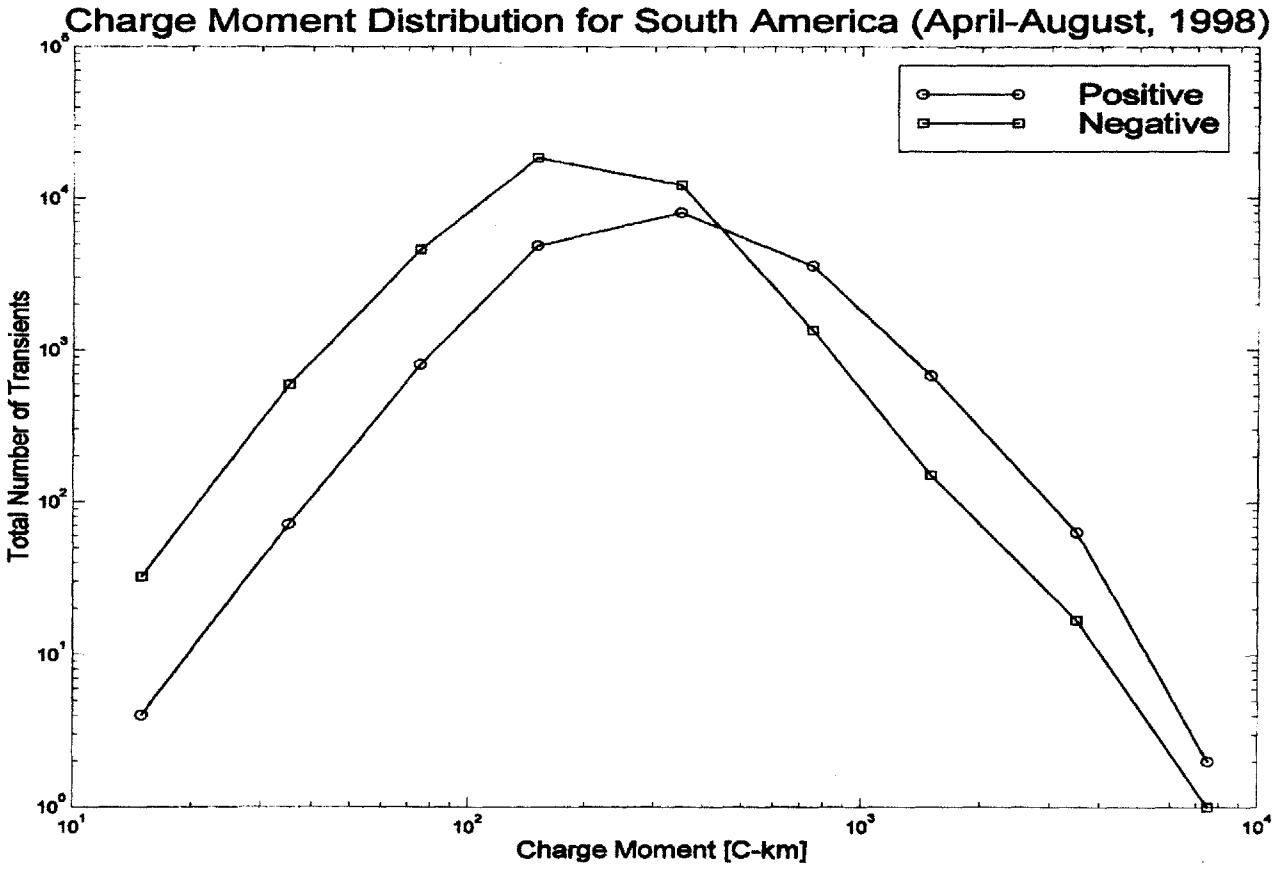

Figure 4-1: Log/Log Plots of Vertical Charge Moment in Africa and South America

4.1 Sprites

4.1.1 Description of Sprite

The upper atmospheric optical phenomenon known as sprites has recently become a heavily studied topic (Huang et al., 1999, Lyons, 1994, Lyons, 1996, Sentman et al., 1995). They are a relatively rare phenomenon and are associated with cloud-to-ground lightning strokes in thunderstorms. Sprites appear directly above an active thunderstorm system and spatially vary in structure. They can appear as small single or multiple vertically elongated spots, to spots with faint extrusions above and below, to bright groupings which extend from the cloud tops to altitudes up to about 95 km. Sprites are predominantly red, with their brightest region in the altitude range of 65-75 km. Above the bright red region there often appears a faint red glow that extends to about 90 km. The bottom portion of a sprite is usually blue and often exhibits a tendril-like filamentary structure that can extend downward as low as 40 km. Sprites are more likely to occur in clusters with some of the very large events seeming to be tightly packed clusters of many individual sprites. Other events are more loosely packed and may extend across horizontal distances of 50 km or more and occupy atmospheric volumes in excess of 10,000 cubic km.

4.1.2 Possible Causes

Although the actual physical processes involved in forming sprites/elves are not yet fully understood, two theories have been proposed. First, because the exponential variation of ambient

electrical conductivity with altitude is controlled primarily by both ultraviolet and cosmic radiation external to the Earth's atmosphere, we expect most of the change occurring in the Earth-Ionosphere cavity to be caused by meteorological processes in the troposphere. In their article, "Heating, Ionization and Upward Discharges in the Mesosphere Due to Intense Quasi-Electrostatic Thundercloud Fields", Victor Pasko et al. suggest that temporary high altitude QE fields, created by large lightning discharges, significantly heat mesospheric electrons causing them to produce optical emissions with characteristics analogous to sprites (Pasko et al., 1995). Furthermore, they argue that, because the conductive upper atmosphere tries to eliminate electric fields imposed from below, "The important physical consequences of the QE system depends on the magnitude and altitude of the removed charge and is essentially independent of the initial charge configuration." Studies in this thesis will thus be more focused on the moment change due to lightning rather than on the charge moment that may have been exhibited by the thunderstorm prior to the lightning.

Another theory which attempts to explain the sprite/elve mystery argues that these same QE fields may cause "runaway electrons" to be driven upward creating a breakdown in the atmosphere as suggested by Tareneko and Rousel-Dupre in their article, "High Altitude Discharges and Gamma-Ray Flashes: a Manifestation of Runaway Air Breakdown." (Tareneko and Rousel-Dupre, 1996) In 1997, Huang found that sprite-producing events have a higher mean charge moment (900 C-km) than elve-producing events (550 C-km) and that, on average, positive transient events have substantially higher charge moments (750 C-km) than negative transient events (350 C-km). Huang also found an apparent charge moment threshold of approximately 500 C-km, below which sprites are unlikely to form and where most elve and negative events fall. The findings are consistent with the theory that large positive ground flashes (CG's) make sprites/elves as stated by Boccippio et al. (1995).

4.1.3 'Negative' Sprites

The fact that sprite observations have rarely been confirmed to be associated with negative-stroke lightning events has led to the widespread belief that they are primarily a positive lightning-induced phenomenon. Given the plausibility that conventional dielectric breakdown is responsible for sprites, results in this thesis provide preliminary evidence that negative lightning events can in fact trigger sprites and, in particular, that these events are more likely oceanic than continental.

If 'negative' sprites do indeed exist, why are there so few reports of their occurrence? One possible explanation is that the likelihood of actually observing a 'negative' sprite is minimal. Figures 4-2 and 4-3 provide partial evidence for this assertion by respectively comparing the diurnal distributions of positive and negative transient events with vertical charge moments sufficiently large to produce sprites (charge moments > 300 C-km, as described in Huang et al., 1999) and the diurnal mean vertical charge moments for positive and negative events. As we can see from Figure 4-2, peak positive transient activity occurs during the local evening (approximately 20:00 local time) as opposed to the bimodal peaks of the negative transients that occur in the local morning and late afternoon (approximately 5:00 and 15:00 local time). The fact that negative transient activity peaks at these particular local times, suggests that negative transients with sprite-producing potential are more likely to occur at times when it is not sufficiently dark to detect sprites. Also, Figure 4-3 shows that the mean vertical charge moment for negative transient events peaks in the afternoon (approximately 12:00 local time) as opposed to the evening peak (approximately 20:00 local time) for positive transients where the mean charge moment for positive transients is almost two times the mean charge moment for negative transients. Therefore, not only is a positive transient more likely to occur at night than a negative transient, but the size of such

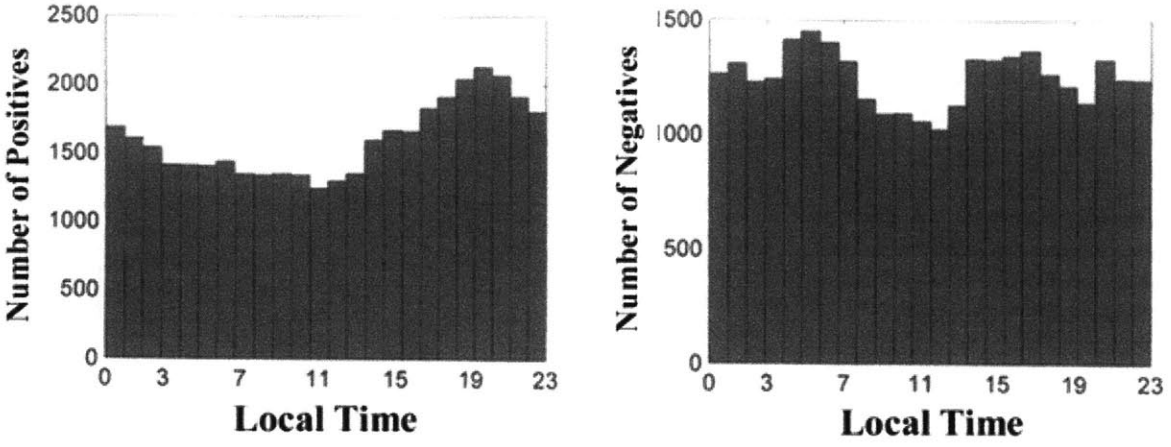

Figure 4-2: Diurnal Distribution of Positive and Negative Events with Charge Moments > 300 C-km

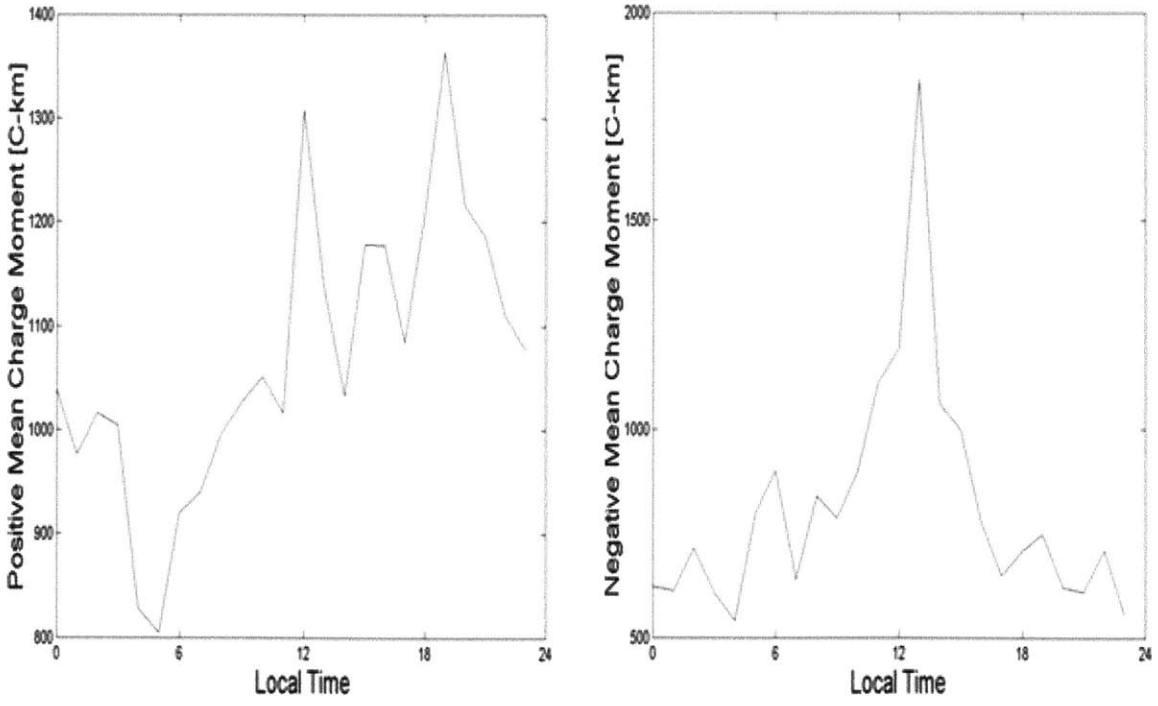

Figure 4-3: Diurnal Variation in Mean Charge Moment for Positive and Negative Transients

positive event is more likely to be significantly larger than a negative event occurring at the same time.

The local morning peak associated with negative transient activity in Figure 4-2 is consistent with previous studies on morning oceanic convection (Gray and Jacobson, 1977). Indeed, another plausible explanation for the minimal number of sprites associated with negative-stroke lightning events stems from recent reports confirming 'negative' sprites over water (Barrington-Leigh et al., 2000). It should also be noted that, although the large MCS's theorized to be necessary for sprite production are common over land, they also develop over the water (Mohr and Zipser, 1996). A schematic drawing, illustrating the structural difference between MCS's and ordinary thunderclouds is included in Figure 4-4. In Figure 4-5, we can see that the spatial distribution of large negative transients is relatively more prevalent over the ocean in comparison to the land-based distribution of positive transients. Since observational networks for sprites over the ocean are extremely limited, it is possible that many negative lightning-induced sprites are undetected.

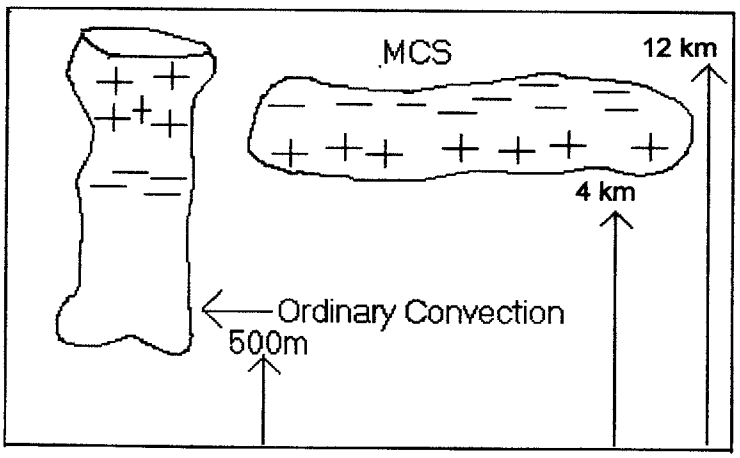

Figure 4-4: Typical Convection for Positive and Negative Lightning

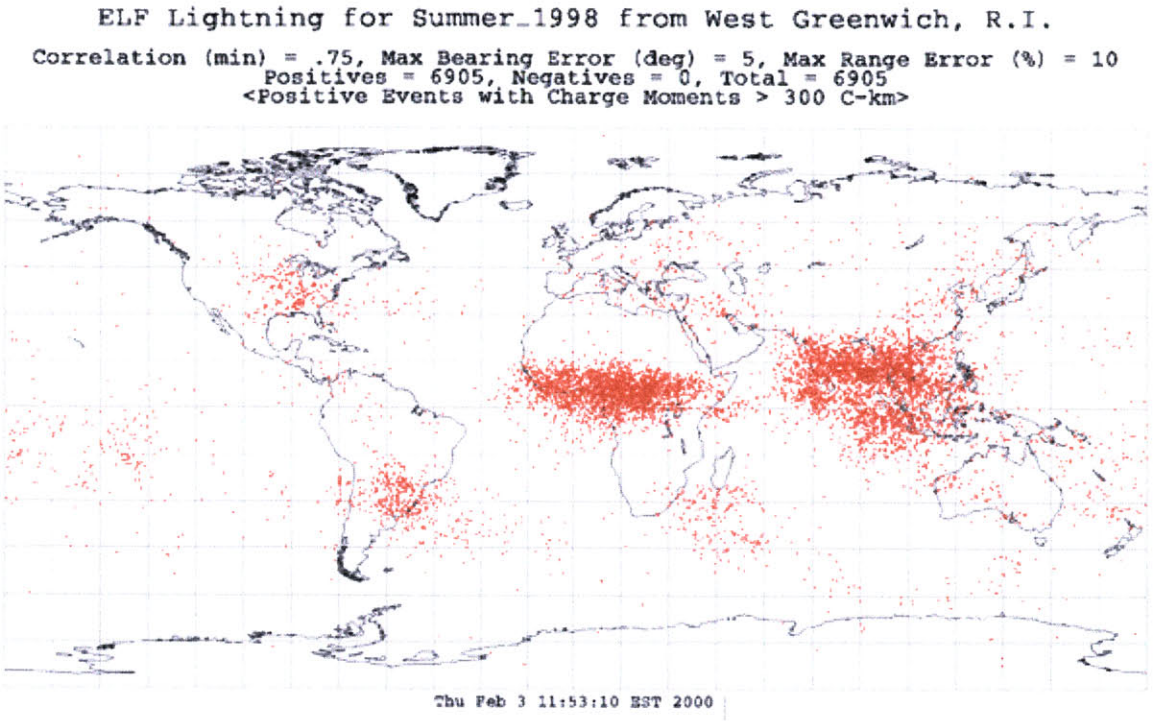

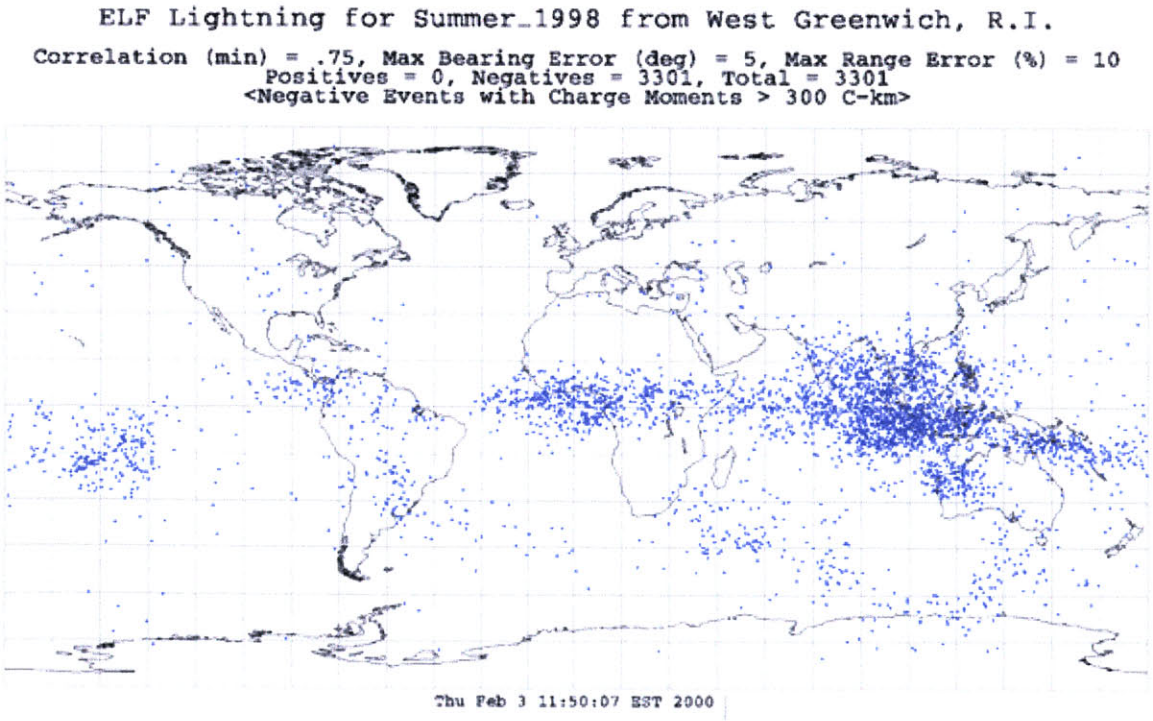

Figure 4-5: Global Distribution of Positive and Negative Events

4.2 Methods for Calculating Charge Moment

4.2.1 Integrative Method

Through integration techniques, the vertical charge moment of a particular lightning event can be determined. This is accomplished by first taking the Fourier transform of the current moment frequency spectrum, thus yielding its time series. The current moment time series is then integrated in order to estimate the amount of charge transferred. This method becomes problematic though because it assumes a constant vertical charge height, leaving no variability with respect to convection. Also, the accuracy of this method is dependent on being able to integrate over a complete bandwidth. The limited bandwidth of the Rhode Island site (120 Hz) therefore, causes much of the actual current waveform information to be lost. An obvious solution would be to simply increase the bandwidth. This would however introduce problems of over-sampling in the system and cause more harmonics from near by power lines to become detected.

4.2.2 Impulsive Estimation Method

Another method to calculate the charge moment is to assume an exponential current and directly use the normal mode equations. In the time domain, the current is then defined as

$$I(t)ds = I_o ds e^{\frac{-t}{\tau}}$$

Transforming to the frequency domain

$$I(f)ds = \frac{I_o ds}{j2\pi f + \frac{1}{\tau}}$$

As the time constant τ approaches zero, the time waveform of the current becomes more impulsive while the frequency spectrum becomes nearly flat. Due to the fact that the time scales of Schumann resonances (i.e. the time for light to propagate around the world) are long compared to most lightning processes, we can replace the *I(f)ds* term in the normal mode equations with *Qds* where Q is simply the total amount of charge transferred by the lightning (Huang et al., 1999).

This impulsive estimate for the amount of charge transferred is more flexible than the integration method because it is independent of bandwidth. Furthermore, it is not necessary to assume an exponential current waveform. Any type of waveform that will cause the function to converge to a delta function as τ approaches zero may be used. This method has yielded results comparable to measurements made by researchers at Stanford University using a different method (Huang, 1997), and this is the method adopted for the computations presented in this thesis.

Chapter 5

Further Work

5.1 Source Strength Calculation

Future Schumann resonance work attempting to study how lightning transient activity in a particular tropical zone is associated with its corresponding electromagnetic ambient, might consider relating the region's intrinsic source strength $\frac{(Qds)^2}{time}$ (charge moment squared per unit time) to transient activity instead of simply its background intensity. Such calculation would be a more accurate assessment of this relationship because regional source strength variation is more closely related to regional mass flux following the results on regional precipitation totals in Chapter 3. Source strength approximations can be made directly from recorded background and transient data, using the normal mode equations (Heckman et al., 1998). First, using transient data, the great circle distance θ of a particular event can be found. Since information about the background magnetic intensity for that region is already recorded, both this and θ can be inserted into the normal mode equations in order to solve for source strength. It should be noted that the calculated pairs of background magnetic intensities are actually $H^2_{ew}(f)/H^2_{ns}(f)$ which require a slight modification of the normal mode equations. Specifically, this modification defines the recorded magnetic background intensity as

$$H^2{}_{xy}(f) = (-\frac{I(f)dsP^1_{\nu(f)}(-\cos\theta)}{4ah\sin(\pi\nu(f))})^2 \frac{[amperes^2]}{[meter^2][Hz]}$$

where $H^2{}_{xy}(f)$ represents either the East-West or North-South component of the magnetic background intensity. Calculations of source strength using the equation above is simplified by assuming that *I(f)* is constant, translating to a delta function in the time domain (similar to the assumption made in the impulsive estimate method for particular transients). Since the vast majority of lightning flashes are indeed characterized as having the white noise spectra described above, this assumption is more likely valid for ordinary lightning than for positive transients that almost always sustain long continuous currents.

Ultimately, the calculated source strengths can be used to create universal graphs plotting great circle distance θ versus all ratios of source strength and background intensity for several different Schumann resonance modes. Figure 5-1 shows plots of these calculations for the first four SR modes (Plots provided courtesy of Dr.Vadim Mushtak)

It should be noted that the curves on these plots are calculated for different spatial sizes of a particular region, in order to demonstrate how the distance dependence of an ELF electromagnetic field depends on the spatial size of the source. Therefore, any estimation of the moment change squared per unit time on the basis of measured fields also depends on what supposed spatial size has the most active (at the period of the measurement) global thunderstorm region.

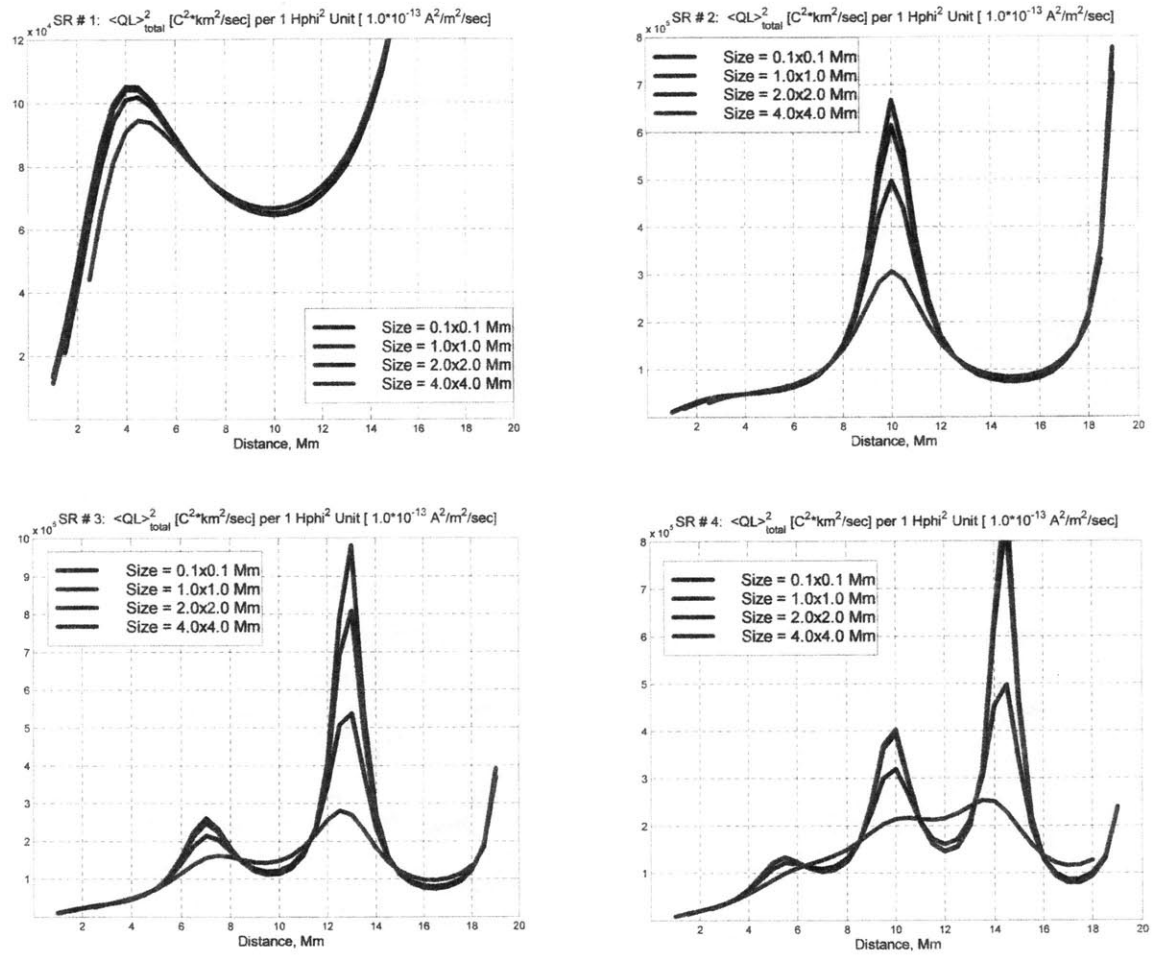

Figure 5-1: Source Strength Conversion Plots for Modes 1-4

Chapter 6

Conclusions

This thesis is concerned with using Schumann resonances to analyze the relationship between ordinary global lightning activity—background Schumann resonances—and larger mesoscale discharges—transient Schumann resonances—that excite the Earth-ionosphere cavity to levels higher than the integration of all other lightning. Regional analysis was conducted for each of the three major areas for tropical thunderstorm activity: Africa, South America, and the Maritime Continent. Analyses conducted in this thesis reveal a rough proportionality between peak background intensity and total number of transients on a regional basis. Furthermore, this thesis shows that local afternoon lightning activity systematically precedes the period of predominant transient activity. These findings provide preliminary evidence that regional afternoon lightning activity—caused by scattered convection—evolve into larger MCS's later in the diurnal cycle providing sufficiently large charge reservoirs necessary to create large transient events.

Simultaneous comparisons of regional precipitation estimates, provided by two independent data sets, with SR data have shown strong evidence for a potential relationship between these two quantities. In particular, daily maps highlighting both global transient and global precipitation activity have revealed a strong spatial relationship. With the exception of Africa though, quantitative comparisons of regional transient activity with corresponding regional precipitation have shown little correlation. There is a strong possibility however that this lack of

correlation is partially caused by inaccuracies of quantifying continental-scale precipitation via satellite. The fact that African precipitation estimates that included data from surface observations yielded slightly higher correlation suggests that this might be true. Another possible explanation is that the geographic location of the Rhode Island site is unfavorable for quantifying transient events in both South America and the Maritime Continent; a phenomenon that is not fully understood. Nevertheless, it is noteworthy that the most 'continental' of the three major tropical 'chimney' regions shows the best correlation between lightning and rainfall.

The strong spatial relationship between transient activity and precipitation suggest the possibility of using SR methods as indicators of latent heat production and regional mass flux on a continental scale. The discovery of a 5-day planetary wave is the strongest evidence toward this goal. Physically, it is possible that these planetary waves are strongly modulating mesoscale activity on a 5-day time cycle. When the isolated convection over Africa, for example, is able to evolve into larger area mesoscale activity, the total latent heat release and mass flux over the continent is substantially enhanced.

Research conducted for this thesis has also provided evidence for sprites being triggered by negative-stroke lightning events. Vertical charge moment distribution plots have shown that, although negative-stroke lightning events with charge moments sufficiently large to produce sprites are less common than positives-stroke lightning events, they do in fact exist. Global transient maps produced for this thesis have shown that the majority of negative transient events occur over the ocean, which partially explains why so few observable sprite events have been associated with negative-stroke lightning. Recent reports of 'negative' sprite events over the ocean provide preliminary evidence for this claim (Barrington-Leigh et al., 2000).

References

Arkin, P. and E. Ardanuy, Estimating climatic-scale precipitation from space: A review, Journal of Climate, 2, 1229-1238, 1989.

Balser, M. and C.A. Wagner, Observations of earth-ionosphere cavity resonances, Nature (London), 188, 638, 1960.

Balser, M. and C.A. Wagner, Diurnal power variations in the Earth-ionosphere cavity modes and their relationship to world-wide thunderstorm activity, J. Geophys. Res., 67, 619, 1962.

Barrington_leigh, C.P., U.S. Inan, M. Stanley, and S.A. Cummer, Sprites triggered by negative lightning discharges, Geophs. Res. Lett., 26, 3605-3608, 1999.

Bliokh, P. V., A. P. Nickolaenko, and Y. V. Filippov, Schumann Resonances in the Earth-Ionosphere Cavity, Peter Perigrinus, London, 1980

Boccippio, D., E. Williams, S. Heckman, W. Lyons, I. Baker, and R. Boldi, Sprites, ELF transients, and positive ground strokes, Science, 269, 1088-1091, 1995.

Boccippio, D., C. Wong, E. Williams, R. Boldi, H. Christian and S. Goodman, Global validation of single-station Schumann resonance lightning location, J. Atmos. Sol. Terr. Phys., 60, 701-712, 1998.

Burpee, R.W., Some features of global-scale 4-5 day waves, J. Atmos. Sci., 33, 2292-2299, 1976.

Chapman, F.W. and D.L. Jones, Earth-ionosphere cavity resonances and the propagation of extremely low frequency radio waves, Nature (London), 202, 654, 1964.

Clayton, M.D. and C. Polk, Diurnal Variation and Absolute Intensity of World-Wide Lightning Activity, September 1970 to May1971, in Proc. conf. Electrical Processes in atmospheres, Garmisch-Partenkirchen, Germany, 1974.

Fellman, E., Analysis of Schumann resonances recorded simultaneously at two widely separated stations, Doctoral Thesis, Universitat des Saarlands, 1973.

Finger, F., J. Laver, K. Bergman, and V. Paterson, The Climate Analysis Center's User Information Service, Bulletin American Meteorological Society, 66, 413-420, 1985.

Gray, W. and R. Jacobson, Diurnal variation of deep cumulonimbus convection, Mon. Wea. Rev., 105, 1171-1188, 1977.

Harth, W., P. Steffen, C. Hofmann, and H. Falcos, The day-to-day variation of atmospheric activity over the South American continent, J. Atmos. Terr. Phys., 123-129, 1982.

Heckman, S., E. Williams, and R. Boldi, Total global lightning inferred from Schumann resonance measurements, J. Geophys. Res., 1998

Herman, A., V. Kumar, P. Arkin, and J. Kousky, Objectively determined 10-day African rainfall estimates created for famine early warning systems, Int. J. Remote Sensing, 18, 2147-2159, 1997.

Huang, E., Electromagnetic Transients, Elves, and Sprites in the Earth-Ionosphere Waveguide, Masters Thesis, Department of Electrical Engineering and Computer Science, Massachusetts Institute of Technology, Cambridge, MA, 1997.

Huang, E., E. Williams, R. Boldi, S. Heckman, W. Lyons, M. Taylor, T. Nelson, and C. Wong, Criteria for sprites and elves based on Schumann resonance observations, J. Geophys. Res., 104, 16943-16964, 1999.

Huffman, G.J., R.F. Adler, M.M. Morrissey, S. Curtis, B. McGavock, J.J. Janowiak, and J. Susskind, Global precipitation at one-degree daily resolution, J. Appl. Meteor., Submitted, 2000

Ishaq, M. and D.L. Jones, Method of obtaining radiowave propagation parameters for the Earth-ionosphere duct at ELF, Electronic Letters, Vol 13, No. 9, p. 253-254, 1977.

Jones, D.L., Schumann resonances and ELF propagation for inhomogeneous isotropic profiles, J. Atmos. Terr. Phys., 29, 1037, 1967.

Jones, D.L. and D.T. Kemp, Experimental and theoretical observations of Schumann resonances, J. Atmos. Terr. Phys., 32, 1095, 1970.

Jones, D.L. and D.T. Kemp, The nature and average magnitude of the sources of transient excitation of the Schumann resonances, J. Atmos. Terr. Phys., 33, 557, 1971.

Kummerow, C., W.S. Olsen, and L. Giglio, A simplified scheme for obtaining precipitation and vertical hydrometeor profiles from passive microwave sensors, IEEE Trans. Geosci. Remote Sens., 34, 1213-1232, 1996

Lazebnyy, B.B and A.P. Nickolaenko, Daily variations of the number of VLF bursts according to synchronous observations at Kharkov and Ulan-Ude, Geomag. Aeron., 15, 218-219, 1976.

Lyons, W., Characteristics of luminous structures in the stratosphere above thunderstorms as images by low-light video, Geophs. Res. Lett., 21, 875, 1994.

Lyons, W., Sprite observations above the U.S. High Plains in relation to their parent thunderstorm systems, J. Geophys. Res., 101, 29, 652, 1996.

Lyons, W., M. Uliasz, and T. Nelson, A climatology of large peak current cloud-to-ground lightning flashes in the contiguous United States, Mon. Weather Rev., 126, 2217-2233, 1998.

Madden, R., Observations of large scale traveling rossby waves, Rev Geophys. Space Phys., 17, 1935-1949, 1979.

Madden, R. and P. Julian, Further evidence of Global-Scale, 5-Day Pressure Waves, J. Atmos. Sci., 29, 1464-1469, 1972.

Madden, T. and J. Stokes, Evidence of global scale 5-day waves in a 73-year pressure record, J. Atmos. Sci., 32, p. 831-836, 1975.

Madden, T. and W. Thompson, Low-frequency electromagnetic oscillations of the Earth-ionosphere cavity, Rev. Geophys., 3, 211, 1965.

Mohr, K. and E.J. Zipser, Mesoscale convective systems defined by their 85 GHz ice scattering signature: size and intensity comparisons over tropical oceans and continents, 124, 2417-2437, 1996.

Nelson, P.H., Ionospheric Perturbations and Schumann Resonance Data, Ph.D. Thesis, Department of Geology and Geophysics Massachusetts Institute of Technology, Cambridge, MA, 1967.

Nickolaenko, A.P. and I.G. Kudiniseva, A modified technique to locate the sources of ELF transient events, J. Atmos. Terr. Phys., 56, 11, 1994.

Ogawa, T., A.C. Fraser-Smith, R. Gendrin, Y. Tanaka, and M. Yasuhara, Worldwide simultaneity of occurrence of a Q-type ELF burst in the Schumann resonance frequency range, J. Geomag. Geoelectr., 19, 377, 1967.

Pasko, V. P., U. S. Inan, Y. N. Taranenko, and T. F. Bell, Heating, ionization, and upward discharges in the mesosphere due to intense quasi-electrostatic thundercloud fields, Geophys. Res. Lett., 22, 365-368, 1995.

Polk, C., Schumann resonances of the earth-ionosphere cavity: extremely low frequency reception at Kingston, R.I., Res. NBS Radio Sci., 66D, 313, 1962.

Price, C., M. Finkelstein, B. Starobinets, and E. Williams, A new Schumann resonance station in the Negev Desert for monitoring global lightning activity, 11th International Conference on Atmospheric Electricity, Huntsville, Alabama, USA, 1999.

Reed, R., D. Norquist, and E. Recker, The structure and properties of African wave disturbances as observed during phase III of GATE, Monthly Weather Review, 105, 317-333, 1977.

Rycroft, M.J., Resonances of the earth-ionosphere cavity observed at Cambridge, England, Radio Sci. J. Res. NBS, 69D, 1071, 1965.

Schumann, W.O., Uber die strahlungslosen eigenschwingungen einer leitenden kugel, die von einer luftschicht und einer ionospharenhull umgeben ist. Z. naturforsch, 7a:149, 1952.

Schumann, W.O., Uber elektrische Eigenschiwingungen des Hohlraumes Erde-Luft-Ionosphare, erregt durch Blitzentladungen, A. Agnew. Phys., 9, 373, 1957.

Sentman, D.D., Magnetic elliptical polarization of Schumann resonances, Radio Sci., 22, 595, 1987.

Sentman, D.D, E. Wescott, D. Osborne, D. Hampton, and M.J. Heavner, Preliminary results from the SPRITES '94 campaign: Red Sprites, Geophs. Res. Lett., 22, 1205-1208, 1995.

Sentman, D.D., M.J. Heavner, D.N. Baker, T.E. Cayton and B. J. Fraser, Effects of solar storms on the Schumann resonances in late 1989, 10th International Conference on Atmospheric Electricity, Osaka, Japan, 696, 1996.

Sentman, D. D., Schumann resonance spectra in a two-scale height earth-ionosphere cavity, J, Geophys. Res., 100, 7097-7103, 1996.

Susskind, J. and J. Pfaendtner, 1989: Impact of interactive physical retrievals on NWP. Report on the Joint ECMWF/EUMETSAT Workshop on the use of Satellite Data in Operational Weather Prediction: 1989-1993, Vol. 1, T. Hollingsworth, Ed., ECMWF, Shinfield Park, Reading RG2 9AV, U.K., 245-270.

Susskind, J., P. Piraino, L. Rokke, L. Iredell, and A. Mehta, Characteristics of the TOVS Pathfinder Path A Dataset. Bull. Amer. Meteor. Soc., 78, 1449-1472, 1997.

Taranenko, Y. and R. Rousell-Dupre, High altitude discharges and gamma ray flashes: a manifestation of runaway air breakdown, Geophys. Res. Lett., 23, 571-574, 1996.

Thomas, A. and V. Patterson, A reliable method for estimating precipitation amounts, Preprints Fifth Symposium on Meteorological Observations and Instrumentation (Toronto, Canada: American Meteorological Society), pp. 554-561, 1983.

Wait, J.R., On the propagation of VLF and ELF radio waves when the ionosphere is not sharply bounded, J. Res. Nat. Bur. Stand., Sect. D., 66, 53, 1962

Wait, J. R., Electromagnetic Waves in Stratified Media, IEEE Press, Piscataway, NJ, 1996.

Wallace, J., Spectral studies of tropospheric wave disturbances in the tropical western pacific, Rev Geophys. Space Phys., 9, 557-603, 1971.

Whipple, F. J., On the association of the diurnal variation of electric potential in fine weather with the distribution of thunderstorms over the globe, Quart. J. Roy. Met. Soc., 55, 1-17, 1929.

Williams, E. R., The positive charge reservoir for sprite-producing lightning, J. Atmos. Terr. Phys., 60, 689-692, 1998

Williams, E.R., D. Castro, R. Boldi, T. Chang, E. Huang, V. Mushtak, W. Lyons, T. Nelson, S. Heckman, and D. Boccippio, The relationship between the background and transient signals in Schumann resonances, 11th International Conference on Atmospheric Electricity, Huntsville, Alabama, USA, 1999.

Wong, C.T., A Global Lightning Transients Detector, Masters Thesis, Department of Electrical Engineering and Computer Science, Massachusetts Institute of Technology, Cambridge, MA, 1996.

Xie, P. and P. Arkin, An intercomparison of gauge observations and satellite estimates of monthly precipitation, J. Appl. Meteor., 34, 1143-1160, 1995.

Appendix A

Background/Transient Plots for Africa and South America (12/13/96 – 12/27/96).

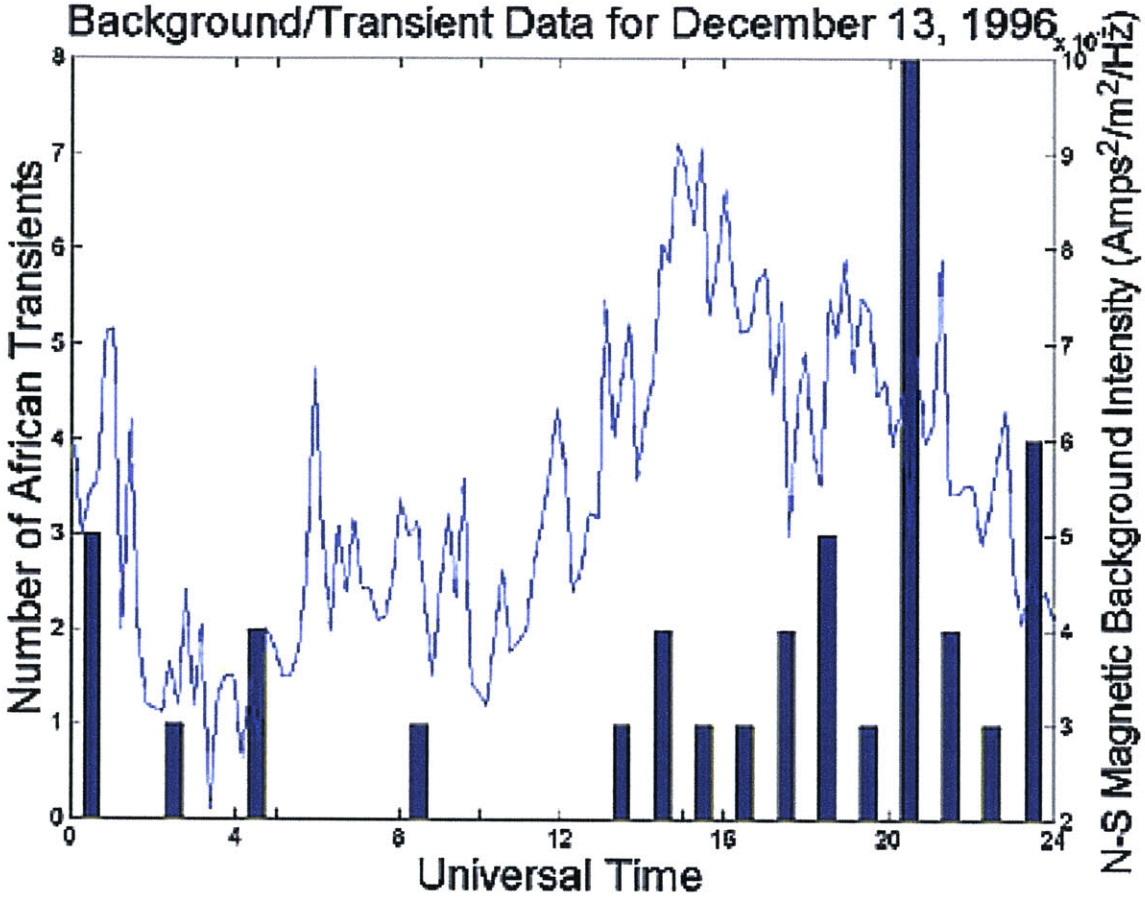
Background/Transient Data for December 13, 1996
Number of African Transients
N-S Magnetic Background Intensity (Amps²/m²/Hz)
Universal Time

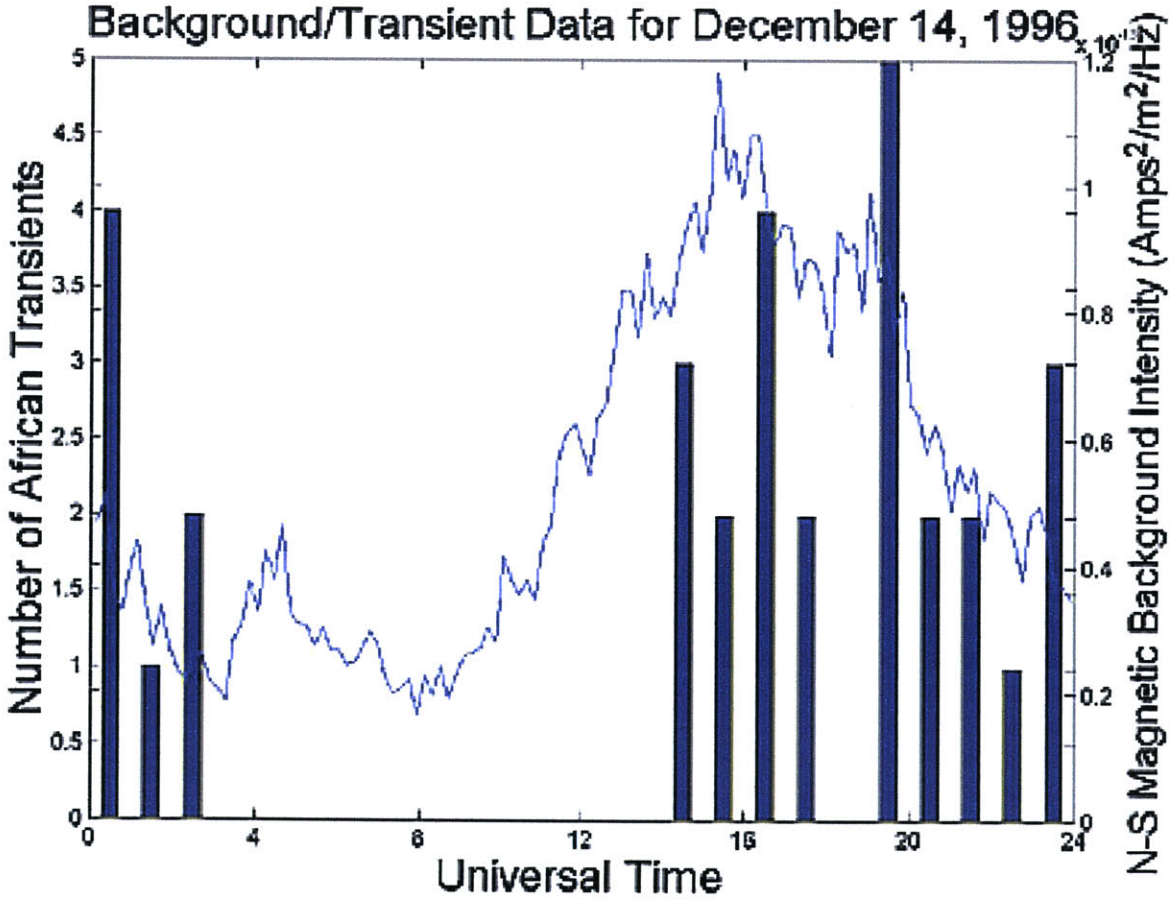
Background/Transient Data for December 14, 1996
Number of African Transients
N-S Magnetic Background Intensity (Amps²/m²/Hz)
Universal Time

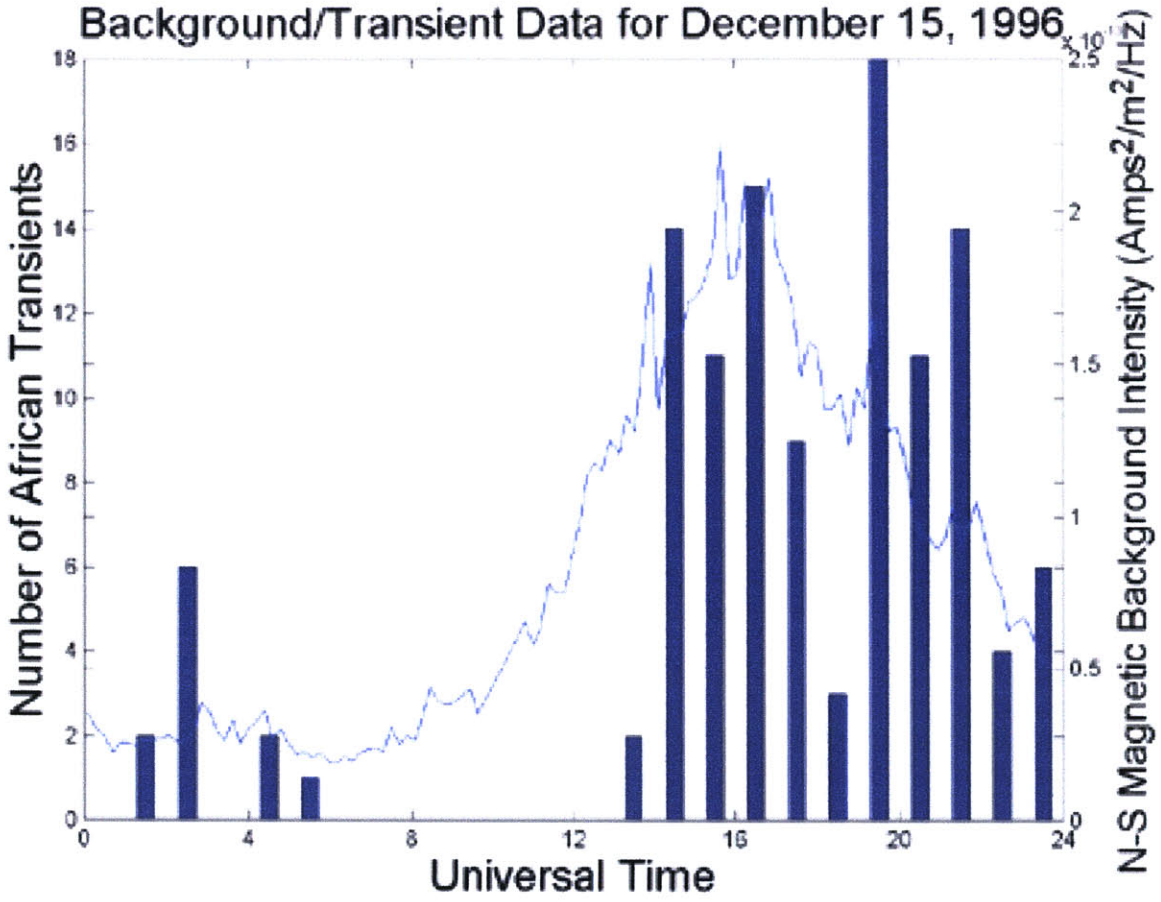
Background/Transient Data for December 15, 1996
Number of African Transients
N-S Magnetic Background Intensity (Amps²/m²/Hz)
Universal Time

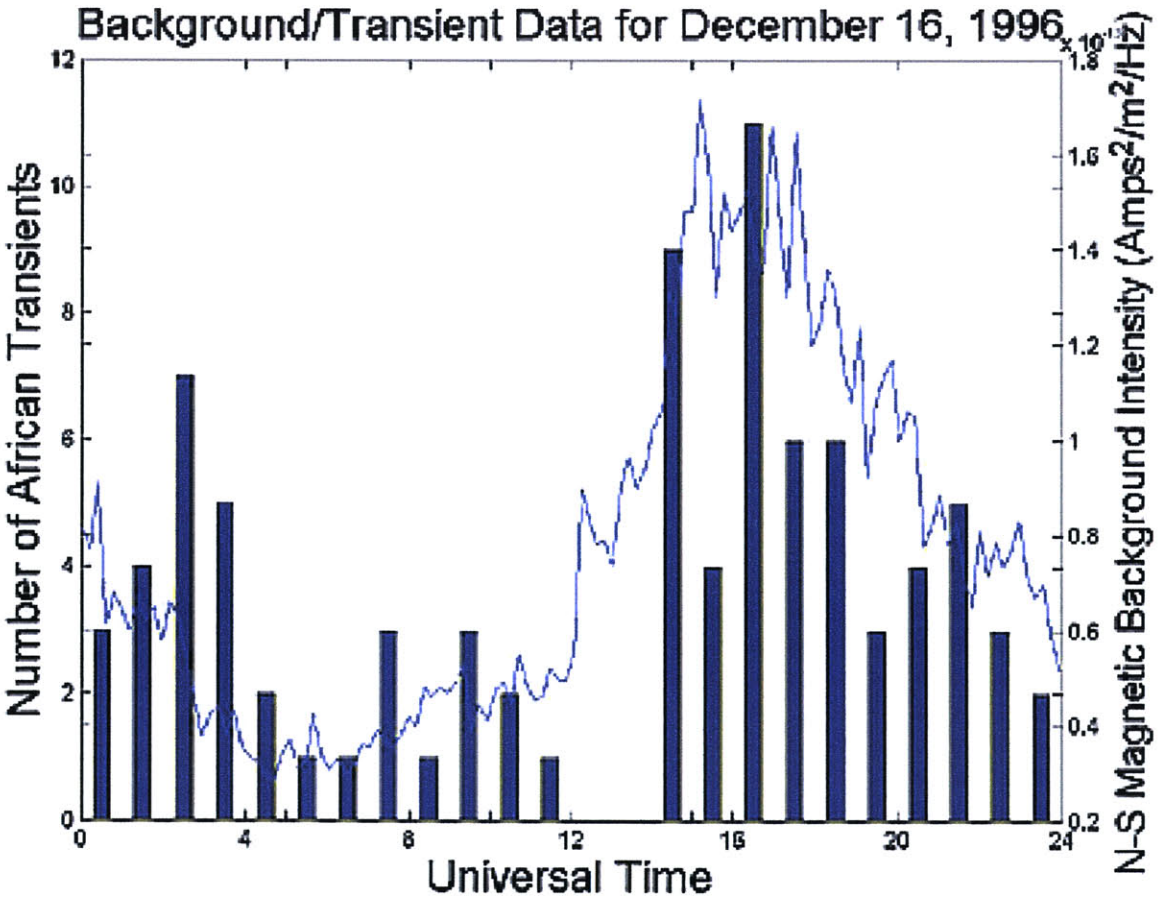
Background/Transient Data for December 16, 1996
Number of African Transients
N-S Magnetic Background Intensity (Amps²/m²/Hz)
Universal Time

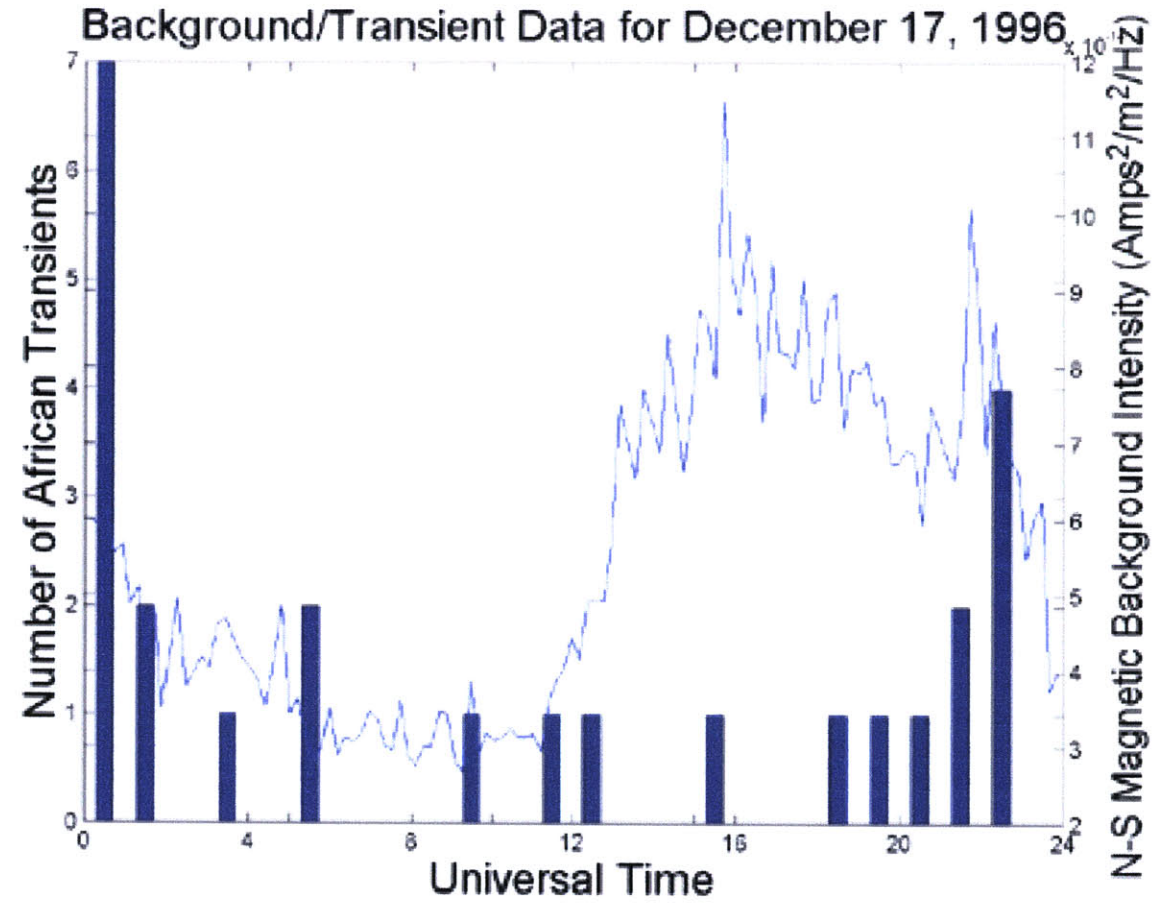
Background/Transient Data for December 17, 1996
Number of African Transients
N-S Magnetic Background Intensity (Amps²/m²/Hz)
Universal Time

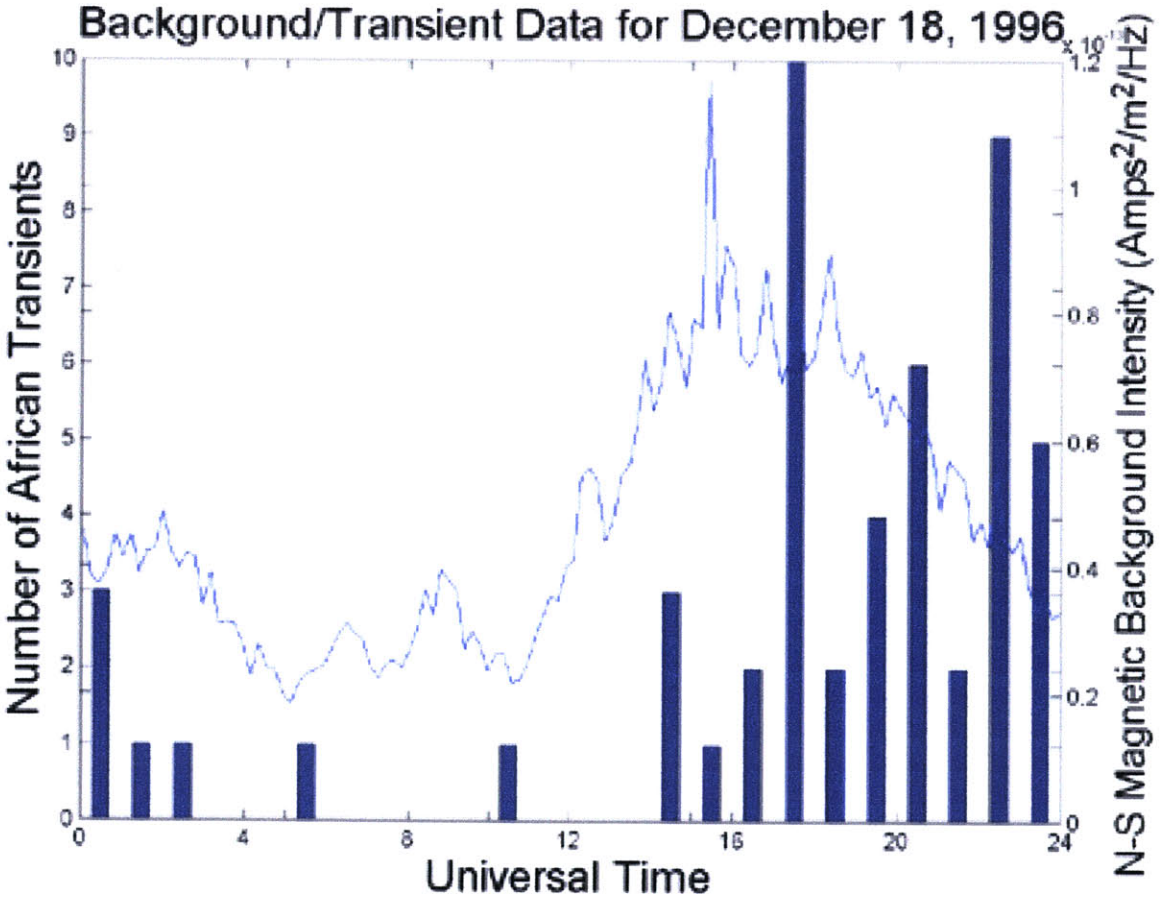
Background/Transient Data for December 18, 1996
Number of African Transients
N-S Magnetic Background Intensity (Amps²/m²/Hz)
Universal Time

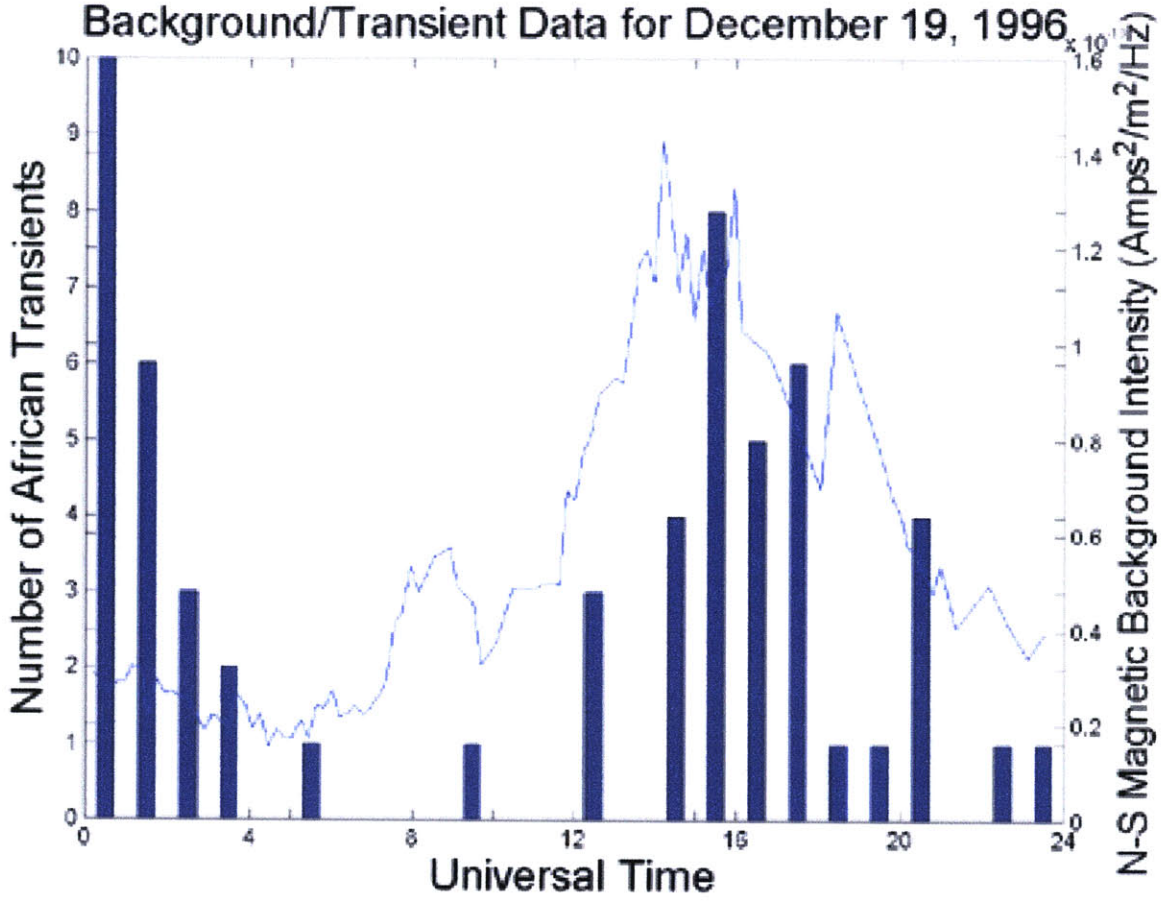
Background/Transient Data for December 19, 1996
Number of African Transients
N-S Magnetic Background Intensity (Amps²/m²/Hz)
Universal Time

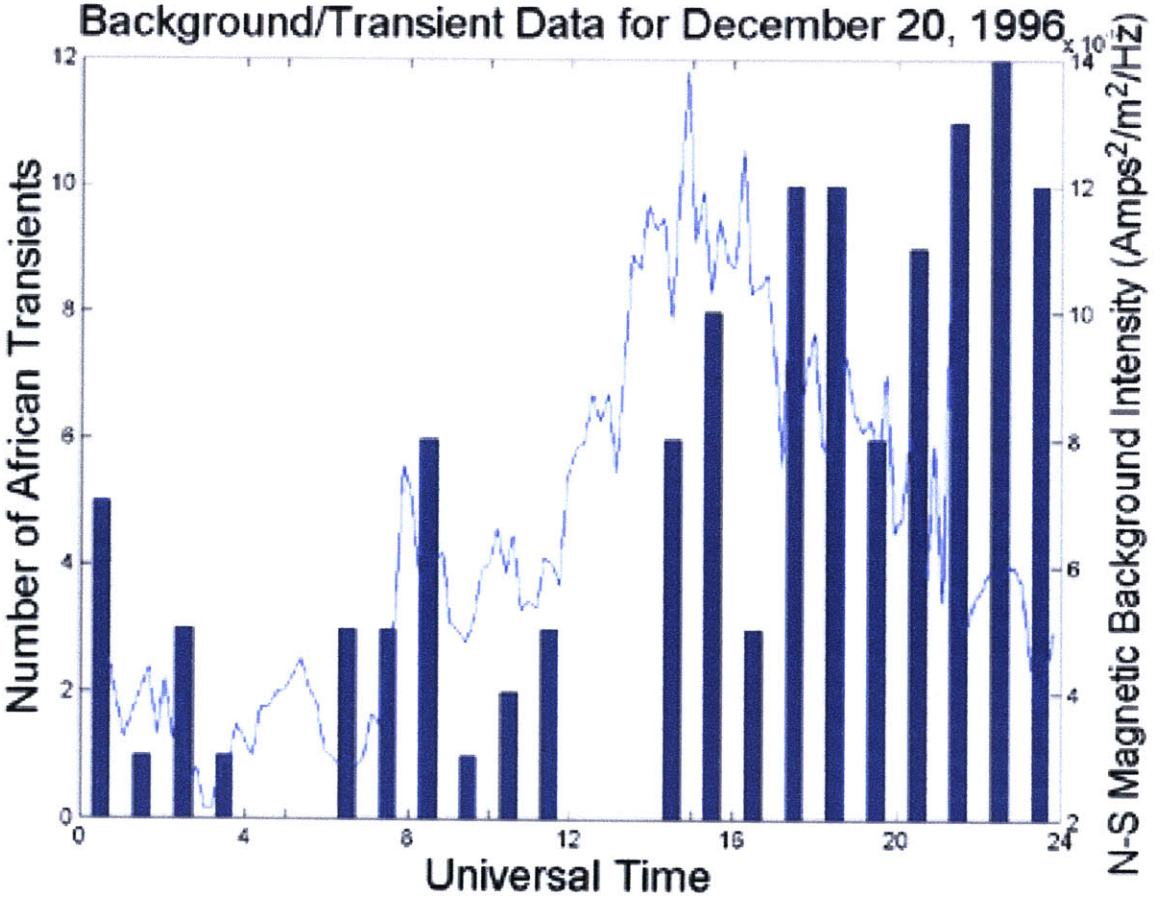
Background/Transient Data for December 20, 1996
Number of African Transients
N-S Magnetic Background Intensity (Amps²/m²/Hz)
Universal Time

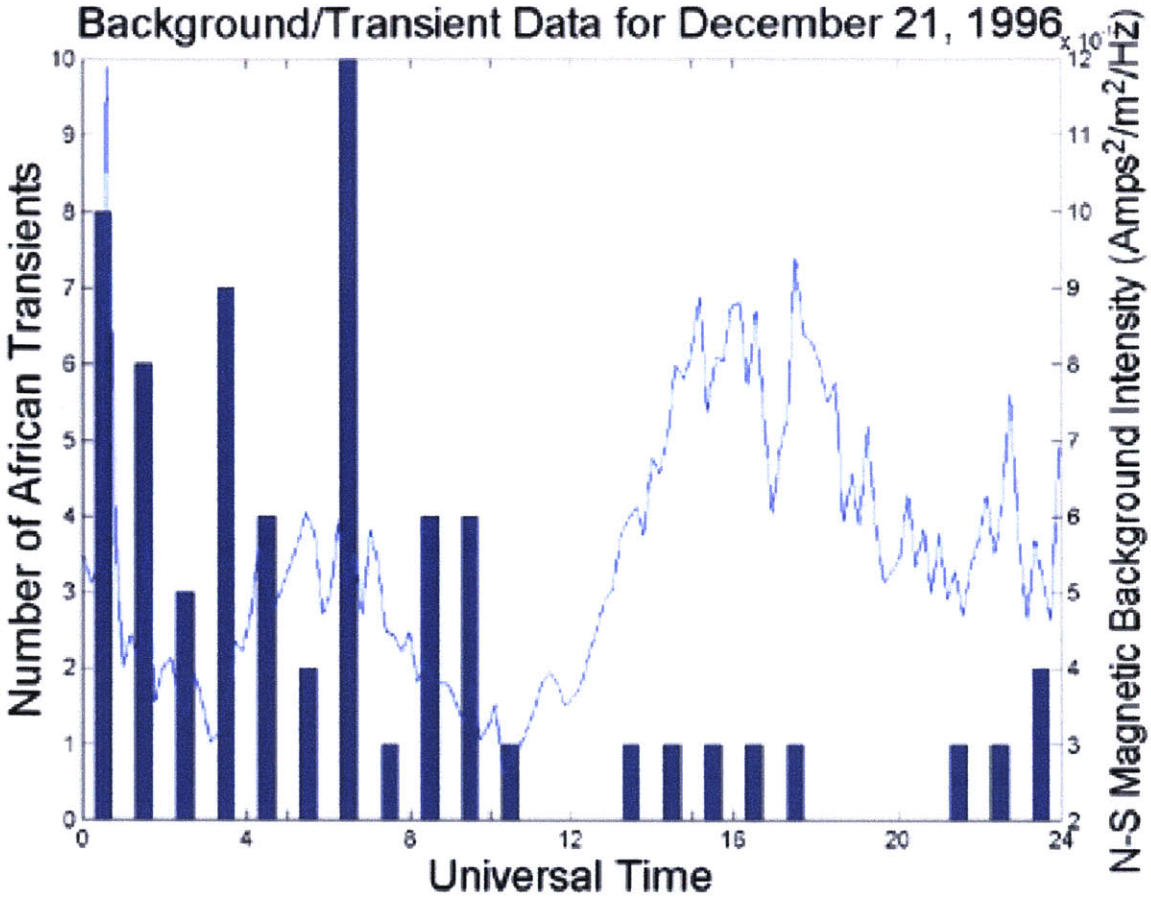
Background/Transient Data for December 21, 1996
Number of African Transients
N-S Magnetic Background Intensity (Amps²/m²/Hz)
Universal Time

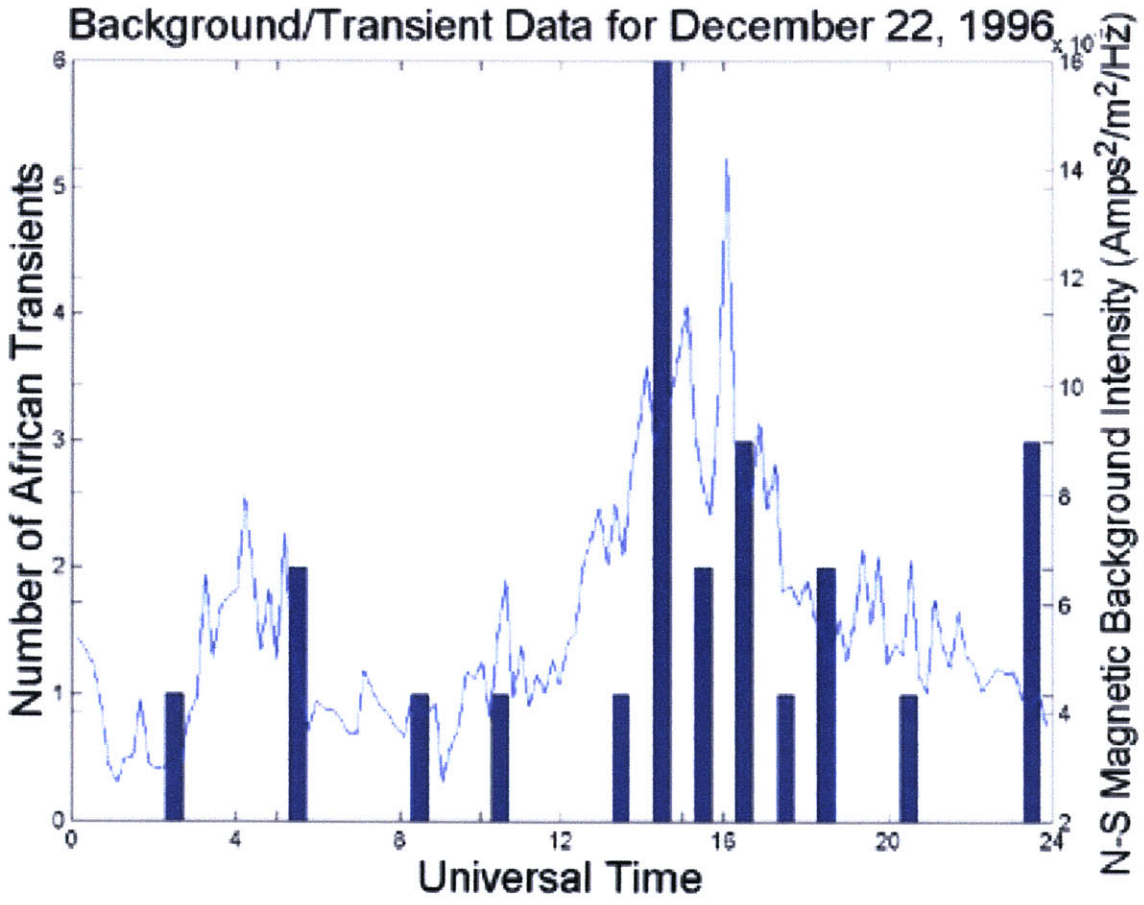
Background/Transient Data for December 22, 1996
Number of African Transients
N-S Magnetic Background Intensity (Amps²/m²/Hz)
Universal Time

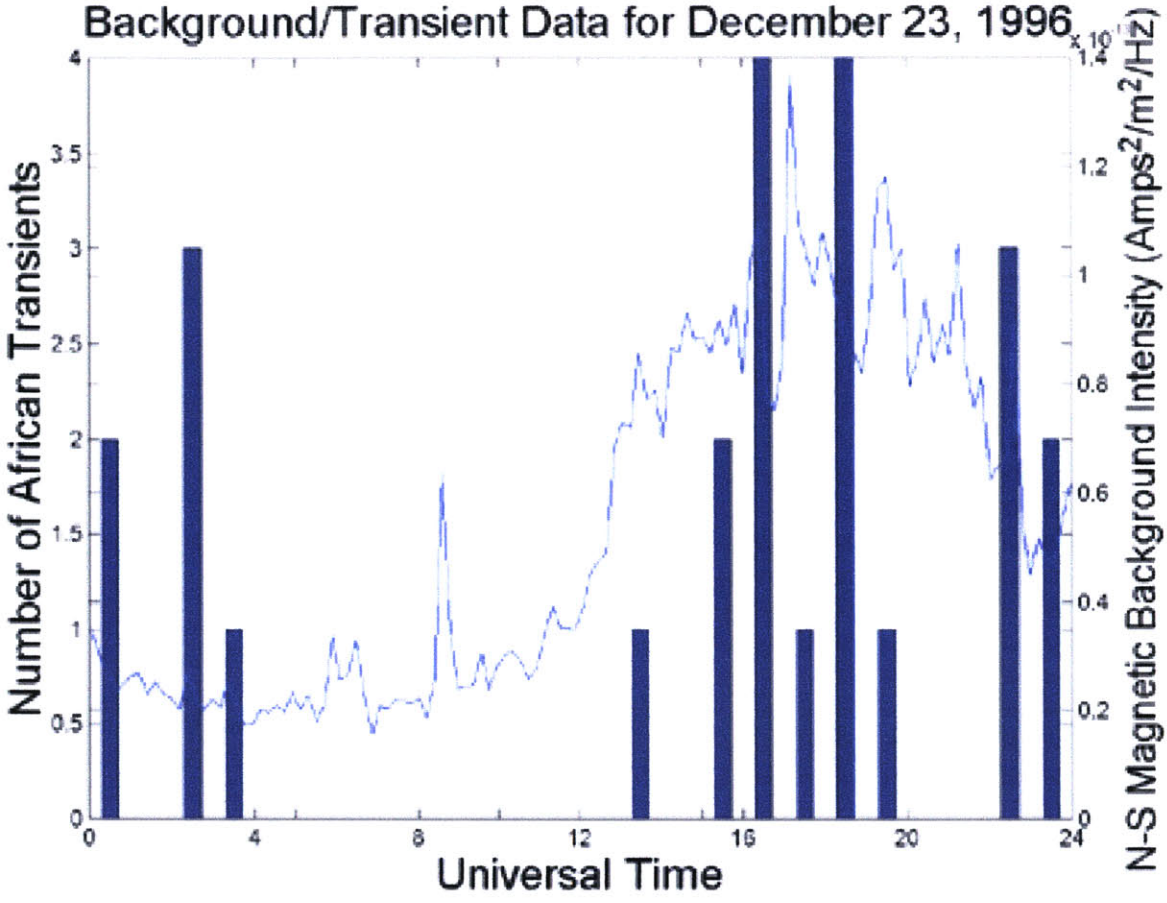
Background/Transient Data for December 23, 1996
Number of African Transients
N-S Magnetic Background Intensity (Amps²/m²/Hz)
Universal Time

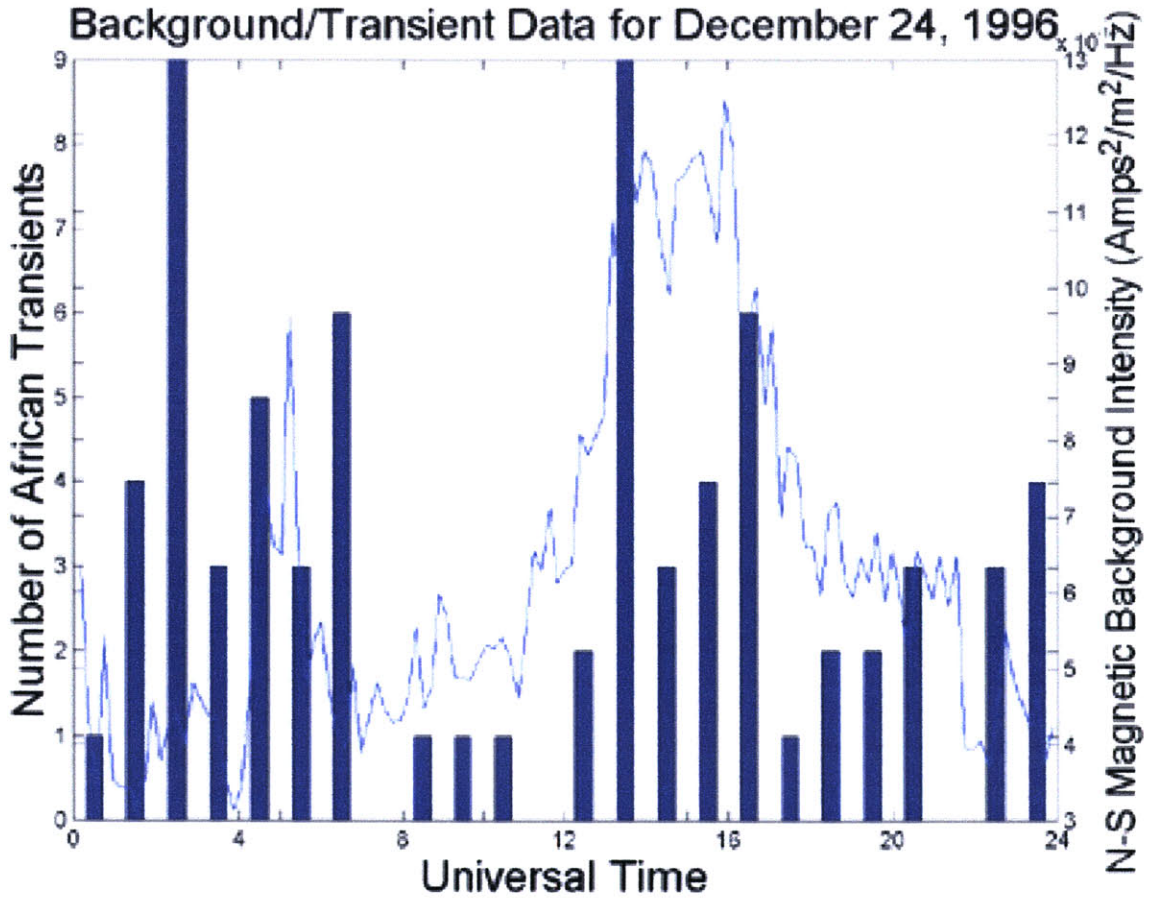
Background/Transient Data for December 24, 1996
Number of African Transients
N-S Magnetic Background Intensity (Amps²/m²/Hz)
Universal Time

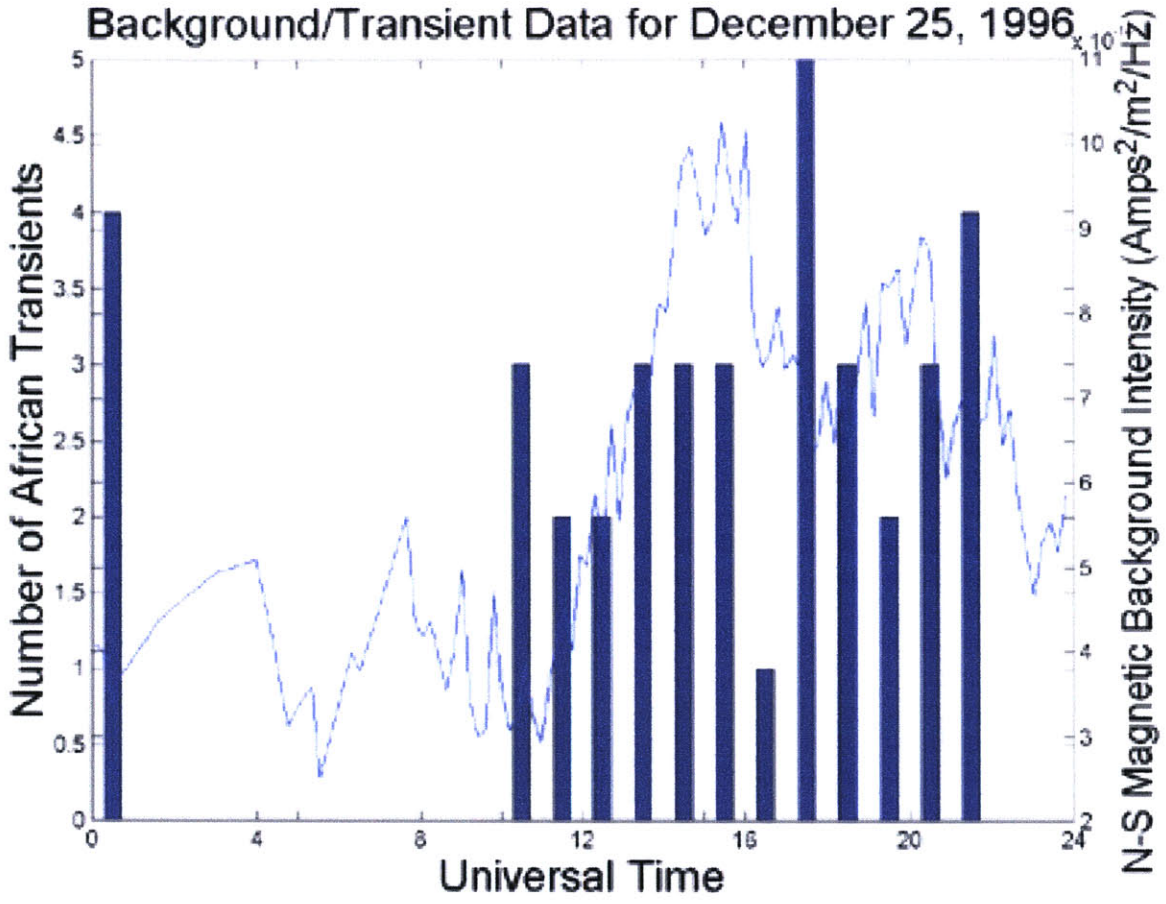
Background/Transient Data for December 25, 1996
Number of African Transients
N-S Magnetic Background Intensity (Amps²/m²/Hz)
Universal Time
0
4
8
12
16
20
24

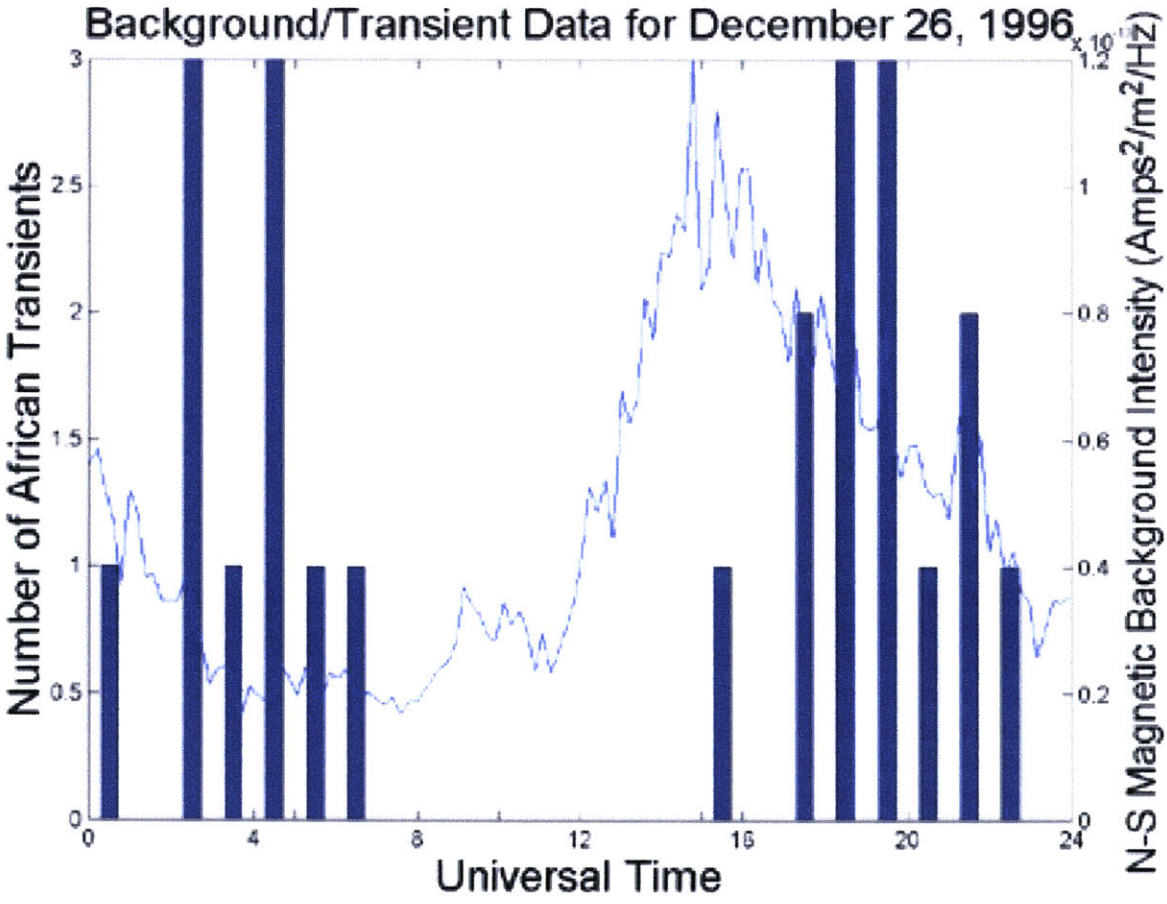
Background/Transient Data for December 26, 1996
Number of African Transients
N-S Magnetic Background Intensity (Amps²/m²/Hz)
Universal Time
0
4
8
12
16
20
24

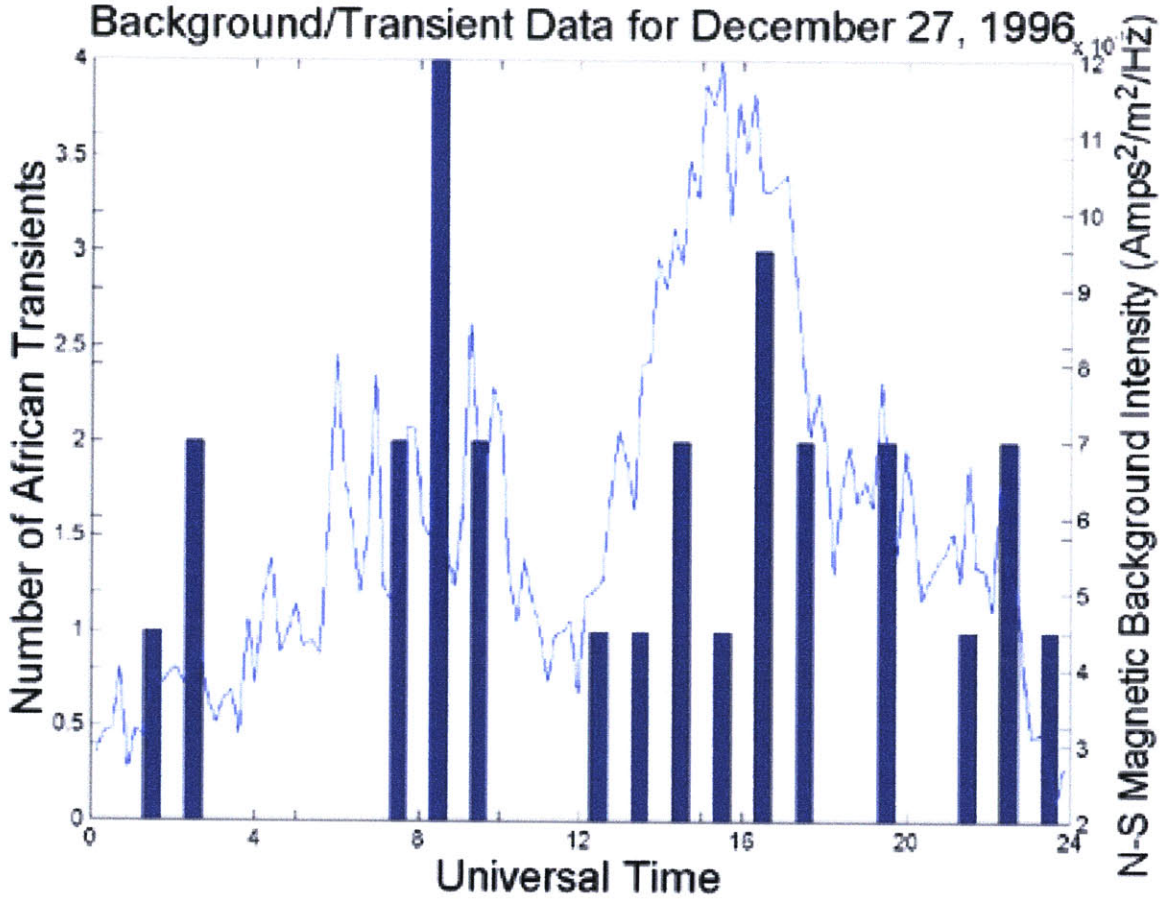
Background/Transient Data for December 27, 1996
Number of African Transients
N-S Magnetic Background Intensity (Amps²/m²/Hz)
Universal Time
0
0.5
1
1.5
2
2.5
3
3.5
4
0
4
8
12
16
20
24
x 10⁻¹²
2
3
4
5
6
7
8
9
10
11
12

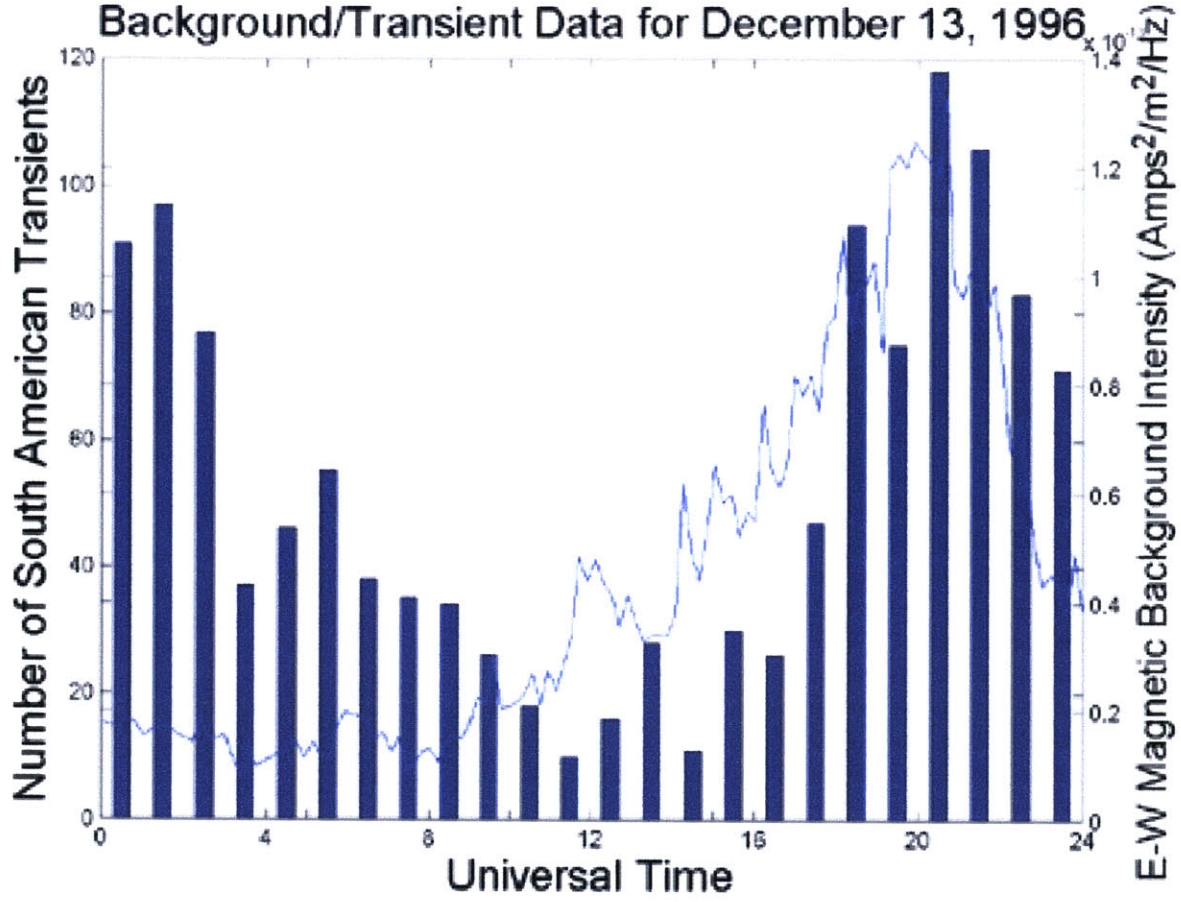
Background/Transient Data for December 13, 1996
Number of South American Transients
E-W Magnetic Background Intensity (Amps²/m²/Hz)
Universal Time
0
20
40
60
80
100
120
4
8
12
16
20
24
0.2
0.4
0.6
0.8
1
1.2
1.4

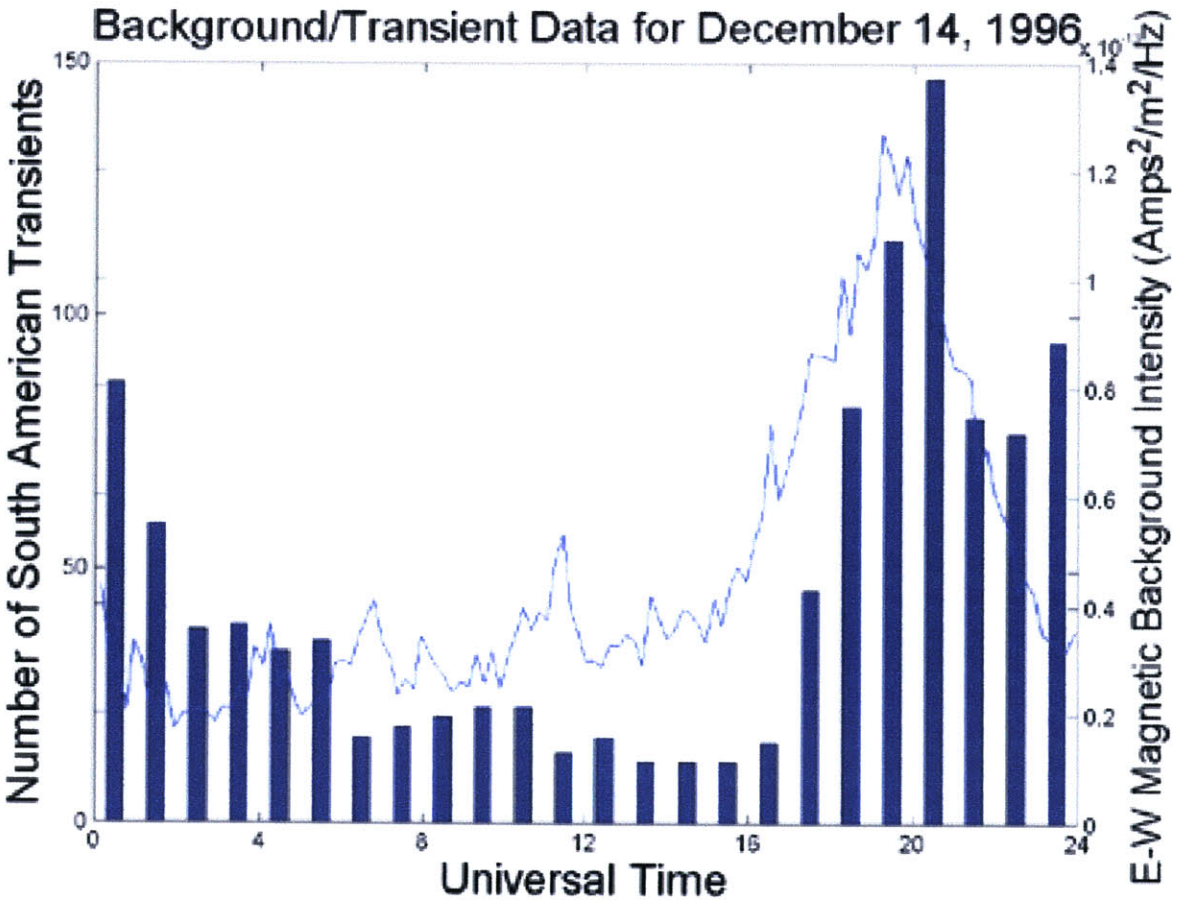
Background/Transient Data for December 14, 1996
Number of South American Transients
E-W Magnetic Background Intensity (Amps²/m²/Hz)
Universal Time
0
50
100
150
4
8
12
16
20
24
0.2
0.4
0.6
1
1.2
1.4

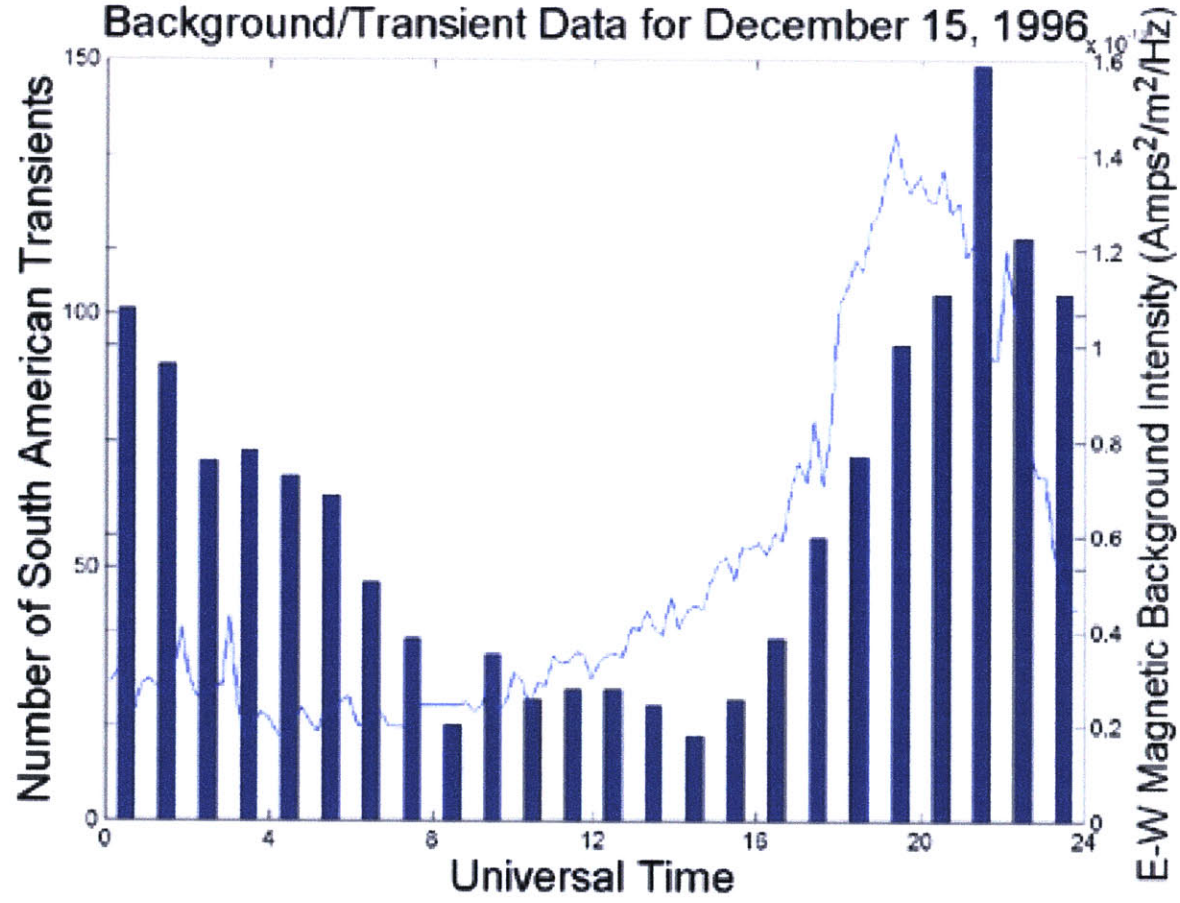
Background/Transient Data for December 15, 1996
Number of South American Transients
E-W Magnetic Background Intensity (Amps²/m²/Hz)
Universal Time
0
4
8
12
16
20
24
50
100
150
0.2
0.4
0.6
0.8
1
1.2
1.4
1.6

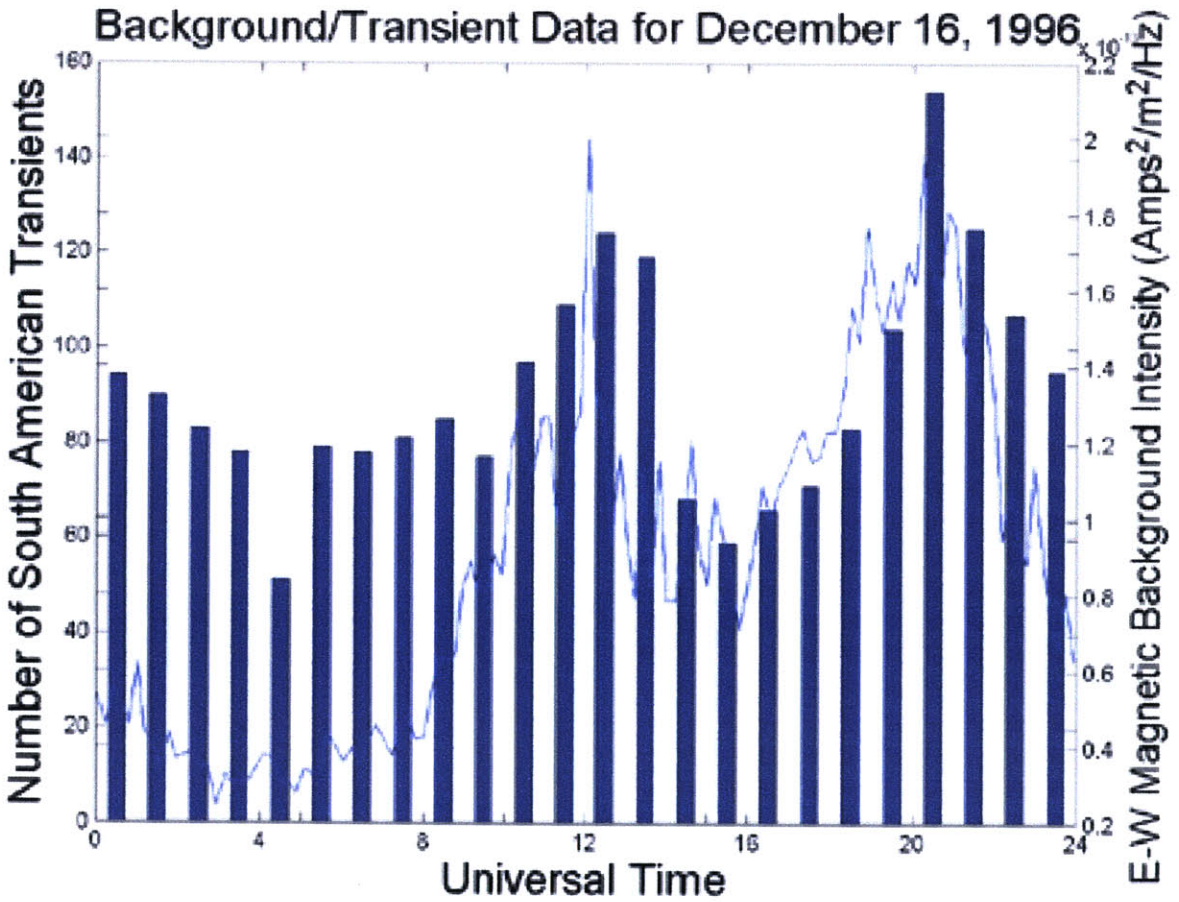
Background/Transient Data for December 16, 1996
Number of South American Transients
E-W Magnetic Background Intensity (Amps²/m²/Hz)
Universal Time
0
4
8
12
16
20
24
20
40
60
80
100
120
140
160
0.2
0.4
0.6
0.8
1
1.2
1.4
1.6
1.8
2
2.2

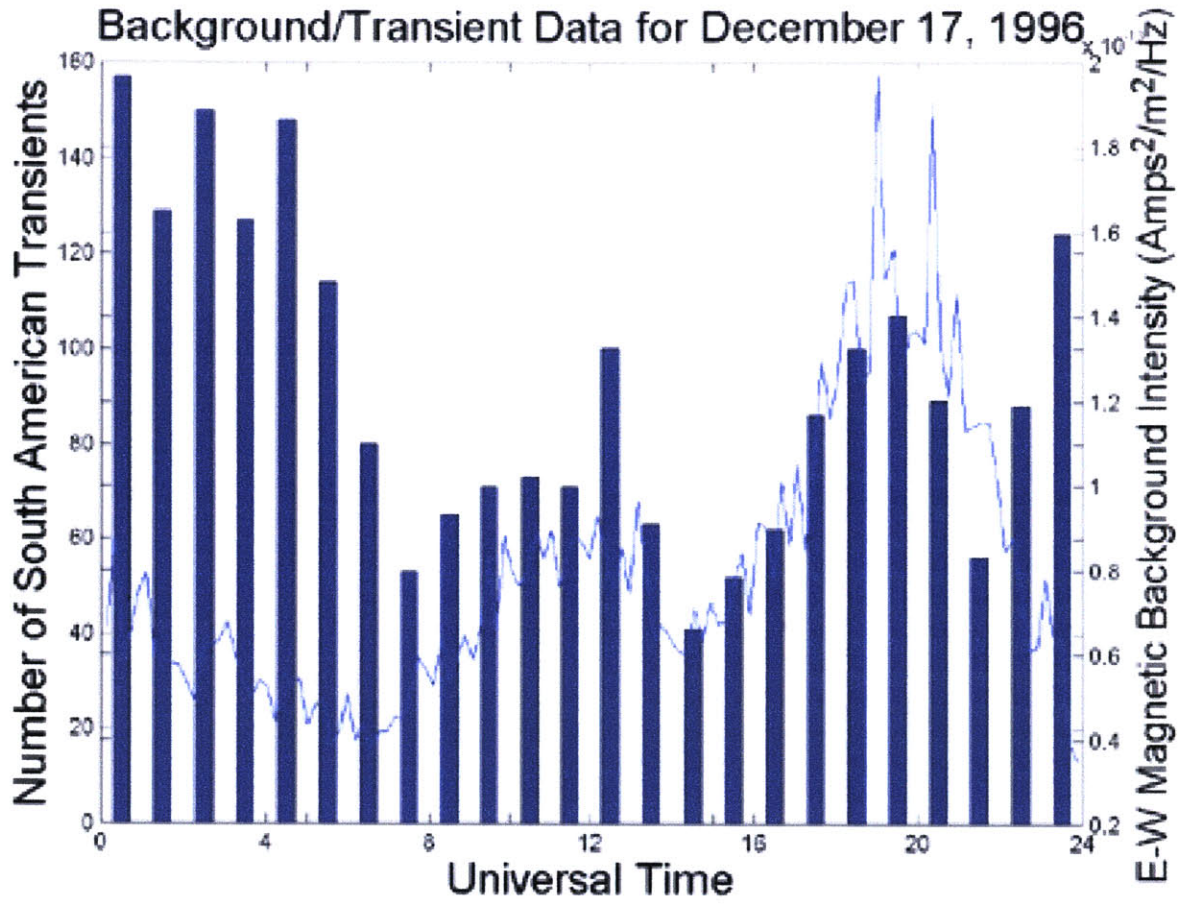
Background/Transient Data for December 17, 1996
Number of South American Transients
E-W Magnetic Background Intensity (Amps²/m²/Hz)
Universal Time
0
20
40
60
80
100
120
140
160
0
4
8
12
16
20
24
0.2
0.4
0.6
0.8
1
1.2
1.4
1.6
1.8
2
x 10⁻¹

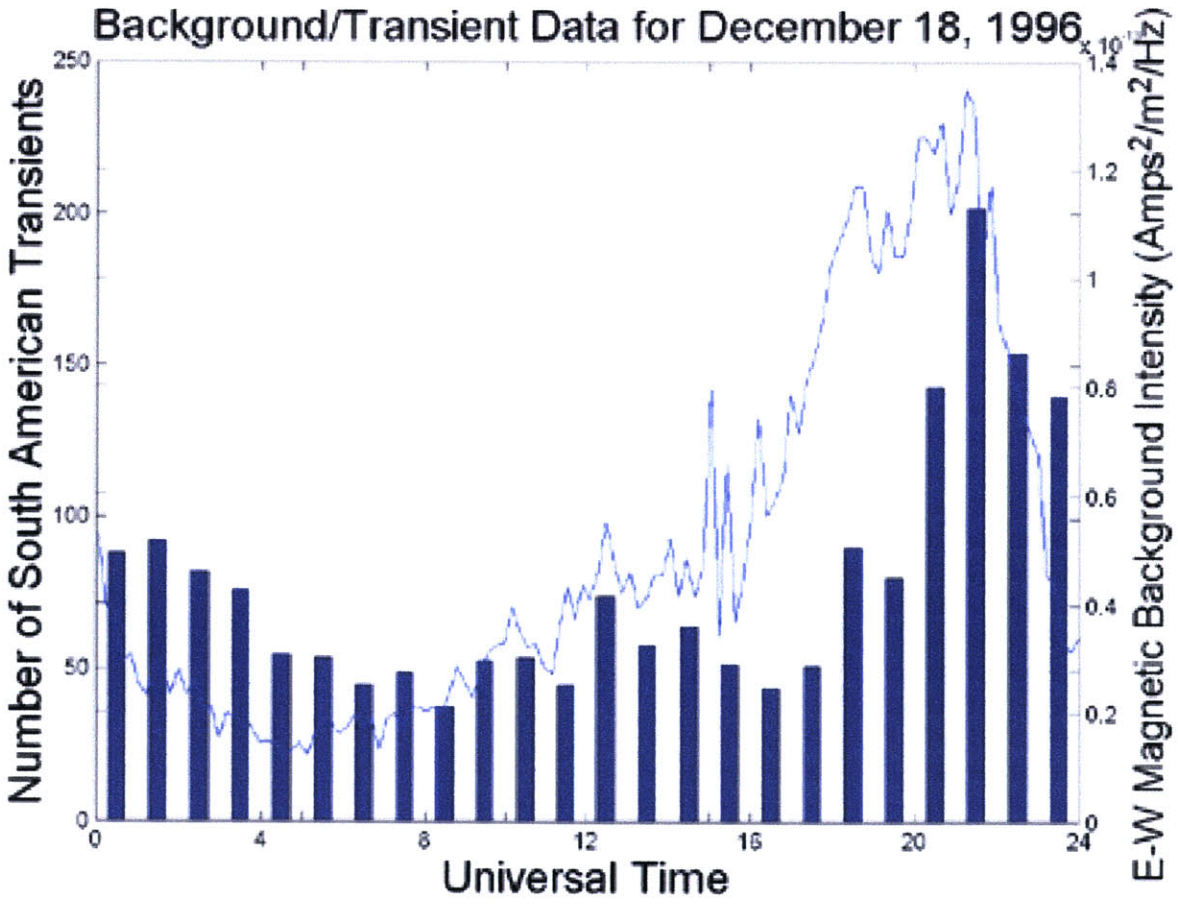
Background/Transient Data for December 18, 1996
Number of South American Transients
E-W Magnetic Background Intensity (Amps²/m²/Hz)
Universal Time
0
50
100
150
200
250
0
4
8
12
16
20
24
0.2
0.4
0.6
0.8
1
1.2
1.4
x 10⁻¹

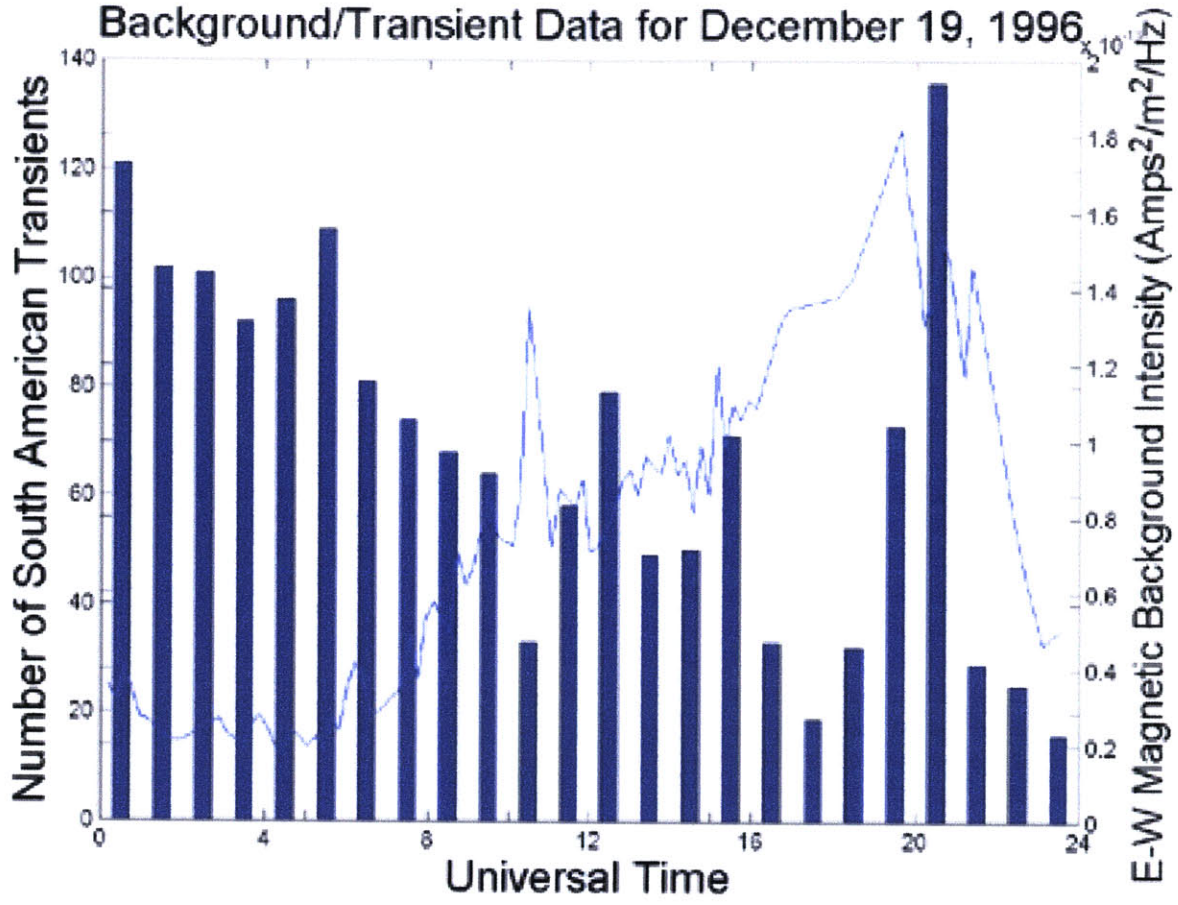
Background/Transient Data for December 19, 1996
Number of South American Transients
E-W Magnetic Background Intensity (Amps²/m²/Hz)
Universal Time
0
20
40
60
80
100
120
140
0
4
8
12
16
20
24
0.2
0.4
0.6
0.8
1
1.2
1.4
1.6

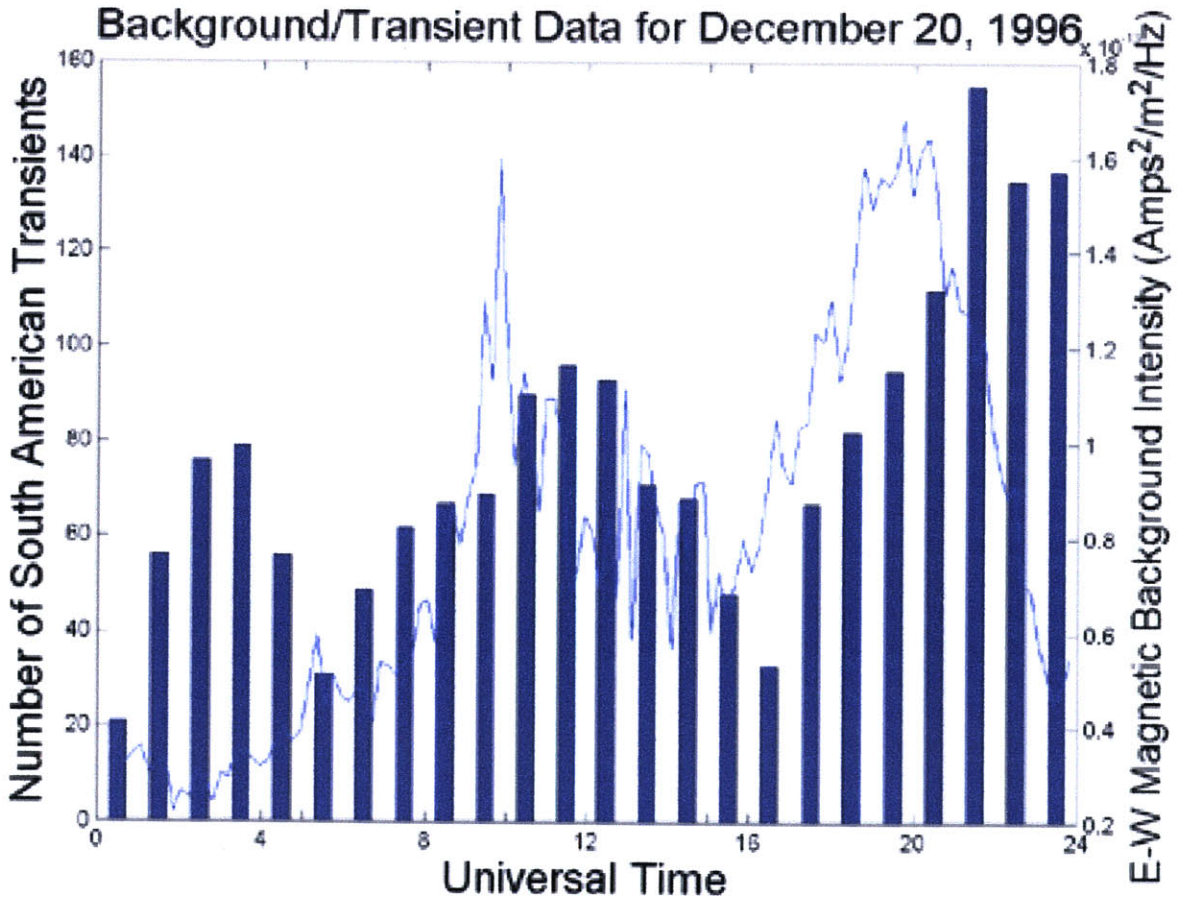
Background/Transient Data for December 20, 1996
Number of South American Transients
E-W Magnetic Background Intensity (Amps²/m²/Hz)
Universal Time
0
20
40
60
80
100
120
140
160
0
4
8
12
16
20
24
0.2
0.4
0.6
0.8
1
1.2
1.4
1.6
1.8

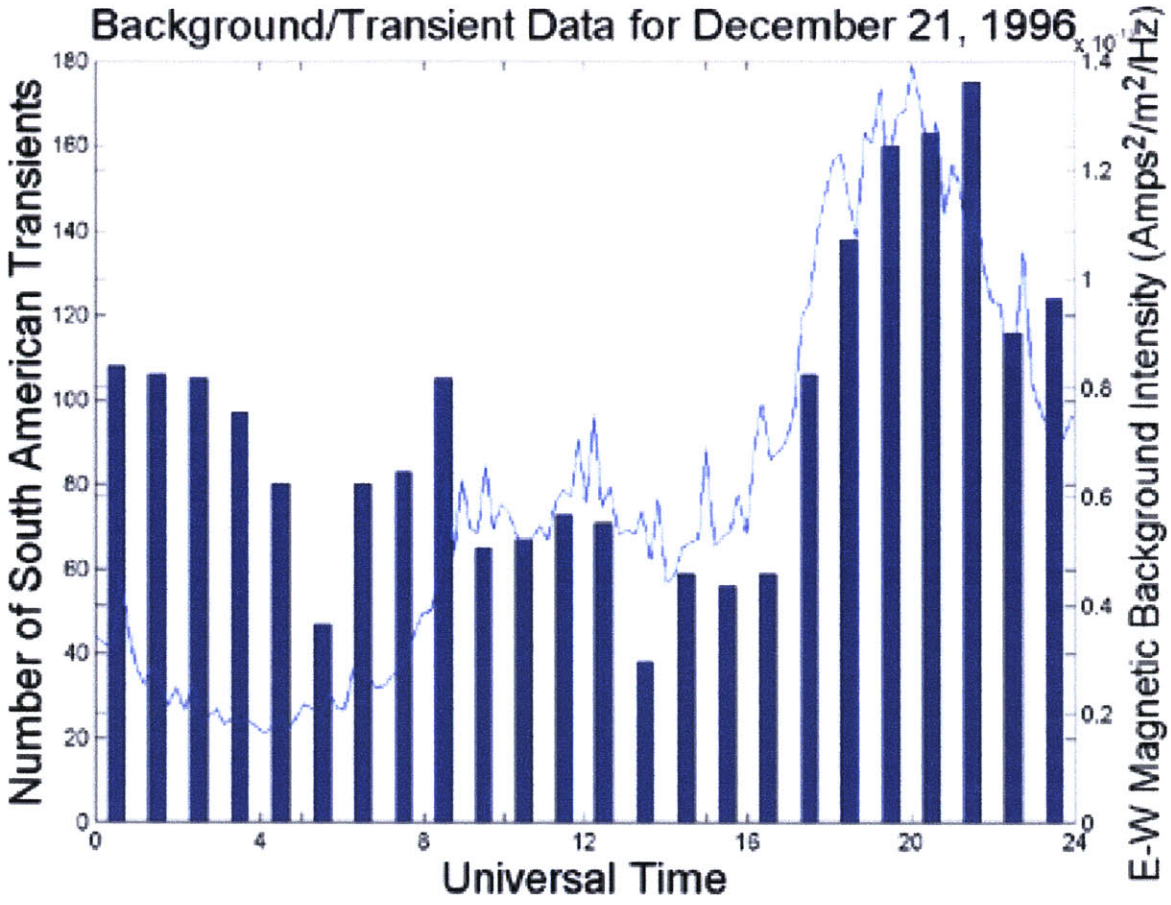
Background/Transient Data for December 21, 1996
Number of South American Transients
E-W Magnetic Background Intensity (Amps²/m²/Hz)
Universal Time

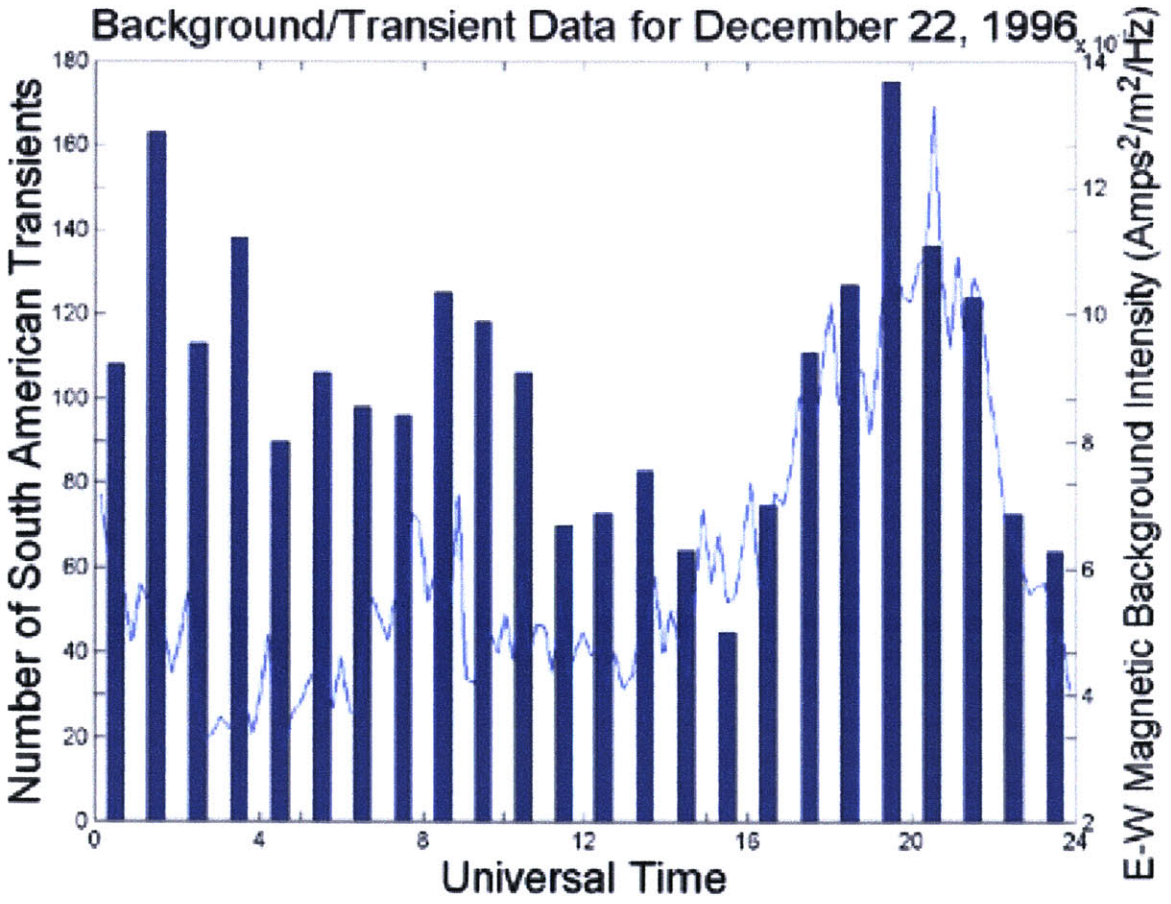
Background/Transient Data for December 22, 1996
Number of South American Transients
E-W Magnetic Background Intensity (Amps²/m²/Hz)
Universal Time

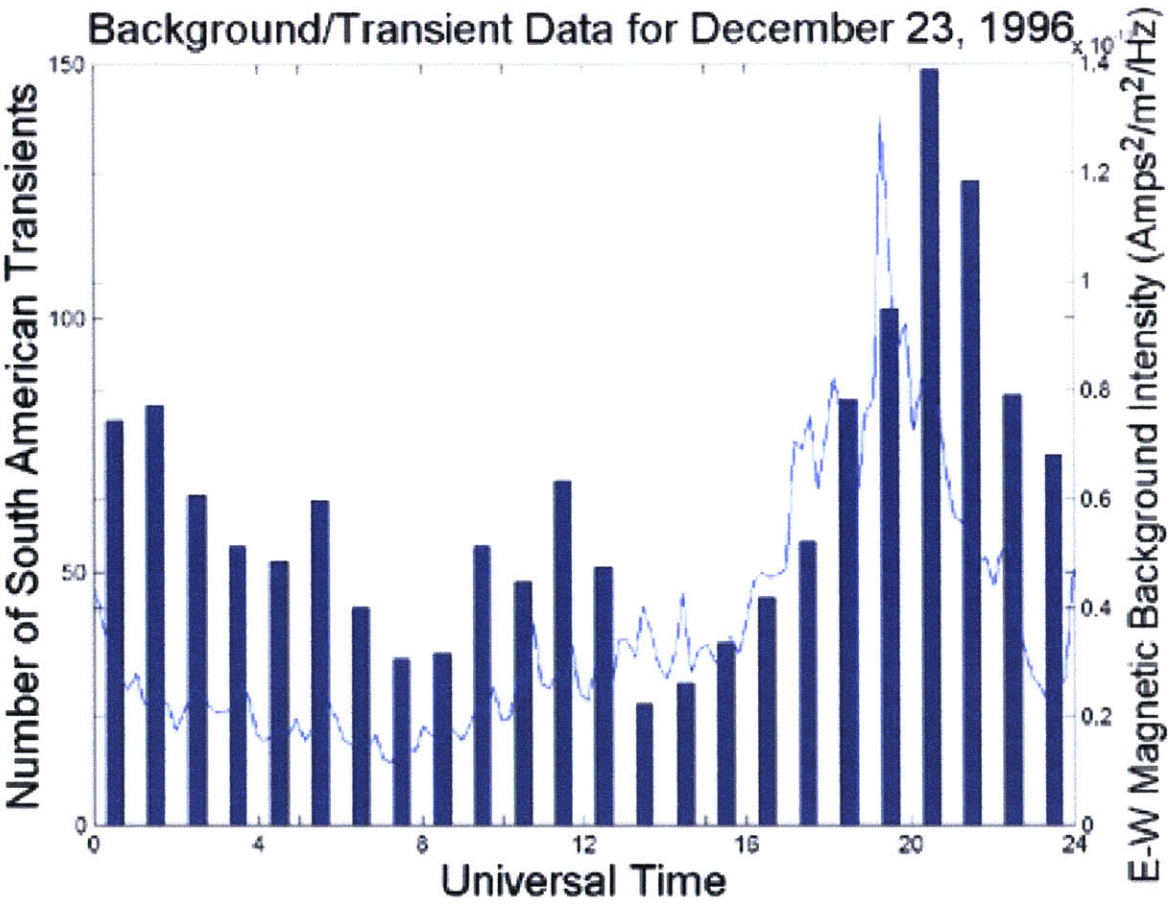
Background/Transient Data for December 23, 1996
Number of South American Transients
E-W Magnetic Background Intensity (Amps²/m²/Hz)
Universal Time
0
50
100
150
0
4
8
12
16
20
24
0.2
0.4
0.6
0.8
1
1.2
1.4

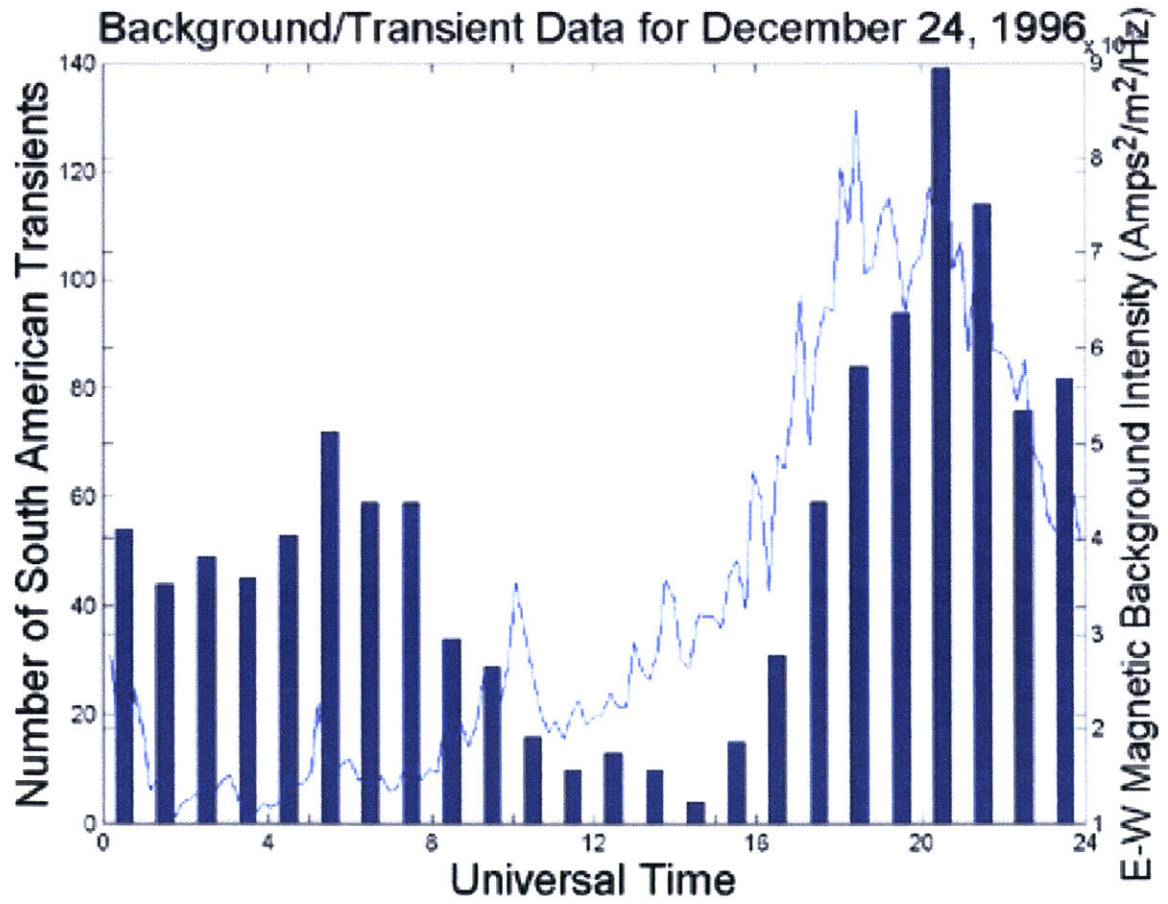
Background/Transient Data for December 24, 1996
Number of South American Transients
E-W Magnetic Background Intensity (Amps²/m²/Hz)
Universal Time
0
20
40
60
80
100
120
140
0
4
8
12
16
20
24
1
2
3
4
5
6
7
8
9

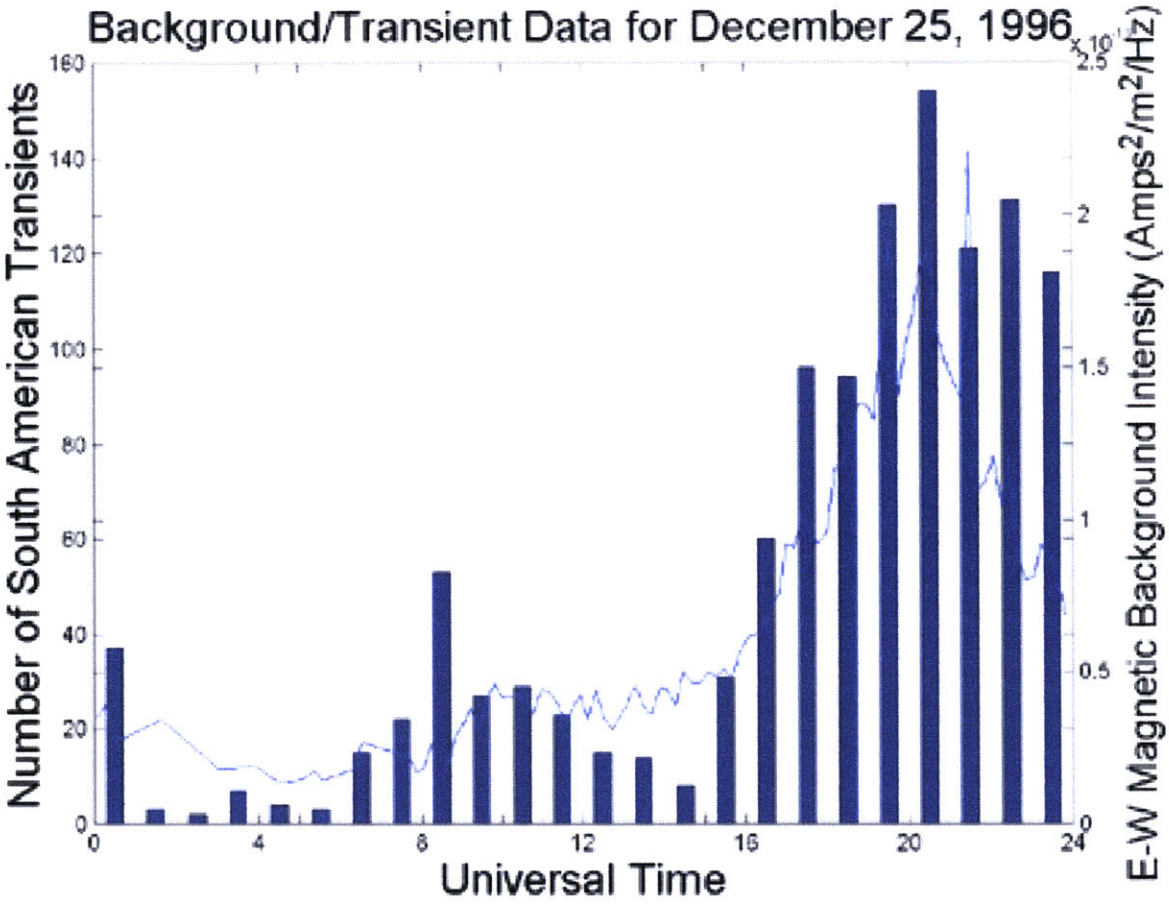
Background/Transient Data for December 25, 1996
Number of South American Transients
E-W Magnetic Background Intensity (Amps²/m²/Hz)
Universal Time
0
4
8
12
16
20
24
0
20
40
60
80
100
120
140
160
0
0.5
1
1.5
2
2.5

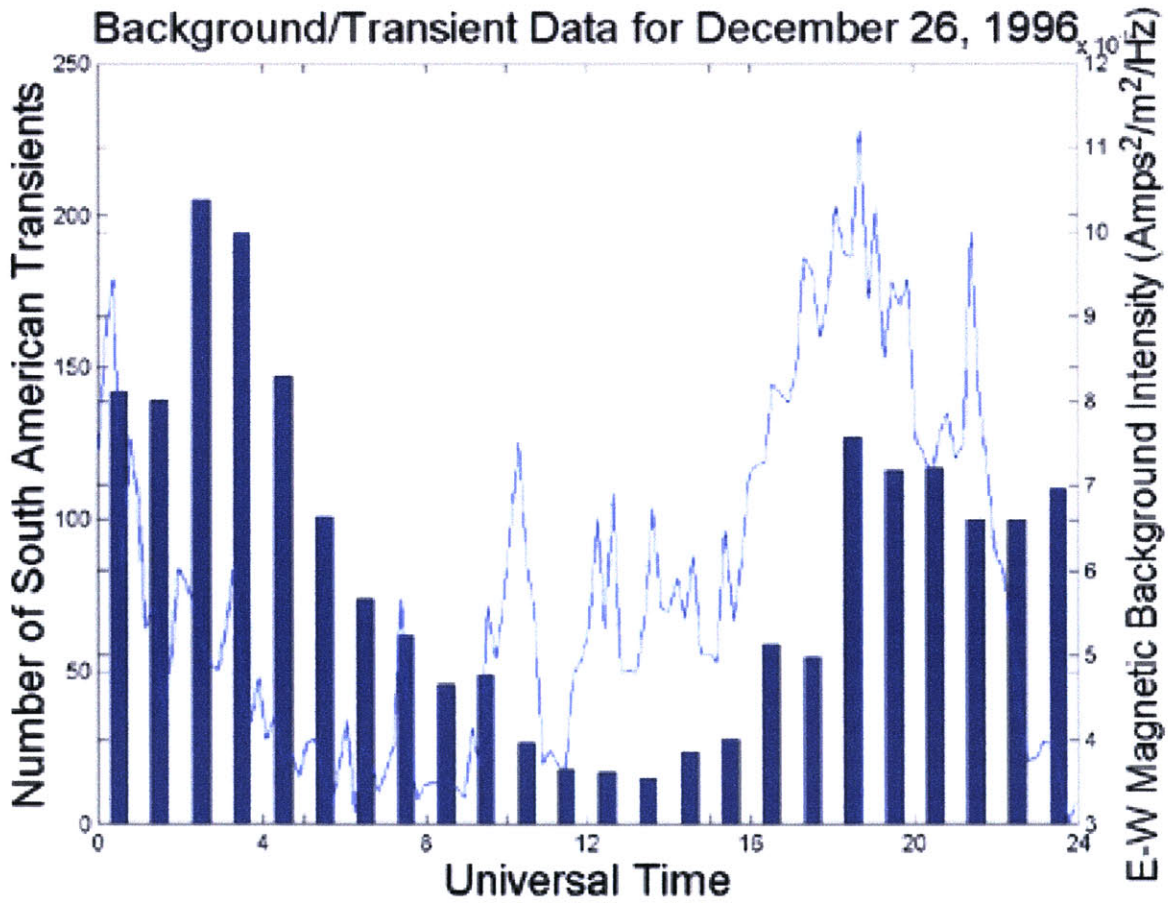
Background/Transient Data for December 26, 1996
Number of South American Transients
E-W Magnetic Background Intensity (Amps²/m²/Hz)
Universal Time
0
4
8
12
16
20
24
0
50
100
150
200
250
3
4
5
6
7
8
9
10
11
12

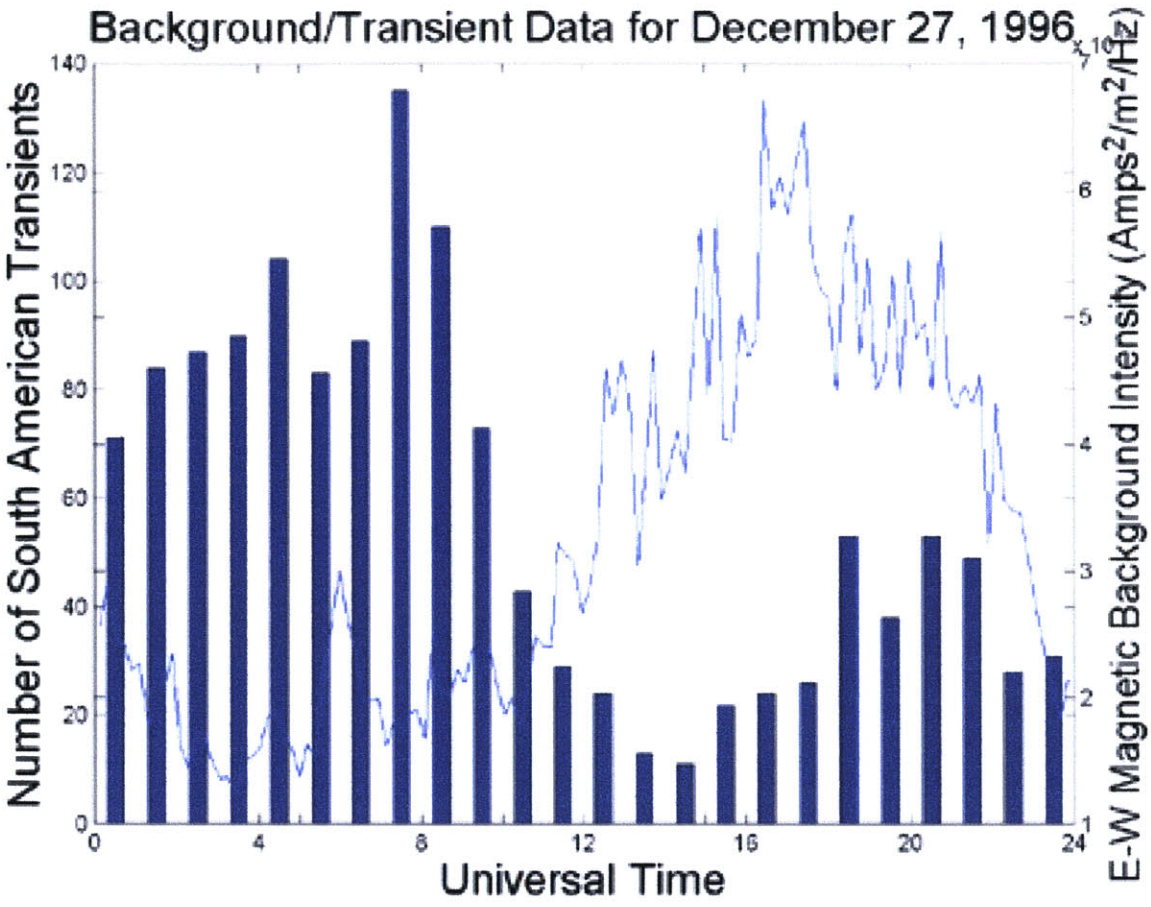
Background/Transient Data for December 27, 1996
Number of South American Transients
E-W Magnetic Background Intensity (Amps²/m²/Hz)
Universal Time
0
20
40
60
80
100
120
140
1
2
3
4
5
6
7
x10⁻¹⁰
0
4
8
12
16
20
24

Appendix B

NASA Global Rainfall/Transient Maps for

5/7/98 – 6/19/98

ELF Lightning for May7.txt from West Greenwich, R.I.

Correlation (min) = .5, Max Bearing Error (deg) = 5, Max Range Error (%) = 10
Positives = 382, Negatives = 357, Total = 739

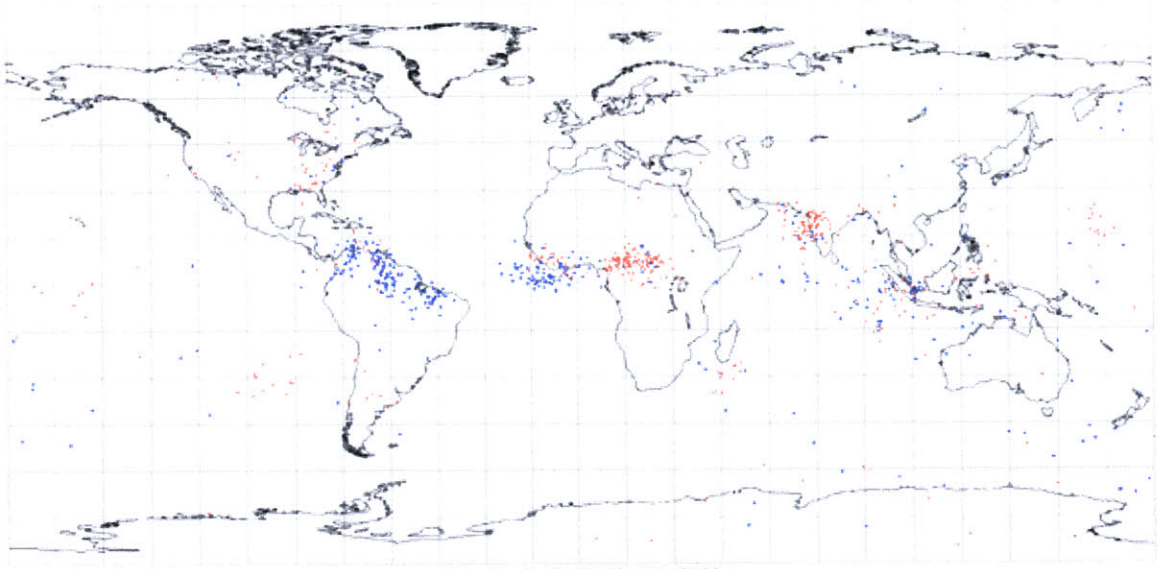

Sat Jan 8 15:36:03 EST 2000

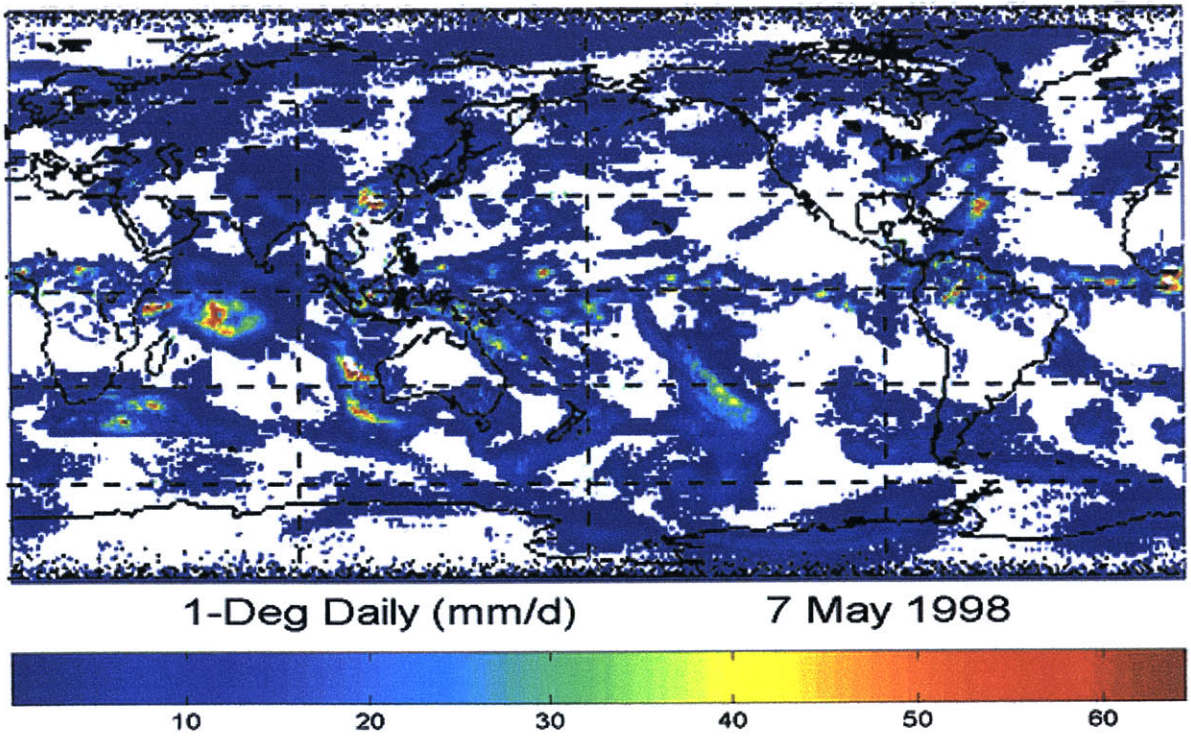

ELF Lightning for May8.txt from West Greenwich, R.I.

Correlation (min) = .5, Max Bearing Error (deg) = 5, Max Range Error (%) = 10
Positives = 973, Negatives = 1107, Total = 2080

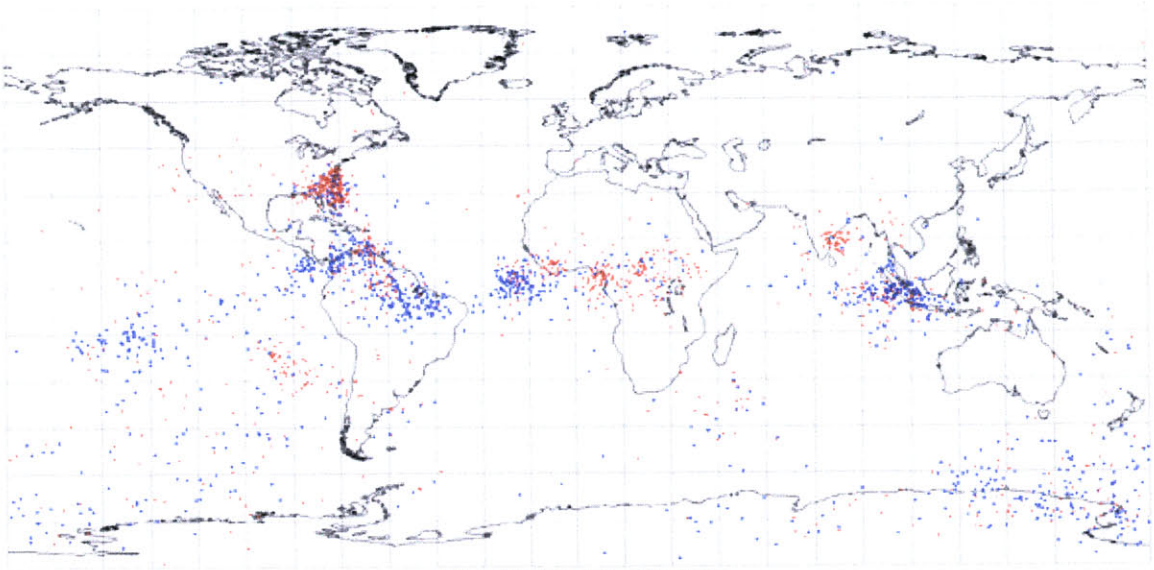

Sat Jan 8 15:36:44 EST 2000

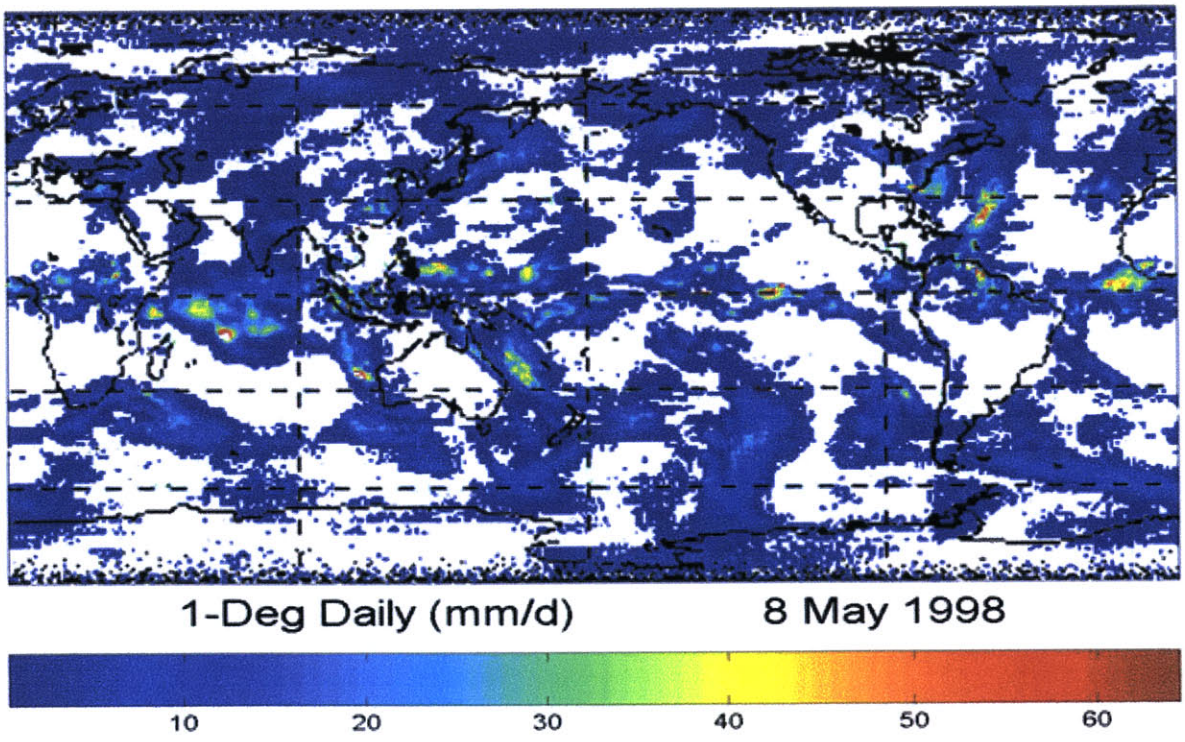

ELF Lightning for May9.txt from West Greenwich, R.I.

Correlation (min) = .5, Max Bearing Error (deg) = 5, Max Range Error (%) = 10
Positives = 1046, Negatives = 1103, Total = 2149
< >

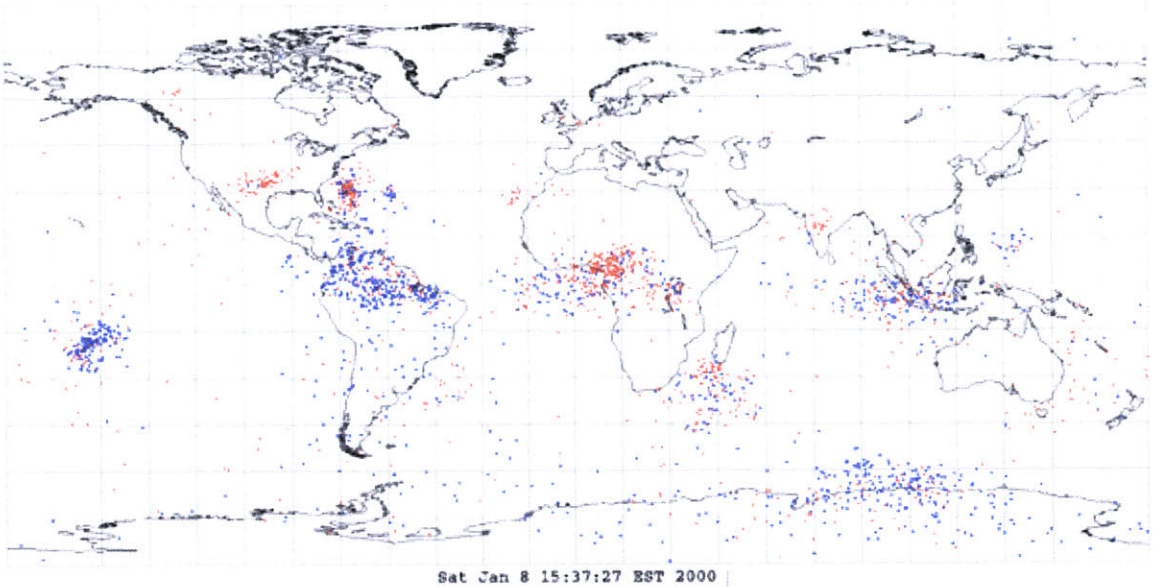

Sat Jan 8 15:37:27 EST 2000

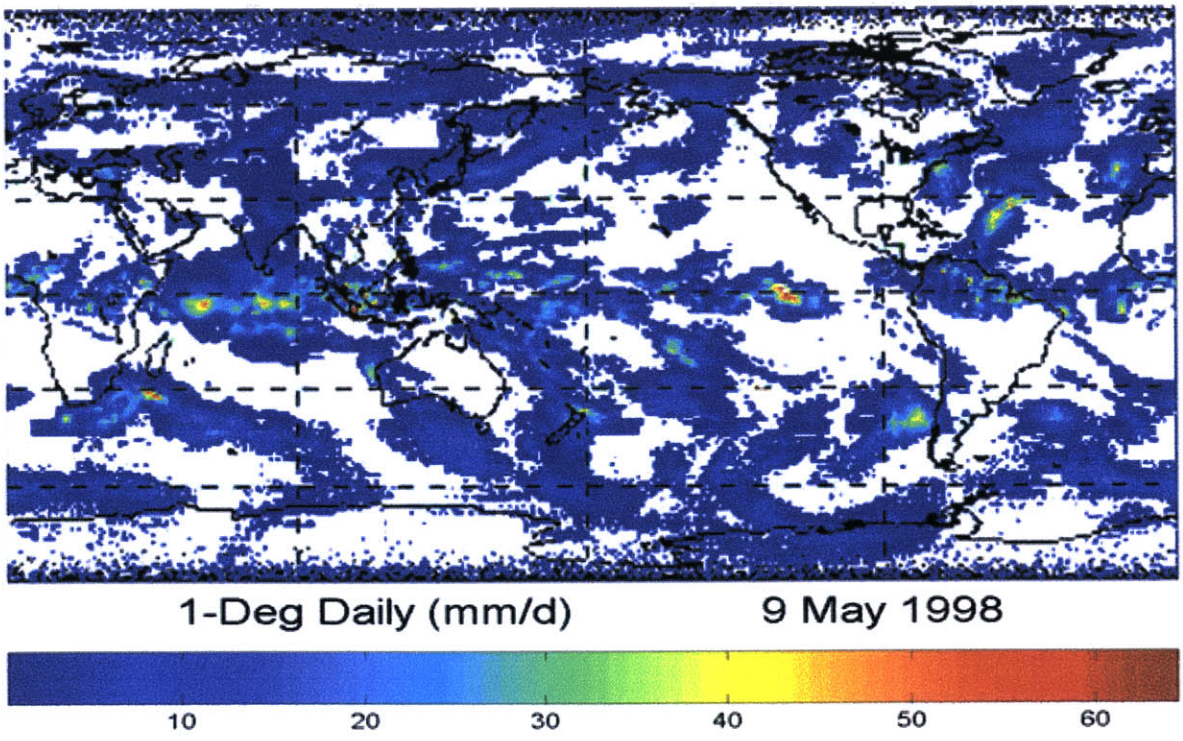

ELF Lightning for May10.txt from West Greenwich, R.I.

Correlation (min) = .5, Max Bearing Error (deg) = 5, Max Range Error (%) = 10
Positives = 1056, Negatives = 1008, Total = 2064
< >

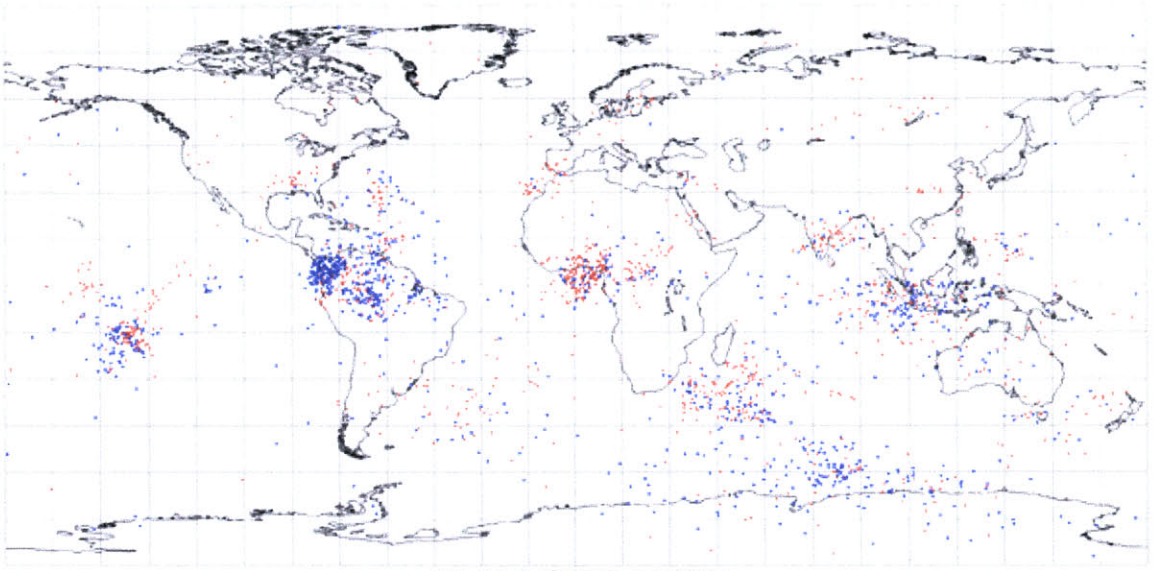

Sat Jan 8 15:38:10 EST 2000

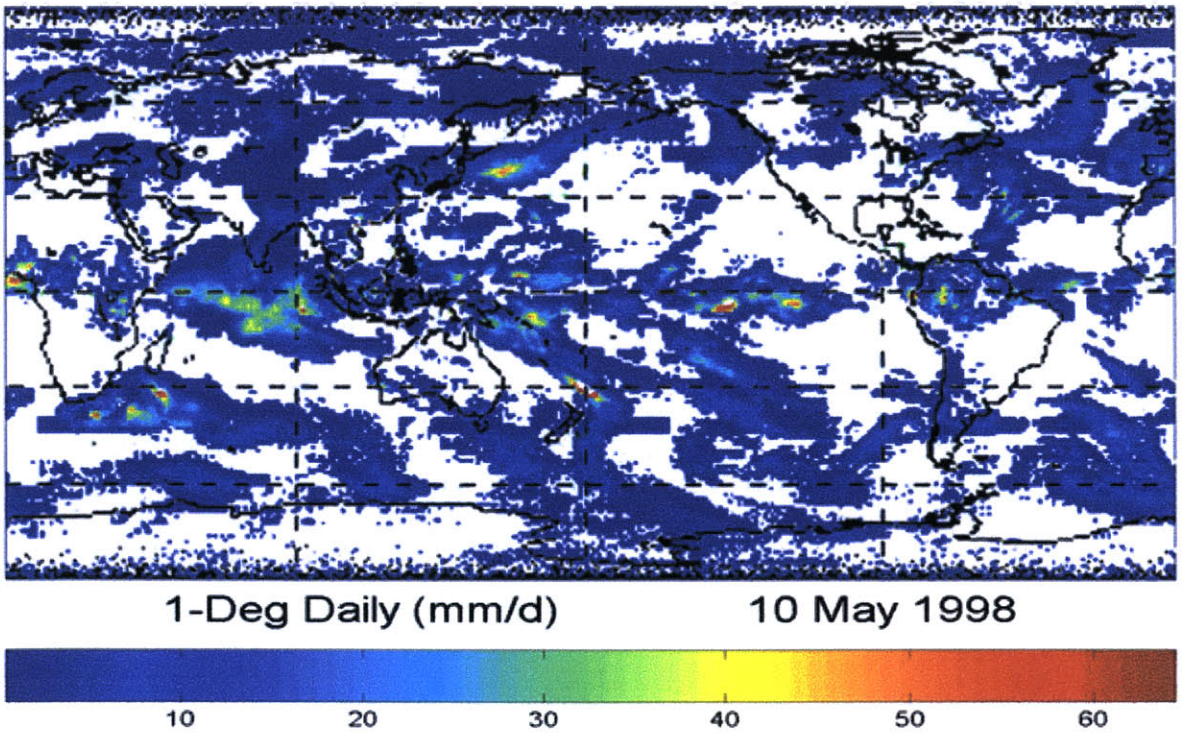

ELF Lightning for May11.txt from West Greenwich, R.I.

Correlation (min) = .5, Max Bearing Error (deg) = 5, Max Range Error (%) = 10
Positives = 1040, Negatives = 1285, Total = 2325

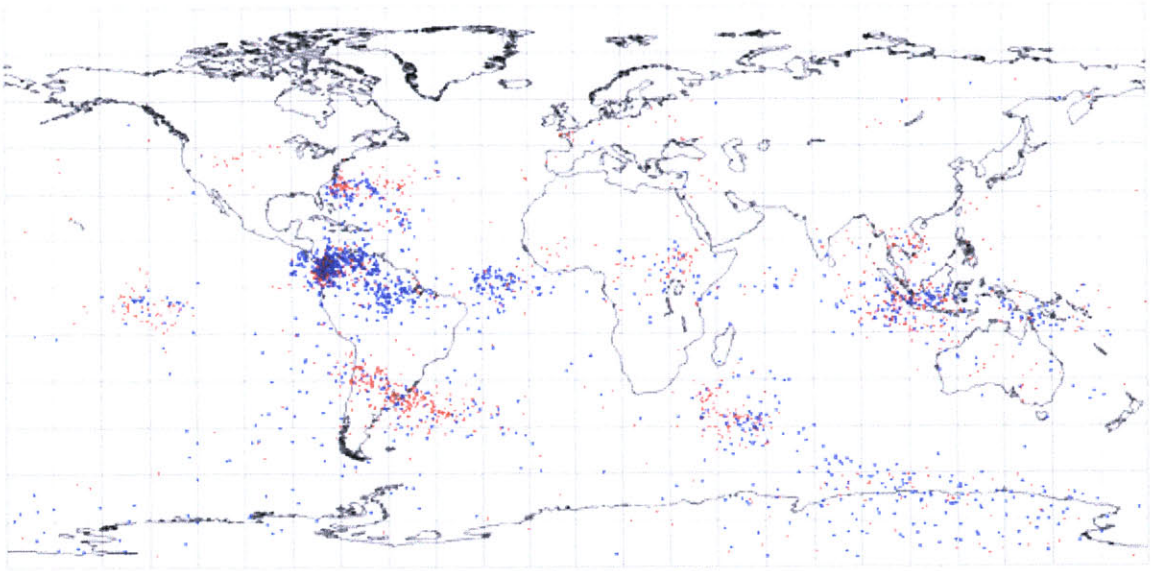

Sat Jan 8 15:39:13 EST 2000

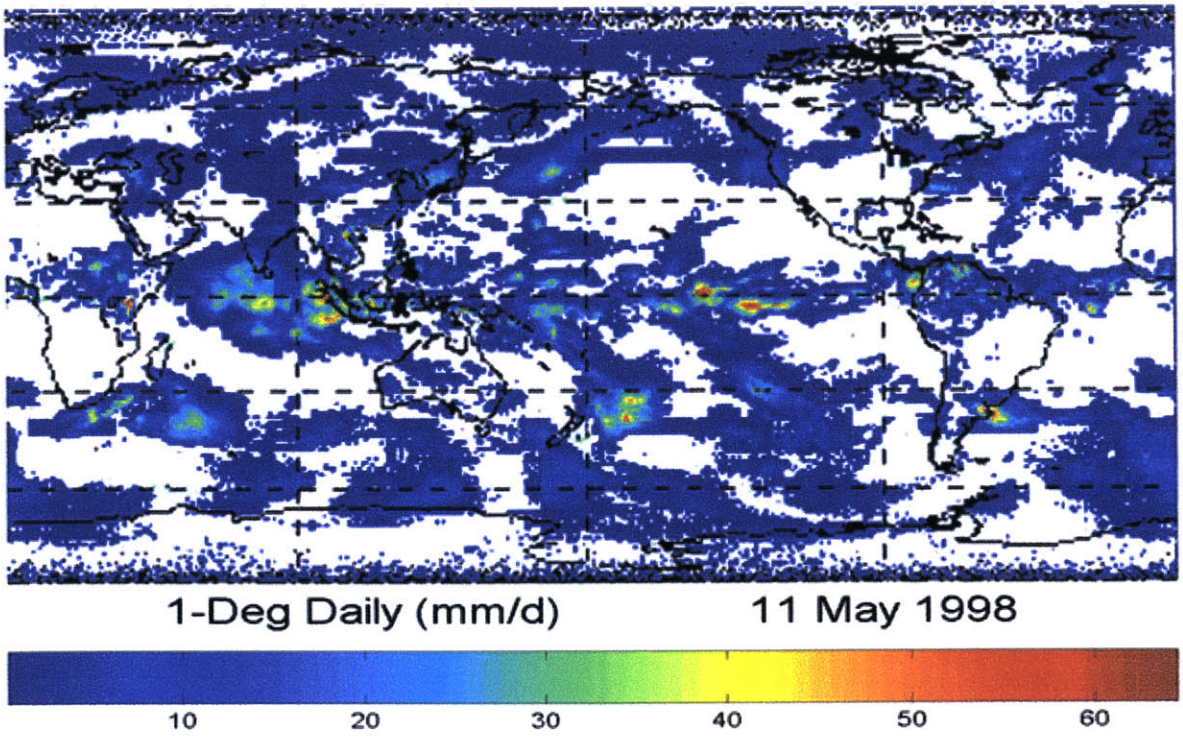

ELF Lightning for May12.txt from West Greenwich, R.I.

Correlation (min) = .5, Max Bearing Error (deg) = 5, Max Range Error (%) = 10
Positives = 844, Negatives = 1254, Total = 2098

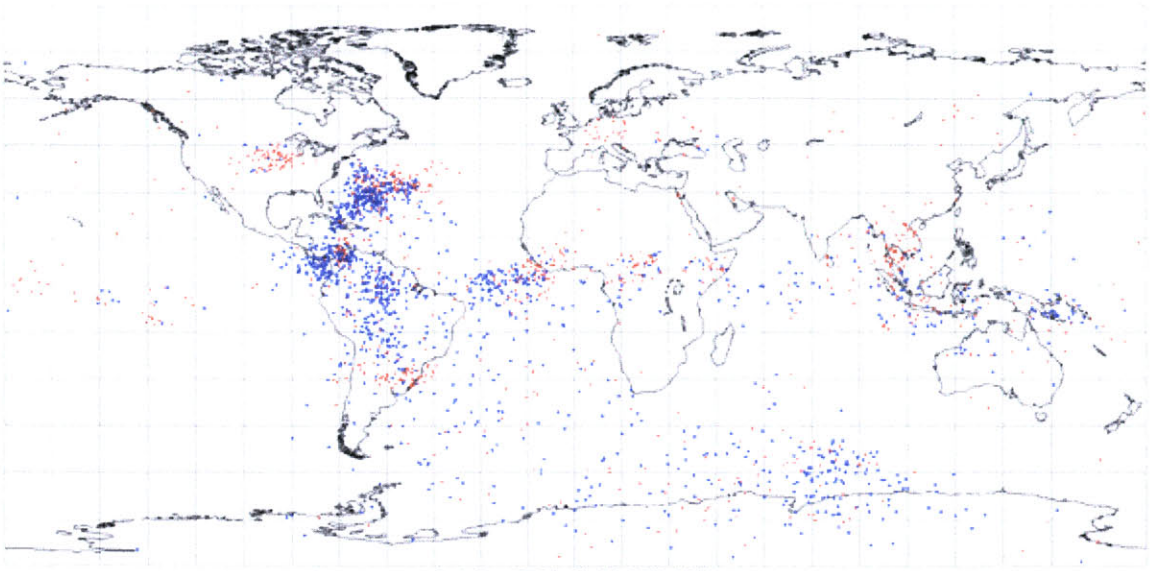

Sat Jan 8 15:40:01 EST 2000

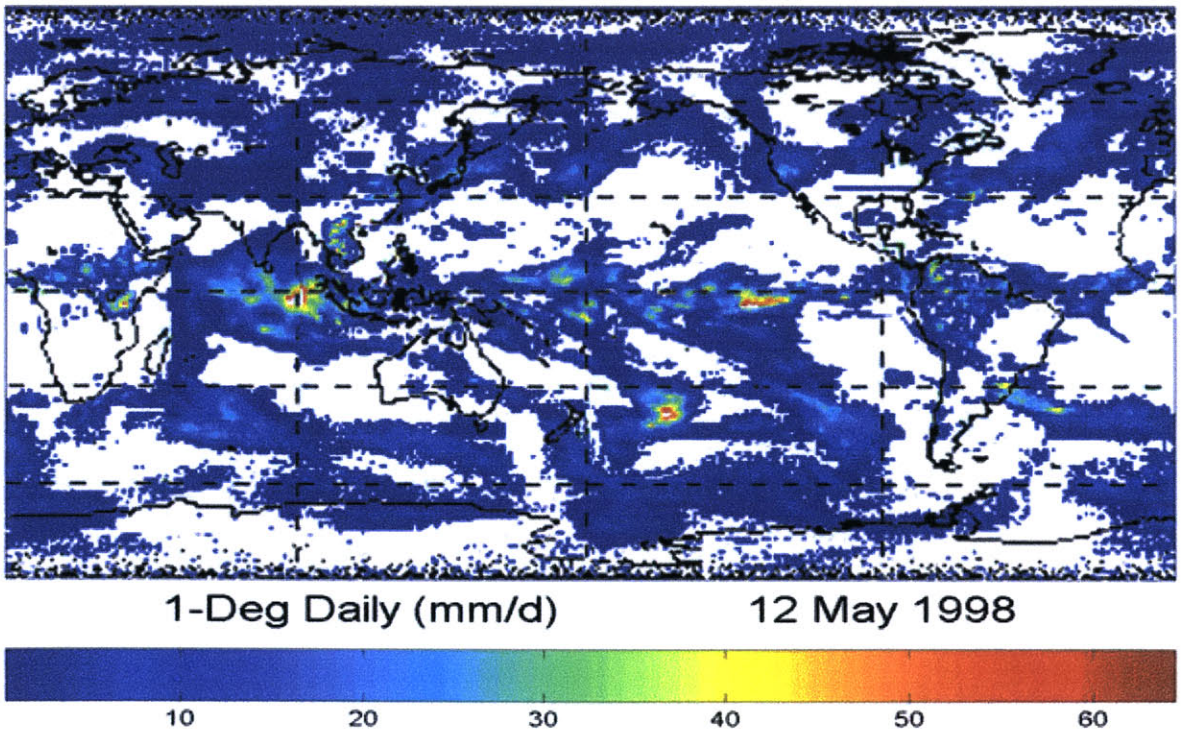

ELF Lightning for May13.txt from West Greenwich, R.I.

Correlation (min) = .5, Max Bearing Error (deg) = 5, Max Range Error (%) = 10
Positives = 1114, Negatives = 1130, Total = 2244

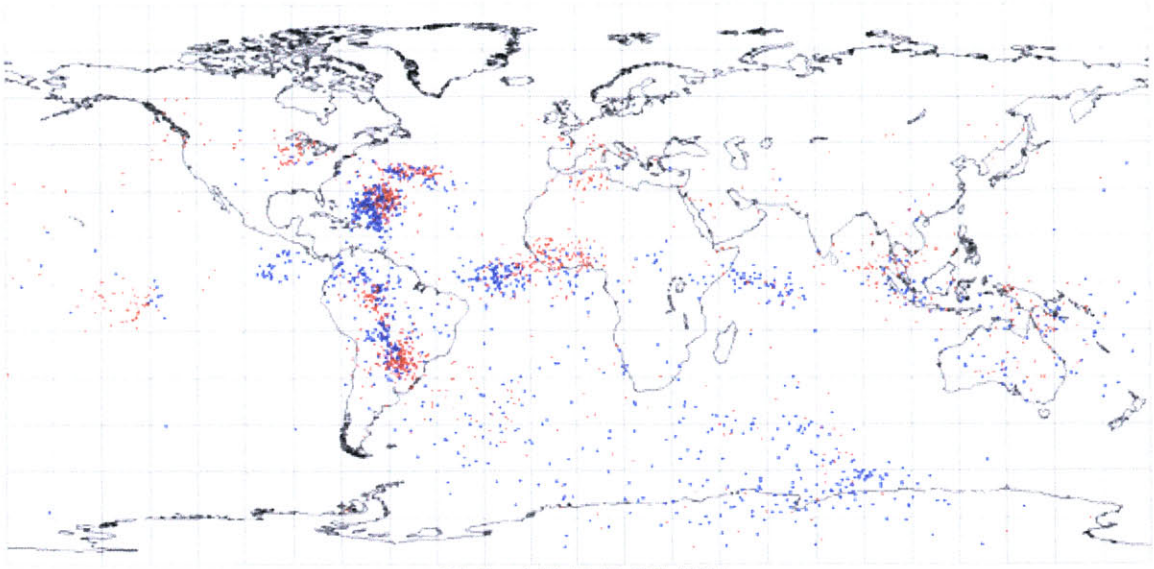

Sat Jan 8 15:41:56 EST 2000

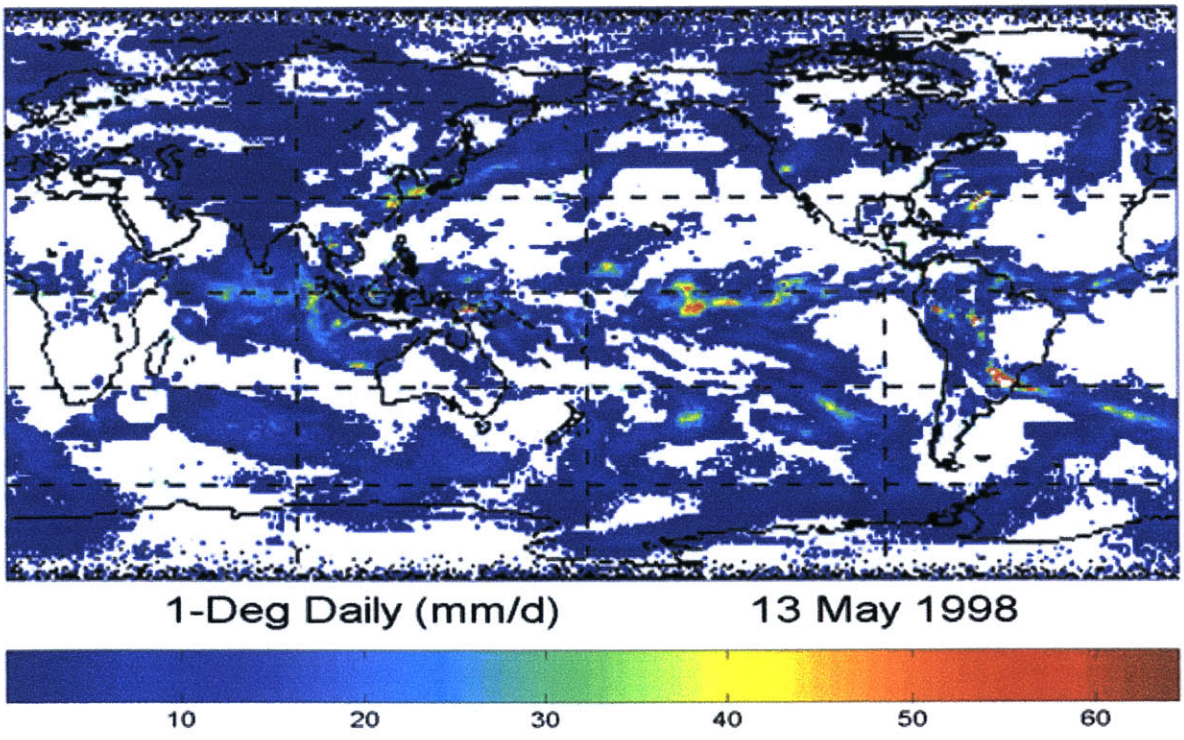

ELF Lightning for May14.txt from West Greenwich, R.I.

Correlation (min) = .5, Max Bearing Error (deg) = 5, Max Range Error (%) = 10
Positives = 1230, Negatives = 1068, Total = 2298
< >

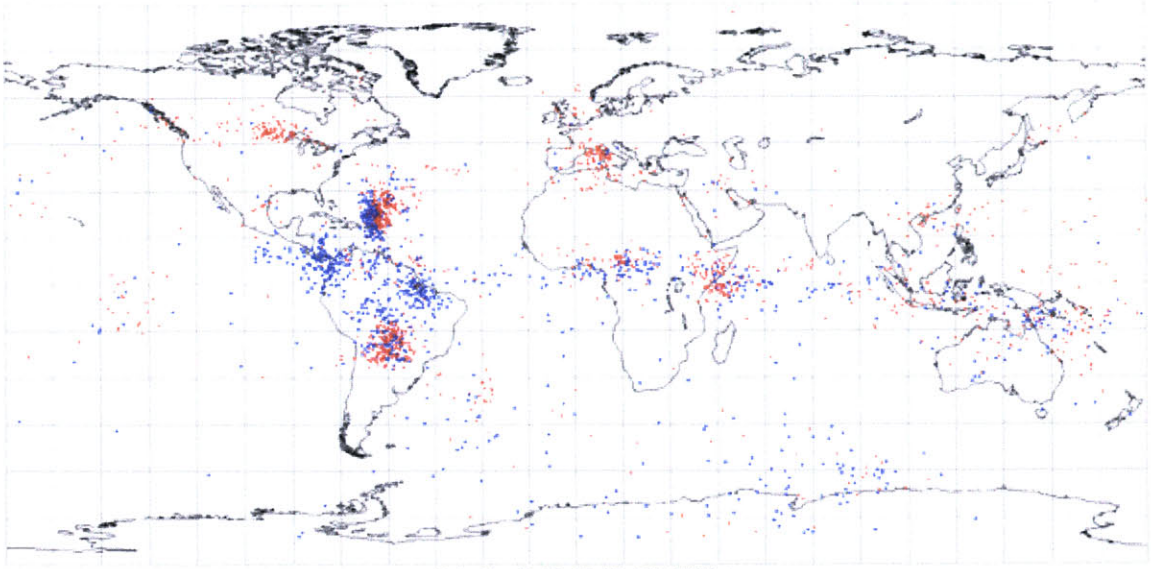

Sat Jan 8 15:42:35 EST 2000

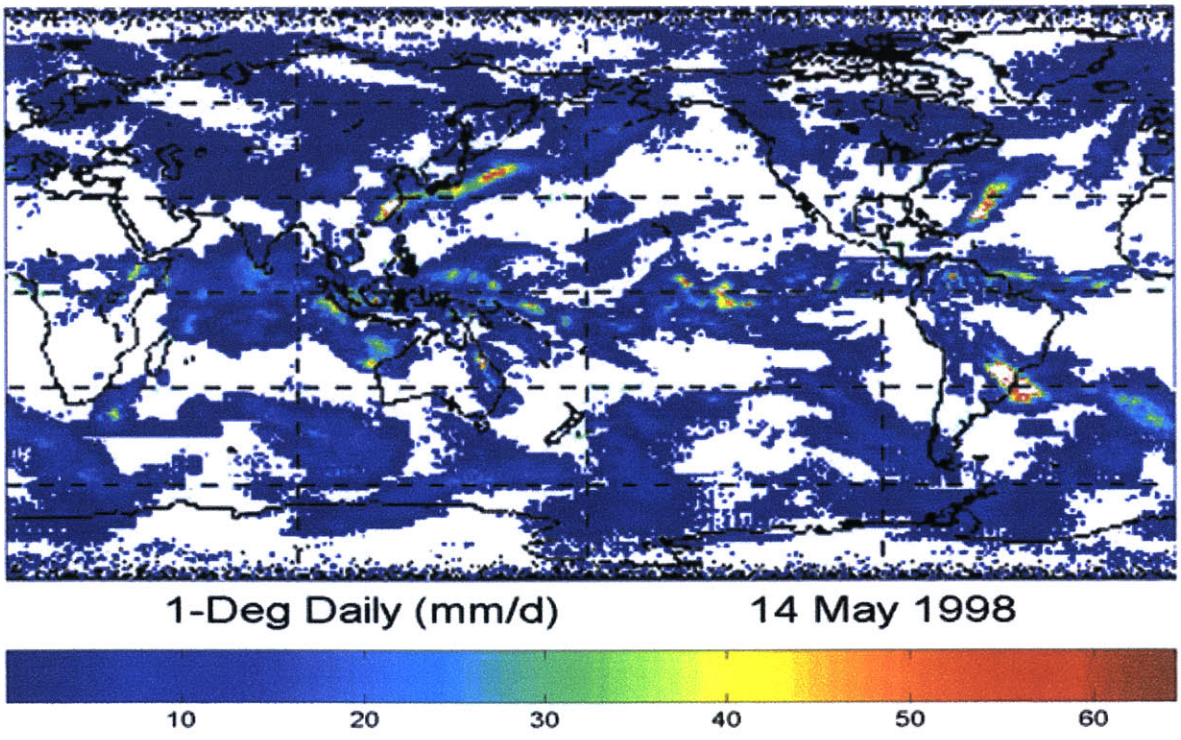

ELF Lightning for May15.txt from West Greenwich, R.I.

Correlation (min) = .5, Max Bearing Error (deg) = 5, Max Range Error (%) = 10
Positives = 1469, Negatives = 988, Total = 2457

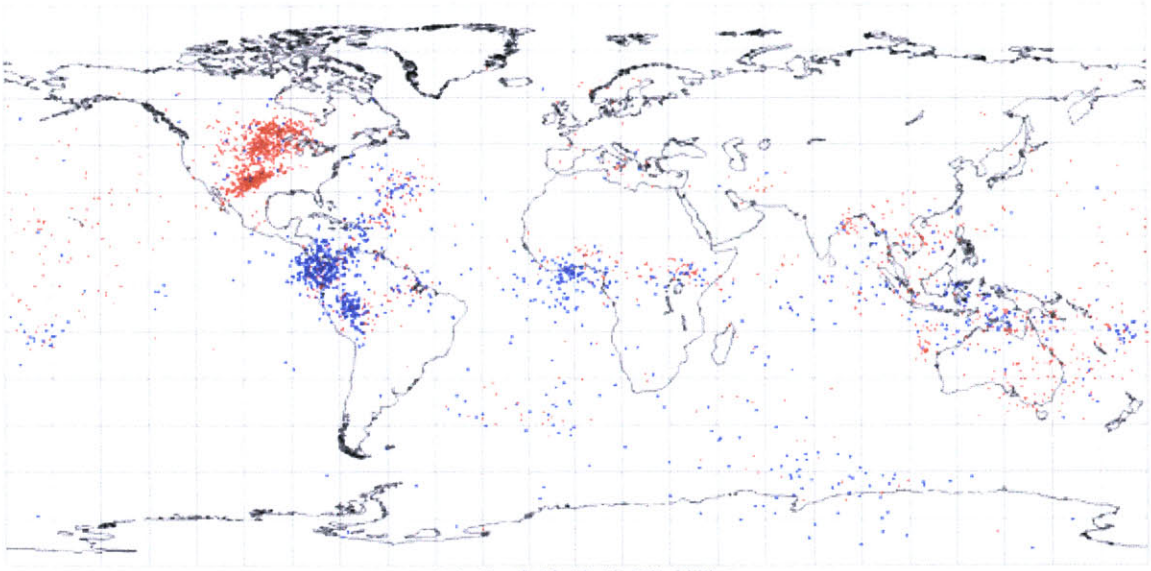

Sat Jan 8 15:43:18 EST 2000

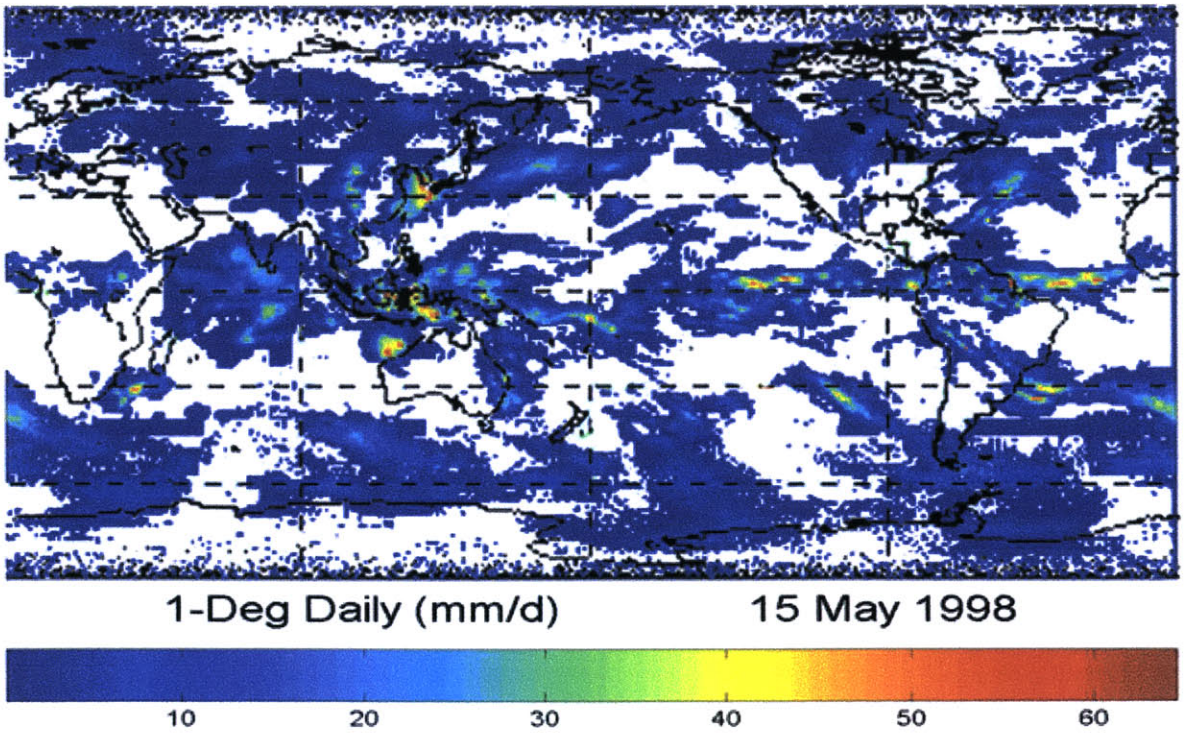

ELF Lightning for May16.txt from West Greenwich, R.I.

Correlation (min) = .5, Max Bearing Error (deg) = 5, Max Range Error (%) = 10
Positives = 1175, Negatives = 901, Total = 2076

< >

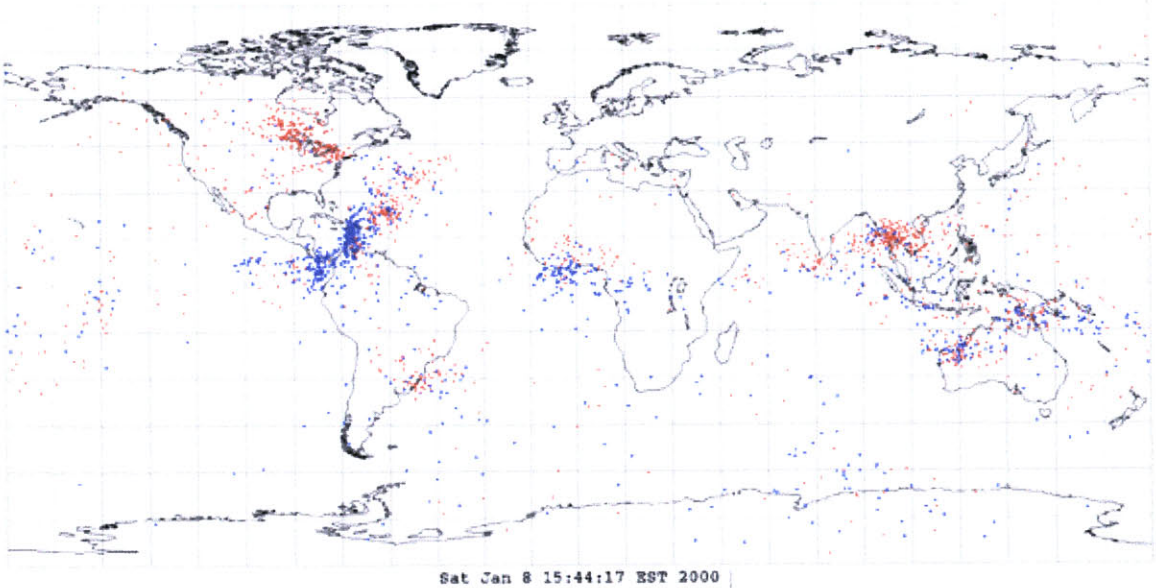

Sat Jan 8 15:44:17 EST 2000

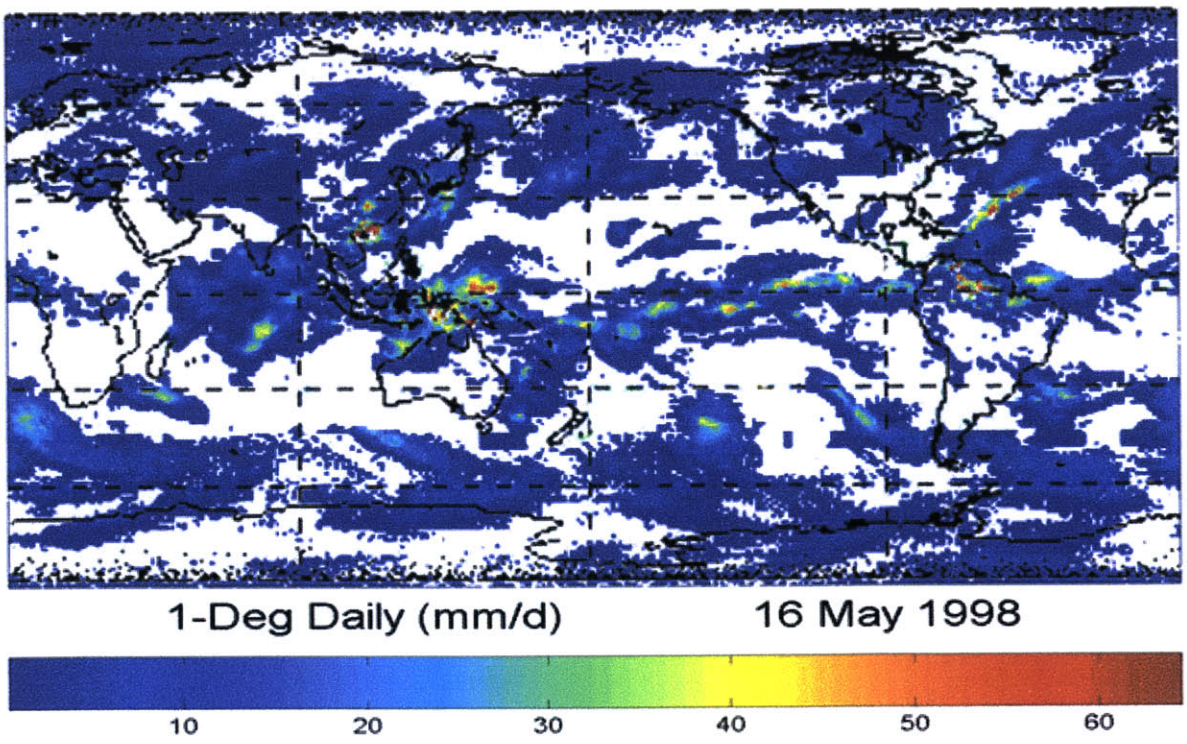

ELF Lightning for May17.txt from West Greenwich, R.I.

Correlation (min) = .5, Max Bearing Error (deg) = 5, Max Range Error (%) = 10
Positives = 961, Negatives = 1089, Total = 2050
< >

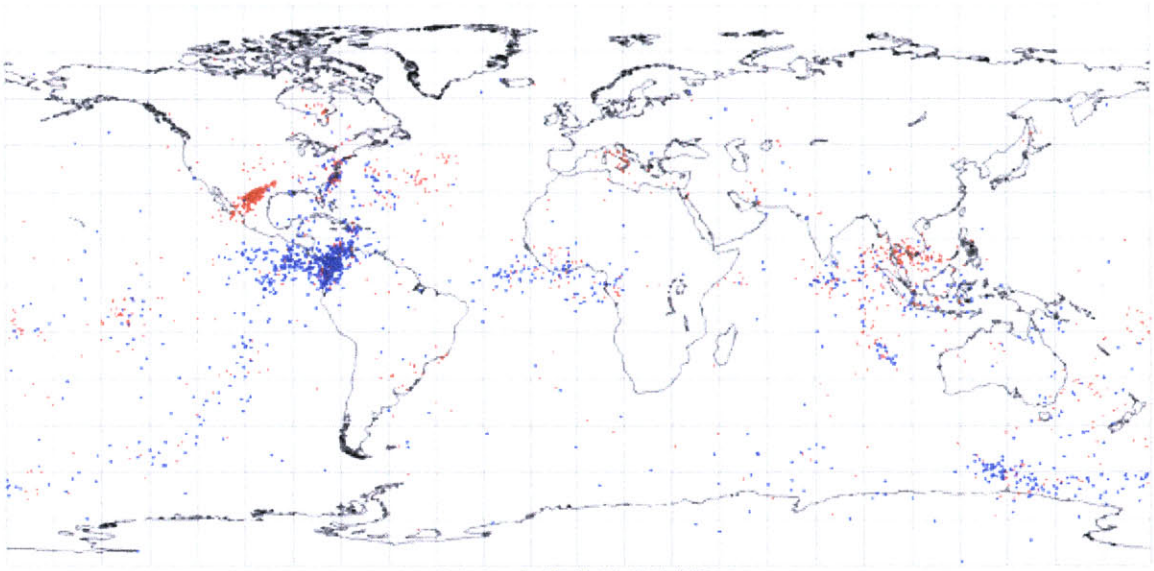

Sat Jan 8 15:45:14 EST 2000

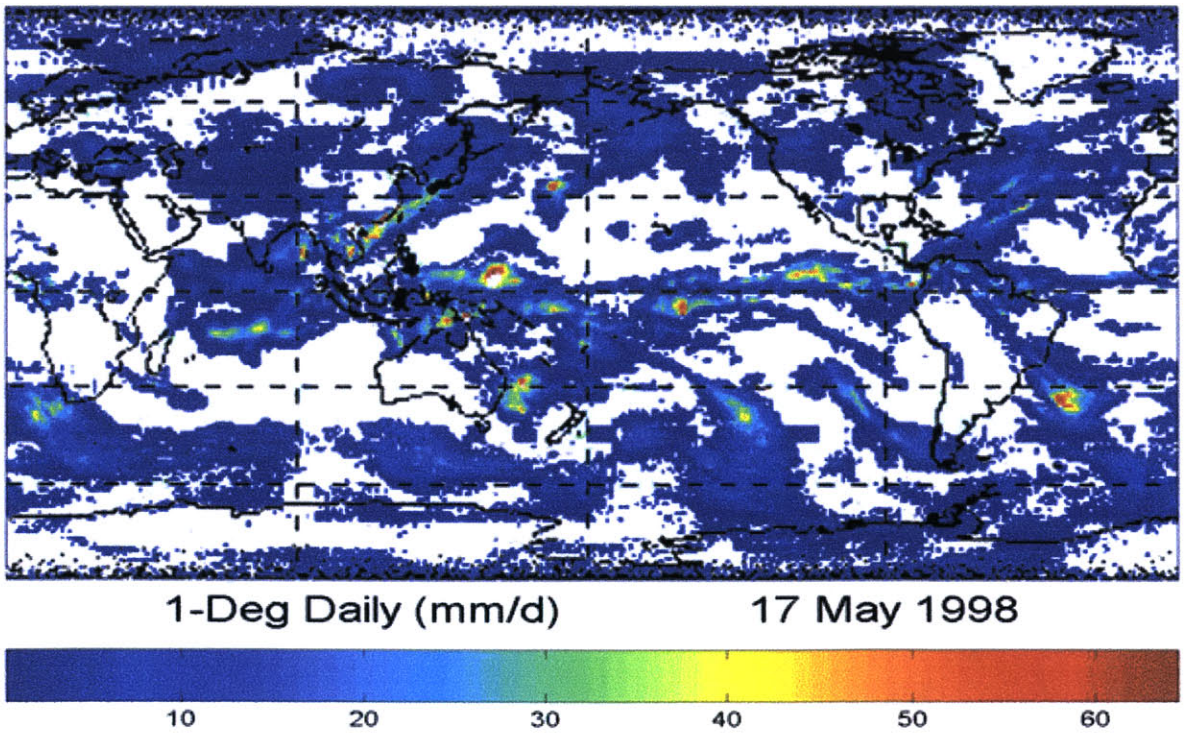

ELF Lightning for May18.txt from West Greenwich, R.I.

Correlation (min) = .5, Max Bearing Error (deg) = 5, Max Range Error (%) = 10
Positives = 803, Negatives = 1042, Total = 1845

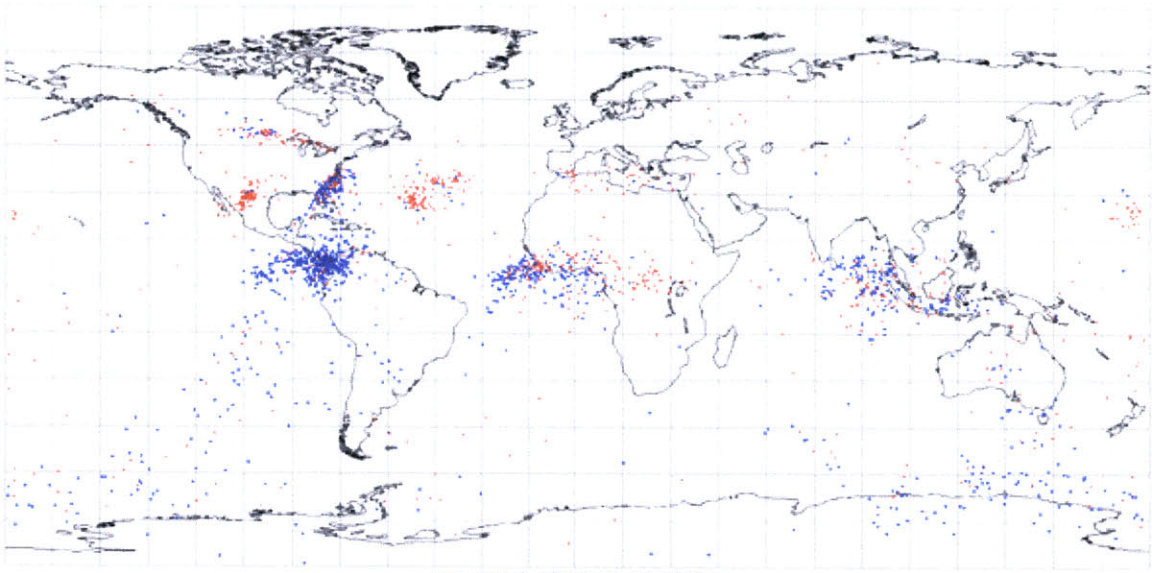

Sat Jan 8 15:46:45 EST 2000

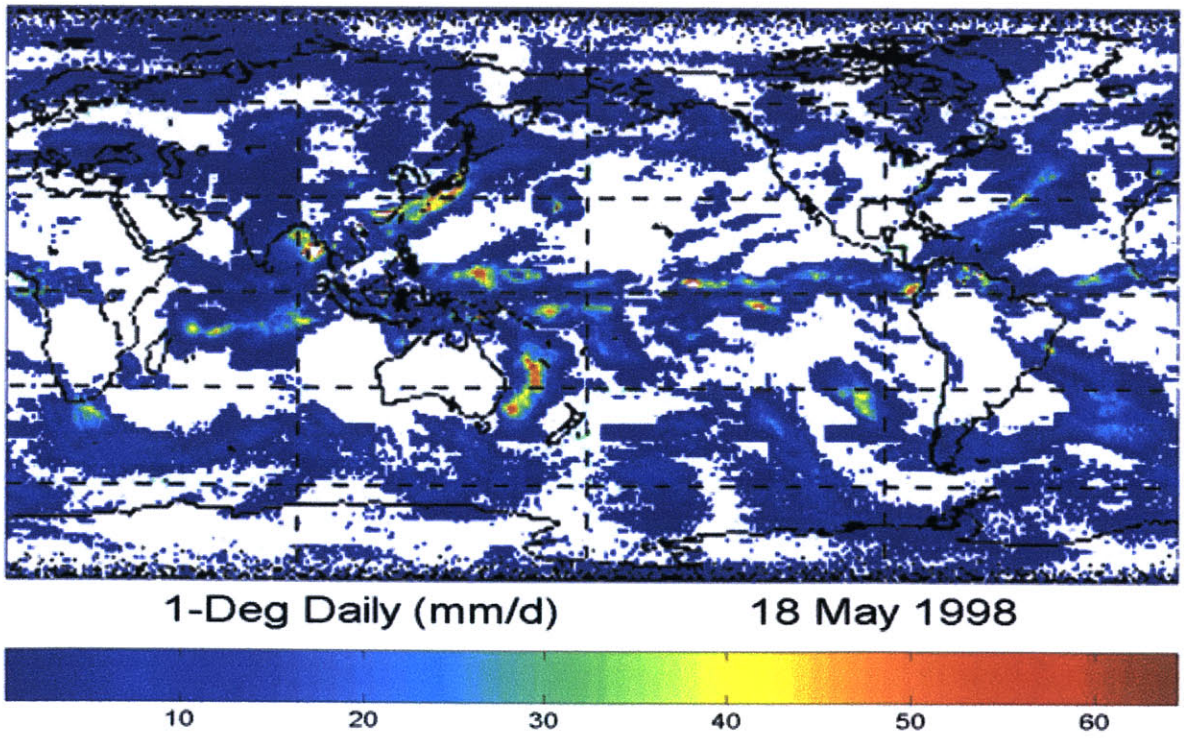

ELF Lightning for May19.txt from West Greenwich, R.I.

Correlation (min) = .5, Max Bearing Error (deg) = 5, Max Range Error (%) = 10
Positives = 1226, Negatives = 894, Total = 2120
< >

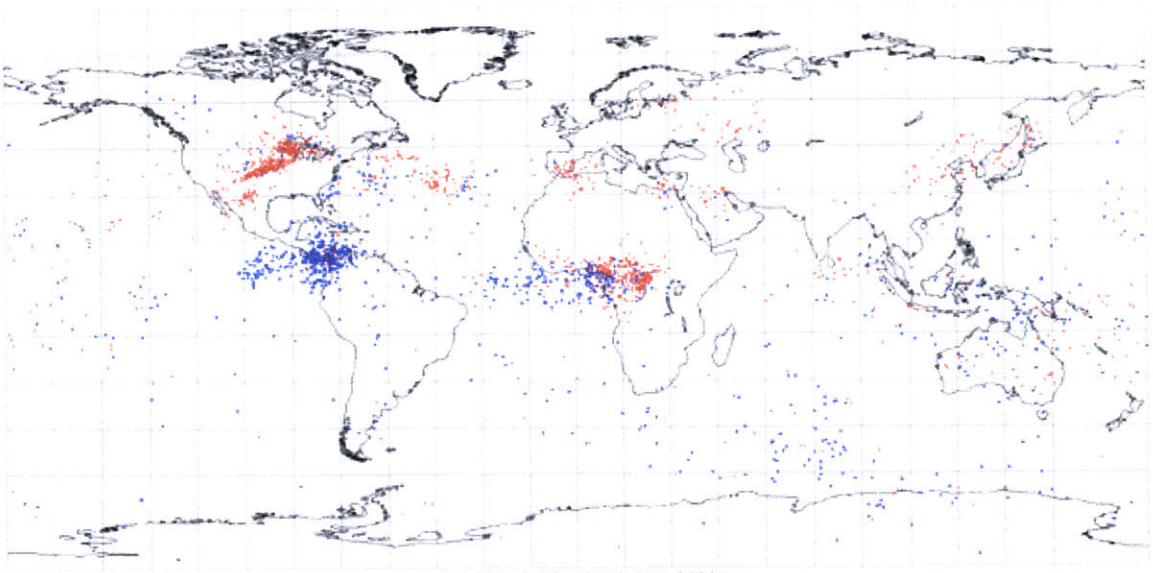

Sat Jan 8 15:47:36 EST 2000

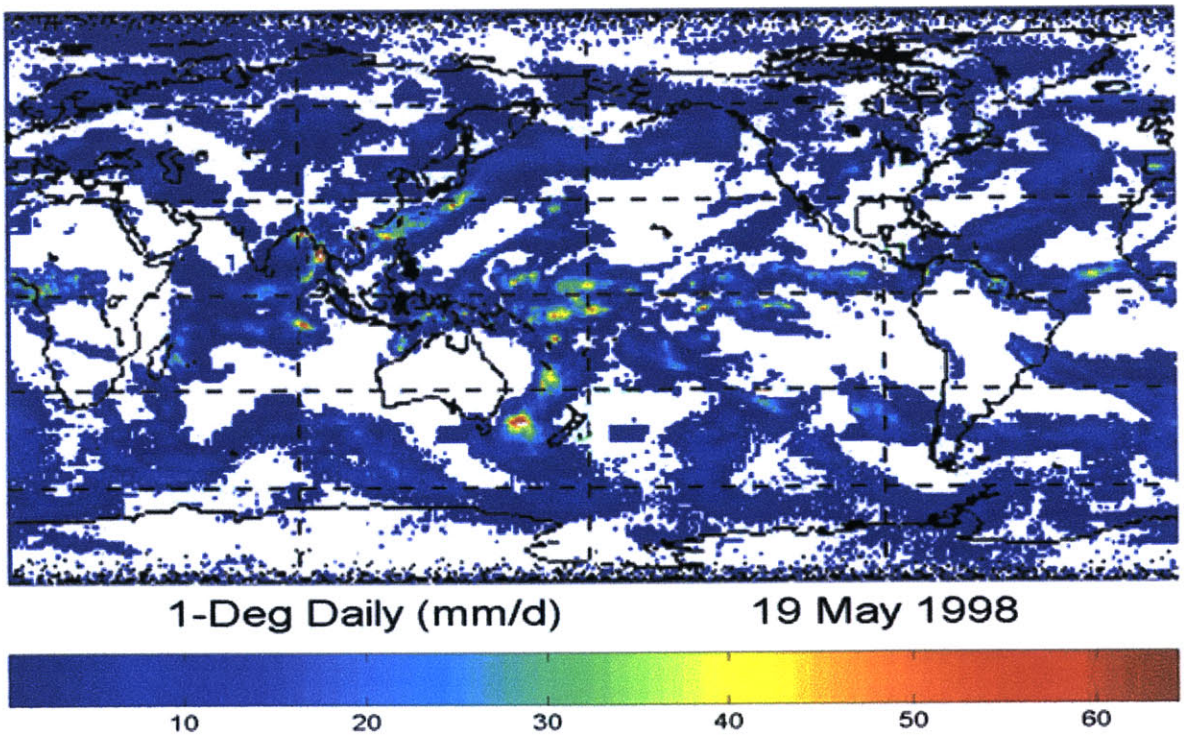

ELF Lightning for May20.txt from West Greenwich, R.I.

Correlation (min) = .5, Max Bearing Error (deg) = 5, Max Range Error (%) = 10
Positives = 1001, Negatives = 906, Total = 1907
< >

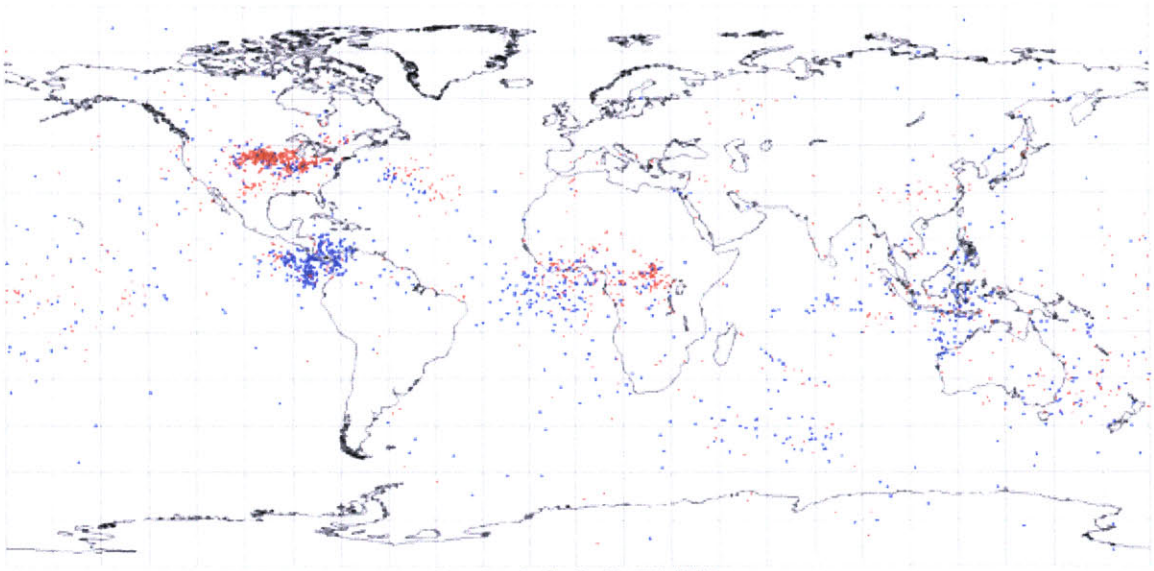

Sat Jan 8 15:48:12 EST 2000

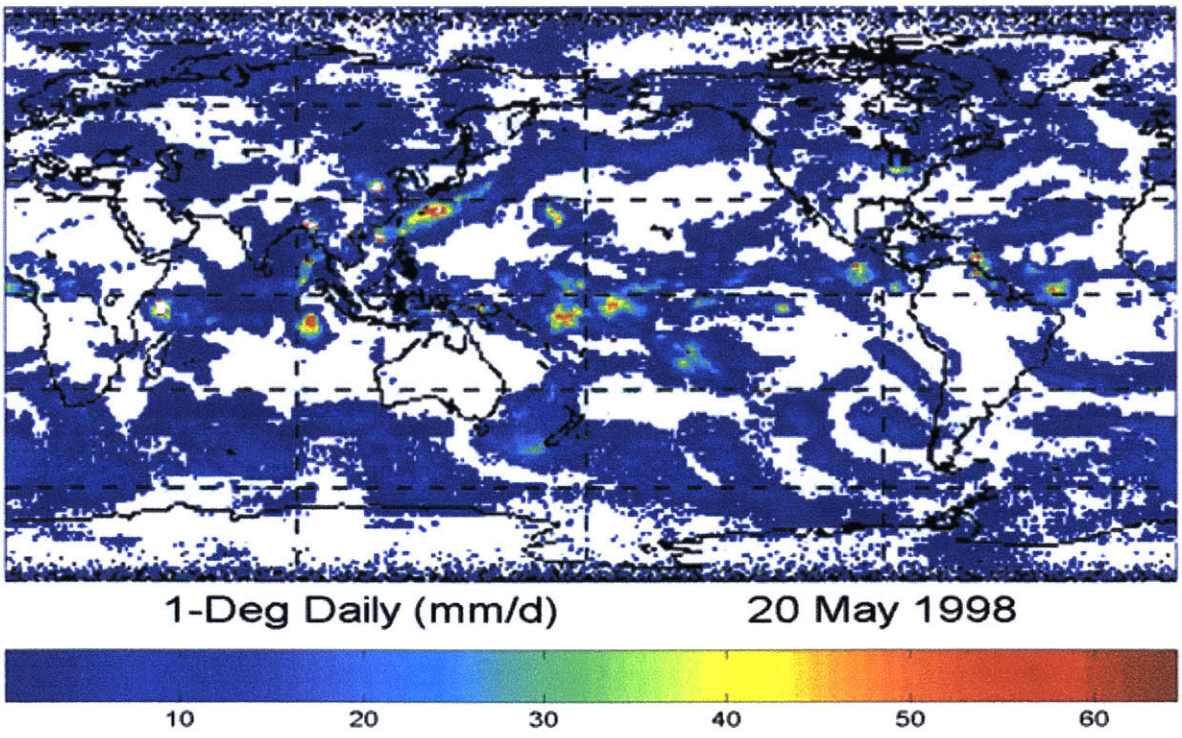

ELF Lightning for May21.txt from West Greenwich, R.I.

Correlation (min) = .5, Max Bearing Error (deg) = 5, Max Range Error (%) = 10
Positives = 837, Negatives = 833, Total = 1670
< >

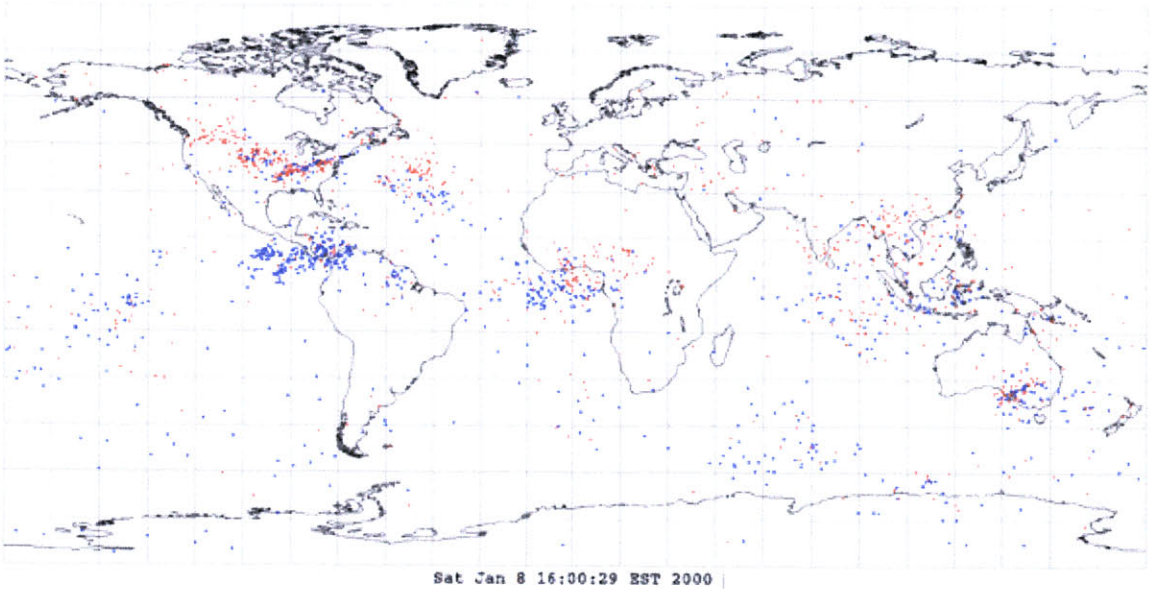

Sat Jan 8 16:00:29 EST 2000

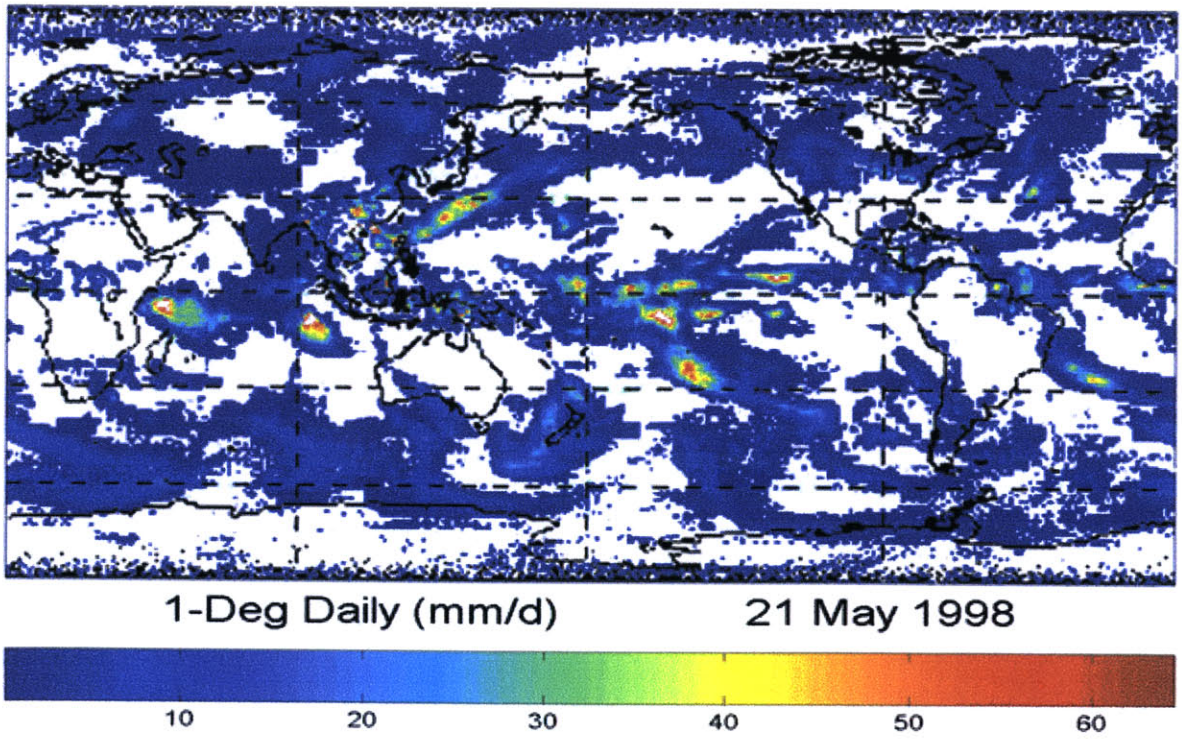

ELF Lightning for May22.txt from West Greenwich, R.I.

Correlation (min) = .5, Max Bearing Error (deg) = 5, Max Range Error (%) = 10
Positives = 742, Negatives = 1110, Total = 1852

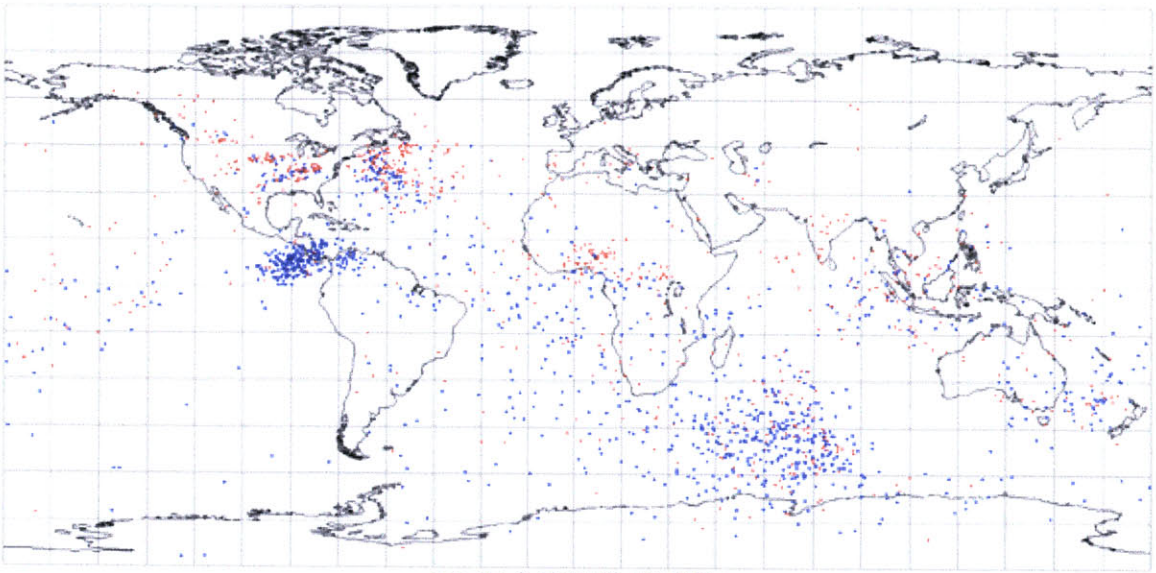

Sat Jan 8 16:01:47 EST 2000

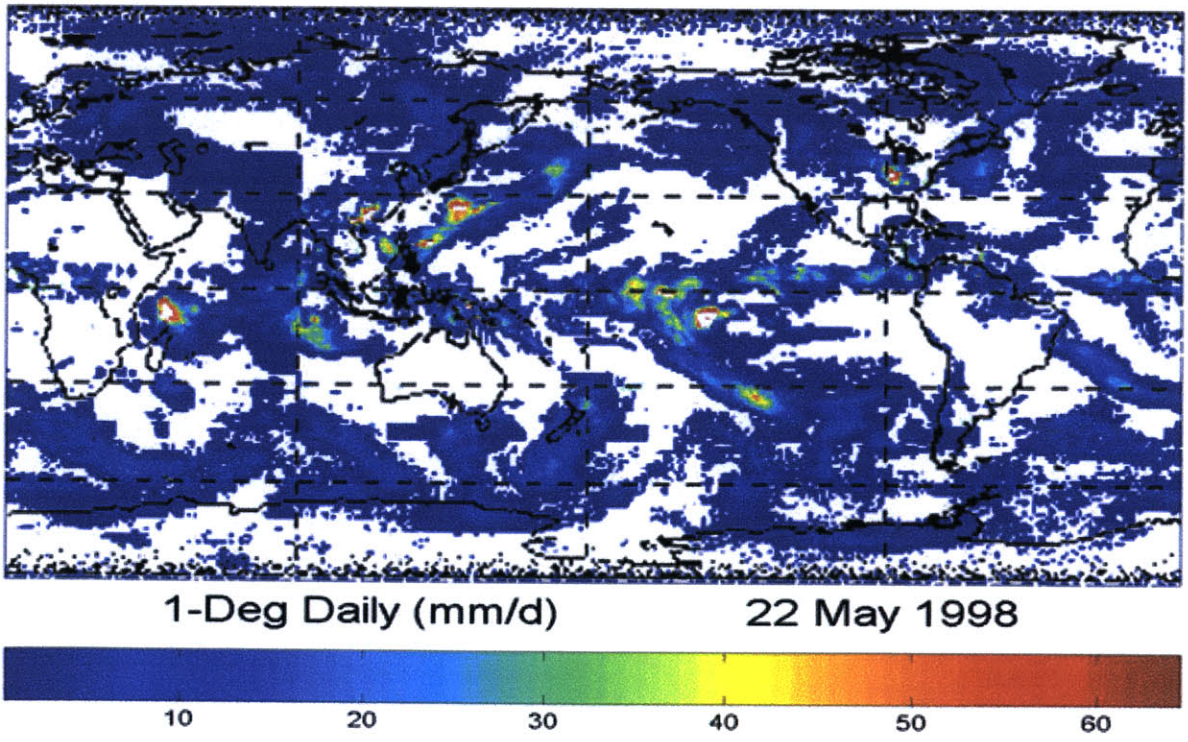

ELF Lightning for May23.txt from West Greenwich, R.I.

Correlation (min) = .5, Max Bearing Error (deg) = 5, Max Range Error (%) = 10
Positives = 876, Negatives = 1174, Total = 2050
< >

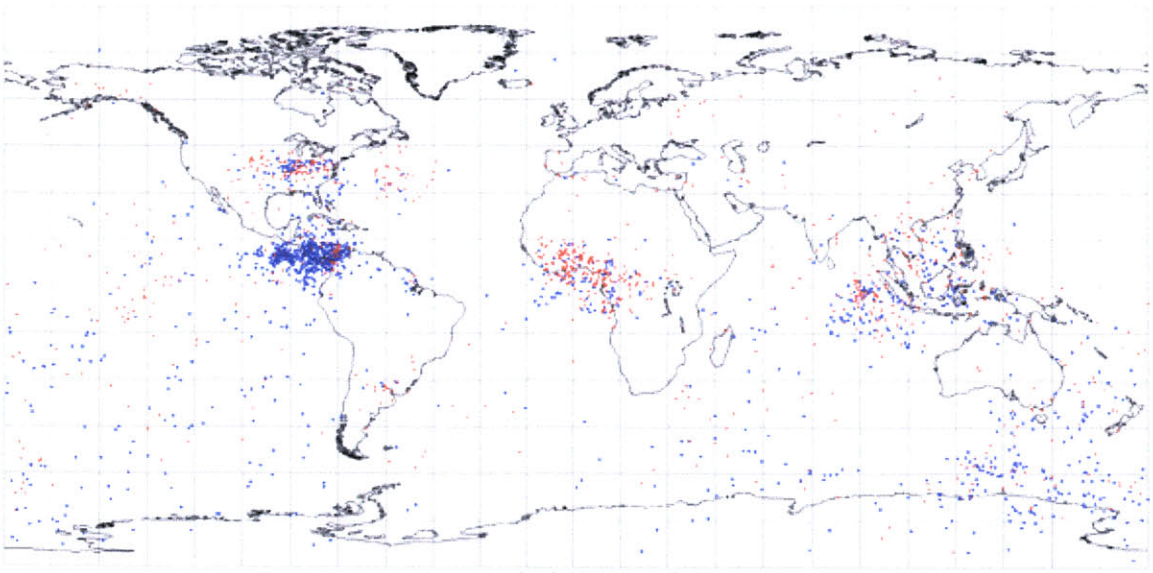

Sat Jan 8 16:23:34 EST 2000

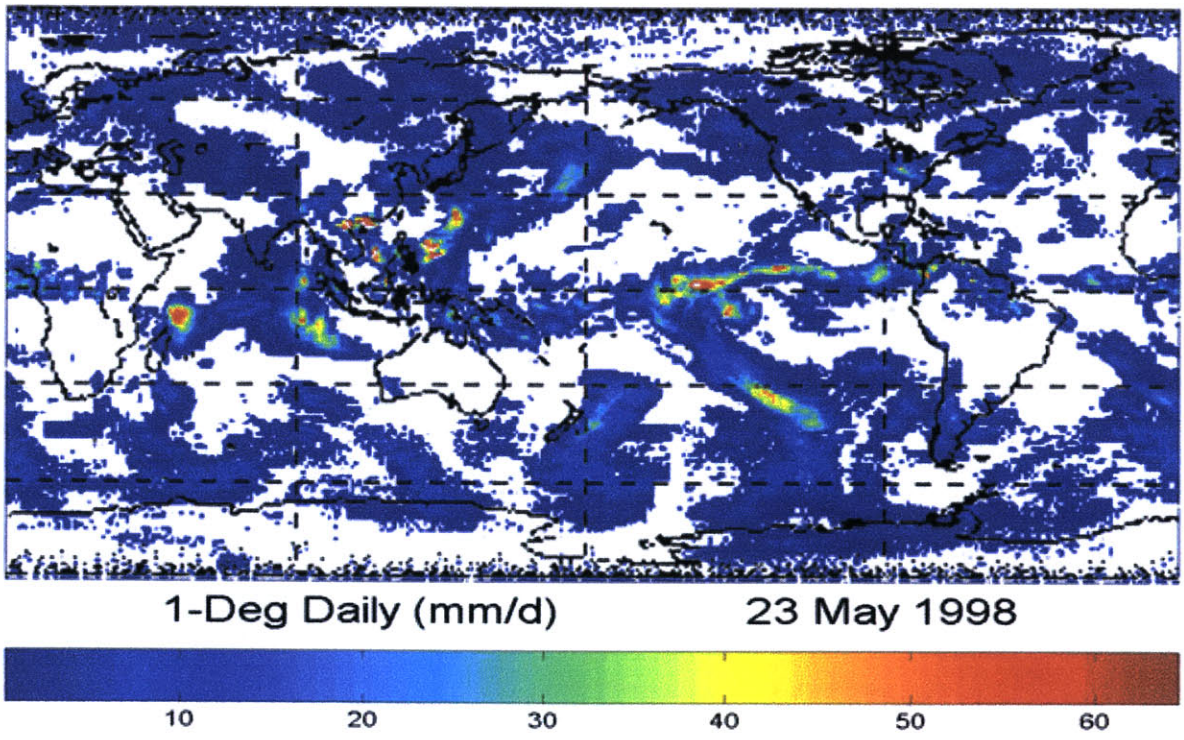

ELF Lightning for May24.txt from West Greenwich, R.I.

Correlation (min) = .5, Max Bearing Error (deg) = 5, Max Range Error (%) = 10
Positives = 1074, Negatives = 916, Total = 1990

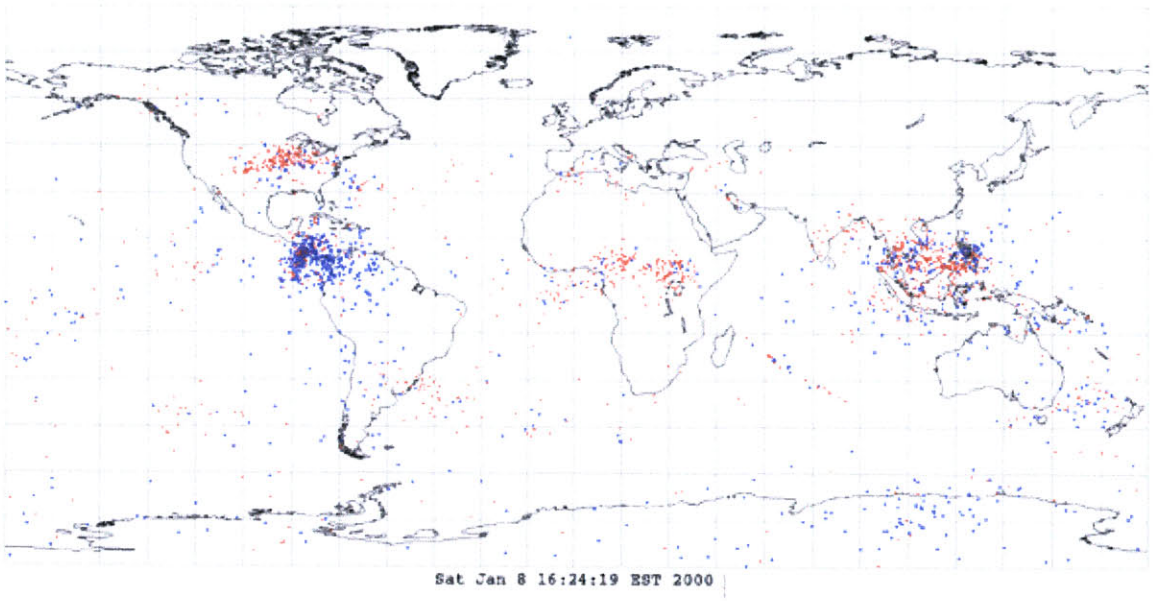

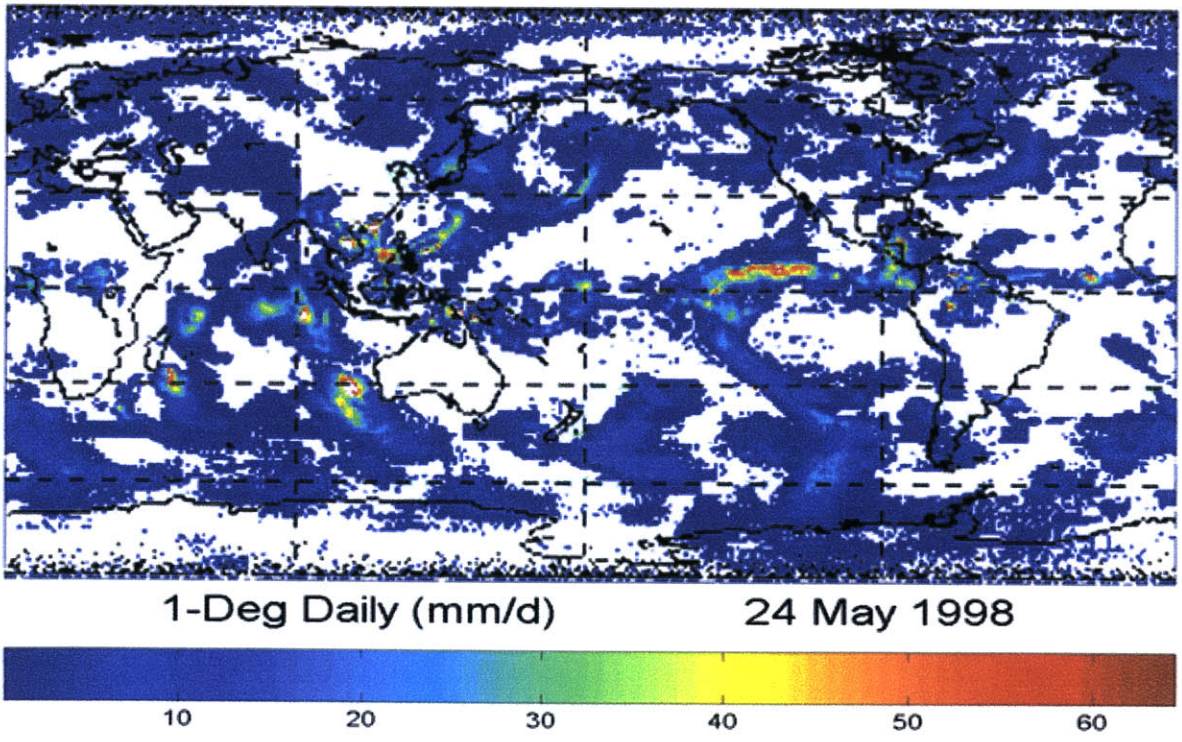

ELF Lightning for May25.txt from West Greenwich, R.I.

Correlation (min) = .5, Max Bearing Error (deg) = 5, Max Range Error (%) = 10
Positives = 1585, Negatives = 1256, Total = 2841
< >

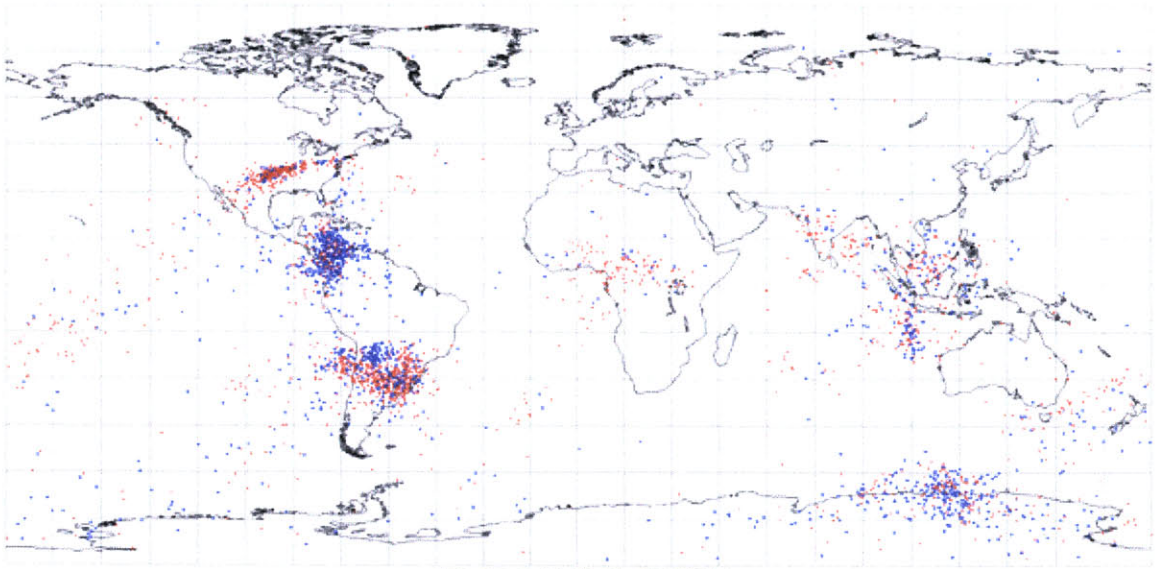

Sat Jan 8 16:25:16 EST 2000

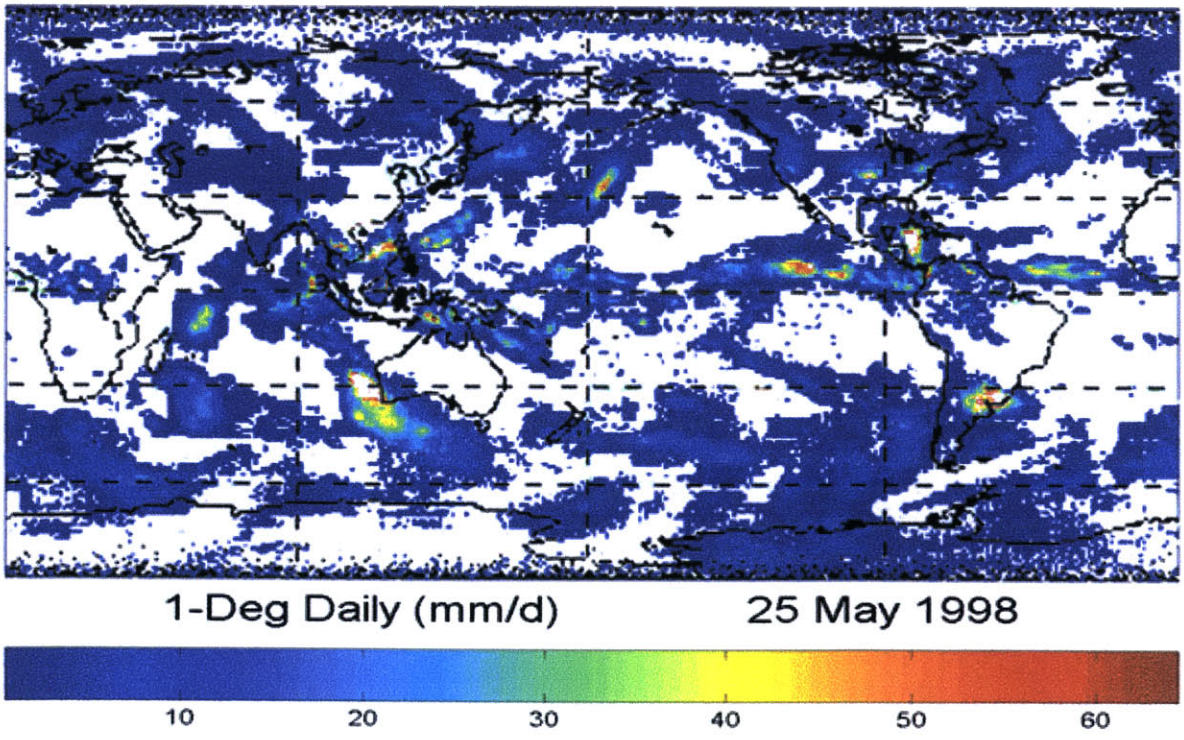

ELF Lightning for May26.txt from West Greenwich, R.I.

Correlation (min) = .5, Max Bearing Error (deg) = 5, Max Range Error (%) = 10
Positives = 1248, Negatives = 969, Total = 2217
< >

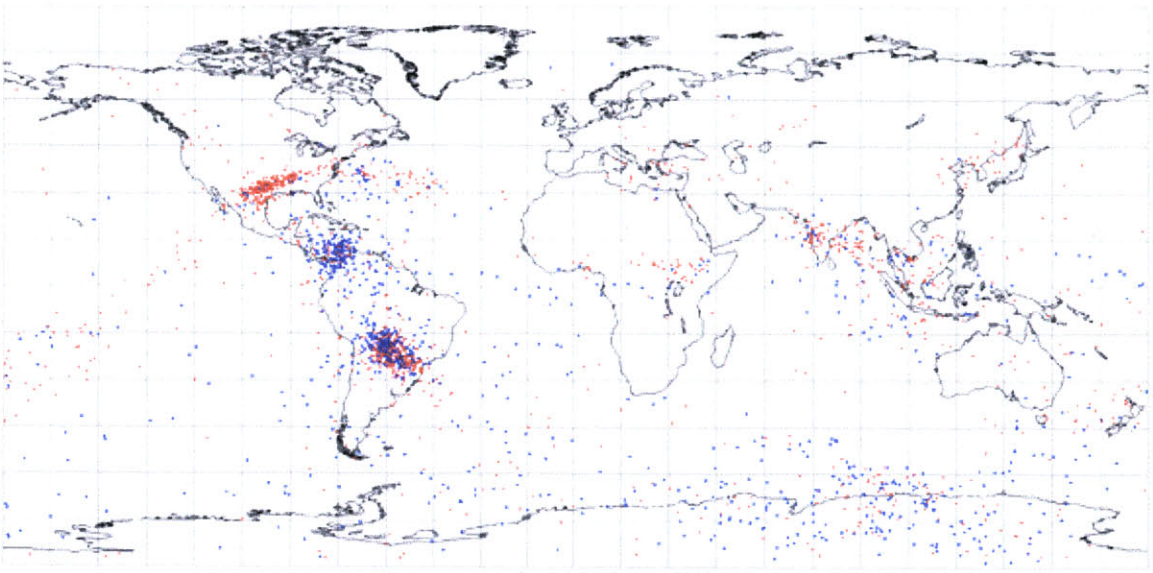

Sat Jan 8 16:26:22 EST 2000

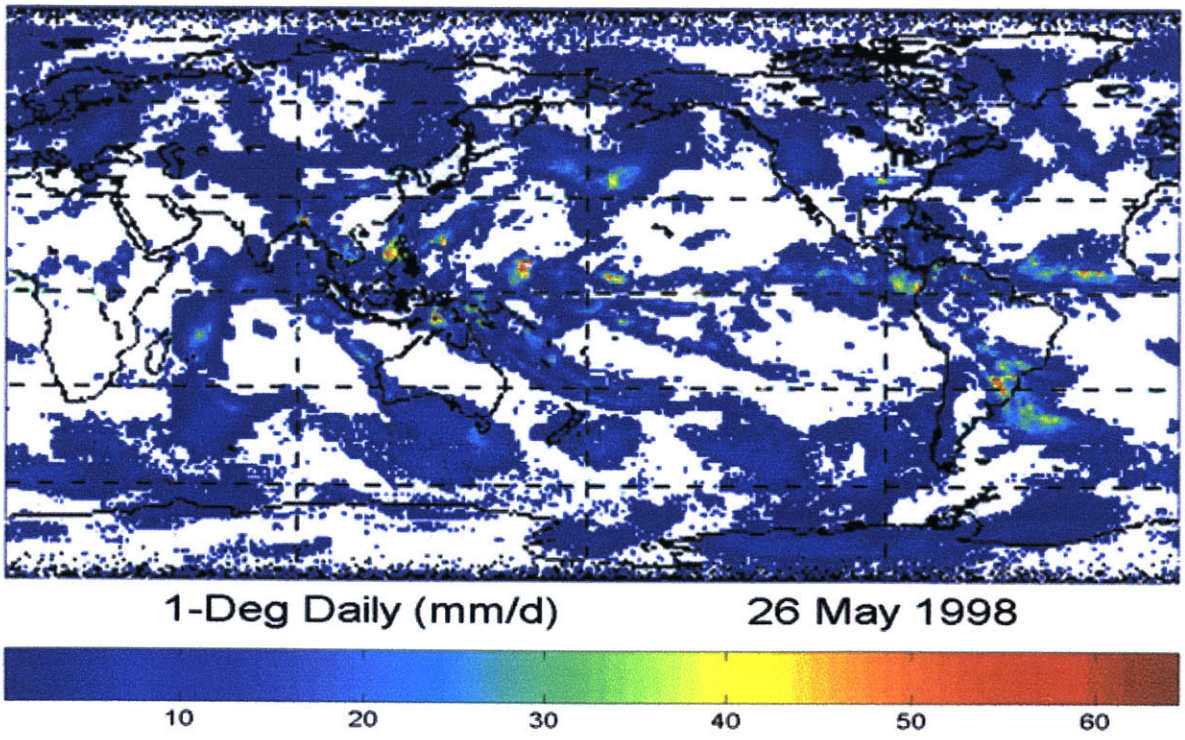

ELF Lightning for May27.txt from West Greenwich, R.I.

Correlation (min) = .5, Max Bearing Error (deg) = 5, Max Range Error (%) = 10
Positives = 1003, Negatives = 748, Total = 1751
< >

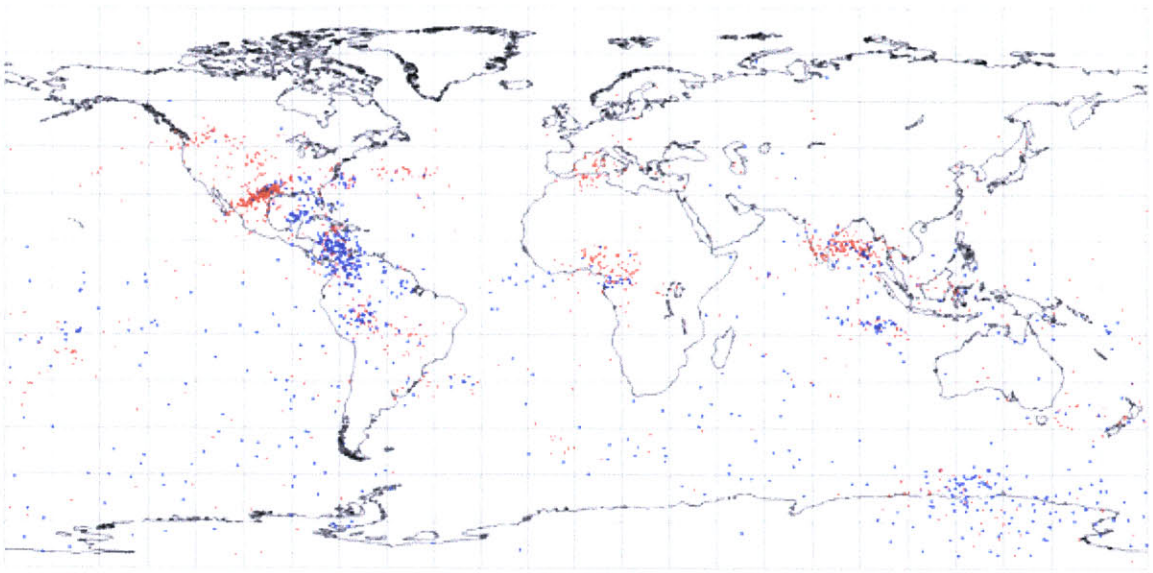

Sat Jan 8 16:36:04 EST 2000

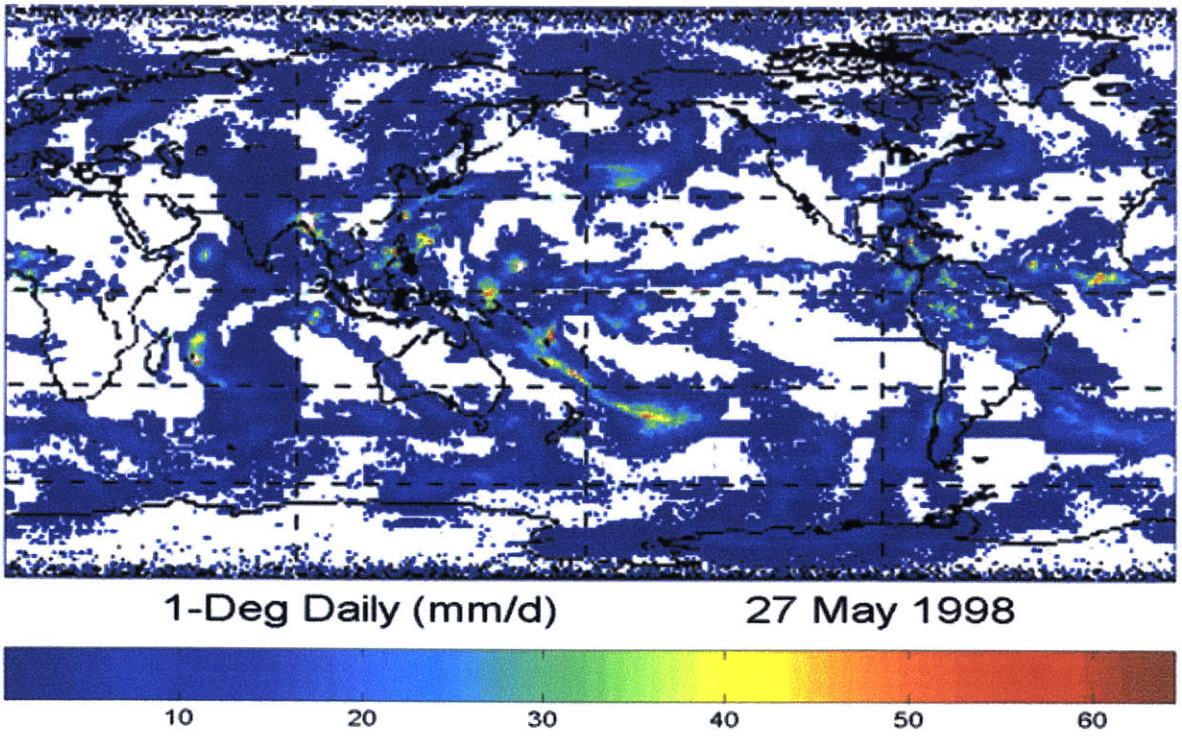

ELF Lightning for May28.txt from West Greenwich, R.I.

Correlation (min) = .5, Max Bearing Error (deg) = 5, Max Range Error (%) = 10
Positives = 832, Negatives = 436, Total = 1268

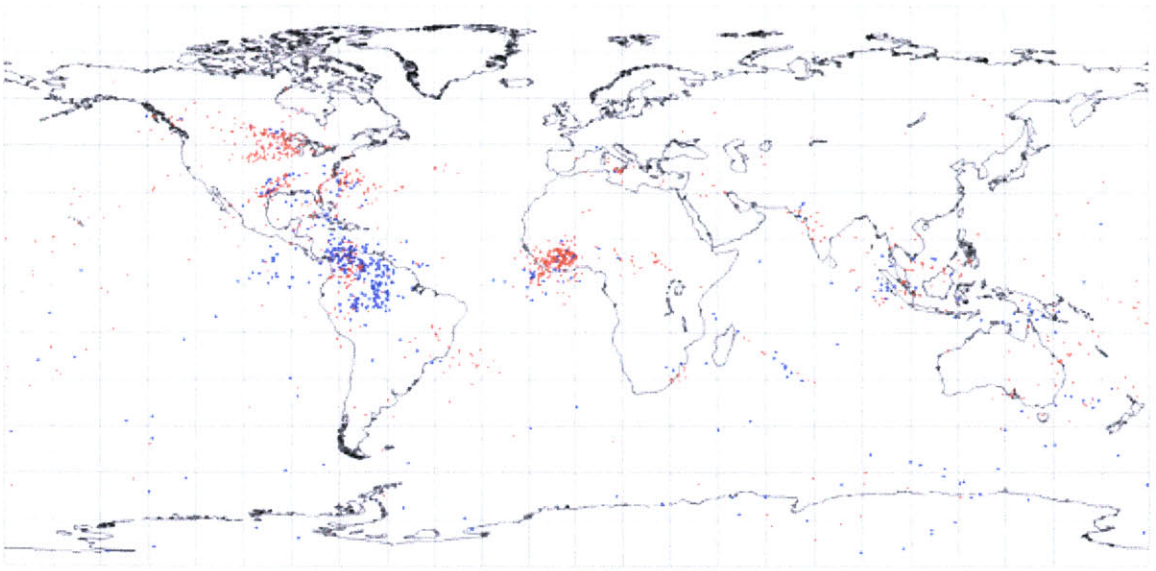

Sat Jan 8 16:37:19 EST 2000

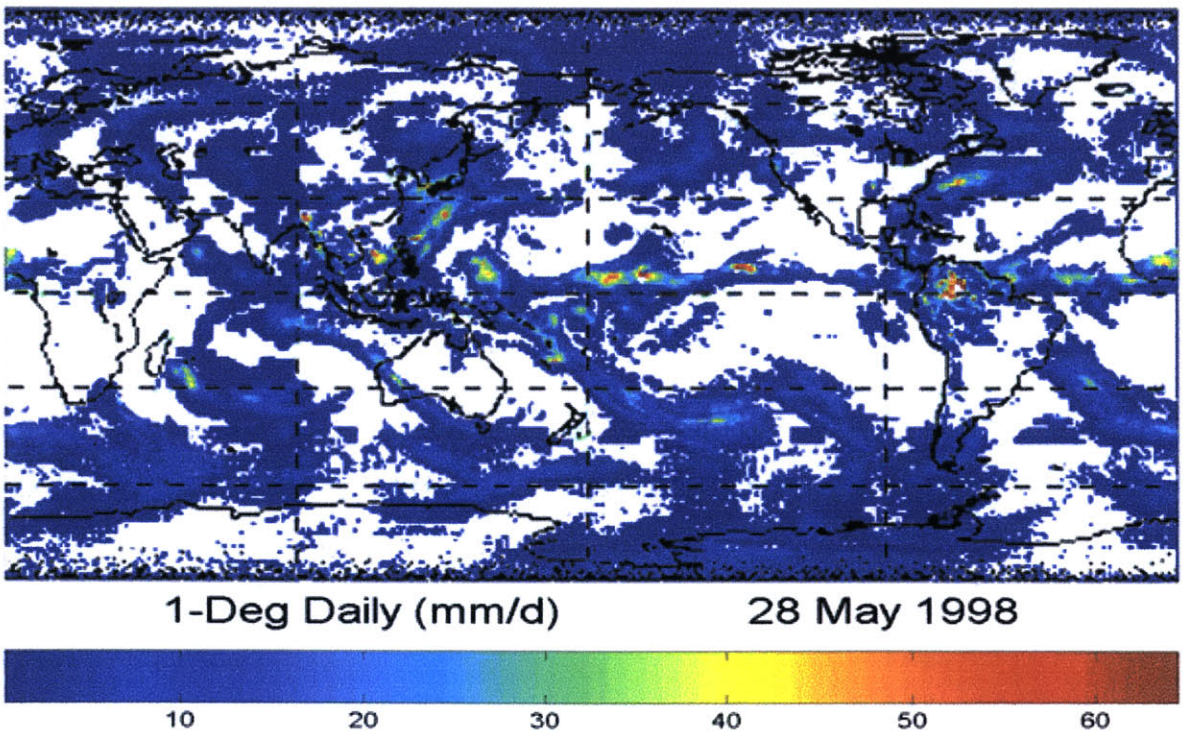

ELF Lightning for May29.txt from West Greenwich, R.I.

Correlation (min) = .5, Max Bearing Error (deg) = 5, Max Range Error (%) = 10
Positives = 1065, Negatives = 861, Total = 1926
< >

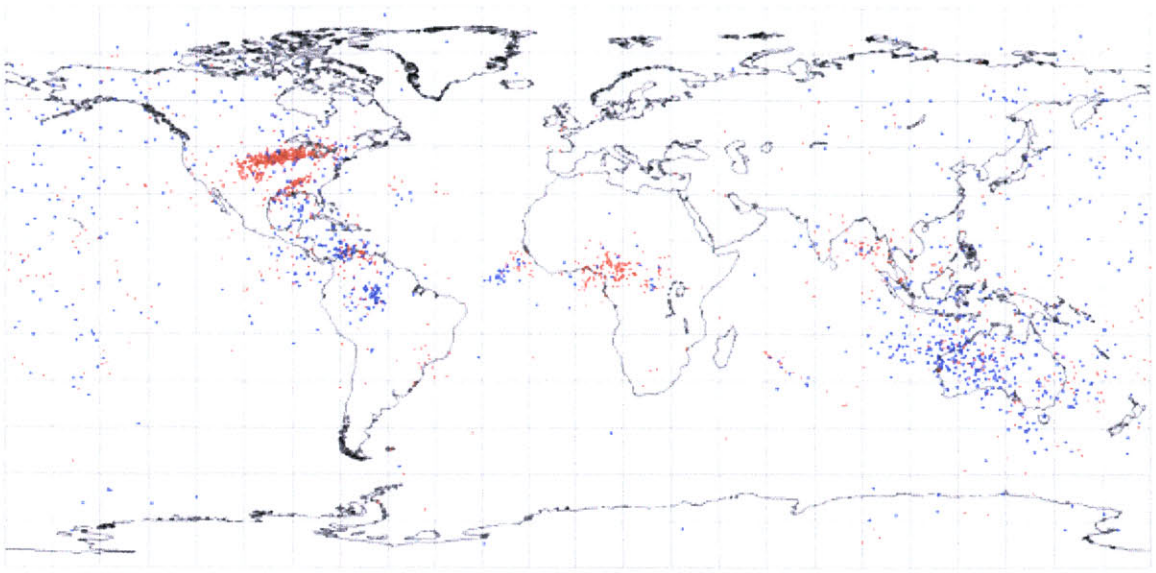

Sat Jan 8 16:37:55 EST 2000

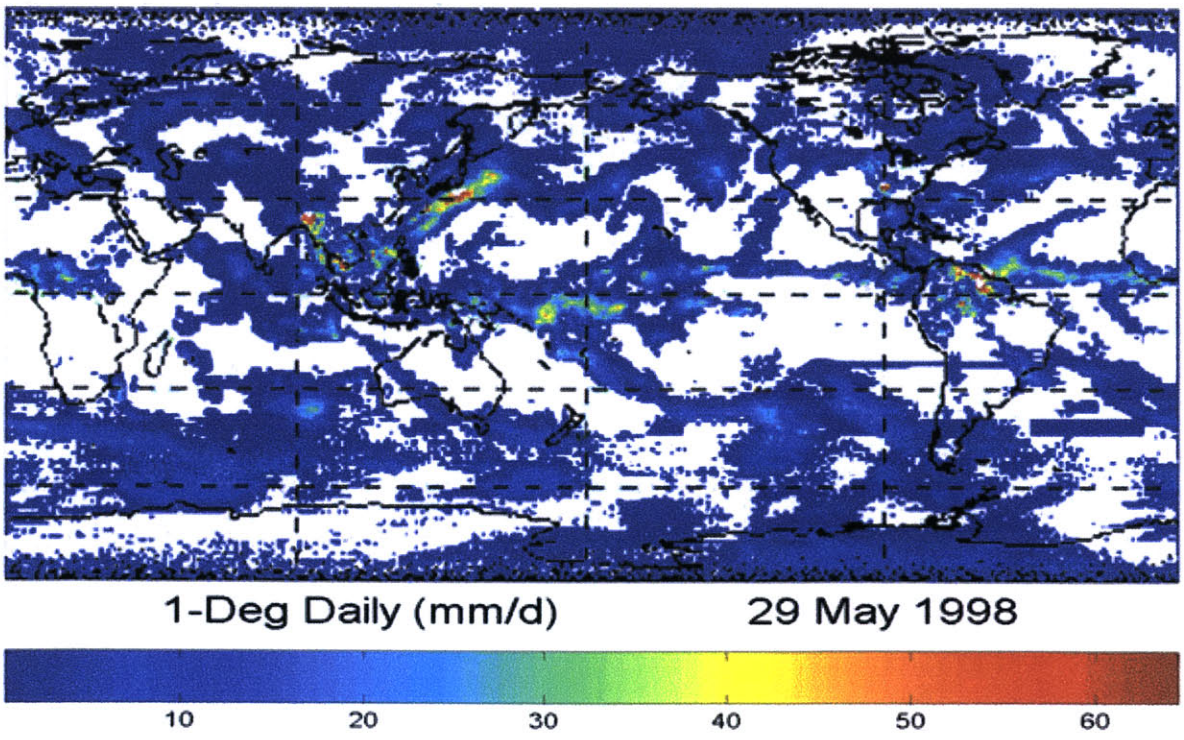

ELF Lightning for May30.txt from West Greenwich, R.I.

Correlation (min) = .5, Max Bearing Error (deg) = 5, Max Range Error (%) = 10
Positives = 421, Negatives = 363, Total = 784

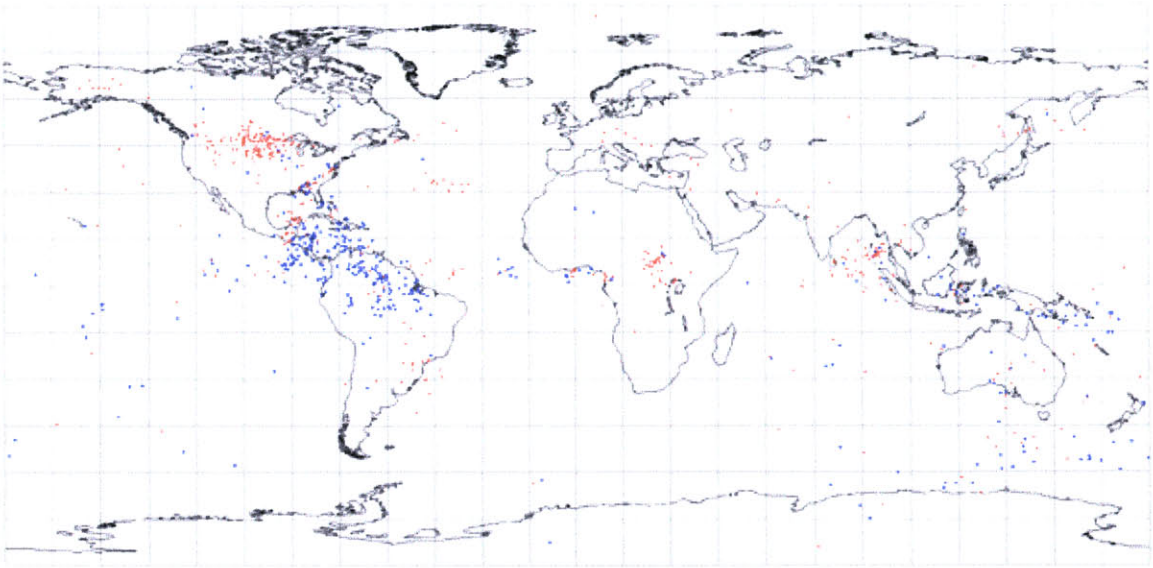

Sat Jan 8 16:39:18 EST 2000

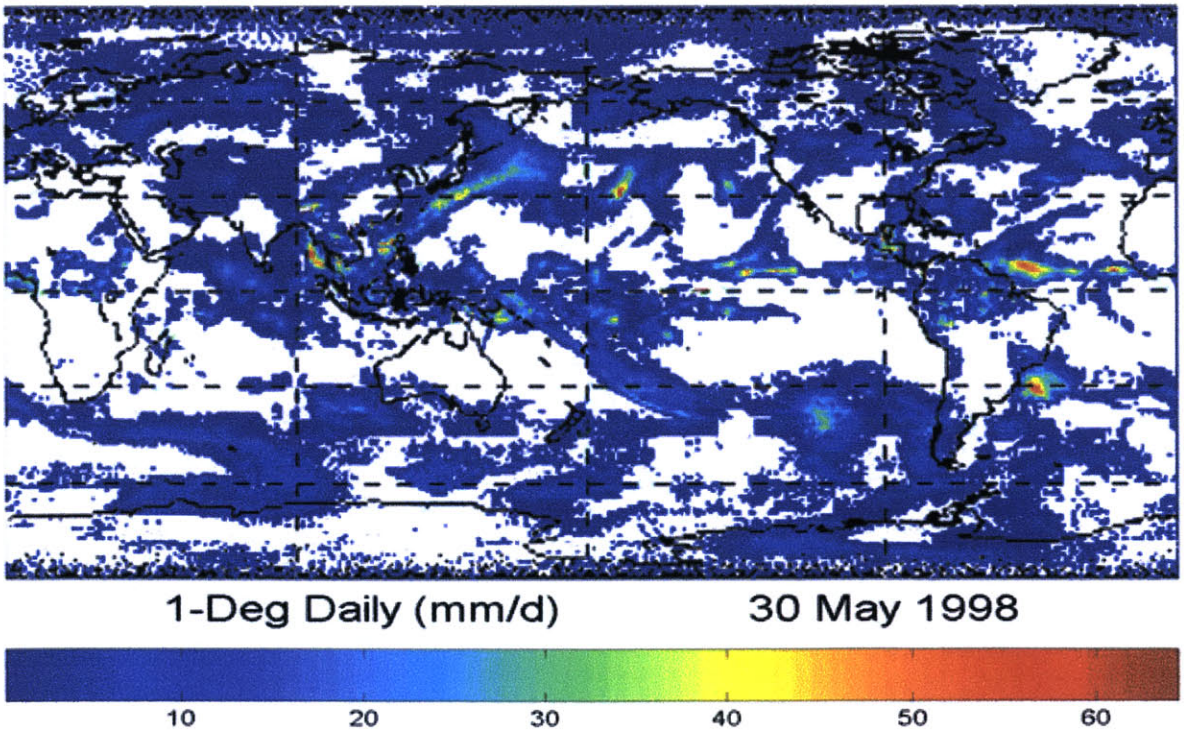

ELF Lightning for May31.txt from West Greenwich, R.I.

Correlation (min) = .5, Max Bearing Error (deg) = 5, Max Range Error (%) = 10
Positives = 1275, Negatives = 1216, Total = 2491
< >

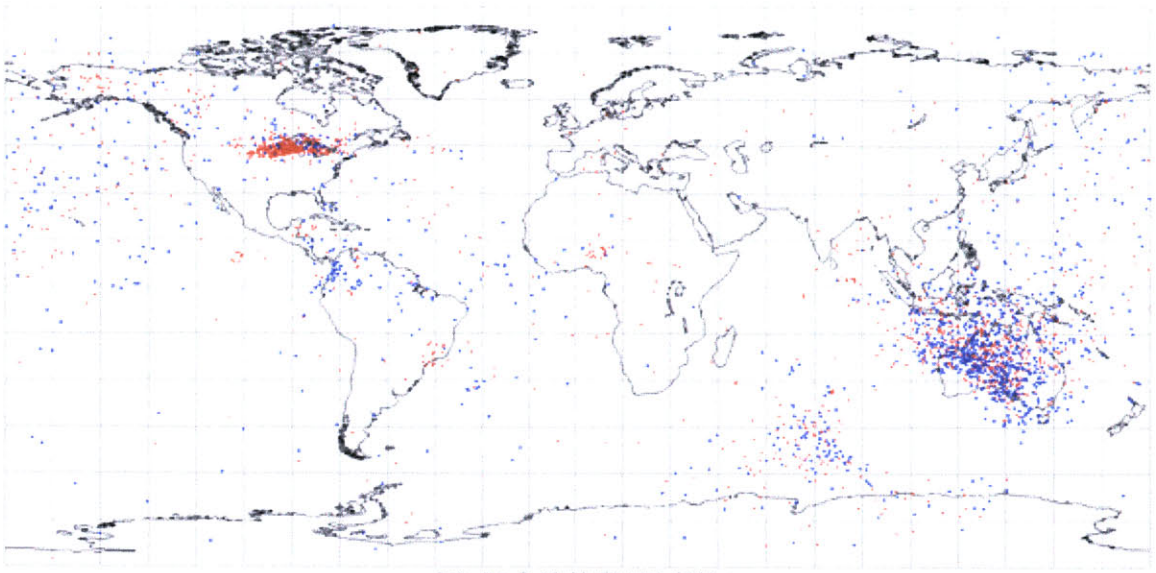

Sat Jan 8 16:39:59 EST 2000

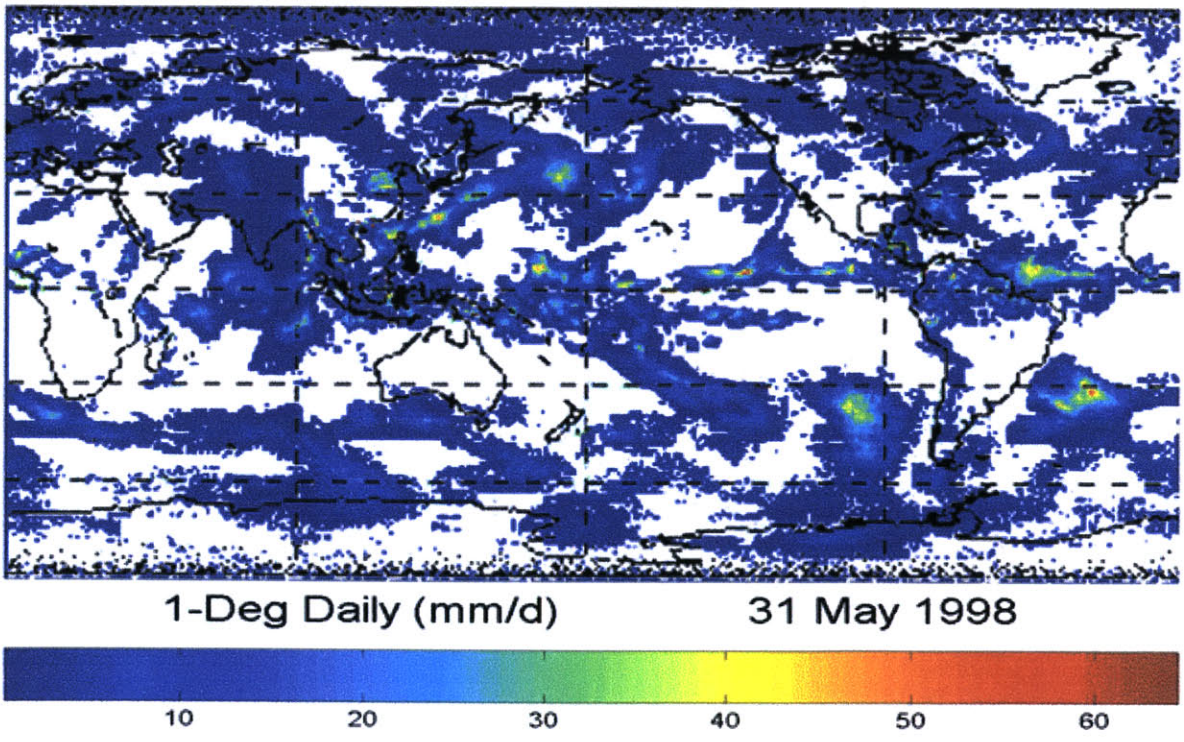

ELF Lightning for June1.txt from West Greenwich, R.I.

Correlation (min) = .5, Max Bearing Error (deg) = 5, Max Range Error (%) = 10
Positives = 1642, Negatives = 1753, Total = 3395
< >

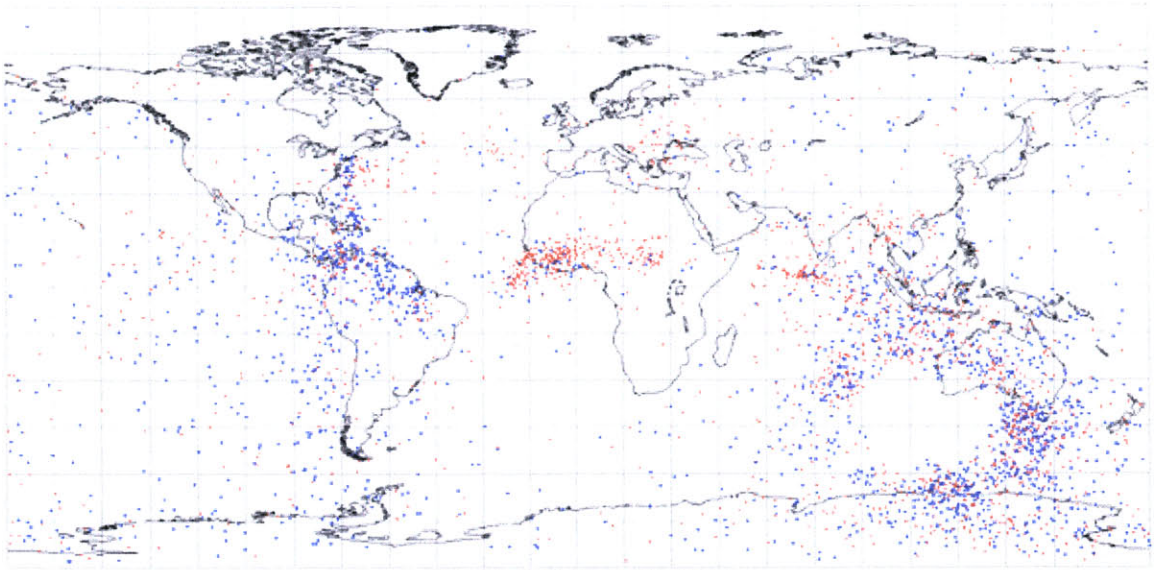

Sun Jan 9 17:19:50 EST 2000

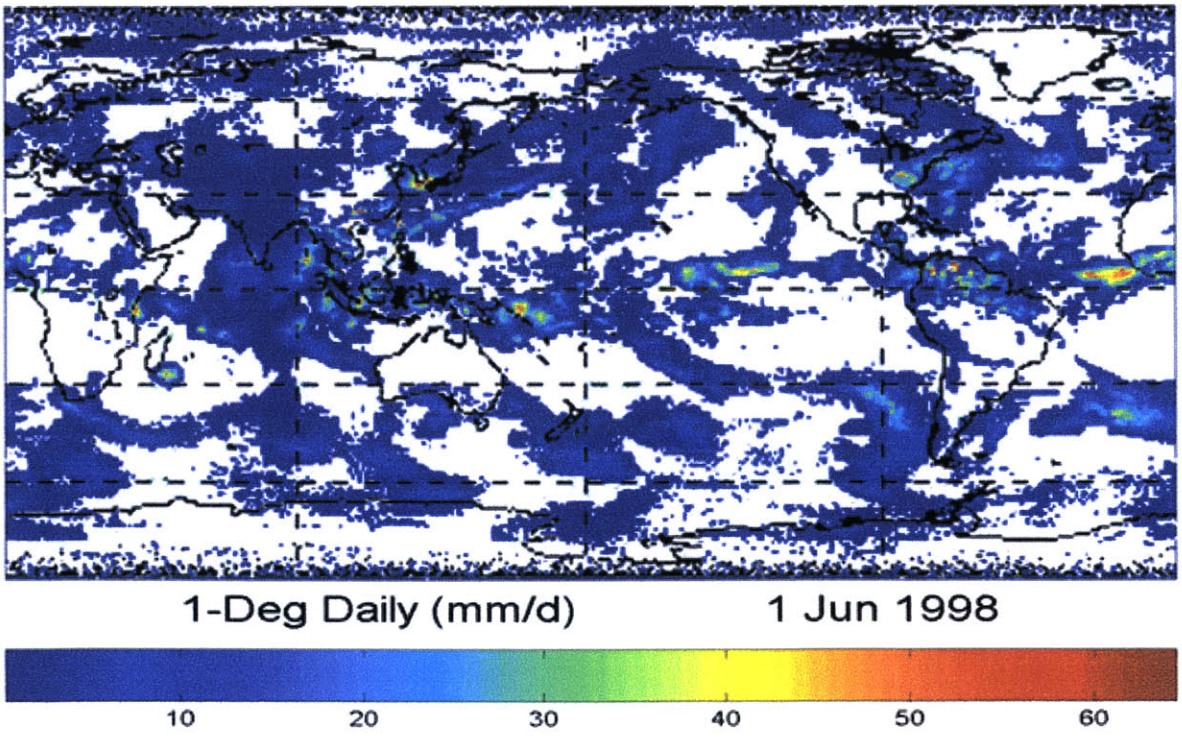

ELF Lightning for June2.txt from West Greenwich, R.I.

Correlation (min) = .5, Max Bearing Error (deg) = 5, Max Range Error (%) = 10
Positives = 1043, Negatives = 1121, Total = 2164
< >

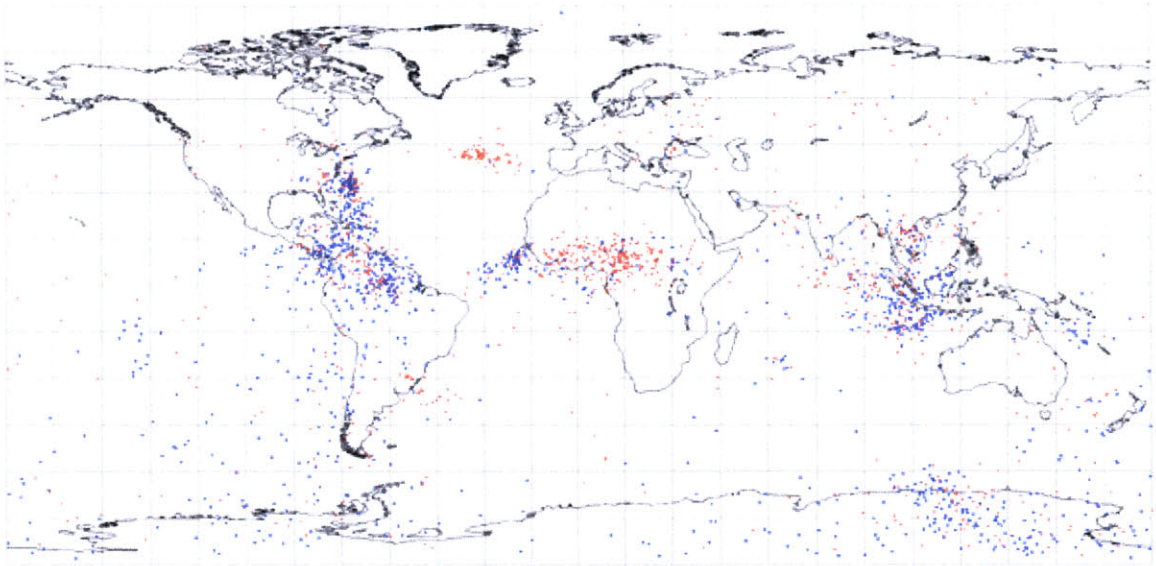

Sun Jan 9 17:19:06 EST 2000

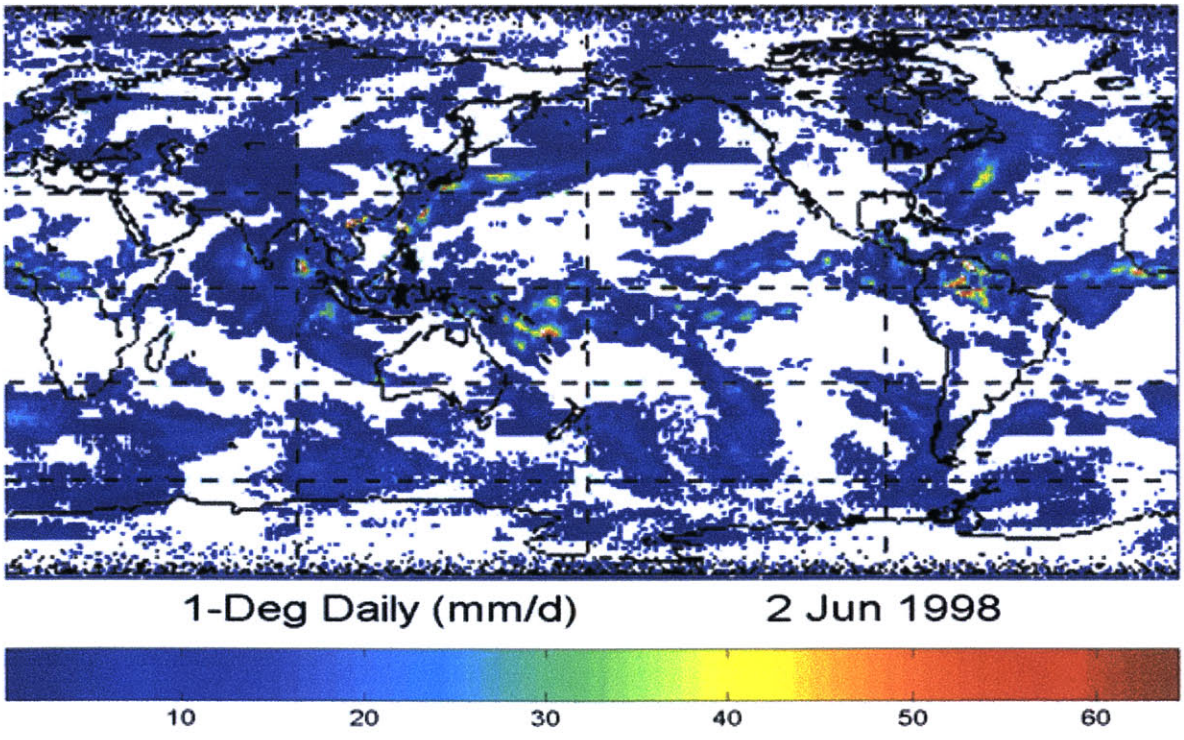

ELF Lightning for June3.txt from West Greenwich, R.I.

Correlation (min) = .5, Max Bearing Error (deg) = 5, Max Range Error (%) = 10
Positives = 1049, Negatives = 1435, Total = 2484

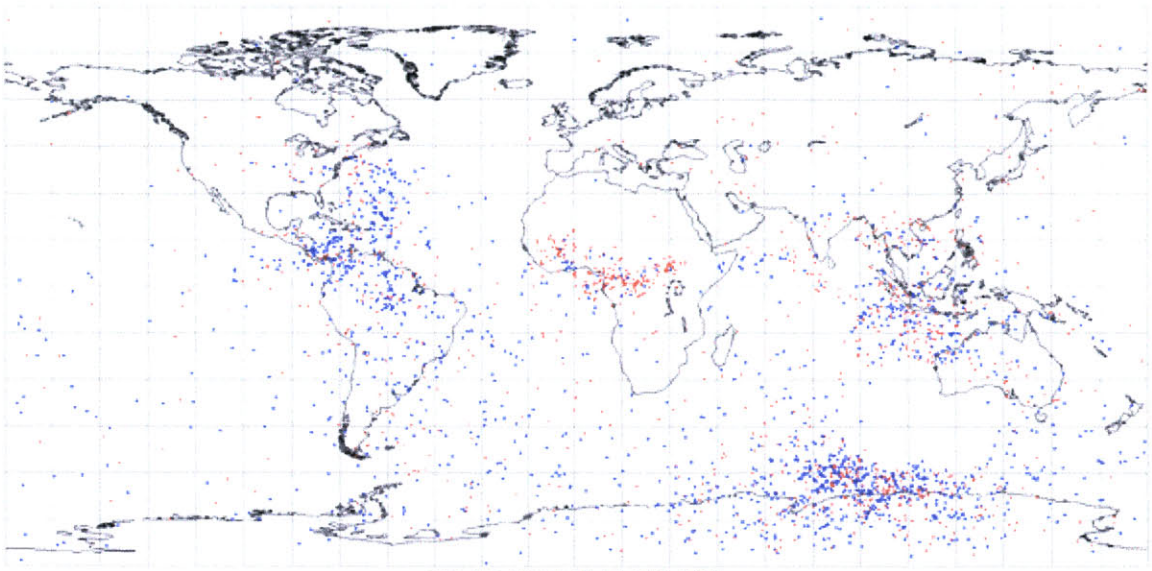

Mon Jan 10 14:33:21 EST 2000

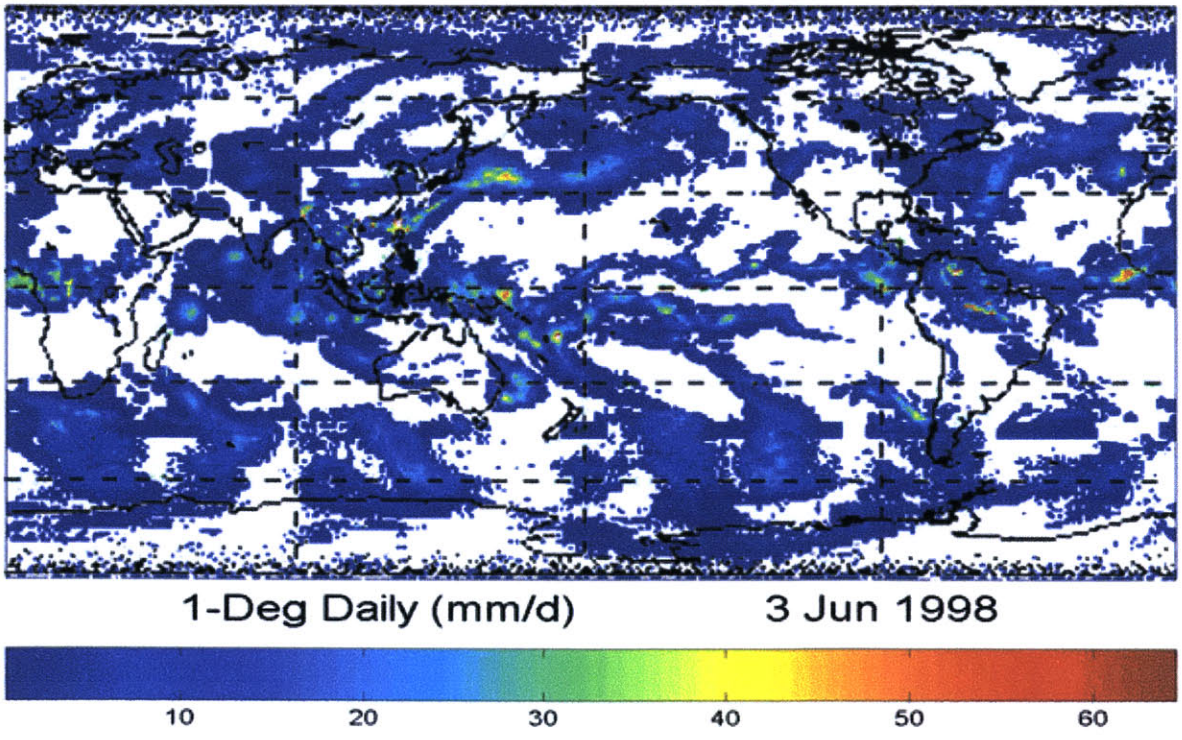

ELF Lightning for June4.txt from West Greenwich, R.I.

Correlation (min) = .5, Max Bearing Error (deg) = 5, Max Range Error (%) = 10
Positives = 52, Negatives = 55, Total = 107

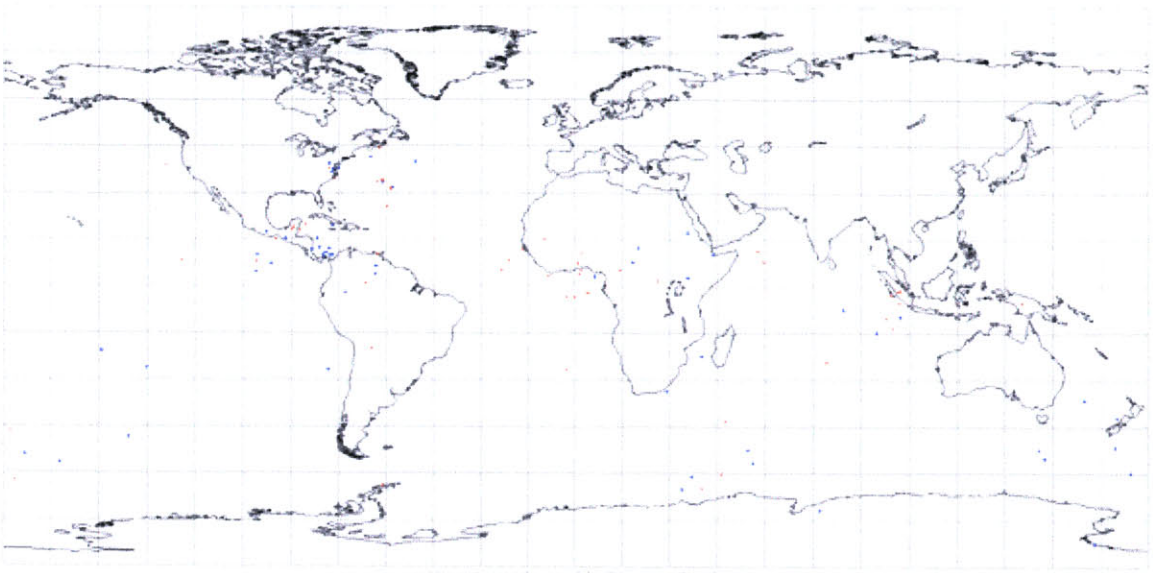

Mon Jan 10 14:33:59 EST 2000

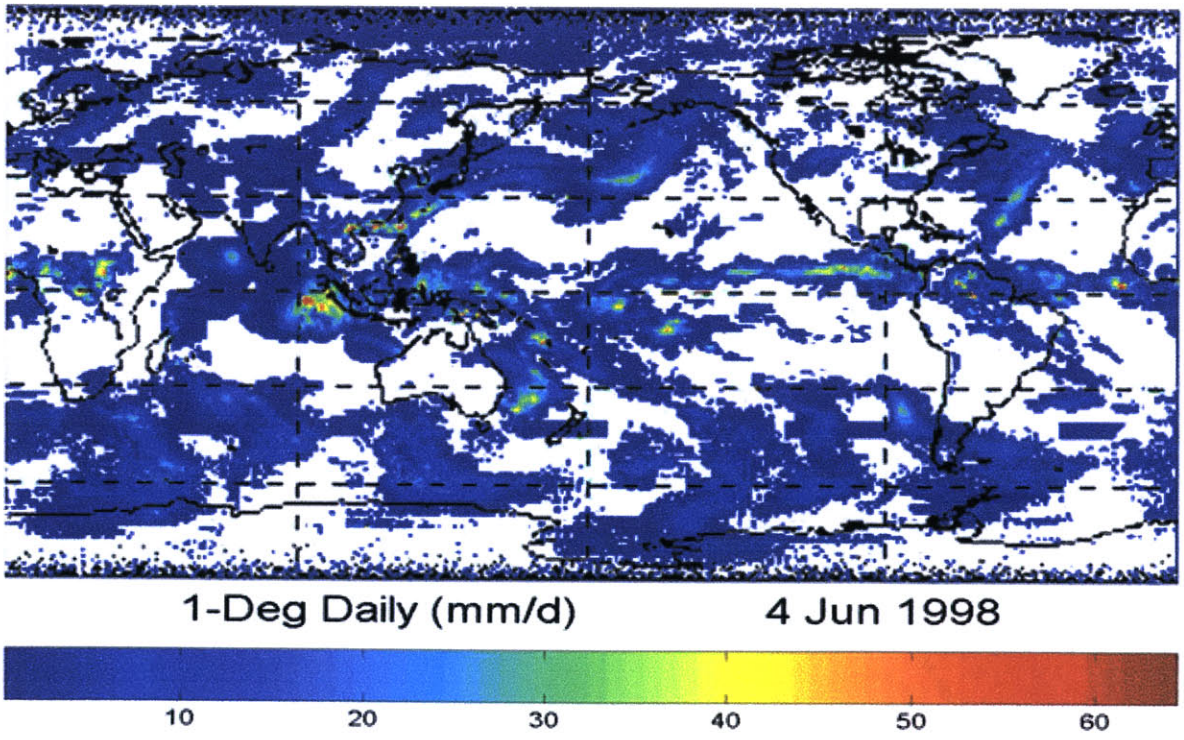

ELF Lightning for June5.txt from West Greenwich, R.I.

Correlation (min) = .5, Max Bearing Error (deg) = 5, Max Range Error (%) = 10
Positives = 672, Negatives = 391, Total = 1063

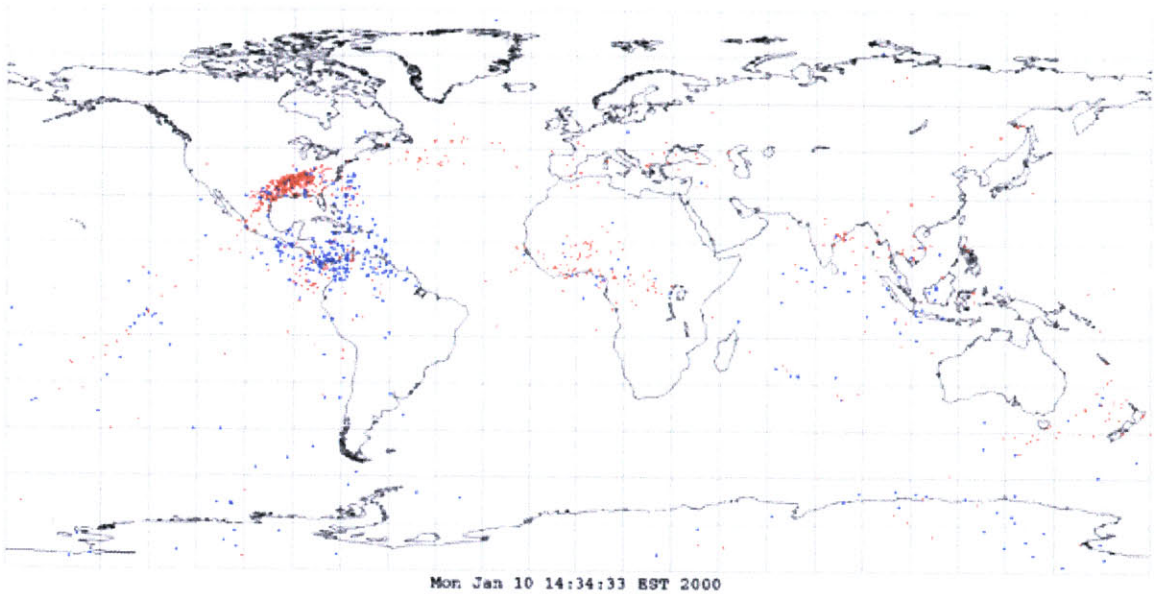

Mon Jan 10 14:34:33 EST 2000

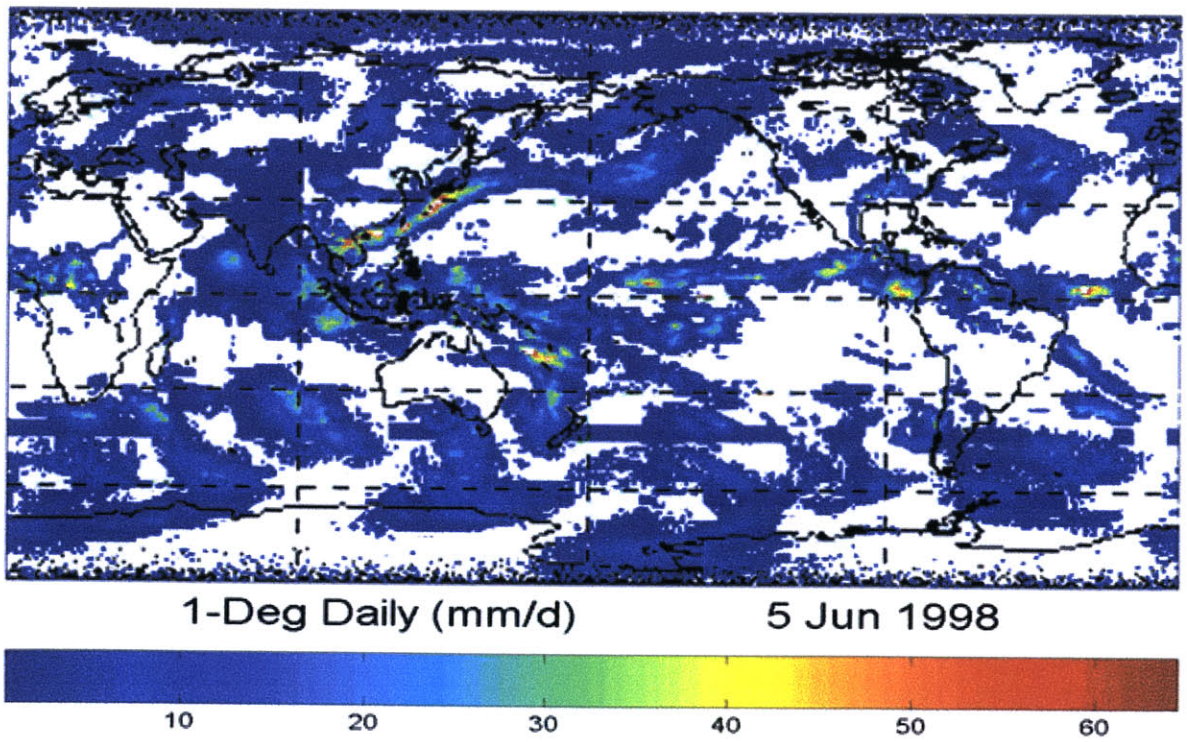

ELF Lightning for June6.txt from West Greenwich, R.I.

Correlation (min) = .5, Max Bearing Error (deg) = 5, Max Range Error (%) = 10
Positives = 714, Negatives = 577, Total = 1291

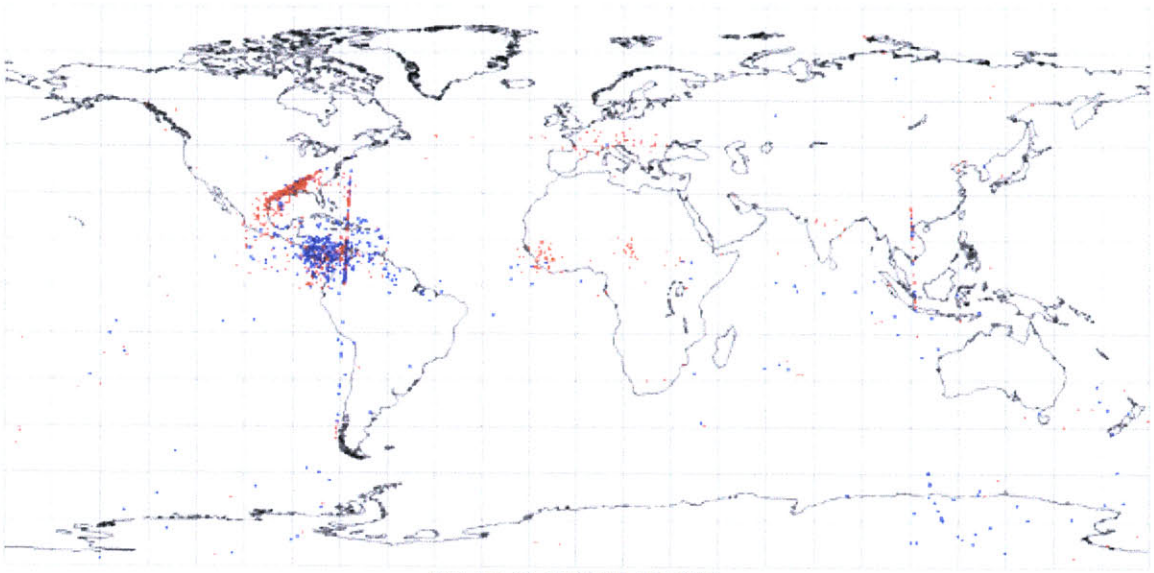

Mon Jan 10 14:37:42 EST 2000

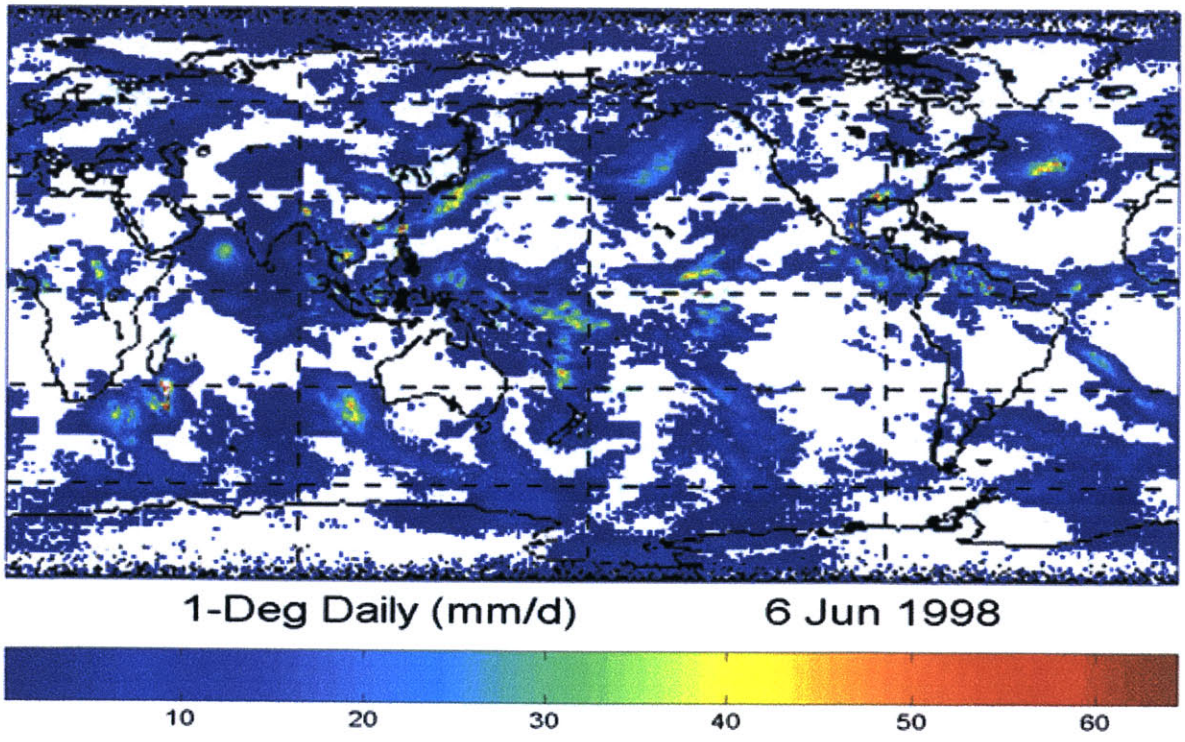

ELF Lightning for June7.txt from West Greenwich, R.I.

Correlation (min) = .5, Max Bearing Error (deg) = 5, Max Range Error (%) = 10
Positives = 475, Negatives = 479, Total = 954

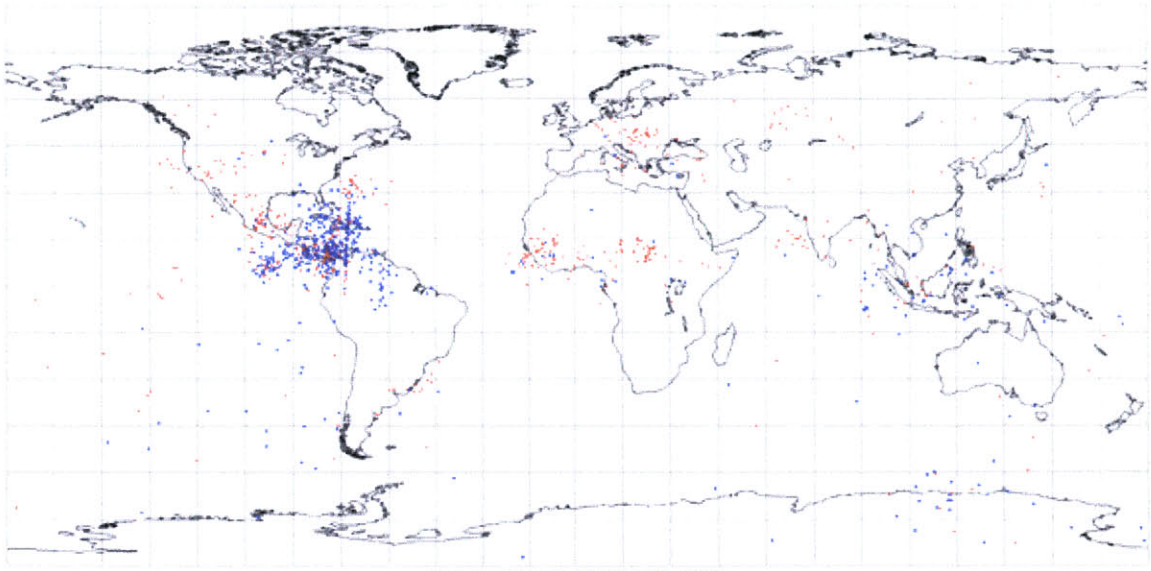

Mon Jan 10 14:38:33 EST 2000

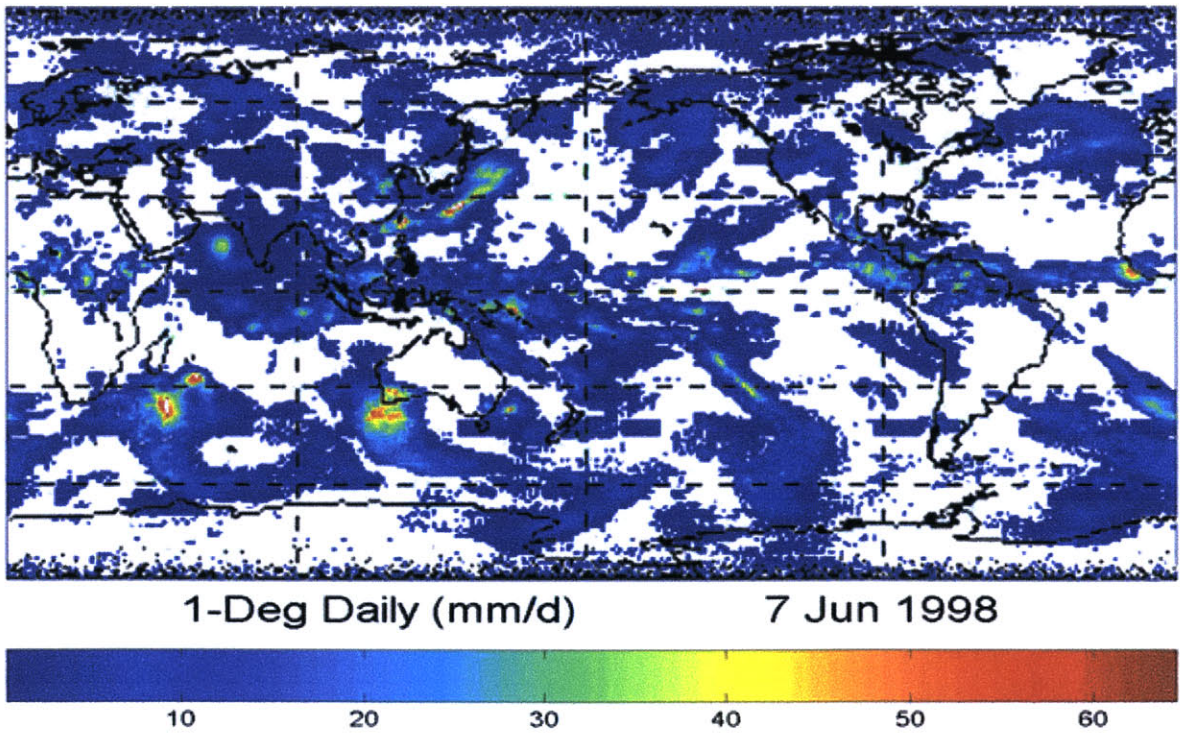

ELF Lightning for June8.txt from West Greenwich, R.I.

Correlation (min) = .5, Max Bearing Error (deg) = 5, Max Range Error (%) = 10
Positives = 442, Negatives = 498, Total = 940
< >

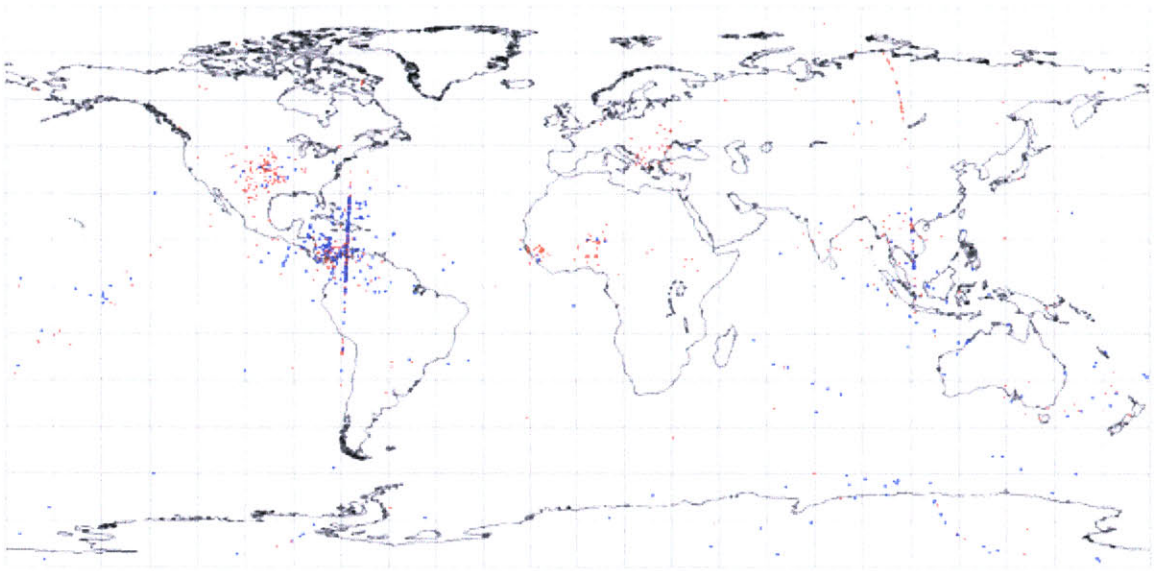

Mon Jan 10 14:39:14 EST 2000

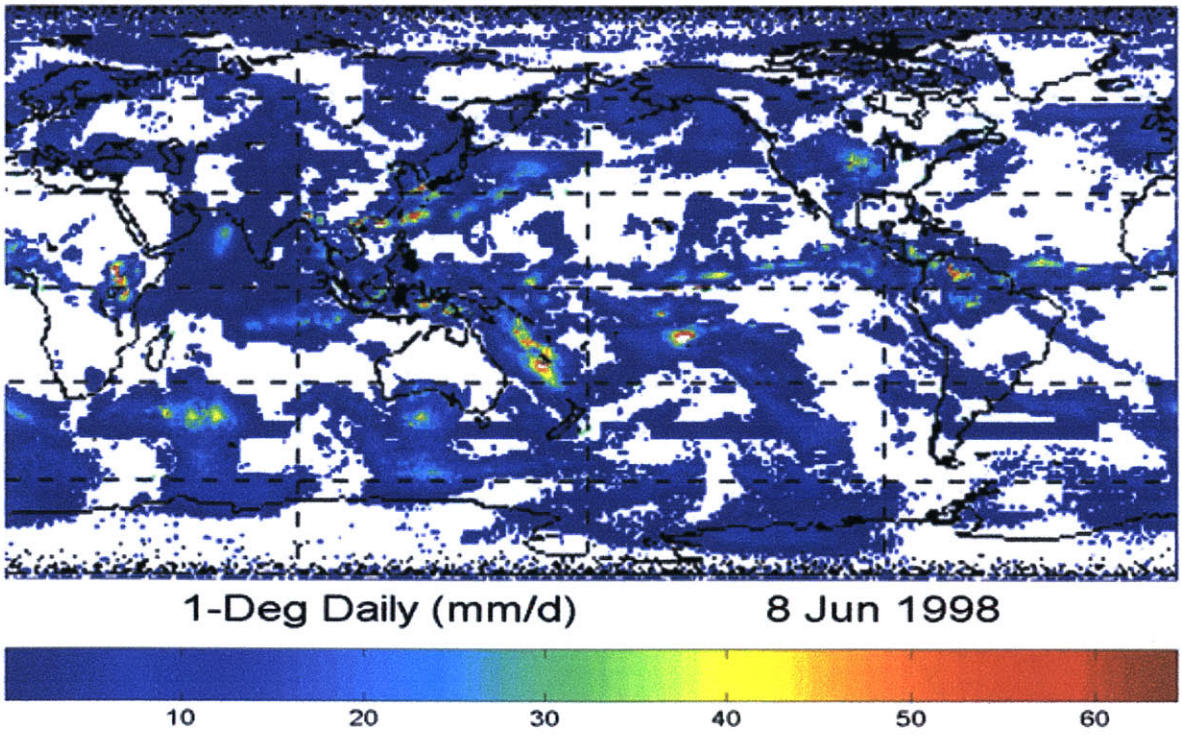

ELF Lightning for June9.txt from West Greenwich, R.I.

Correlation (min) = .5, Max Bearing Error (deg) = 5, Max Range Error (%) = 10
Positives = 744, Negatives = 499, Total = 1243
< >

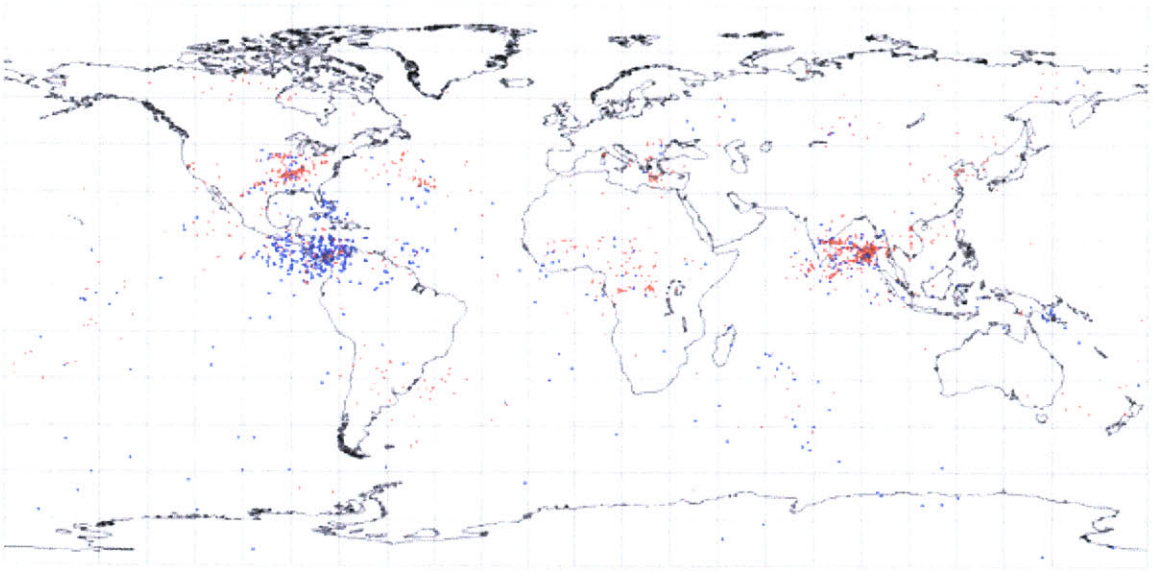

Mon Jan 10 14:39:54 EST 2000

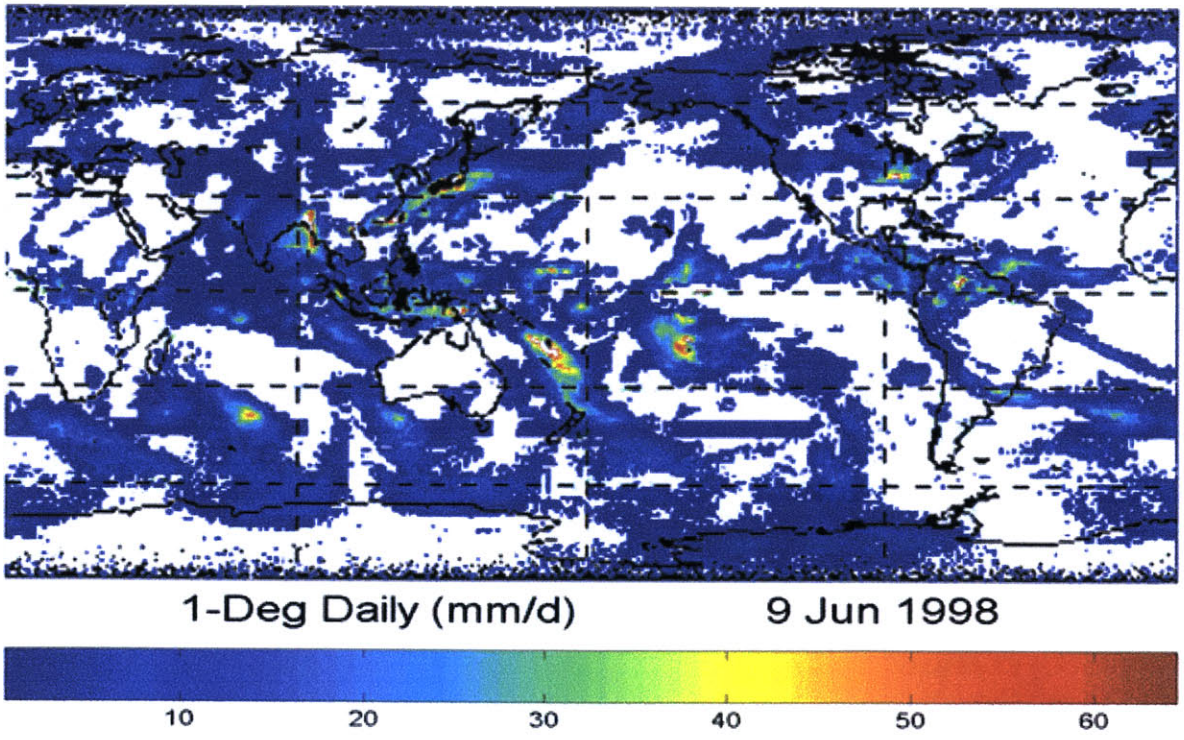

ELF Lightning for June10.txt from West Greenwich, R.I.

Correlation (min) = .5, Max Bearing Error (deg) = 5, Max Range Error (%) = 10
Positives = 674, Negatives = 401, Total = 1075
< >

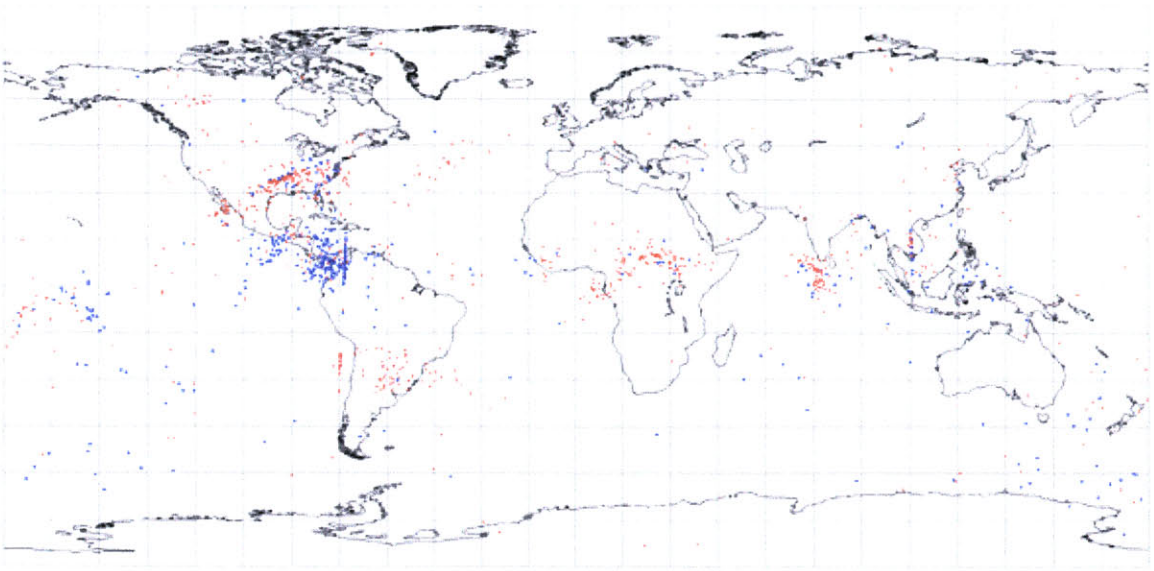

Mon Jan 10 14:40:51 EST 2000

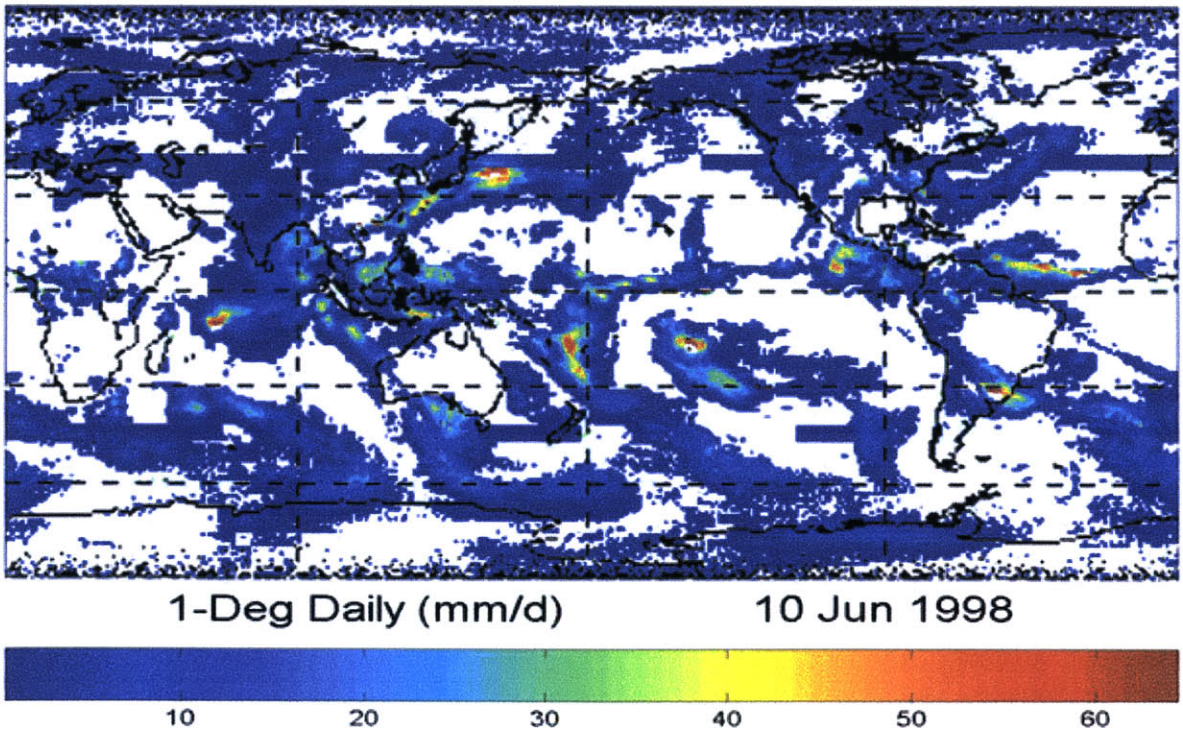

ELF Lightning for June11.txt from West Greenwich, R.I.

Correlation (min) = .5, Max Bearing Error (deg) = 5, Max Range Error (%) = 10
Positives = 700, Negatives = 678, Total = 1378
< >

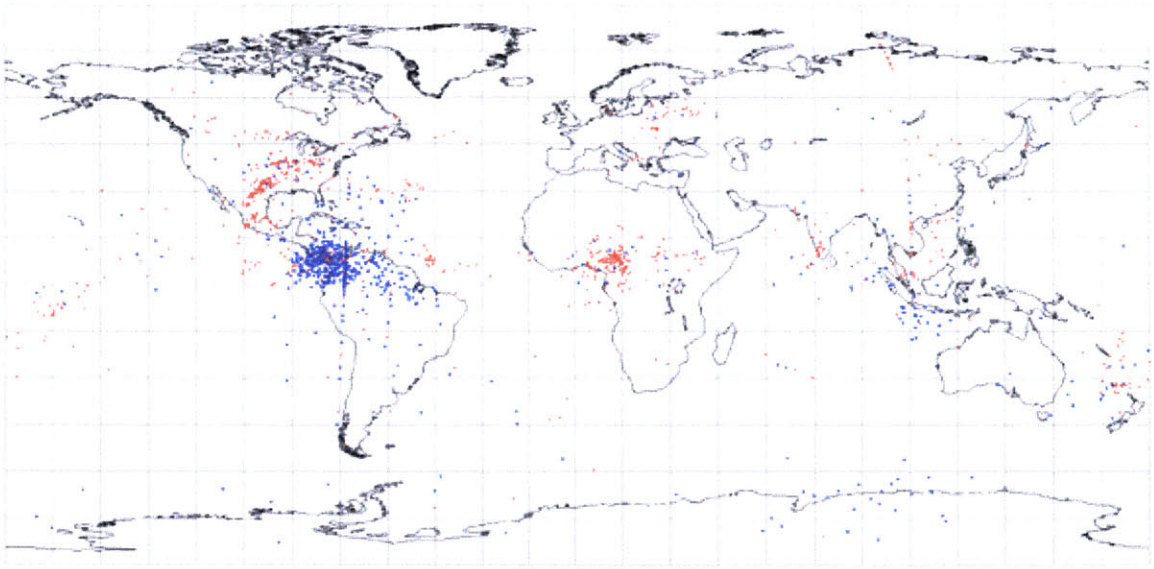

Mon Jan 10 14:41:49 EST 2000

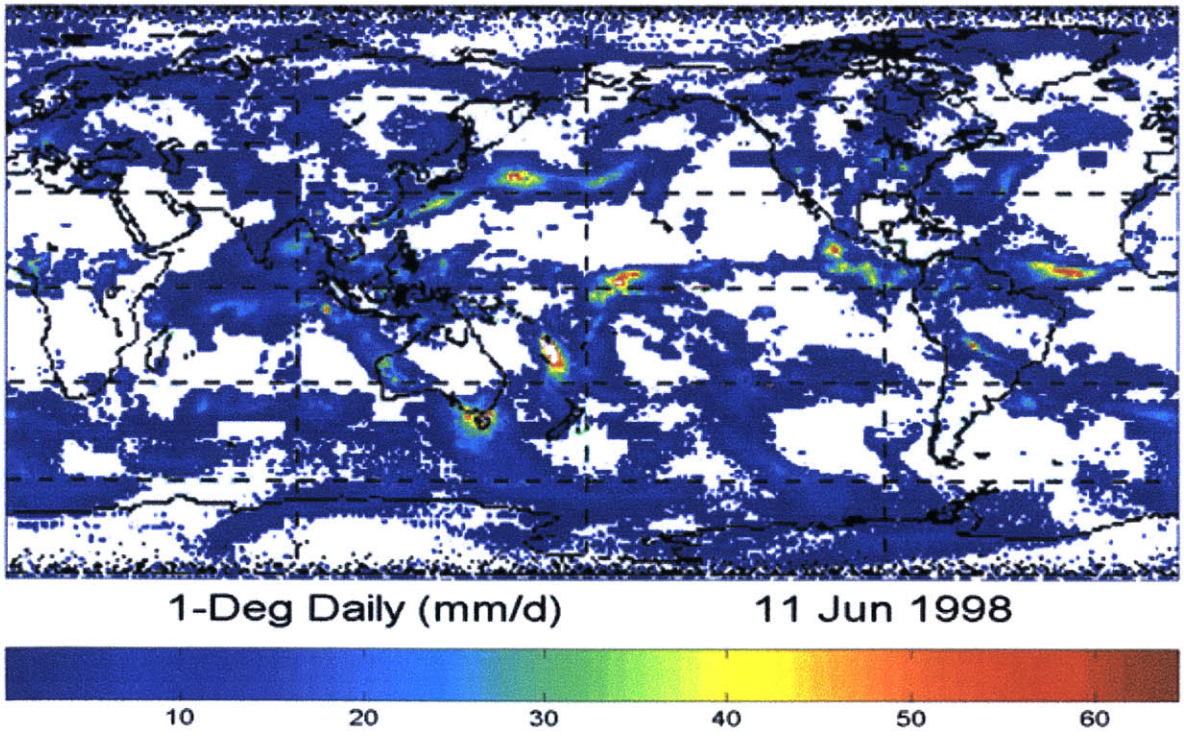

ELF Lightning for June12.txt from West Greenwich, R.I.

Correlation (min) = .5, Max Bearing Error (deg) = 5, Max Range Error (%) = 10
Positives = 782, Negatives = 1061, Total = 1843

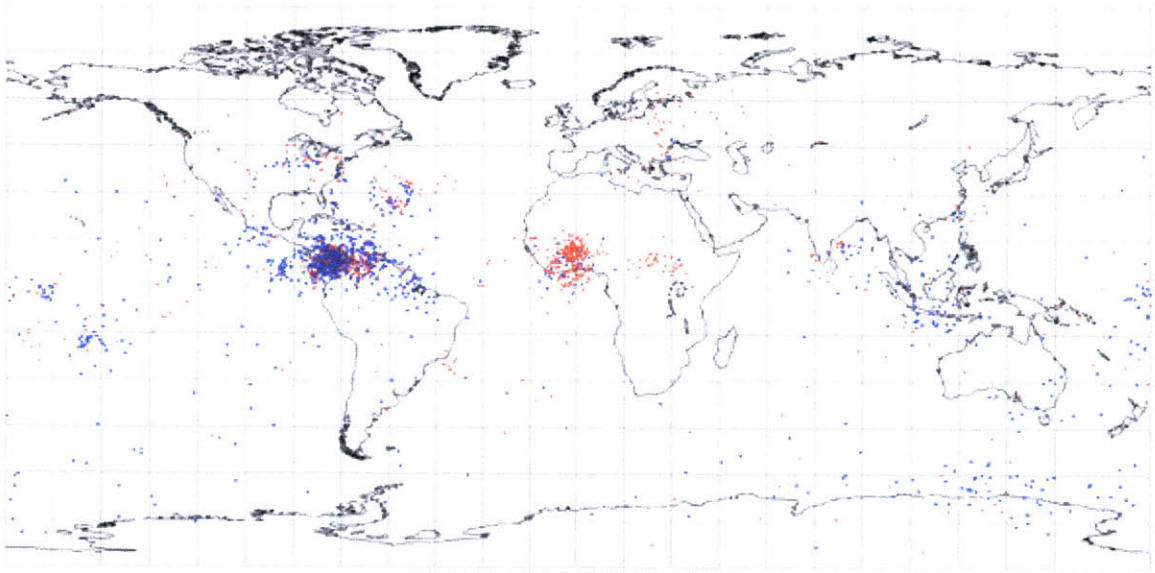

Mon Jan 10 14:42:26 EST 2000

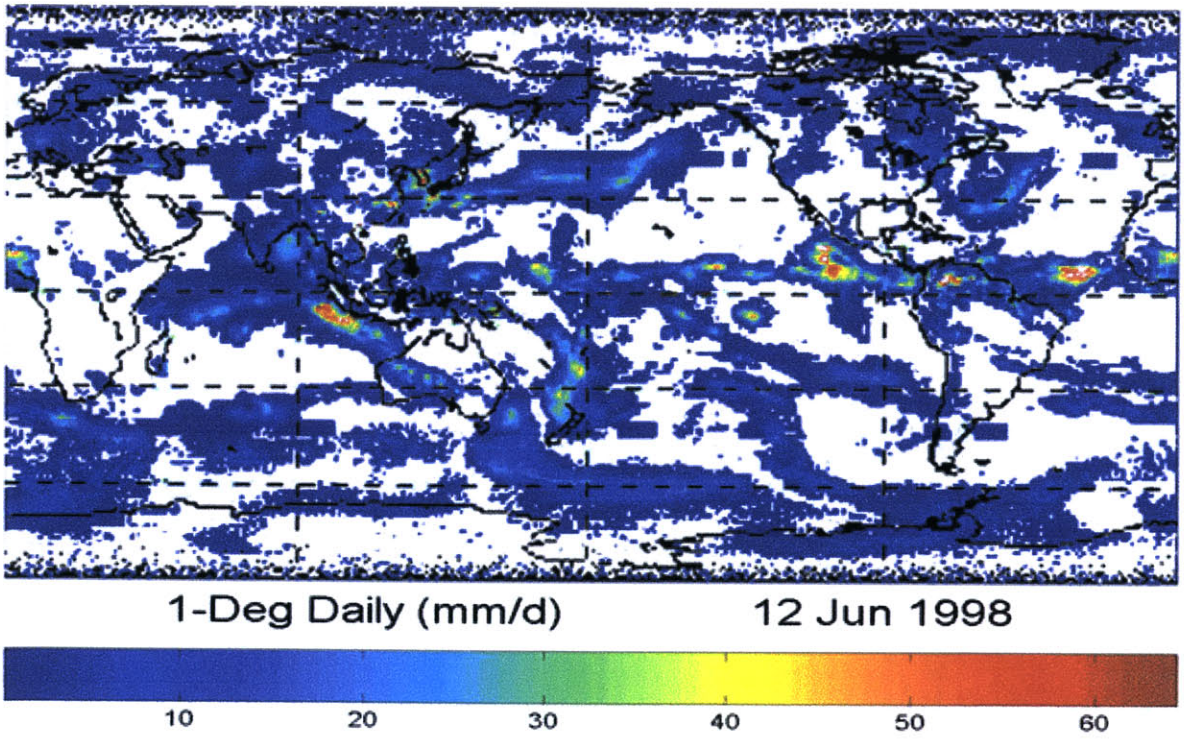

ELF Lightning for June13.txt from West Greenwich, R.I.

Correlation (min) = .5, Max Bearing Error (deg) = 5, Max Range Error (%) = 10
Positives = 1036, Negatives = 1353, Total = 2389

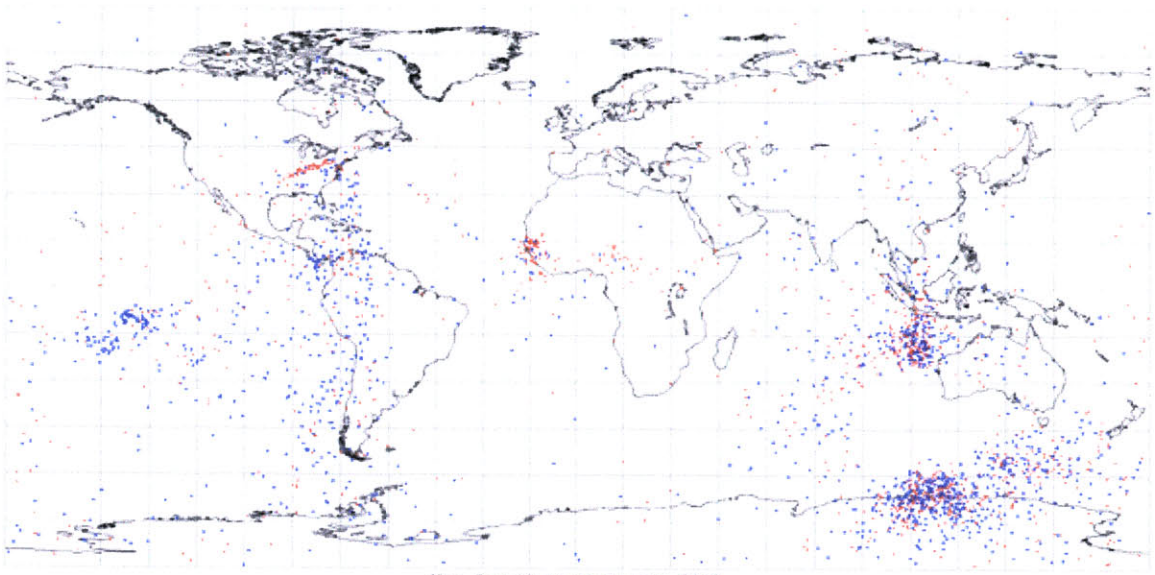

Mon Jan 10 14:43:22 EST 2000

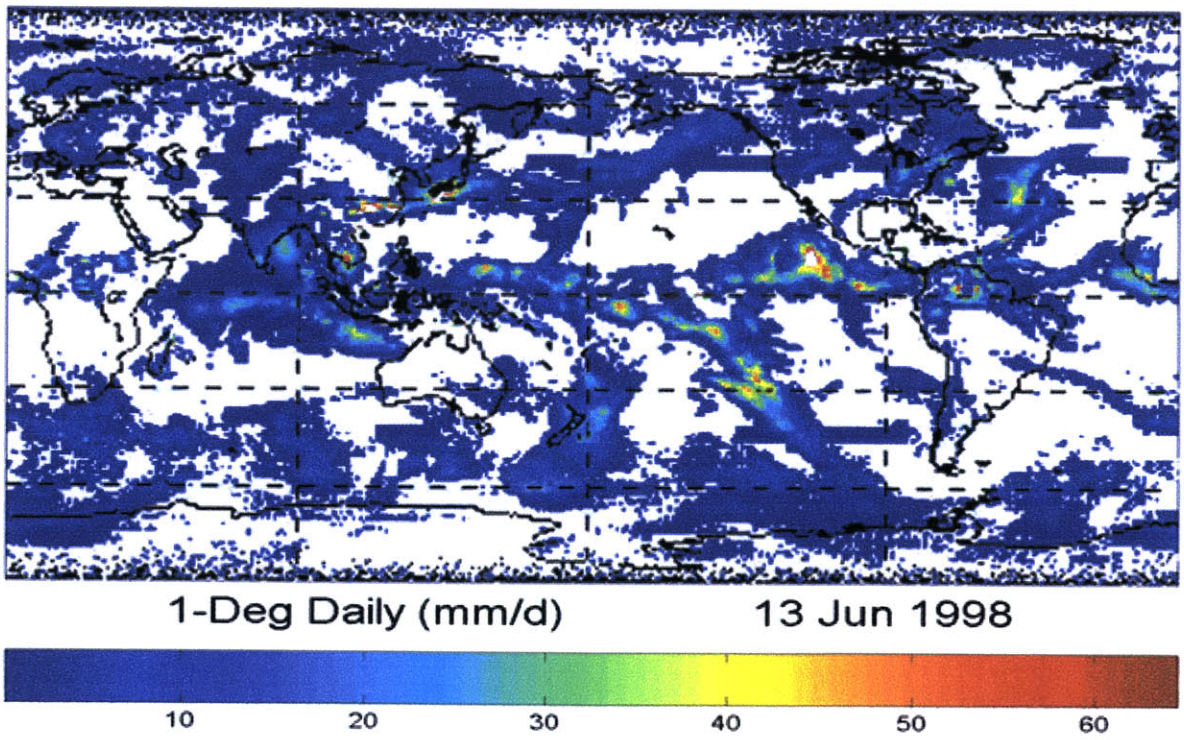

ELF Lightning for June14.txt from West Greenwich, R.I.

Correlation (min) = .5, Max Bearing Error (deg) = 5, Max Range Error (%) = 10
Positives = 836, Negatives = 909, Total = 1745

< >

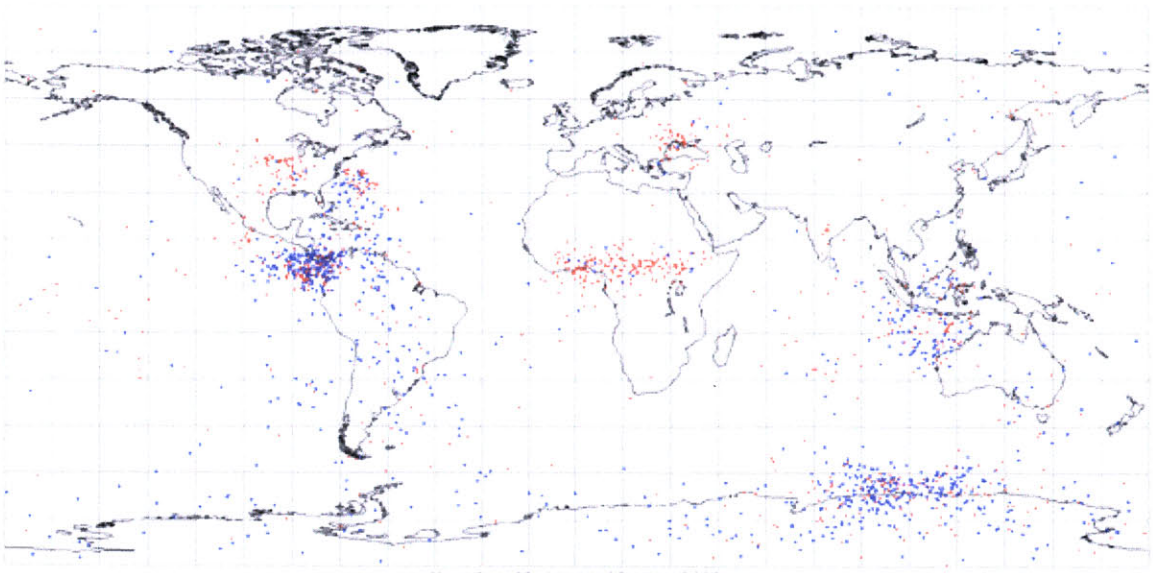

Mon Jan 10 14:44:15 EST 2000

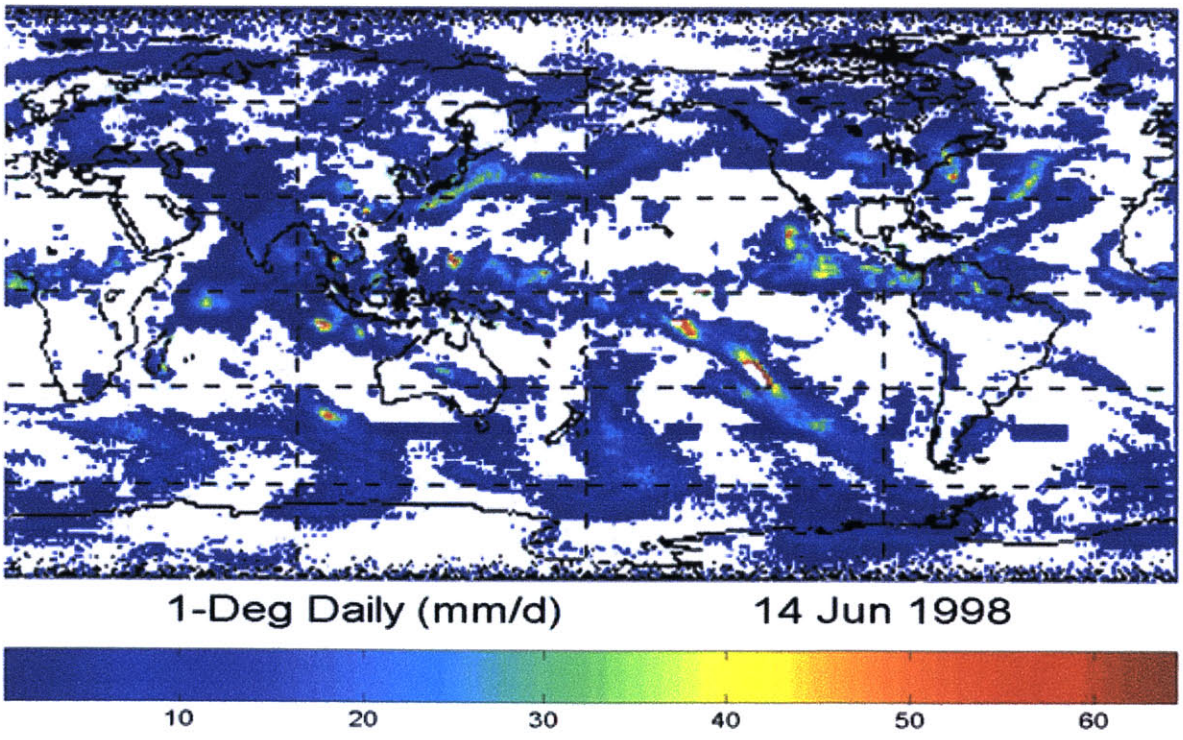

ELF Lightning for June15.txt from West Greenwich, R.I.

Correlation (min) = .5, Max Bearing Error (deg) = 5, Max Range Error (%) = 10
Positives = 705, Negatives = 471, Total = 1176

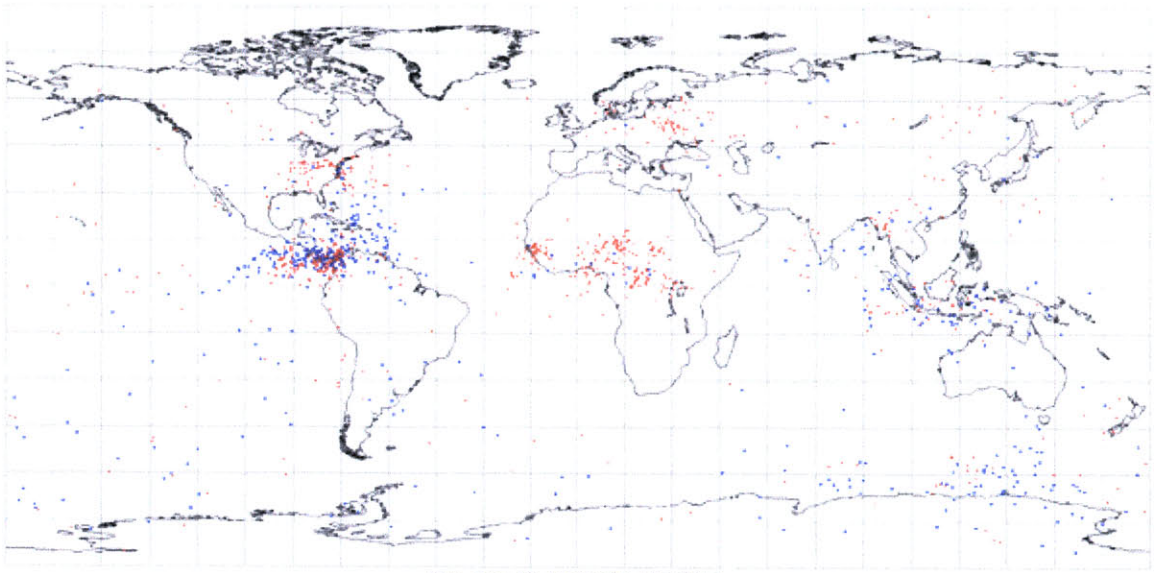

Mon Jan 10 14:44:53 EST 2000

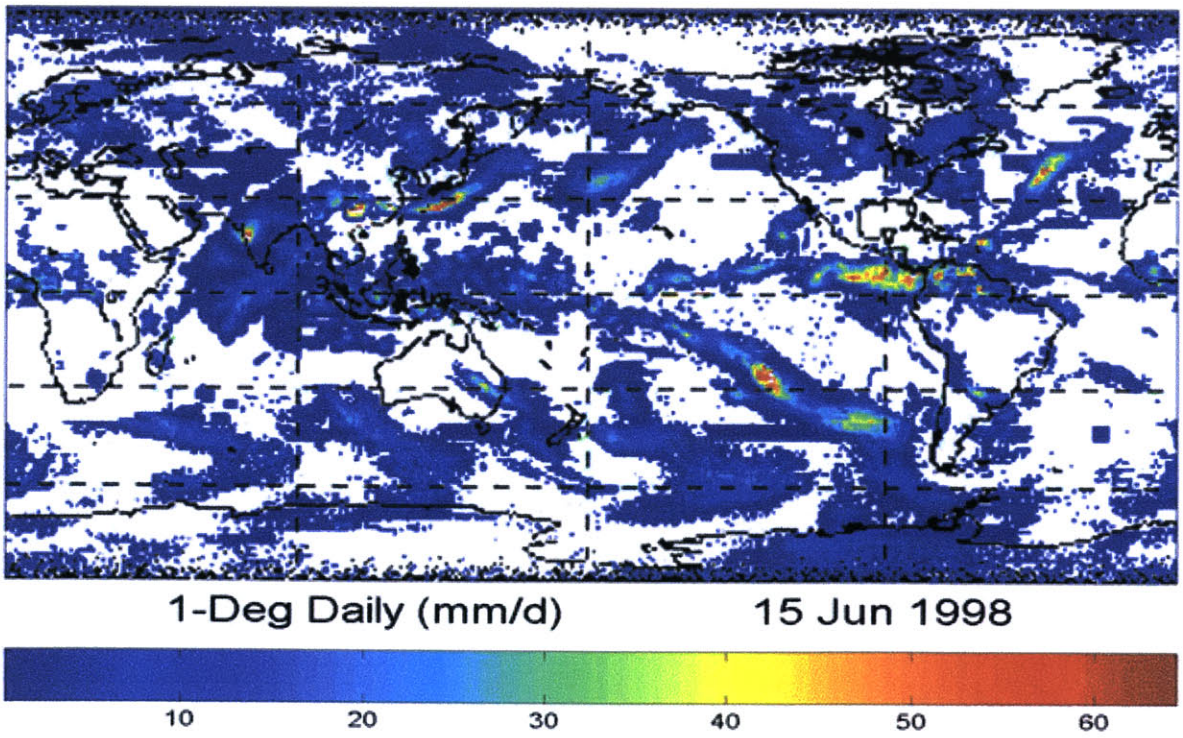

ELF Lightning for June16.txt from West Greenwich, R.I.

Correlation (min) = .5, Max Bearing Error (deg) = 5, Max Range Error (%) = 10
Positives = 852, Negatives = 862, Total = 1714

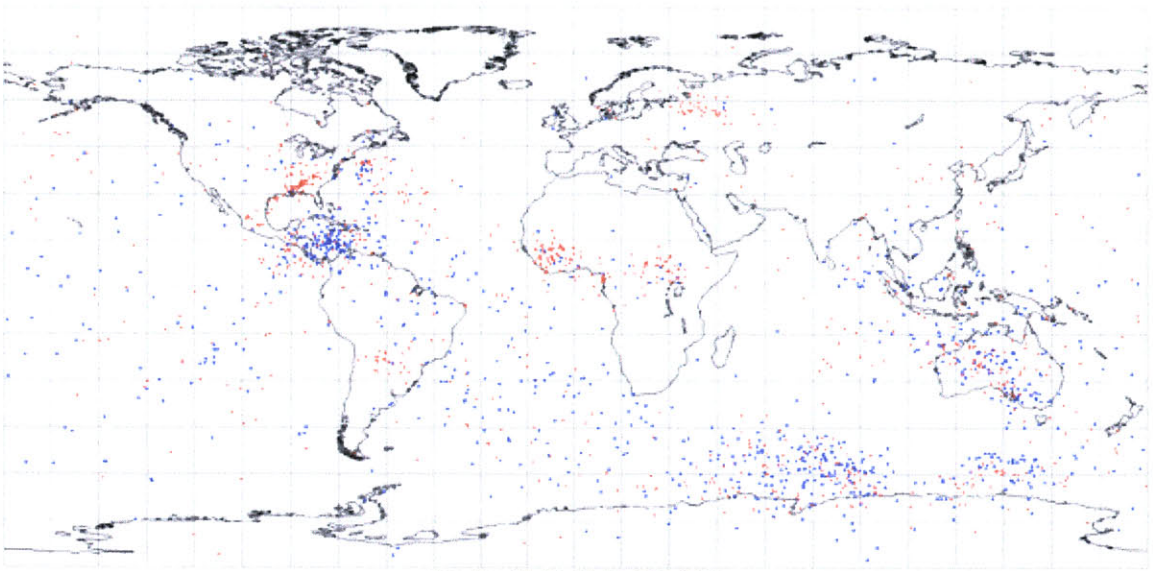

Mon Jan 10 14:46:10 EST 2000

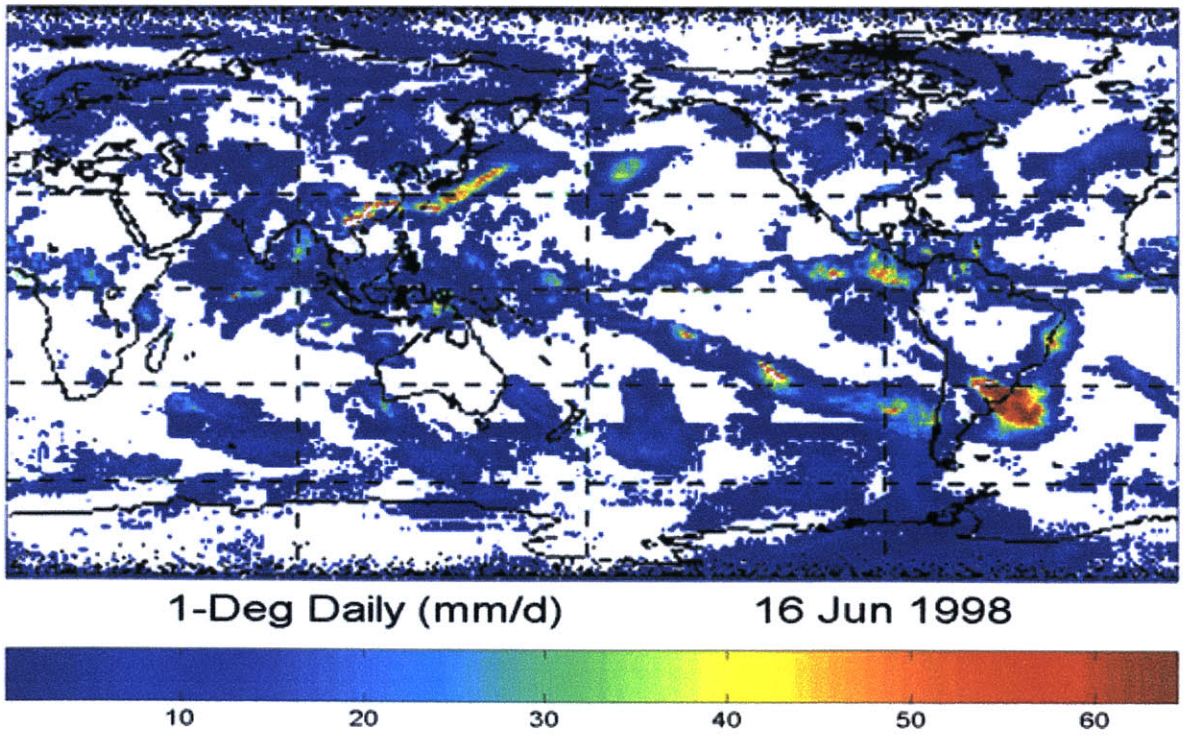

ELF Lightning for June17.txt from West Greenwich, R.I.

Correlation (min) = .5, Max Bearing Error (deg) = 5, Max Range Error (%) = 10
Positives = 577, Negatives = 930, Total = 1507

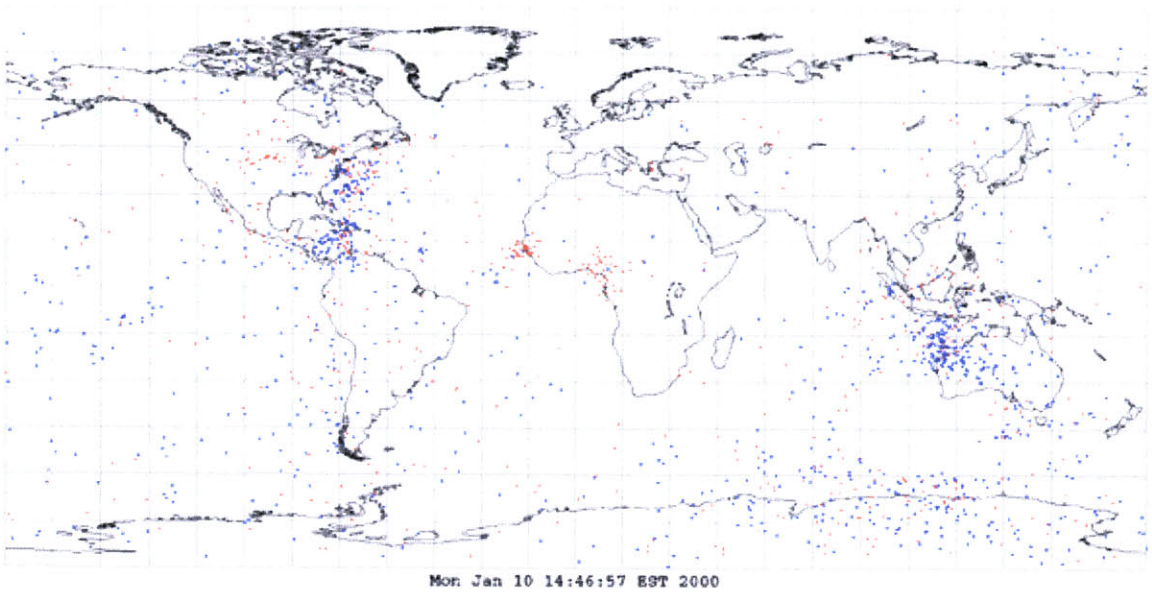

Mon Jan 10 14:46:57 EST 2000

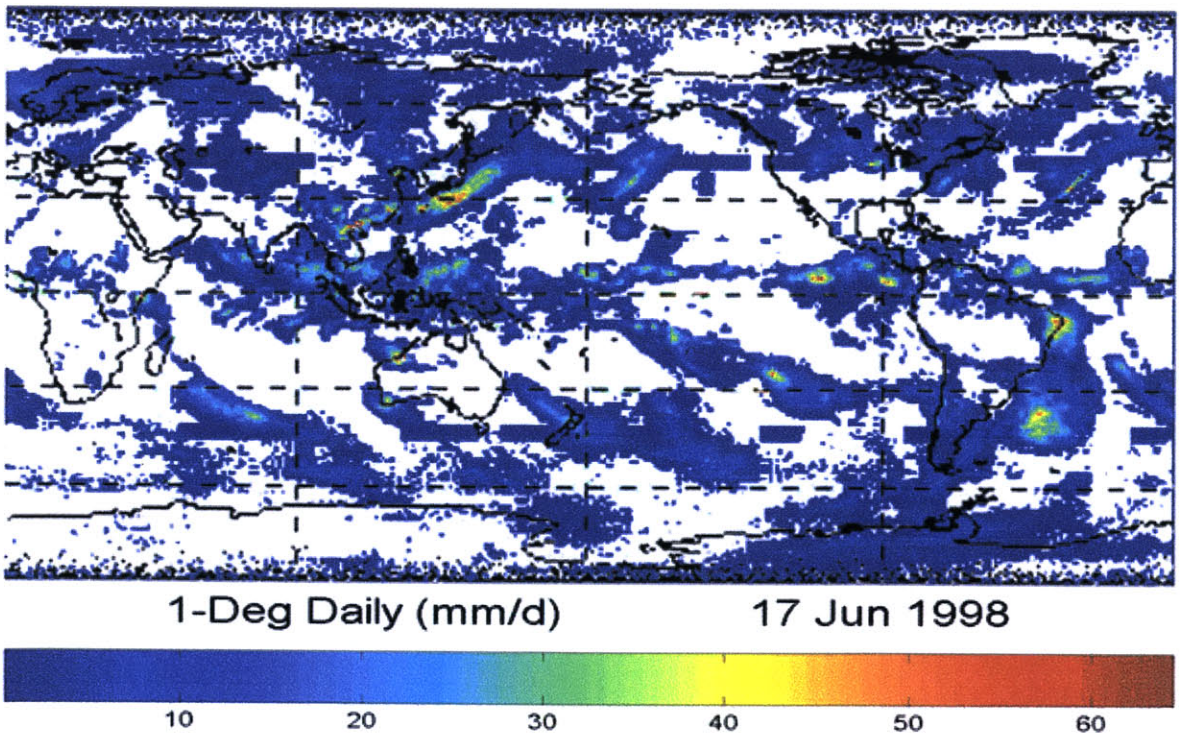

ELF Lightning for June18.txt from West Greenwich, R.I.

Correlation (min) = .5, Max Bearing Error (deg) = 5, Max Range Error (%) = 10
Positives = 749, Negatives = 790, Total = 1539

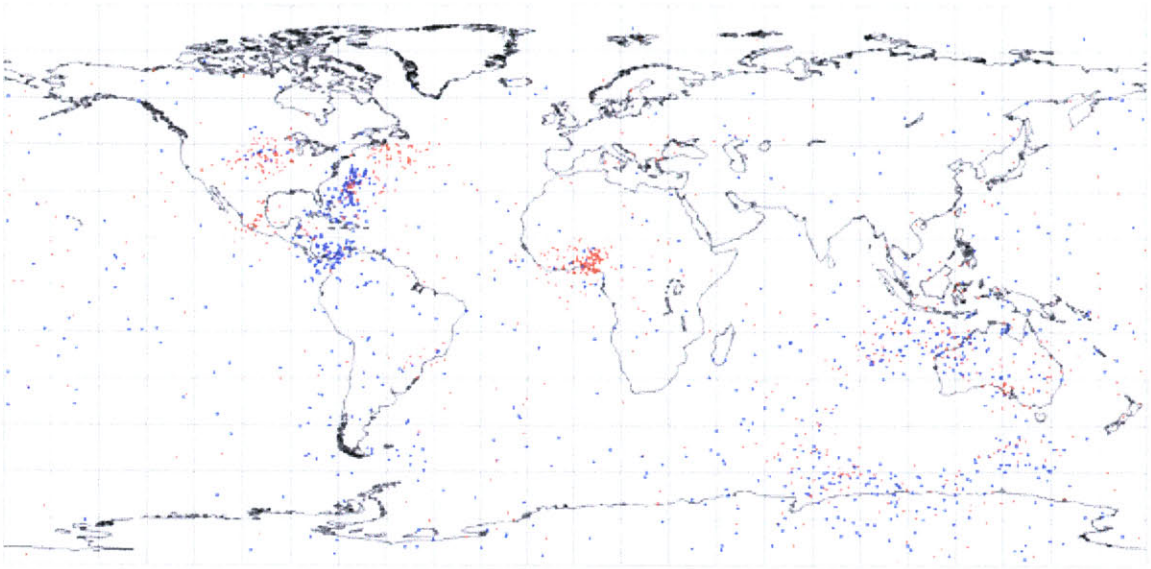

Mon Jan 10 14:47:32 EST 2000

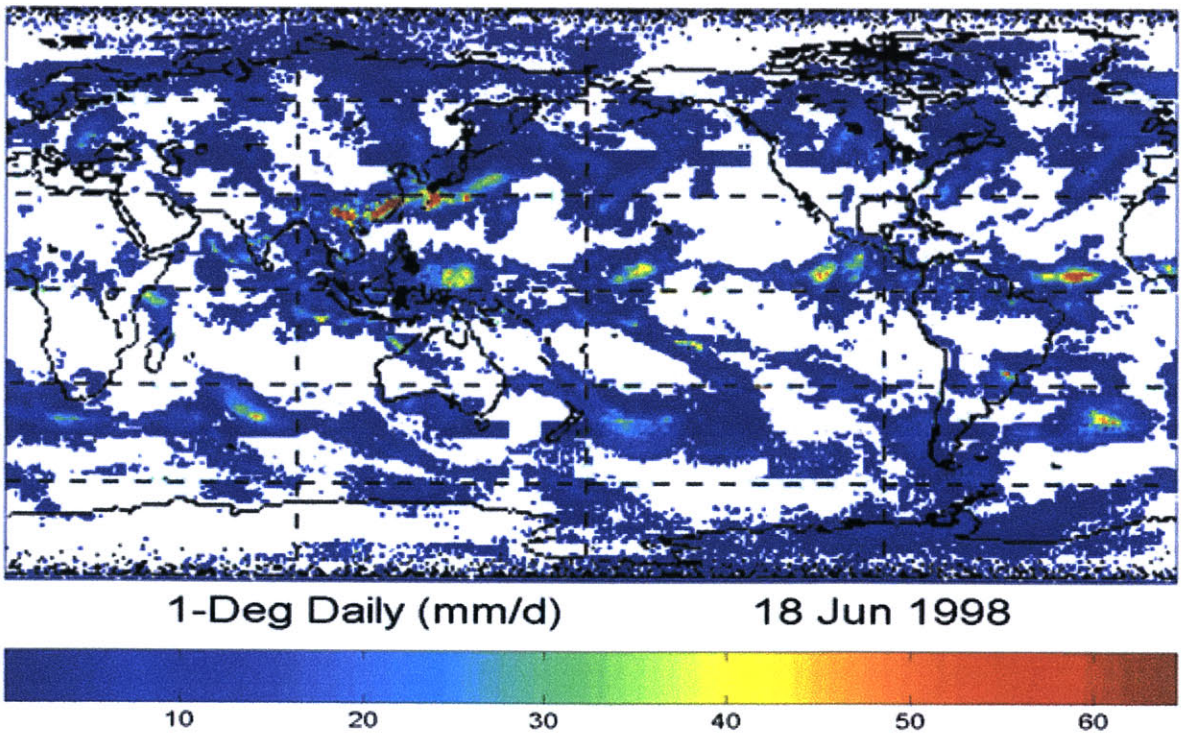

ELF Lightning for June19.txt from West Greenwich, R.I.

Correlation (min) = .5, Max Bearing Error (deg) = 5, Max Range Error (%) = 10
Positives = 517, Negatives = 621, Total = 1138
< >

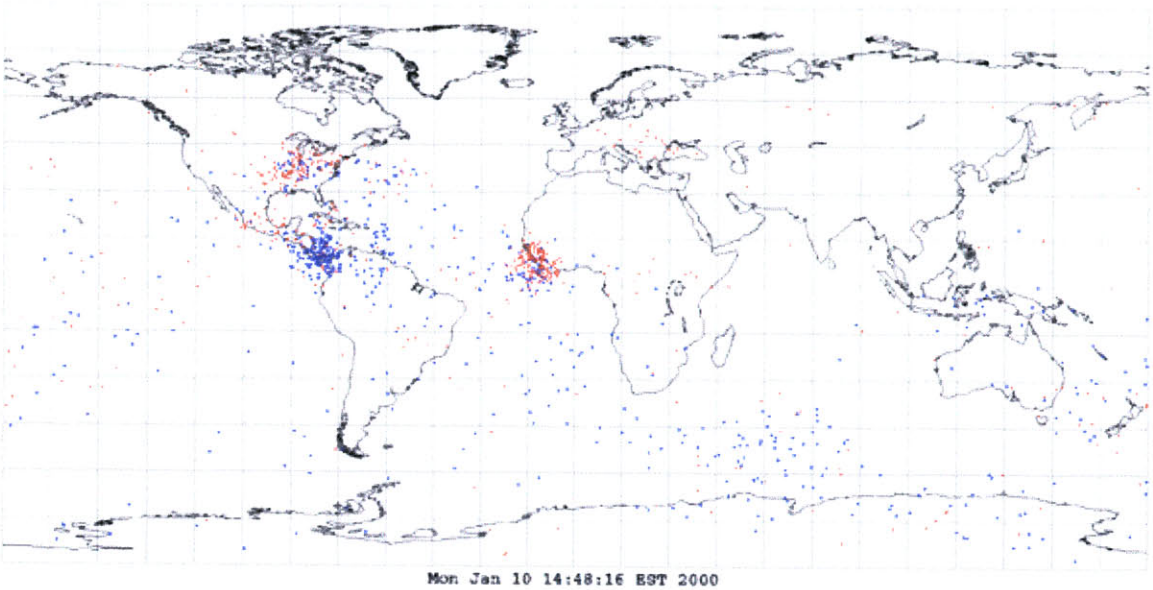

Mon Jan 10 14:48:16 EST 2000

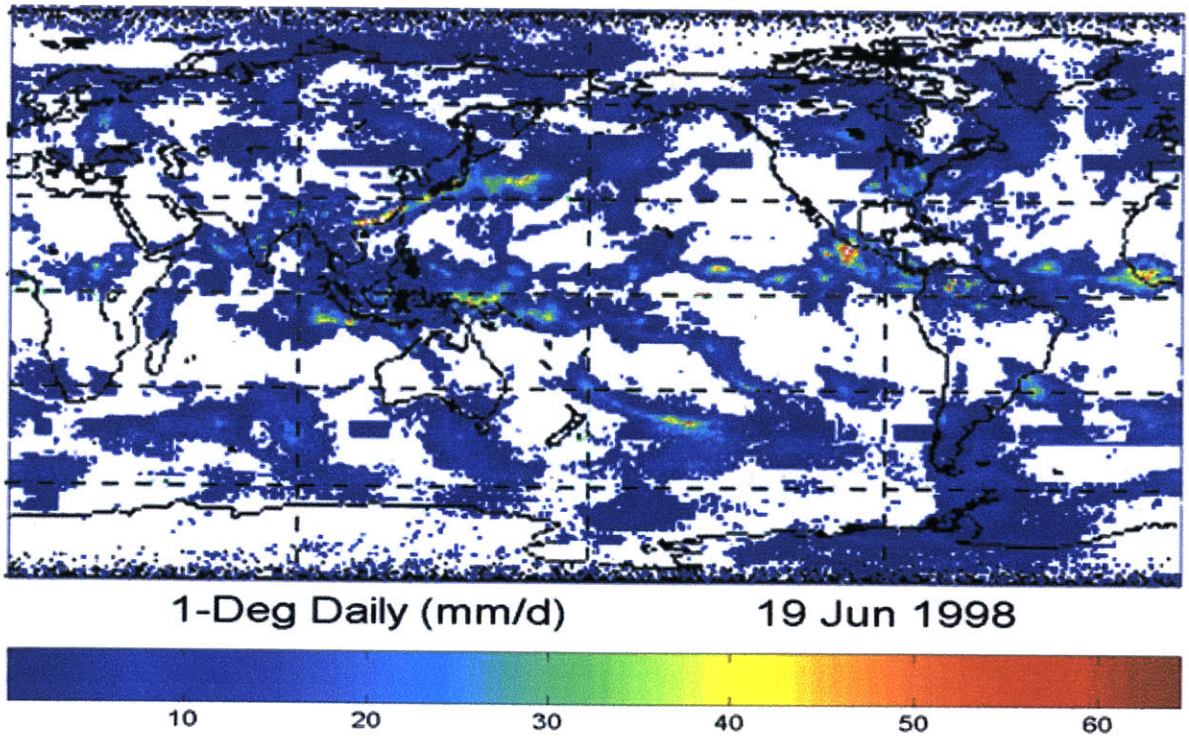

Appendix C

NOAA African Rainfall/Transient Maps for

5/7/98 – 6/19/98

NOAA 0.1 Deg Daily (mm/d) 7 May 1998

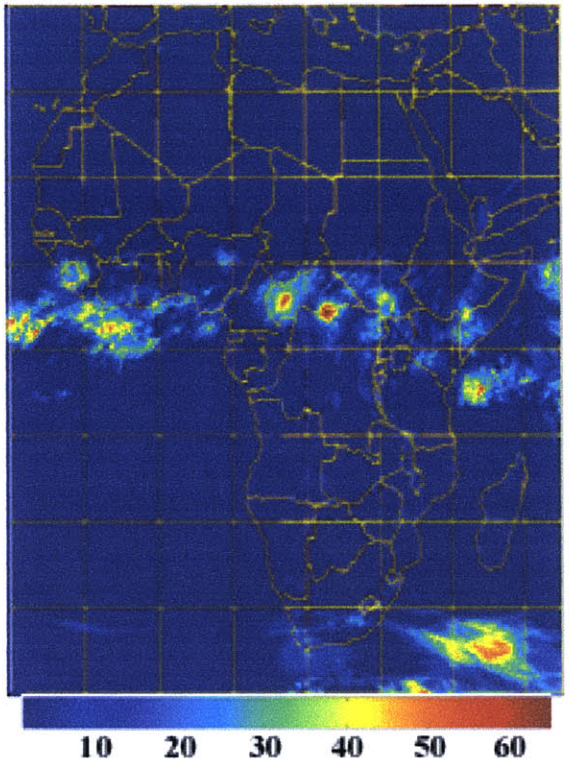

Red = Positive-Stroke
Blue = Negative-Stroke May 7, 1998

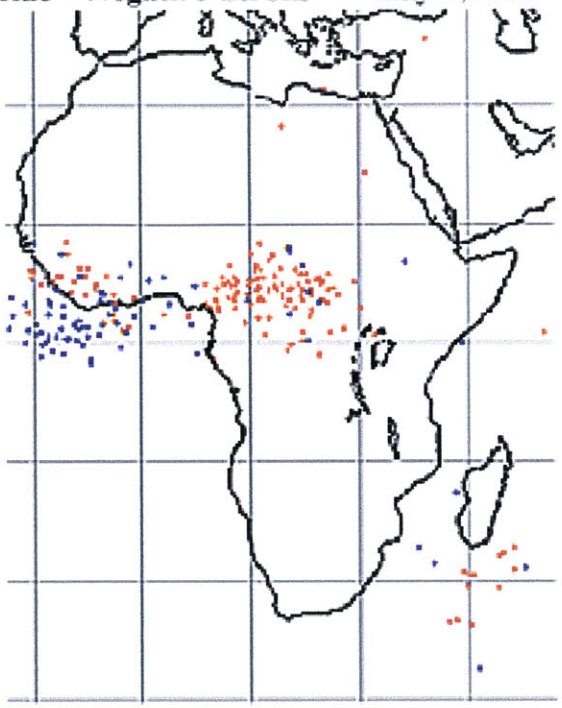

NOAA 0.1 Deg Daily (mm/d) 8 May 1998

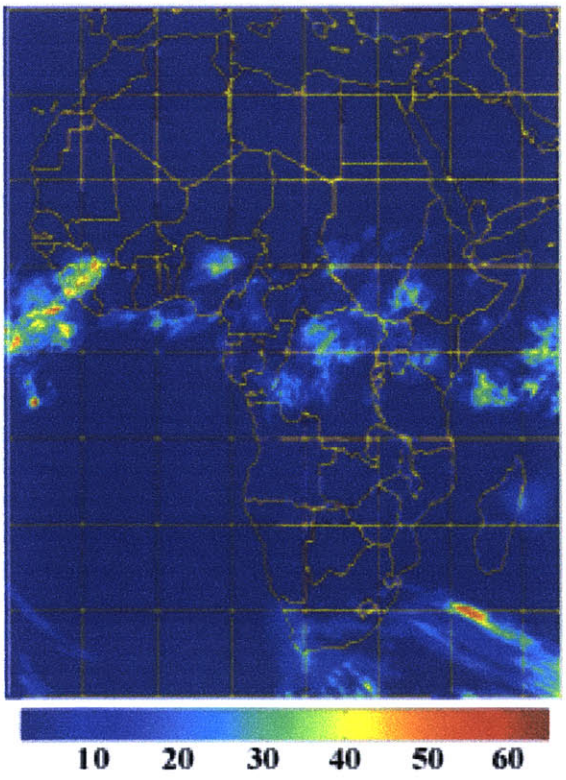

Red = Positive-Stroke
Blue = Negative-Stroke May 8, 1998

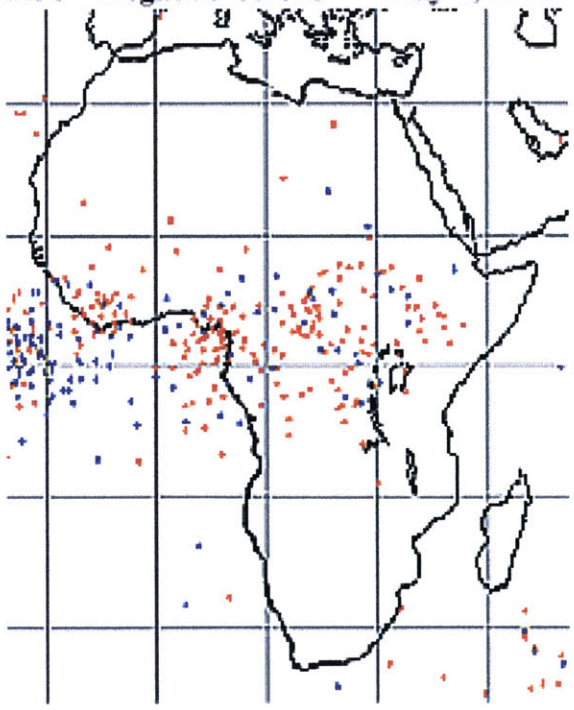

NOAA 0.1 Deg Daily (mm/d) 9 May 1998

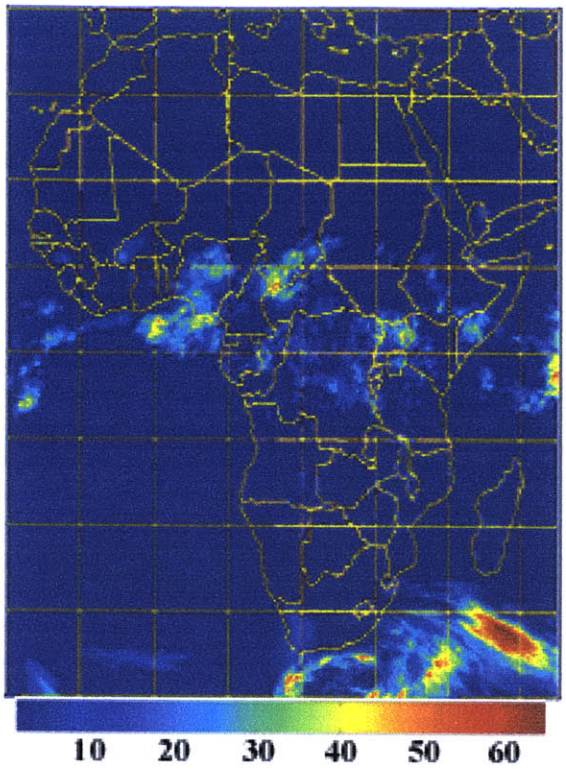

Red = Positive-Stroke
Blue = Negative-Stroke May 9, 1998

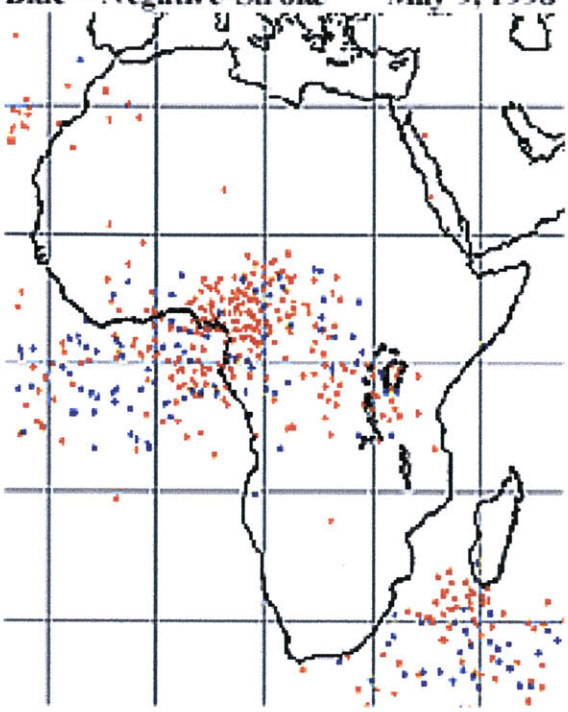

NOAA 0.1 Deg Daily (mm/d) 10 May 1998

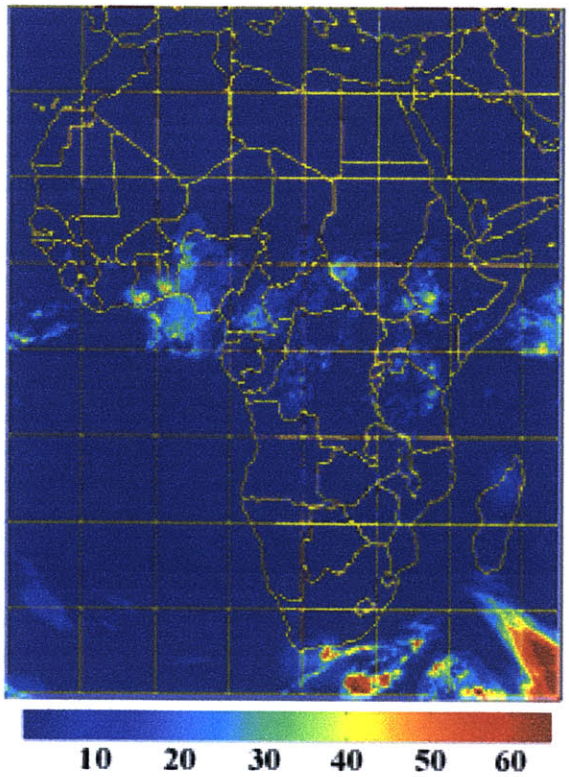

Red = Positive-Stroke
Blue = Negative-Stroke May 10, 1998

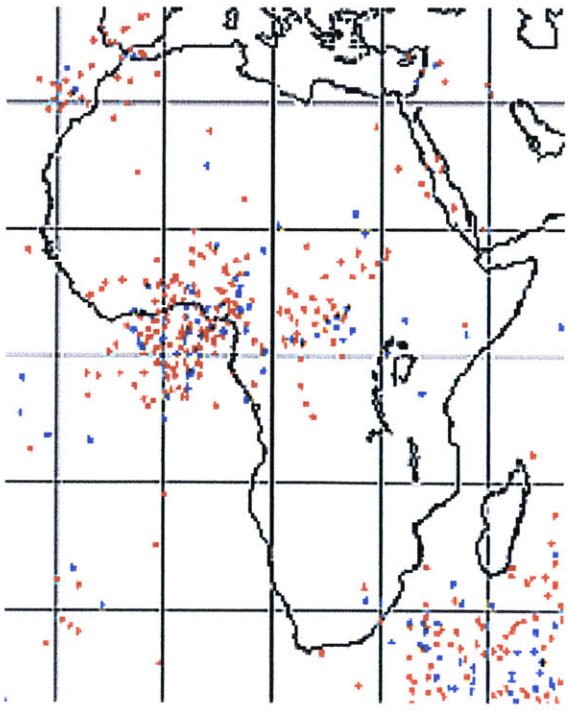

NOAA 0.1 Deg Daily (mm/d) 11 May 1998

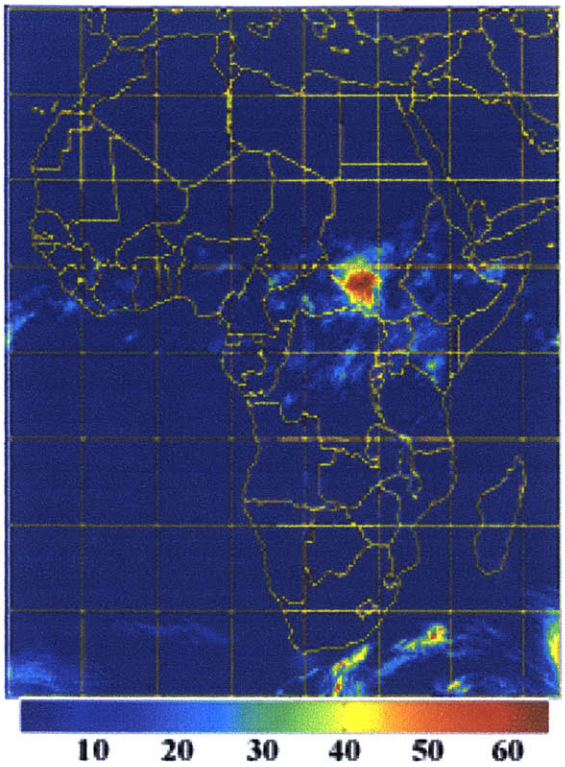

Red = Positive-Stroke
Blue = Negative-Stroke May 11, 1998

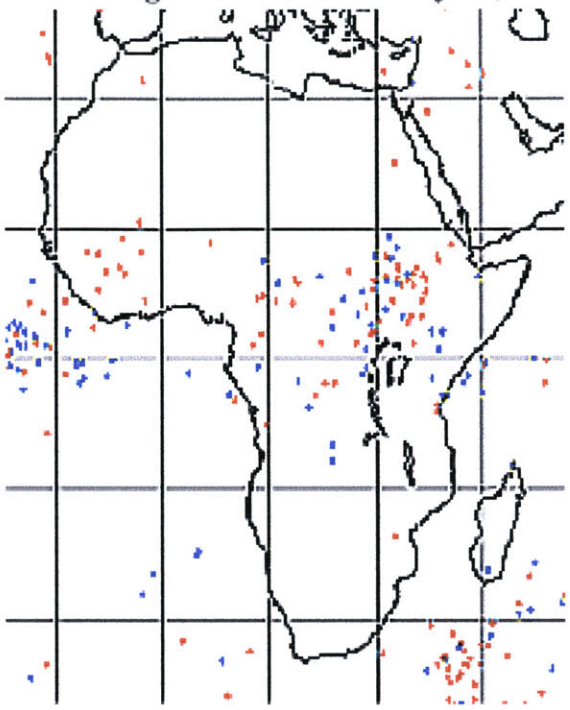

NOAA 0.1 Deg Daily (mm/d) 12 May 1998

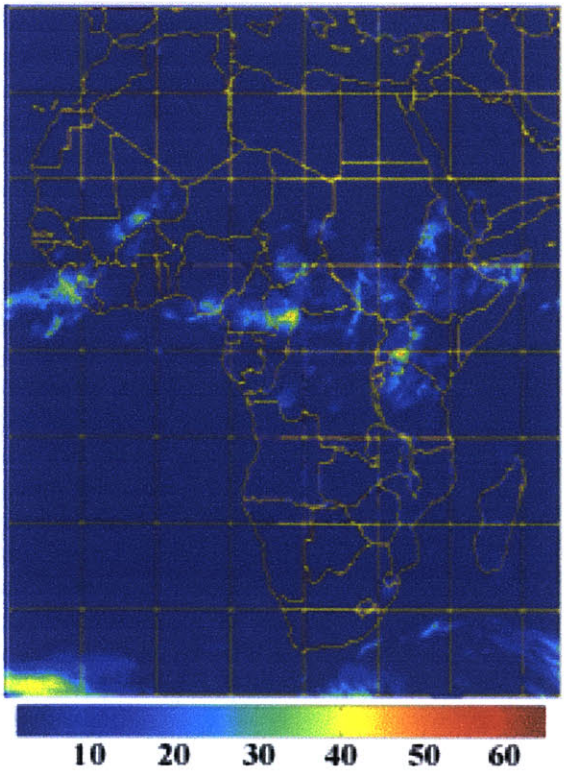

Red = Positive-Stroke
Blue = Negative-Stroke May 12, 1998

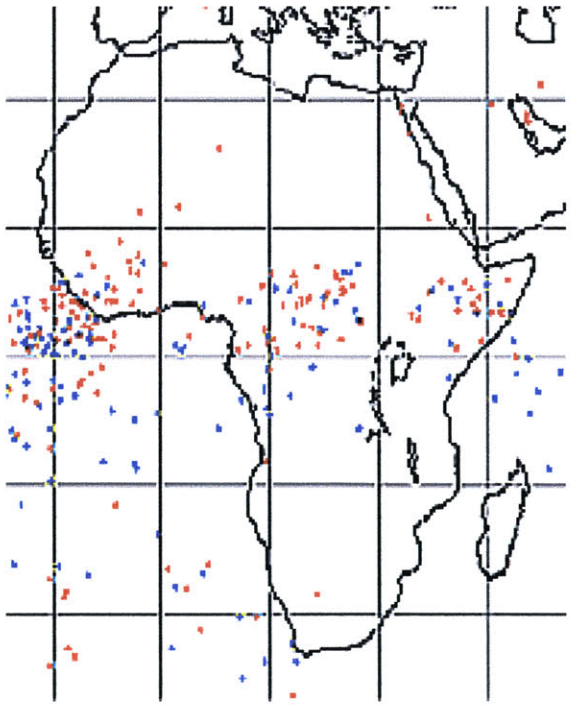

NOAA 0.1 Deg Daily (mm/d) 13 May 1998

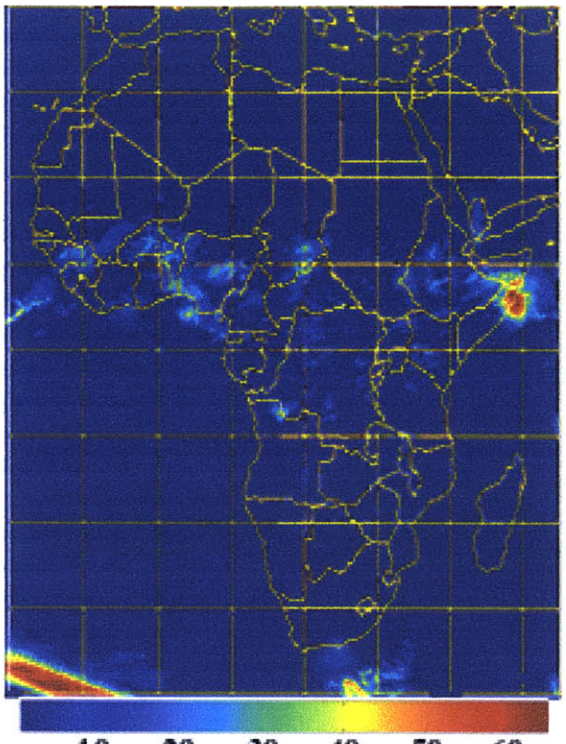

Red = Positive-Stroke
Blue = Negative-Stroke May 13, 1998

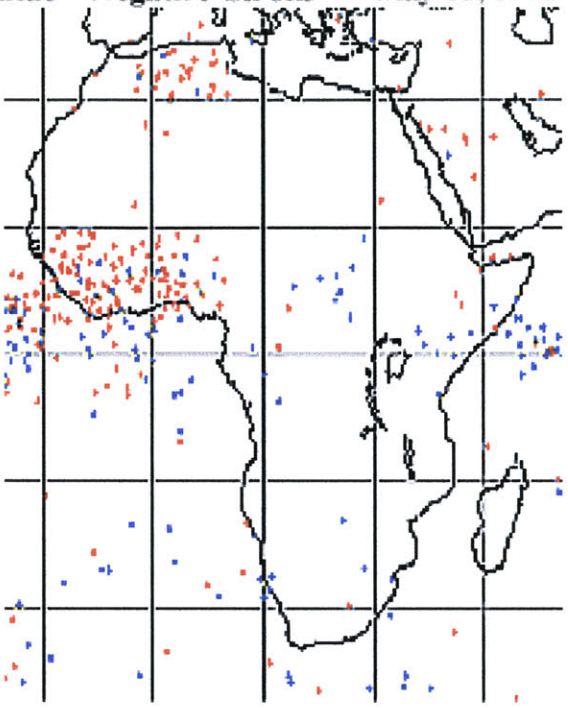

NOAA 0.1 Deg Daily (mm/d) 14 May 1998

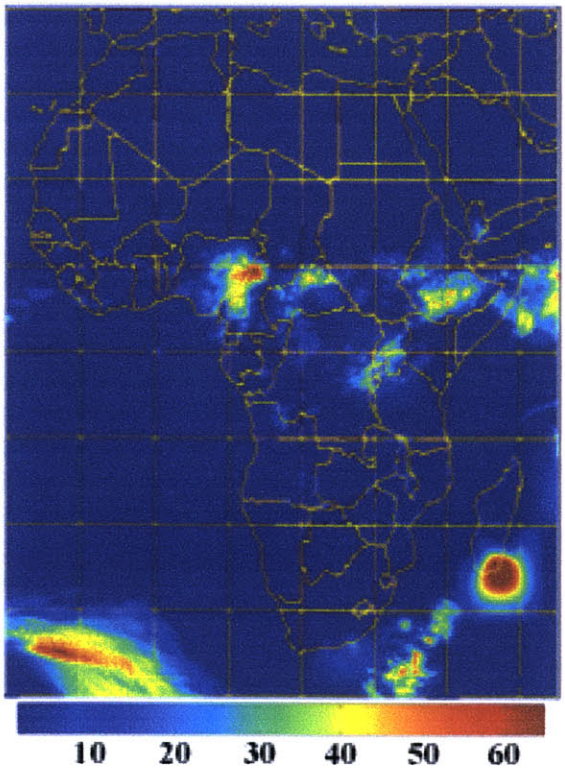

Red = Positive-Stroke
Blue = Negative-Stroke May 14, 1998

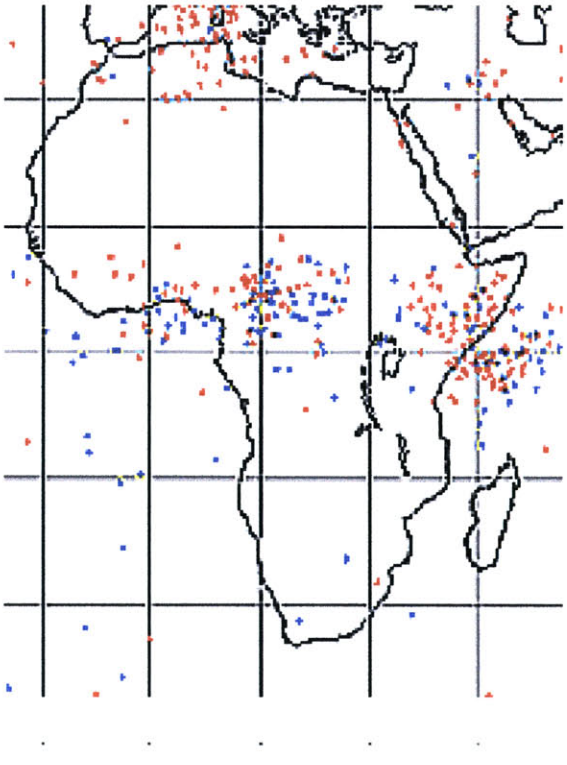

NOAA 0.1 Deg Daily (mm/d) 15 May 1998

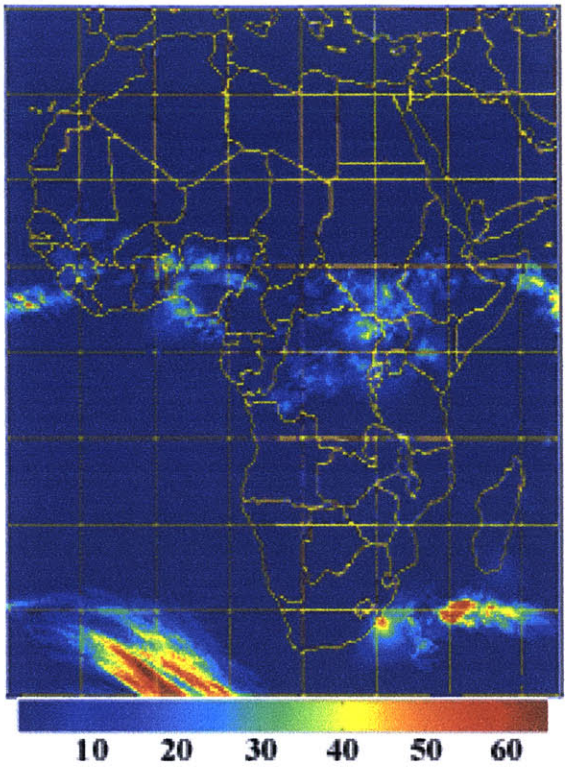

Red = Positive-Stroke
Blue = Negative-Stroke May 15, 1998

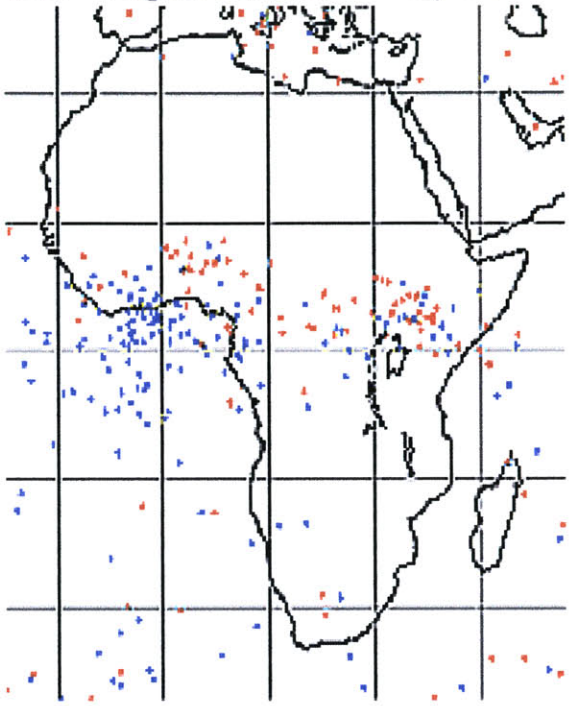

NOAA 0.1 Deg Daily (mm/d) 16 May 1998

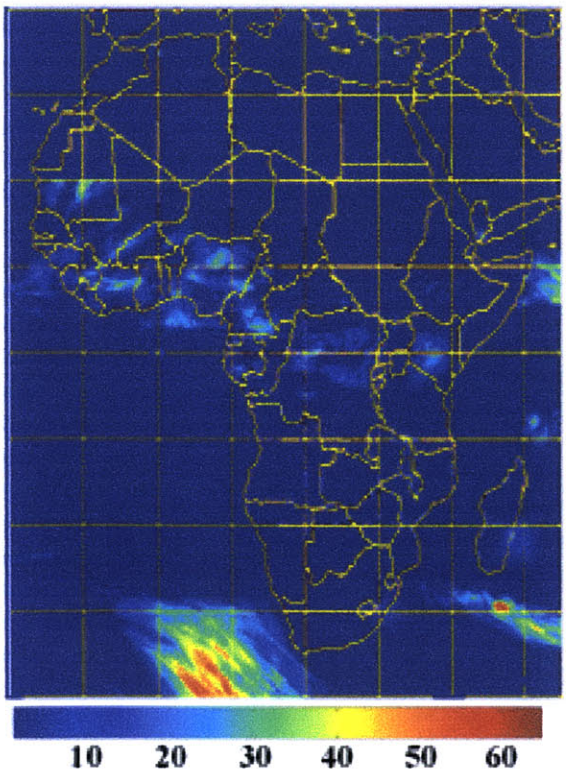

Red = Positive-Stroke
Blue = Negative-Stroke May 16, 1998

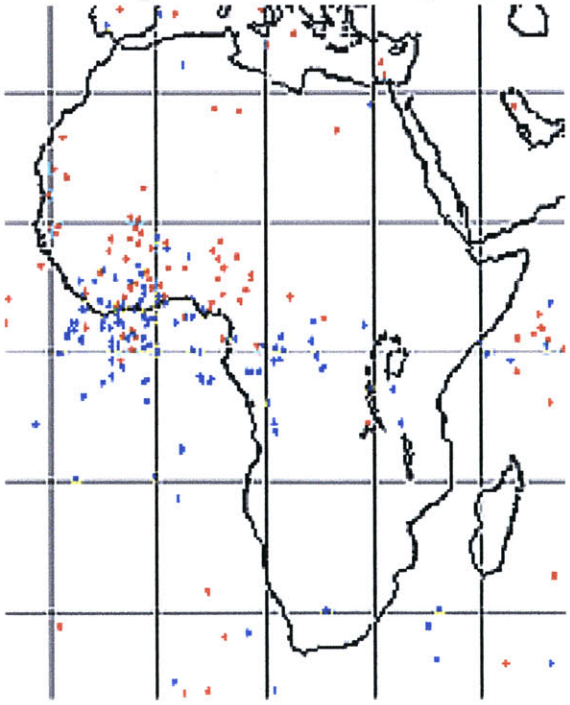

NOAA 0.1 Deg Daily (mm/d) 17 May 1998

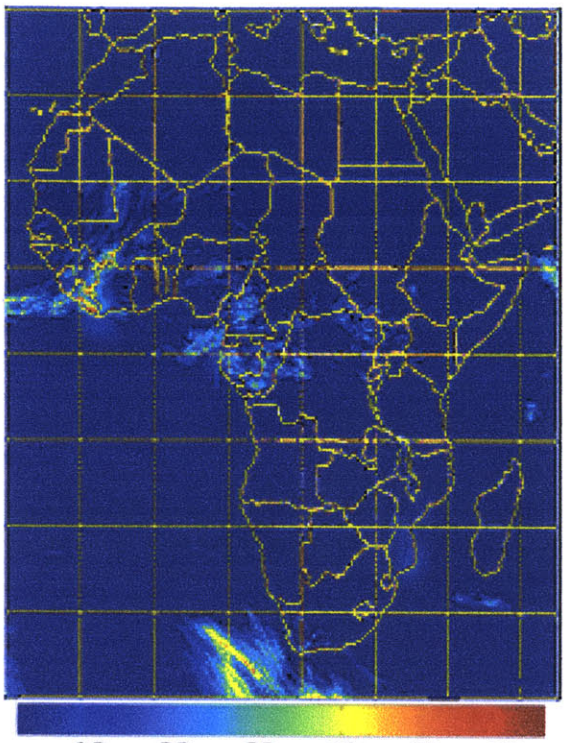

Red = Positive-Stroke
Blue = Negative-Stroke May 17, 1998

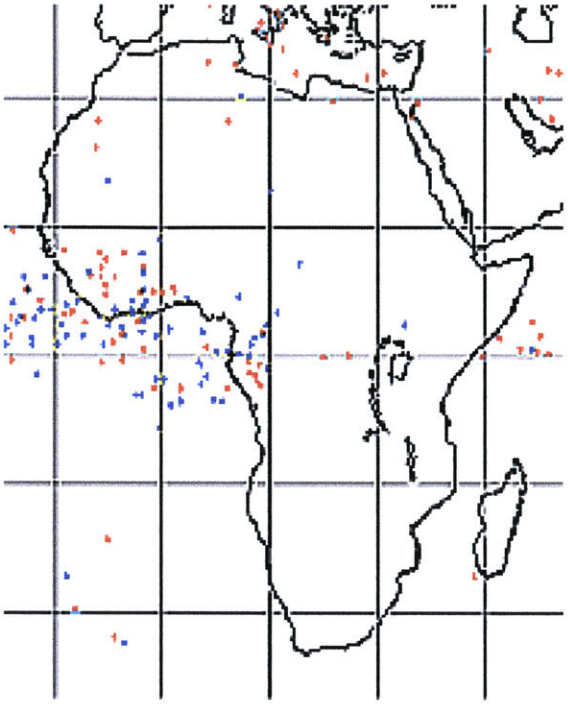

NOAA 0.1 Deg Daily (mm/d) 18 May 1998

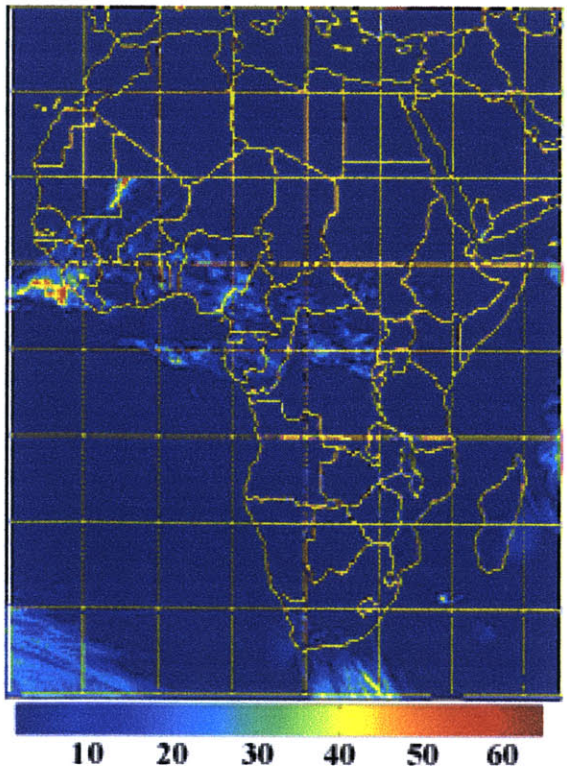

Red = Positive-Stroke
Blue = Negative-Stroke May 18, 1998

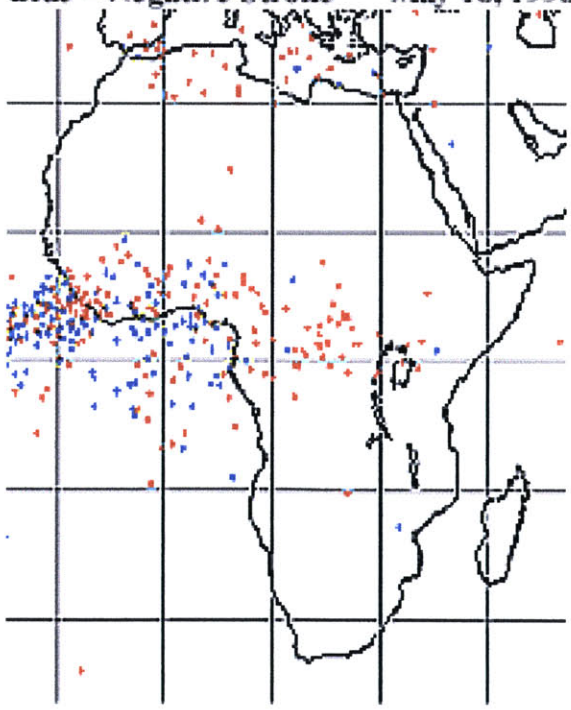

NOAA 0.1 Deg Daily (mm/d) 19 May 1998

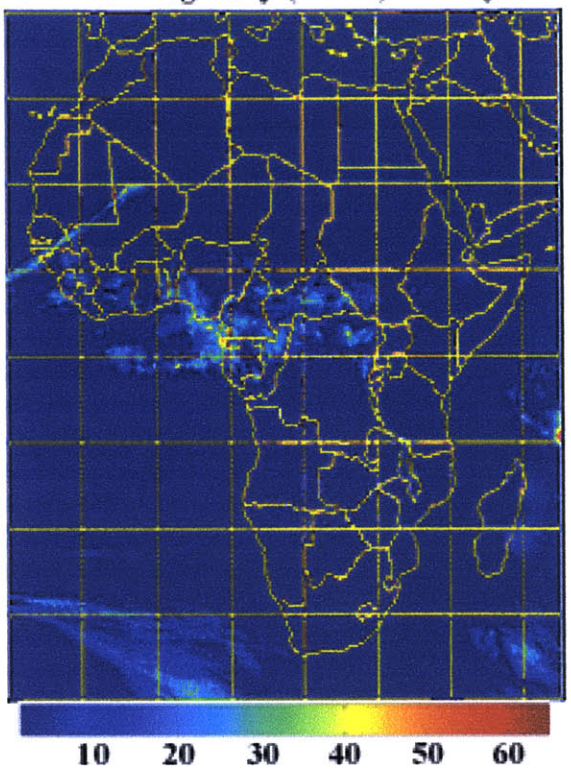

Red = Positive-Stroke
Blue = Negative-Stroke May 19, 1998

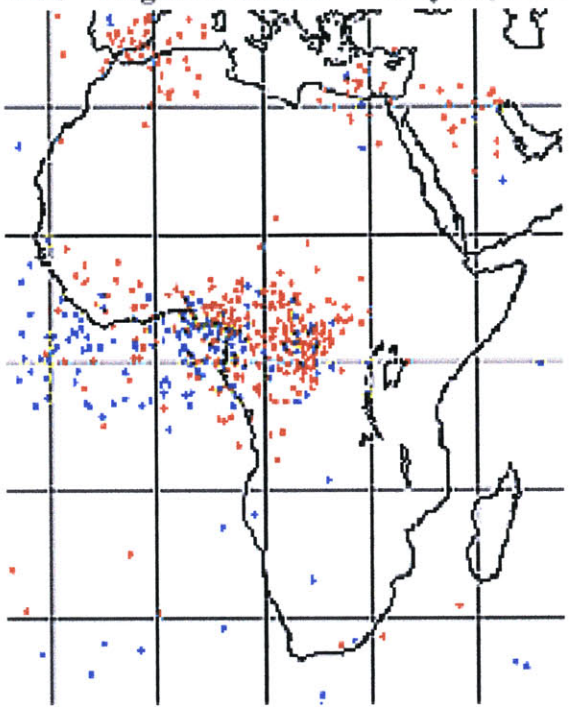

NOAA 0.1 Deg Daily (mm/d) 20 May 1998

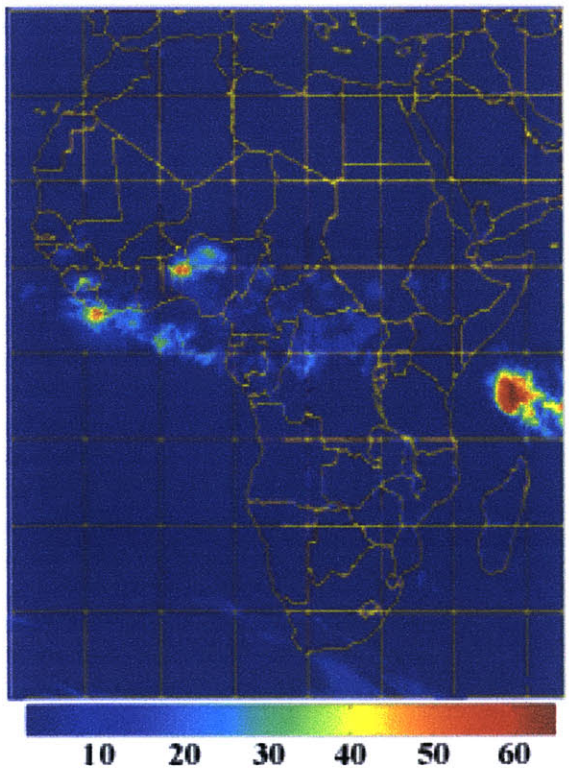

Red = Positive-Stroke
Blue = Negative-Stroke May 20, 1998

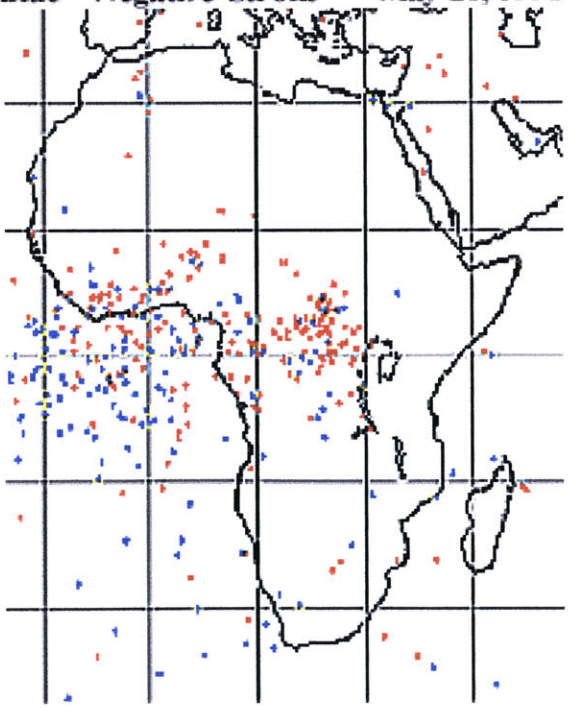

NOAA 0.1 Deg Daily (mm/d) 21 May 1998

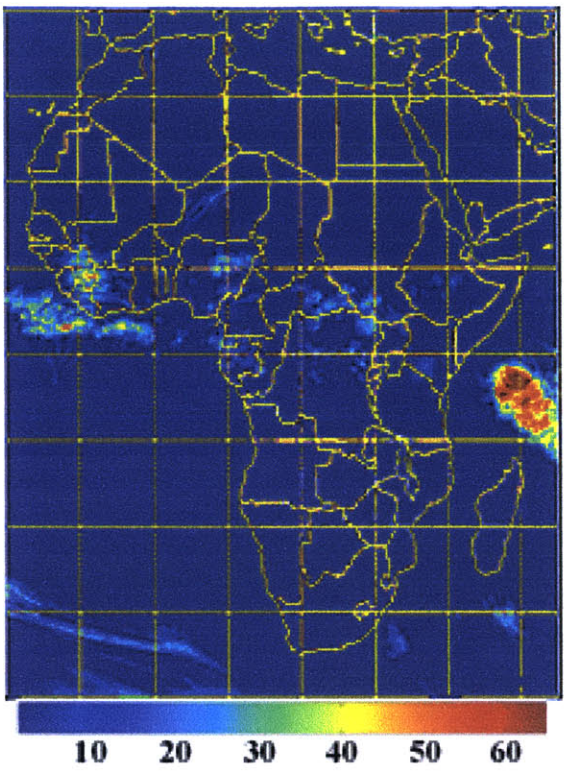

Red = Positive-Stroke
Blue = Negative-Stroke May 21, 1998

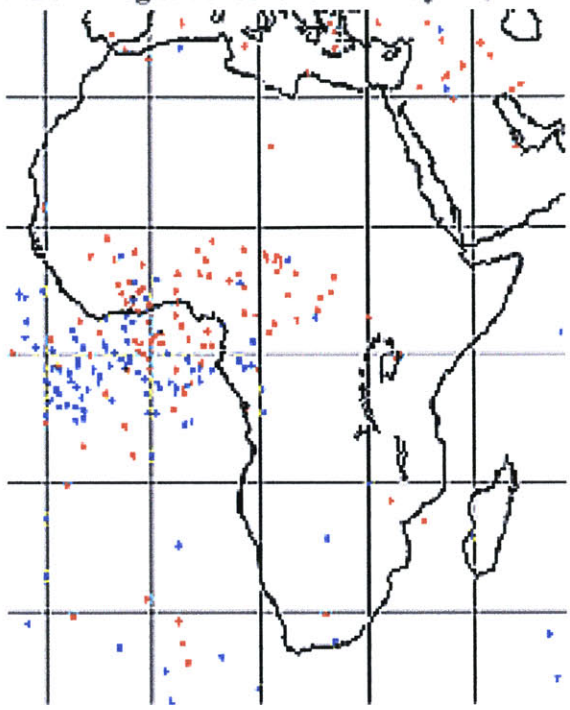

NOAA 0.1 Deg Daily (mm/d) 22 May 1998

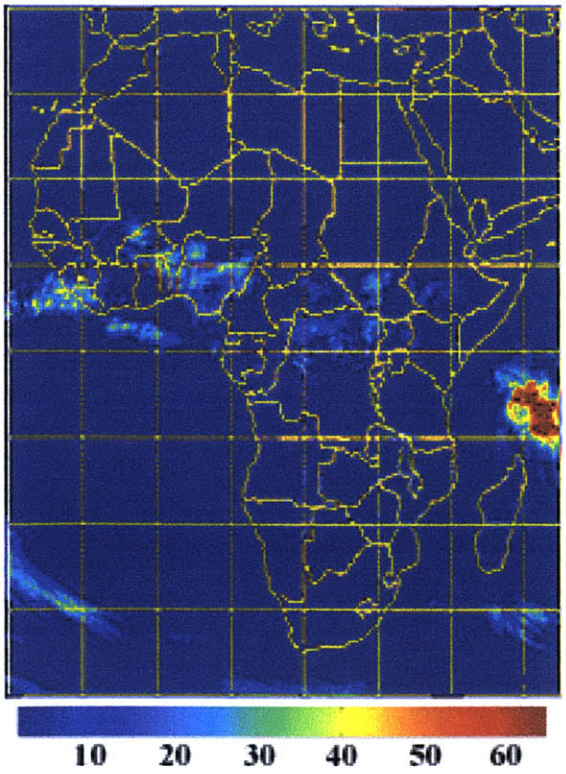

Red = Positive-Stroke
Blue = Negative-Stroke May 22, 1998

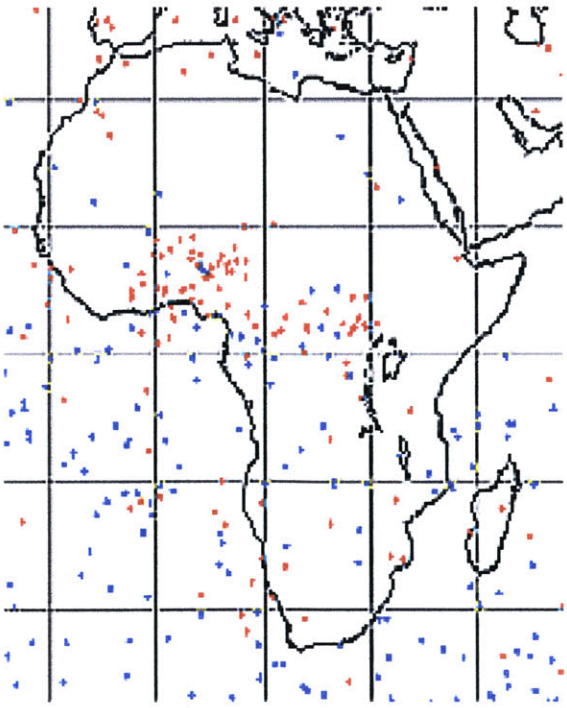

NOAA 0.1 Deg Daily (mm/d) 23 May 1998

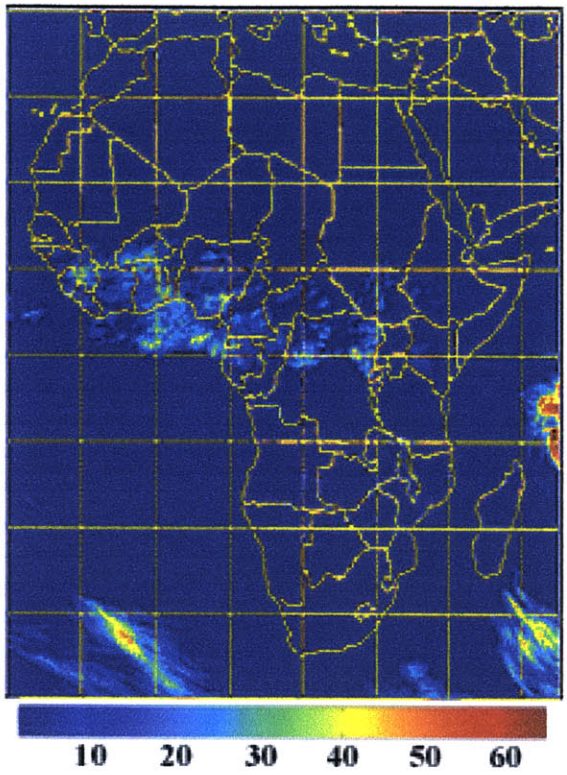

Red = Positive-Stroke
Blue = Negative-Stroke May 23, 1998

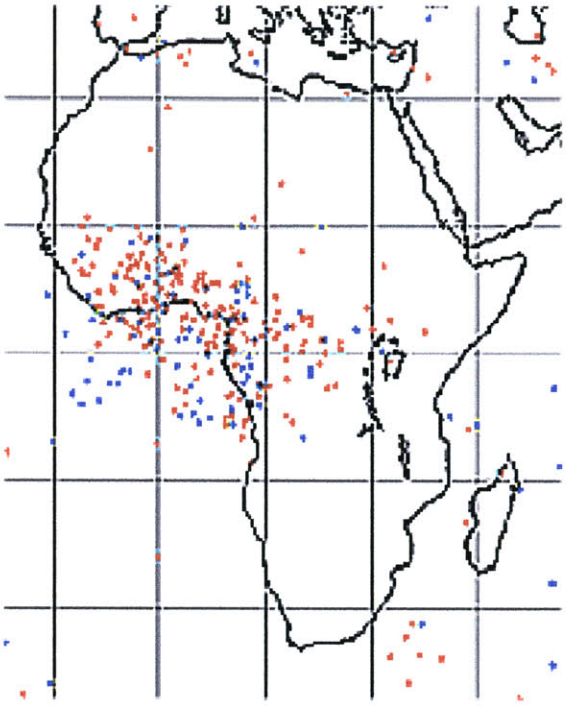

NOAA 0.1 Deg Daily (mm/d) 24 May 1998

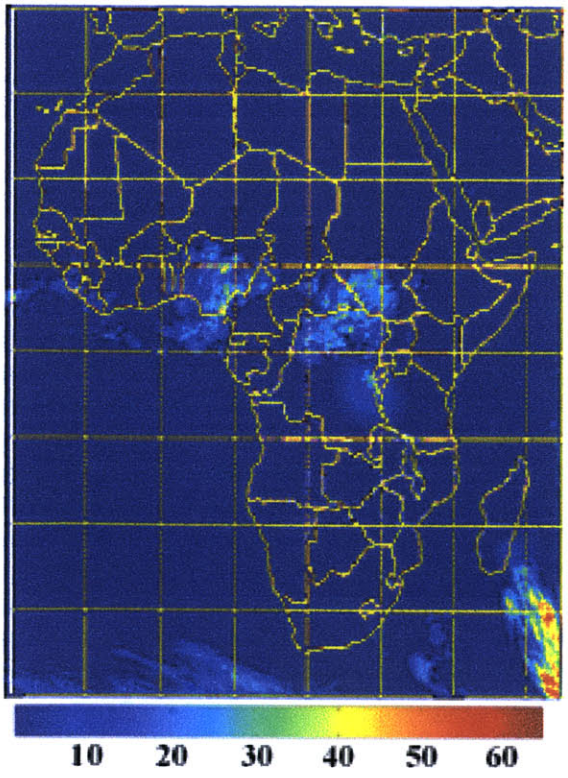

Red = Positive-Stroke
Blue = Negative-Stroke May 24, 1998

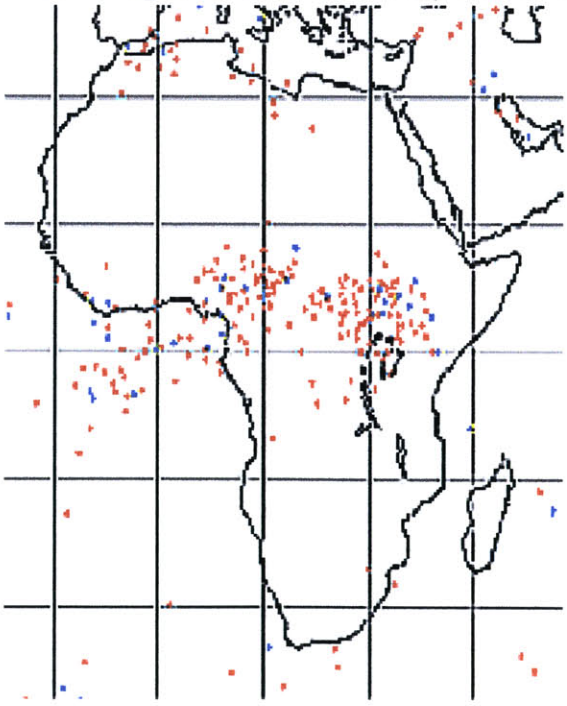

NOAA 0.1 Deg Daily (mm/d) 25 May 1998

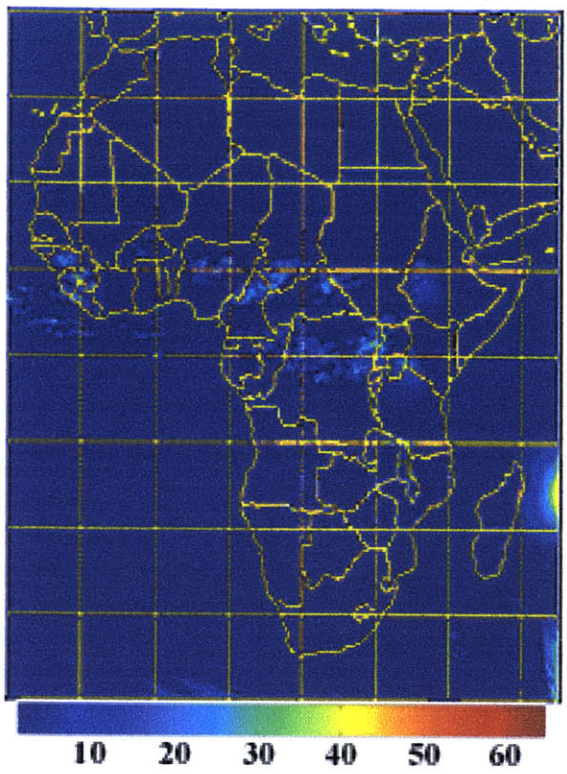

Red = Positive-Stroke
Blue = Negative-Stroke May 25, 1998

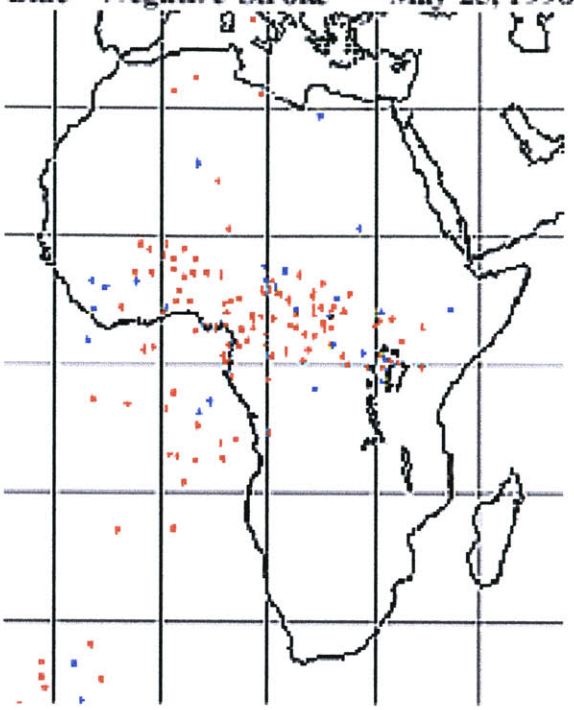

NOAA 0.1 Deg Daily (mm/d) 26 May 1998

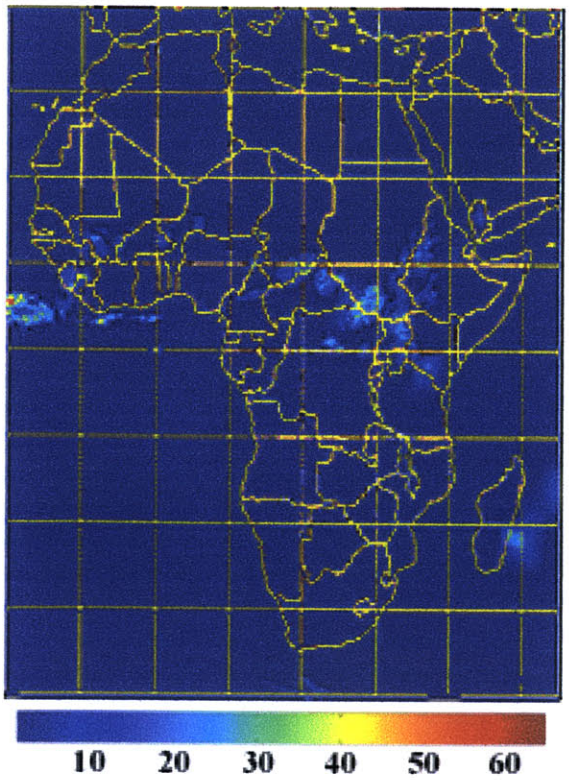

Red = Positive-Stroke
Blue = Negative-Stroke May 26, 1998

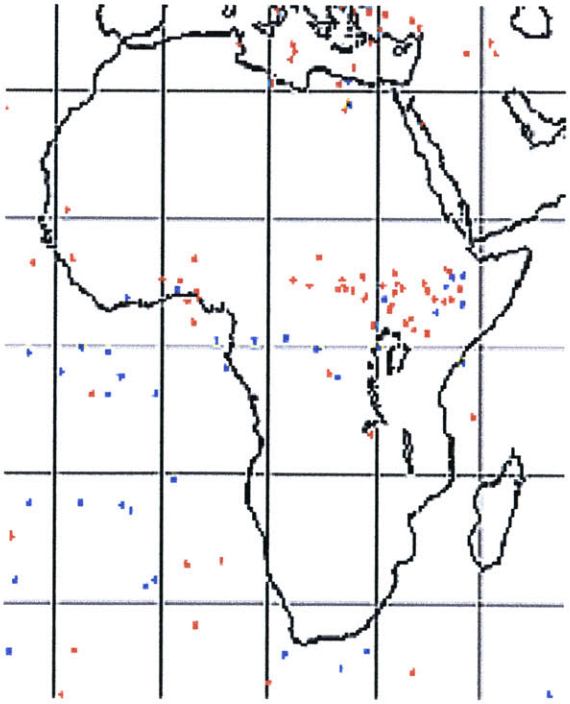

NOAA 0.1 Deg Daily (mm/d) 27 May 1998

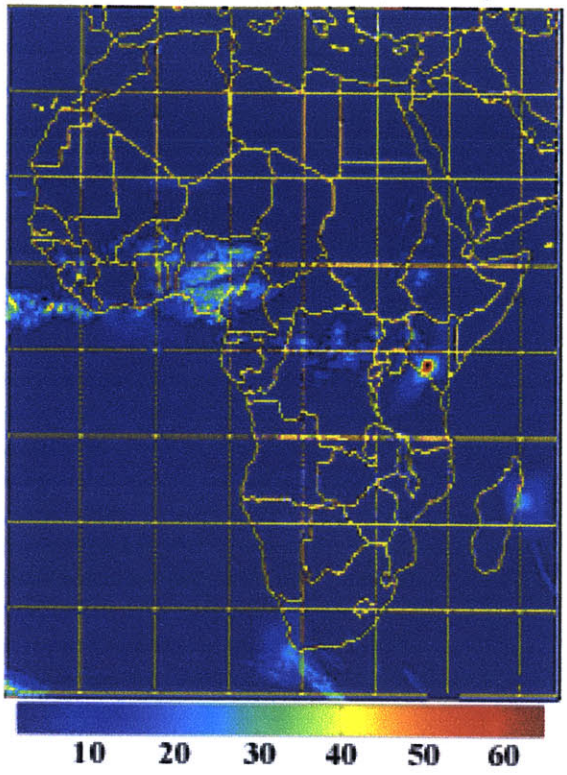

Red = Positive-Stroke
Blue = Negative-Stroke May 27, 1998

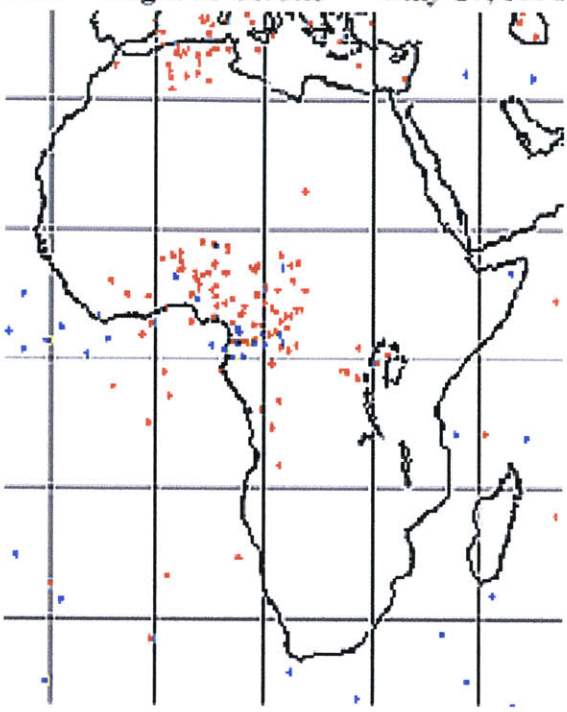

NOAA 0.1 Deg Daily (mm/d) 28 May 1998

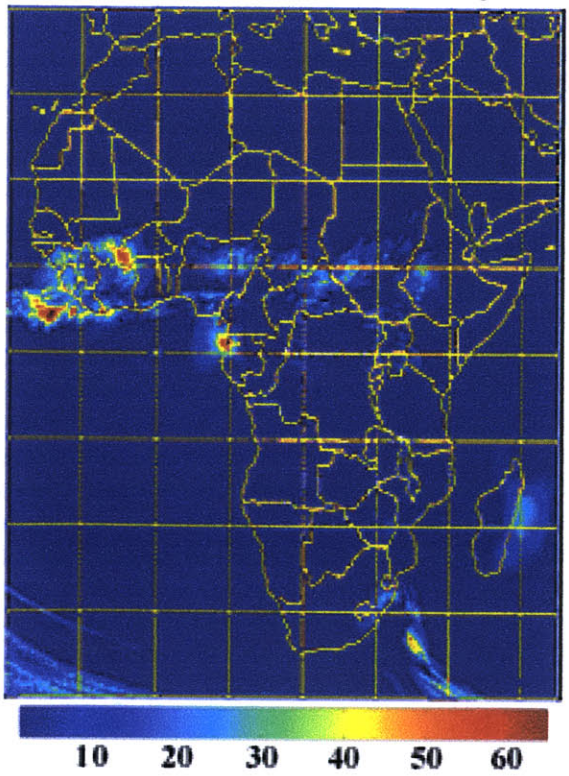

Red = Positive-Stroke
Blue = Negative-Stroke May 28, 1998

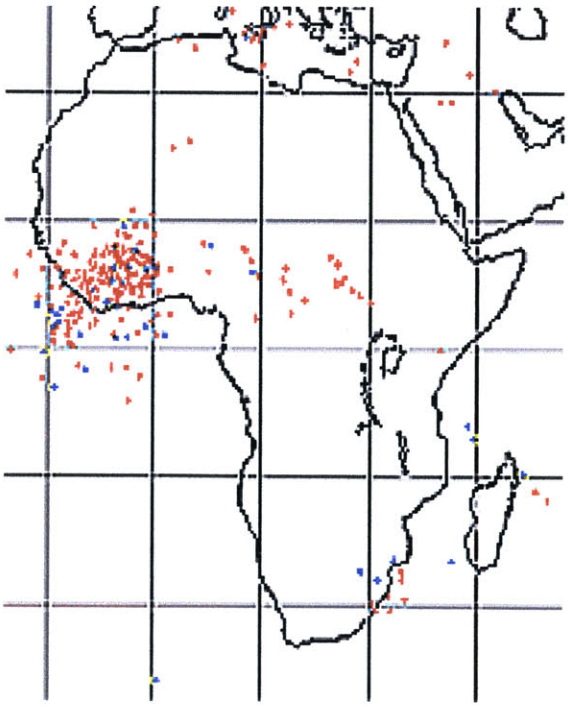

NOAA 0.1 Deg Daily (mm/d) 29 May 1998

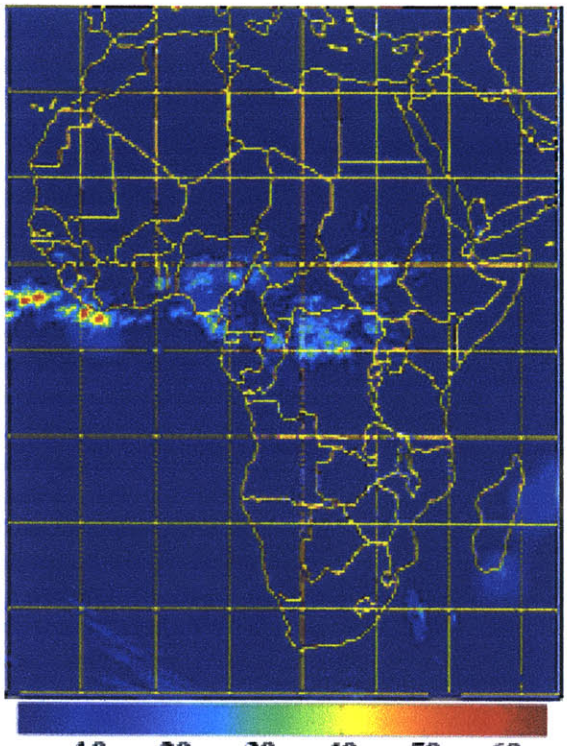

Red = Positive-Stroke
Blue = Negative-Stroke May 29, 1998

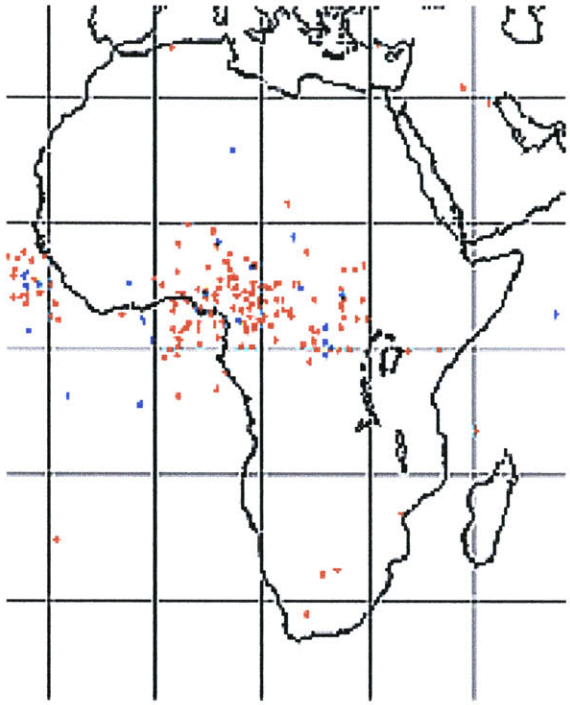

NOAA 0.1 Deg Daily (mm/d) 30 May 1998

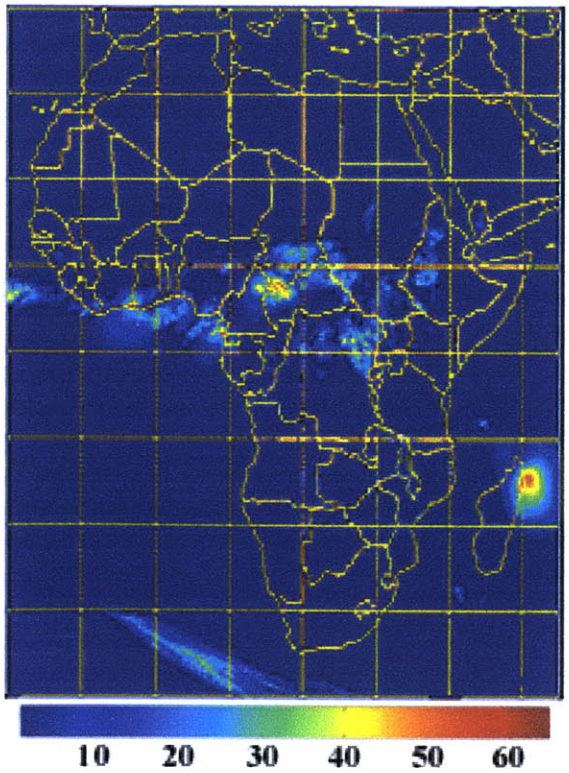

Red = Positive-Stroke
Blue = Negative-Stroke May 30, 1998

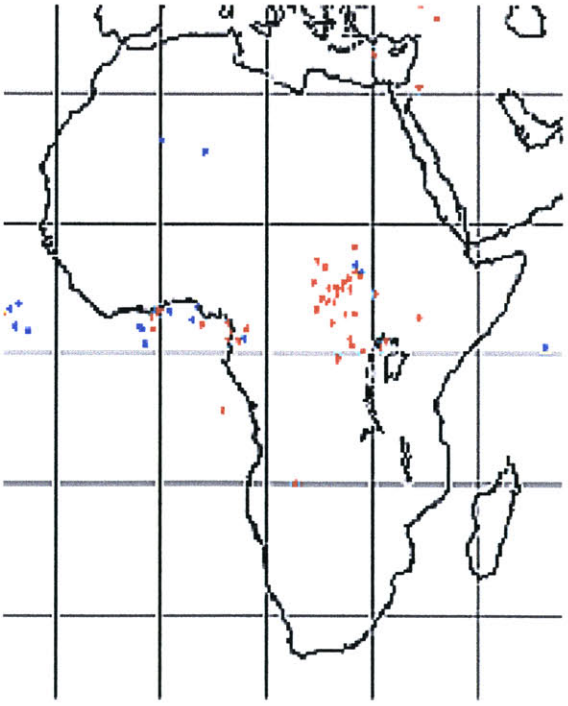

NOAA 0.1 Deg Daily (mm/d) 31 May 1998

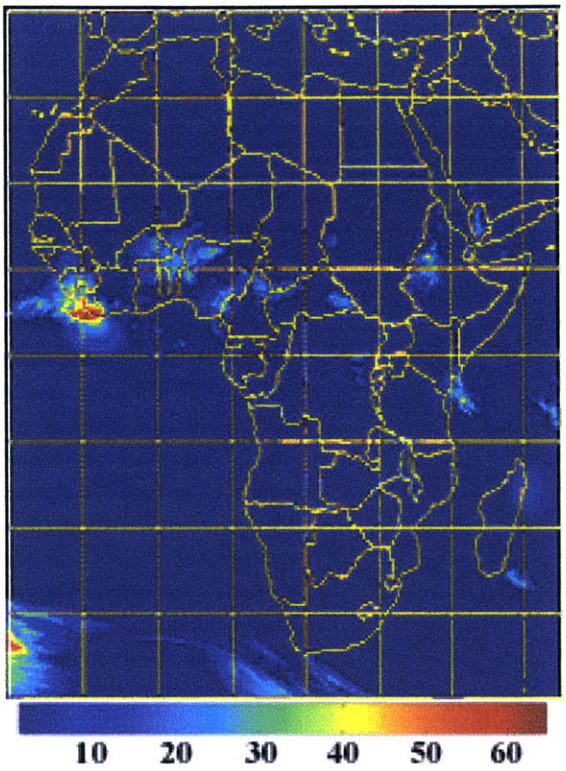

Red = Positive-Stroke
Blue = Negative-Stroke May 31, 1998

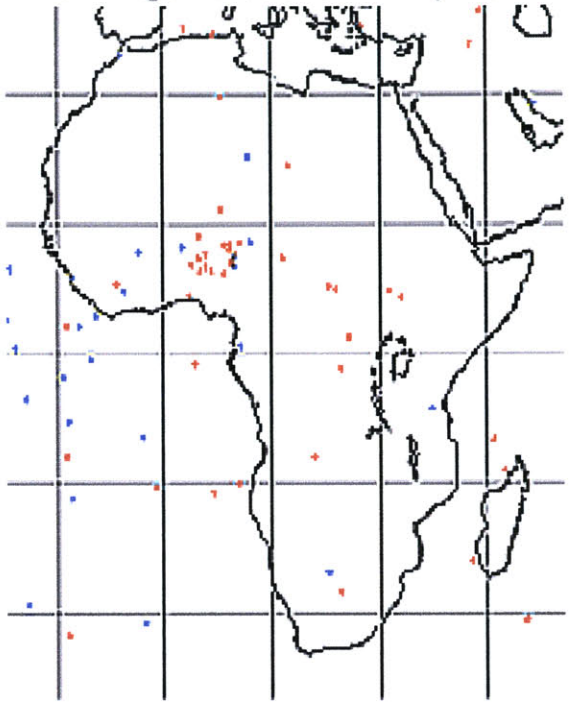

NOAA 0.1 Deg Daily (mm/d) 1 Jun 1998

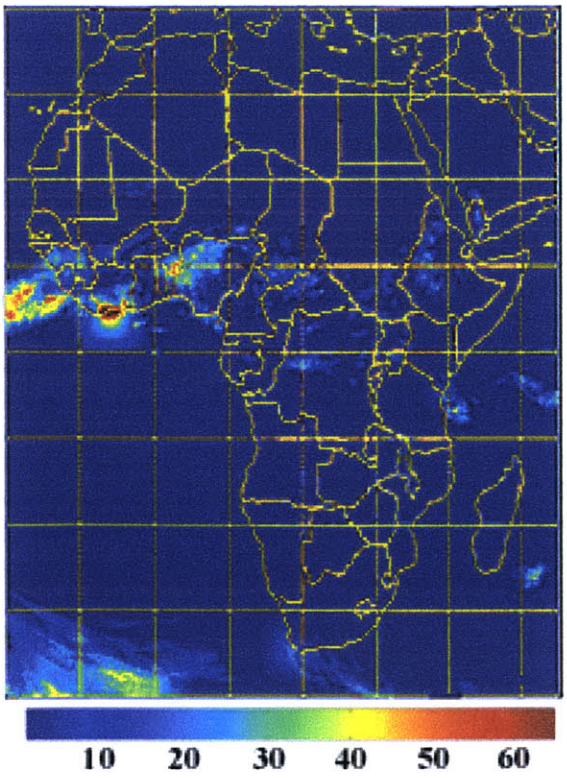

Red = Positive-Stroke
Blue = Negative-Stroke June 1, 1998

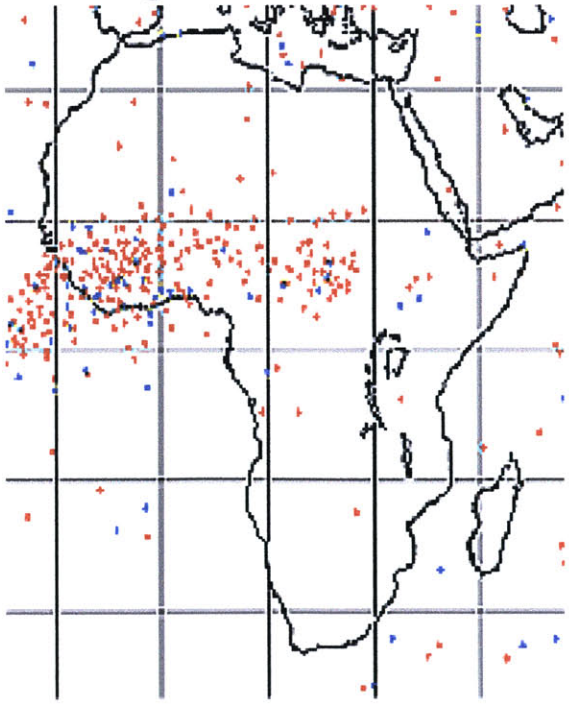

NOAA 0.1 Deg Daily (mm/d) 2 Jun 1998

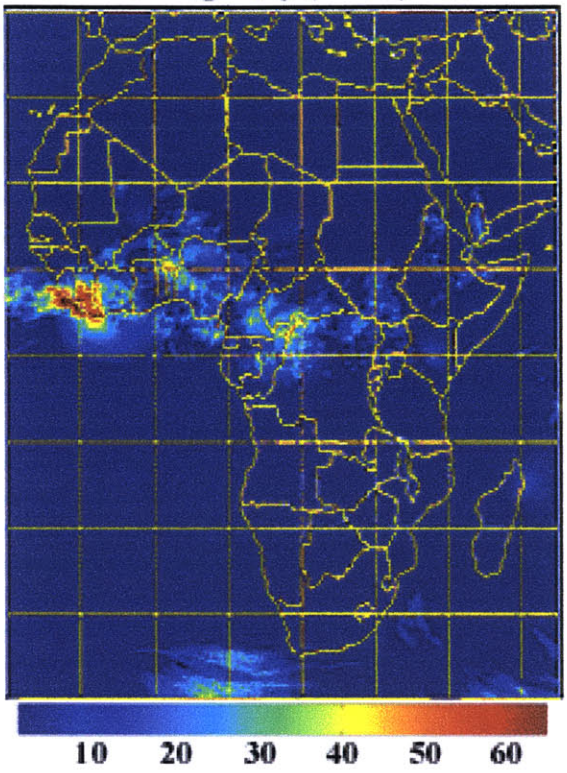

Red = Positive-Stroke
Blue = Negative-Stroke June 2, 1998

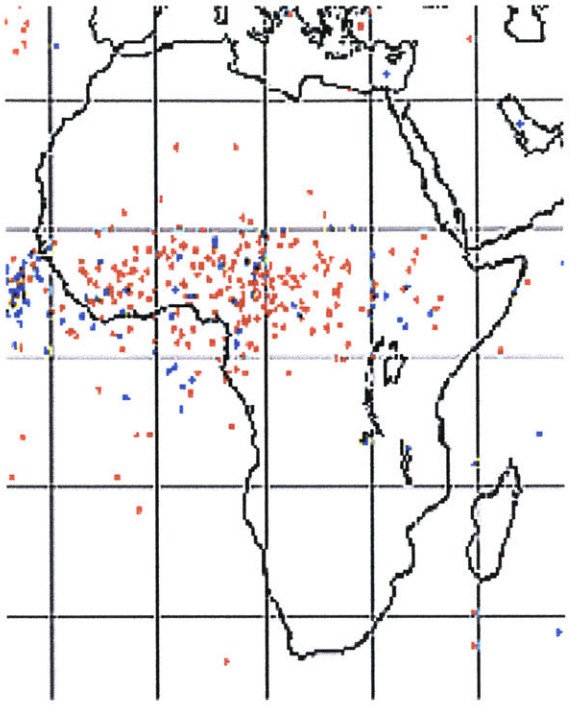

NOAA 0.1 Deg Daily (mm/d) 3 Jun 1998

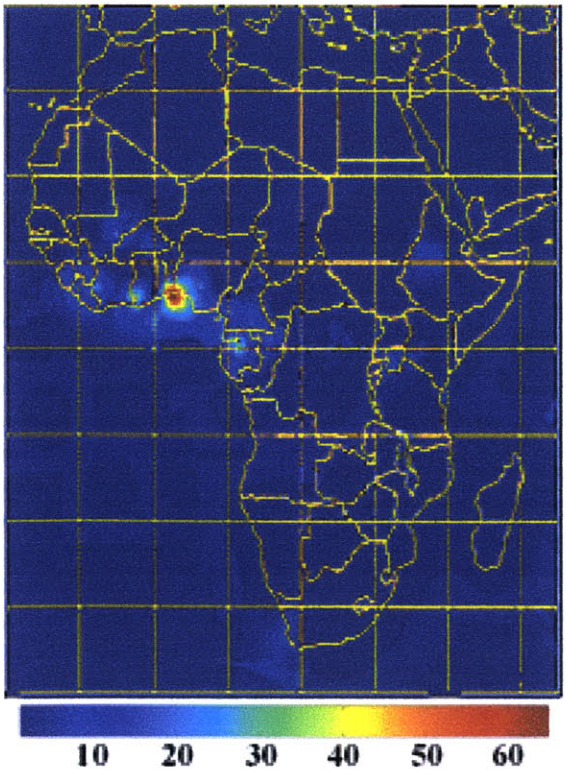

Red = Positive-Stroke
Blue = Negative-Stroke June 3, 1998

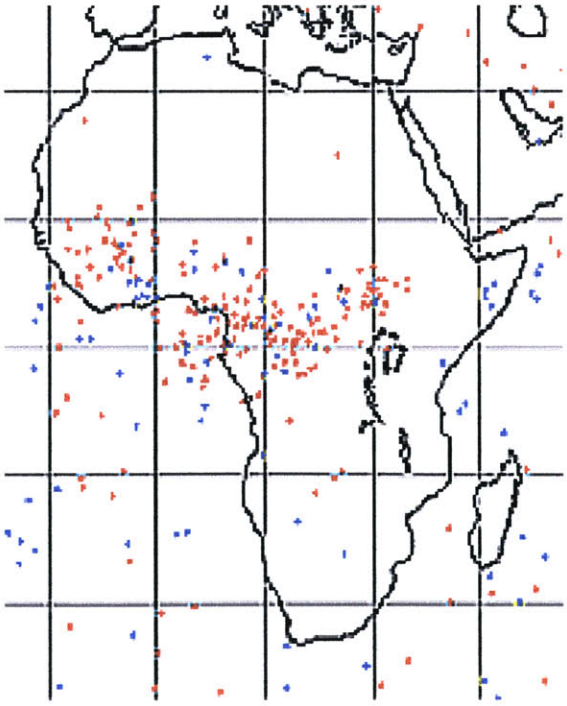

NOAA 0.1 Deg Daily (mm/d) 4 Jun 1998

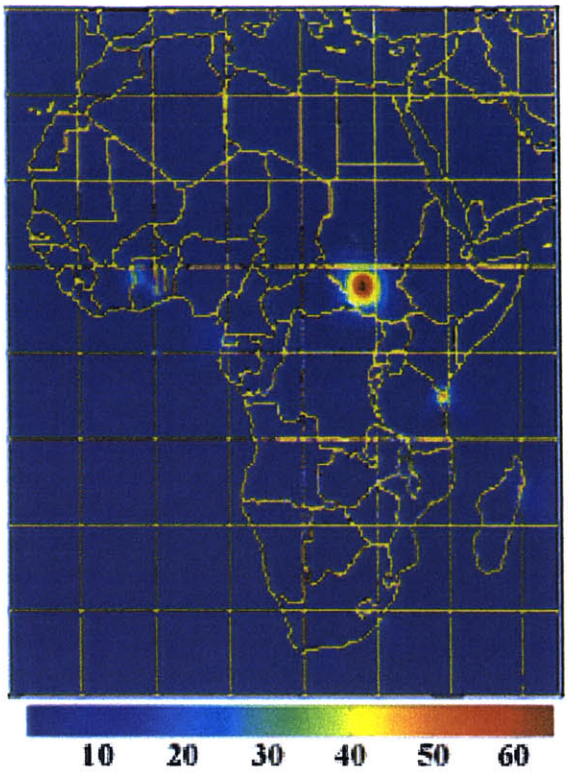

Red = Positive-Stroke
Blue = Negative-Stroke June 4, 1998

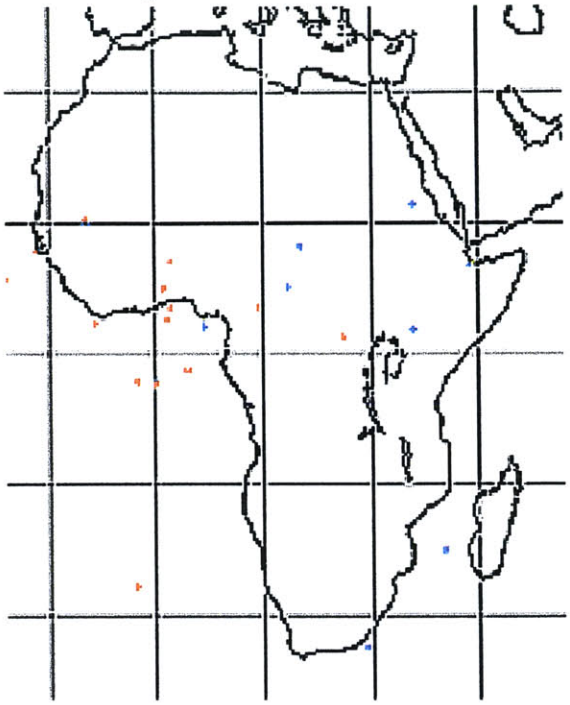

NOAA 0.1 Deg Daily (mm/d) 5 Jun 1998

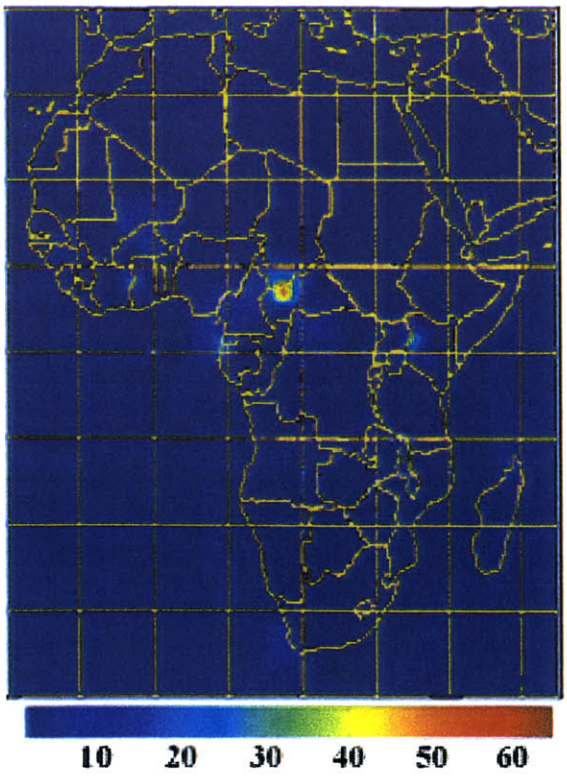

Red = Positive-Stroke
Blue = Negative-Stroke June 5, 1998

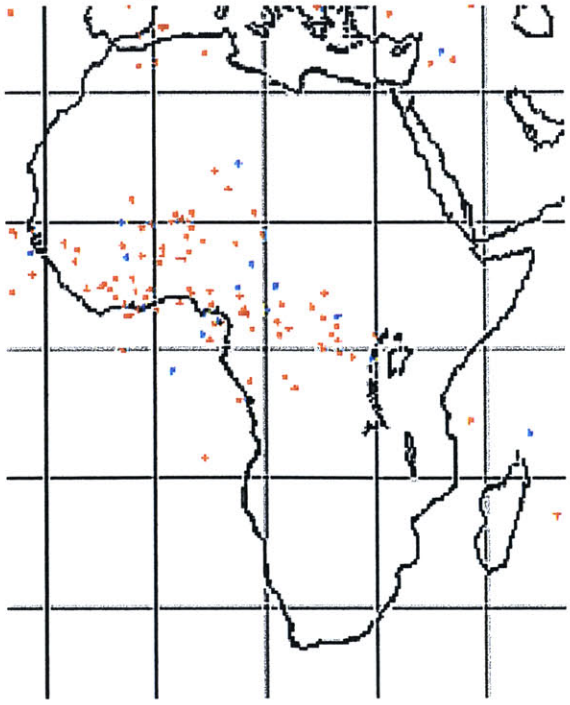

NOAA 0.1 Deg Daily (mm/d) 6 Jun 1998

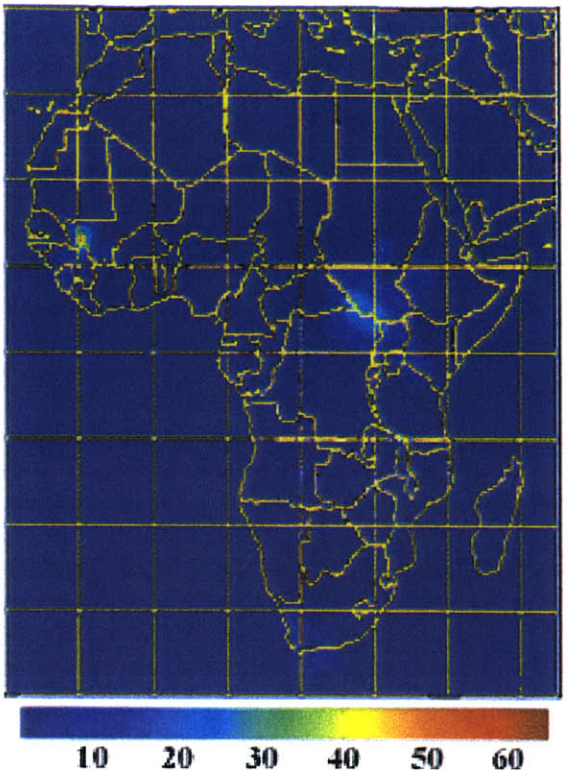

Red = Positive-Stroke
Blue = Negative-Stroke June 6, 1998

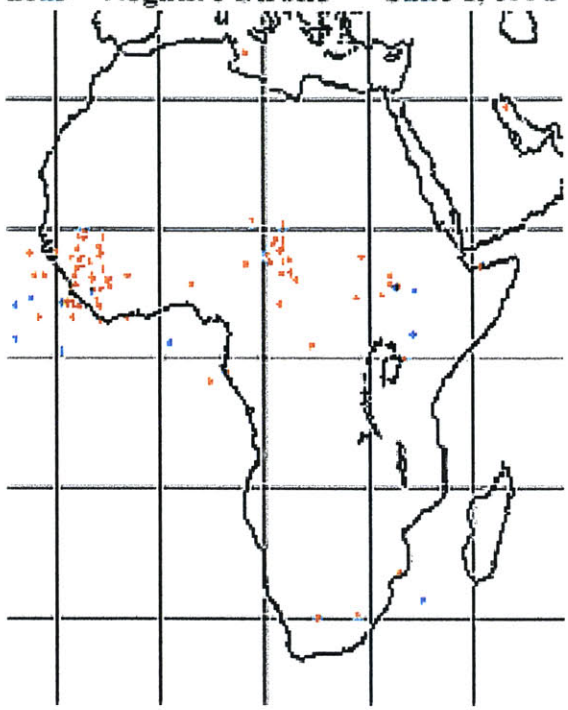

NOAA 0.1 Deg Daily (mm/d) 7 Jun 1998

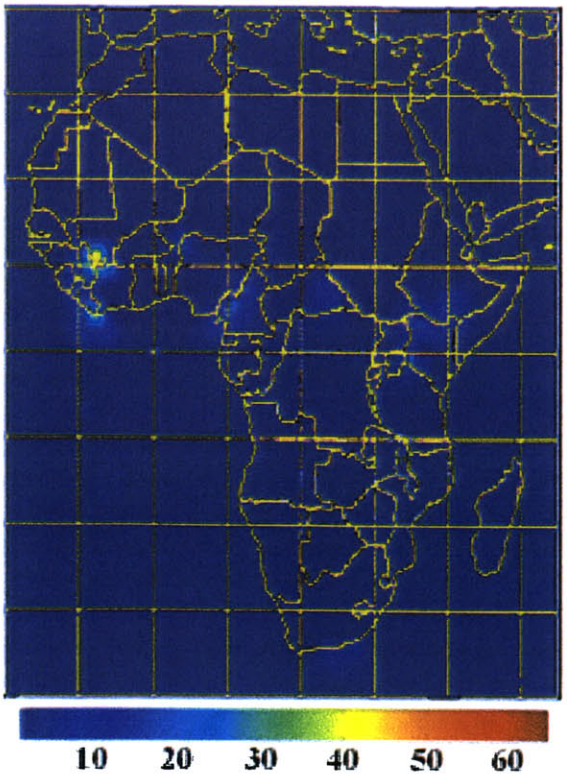

Red = Positive-Stroke
Blue = Negative-Stroke June 7, 1998

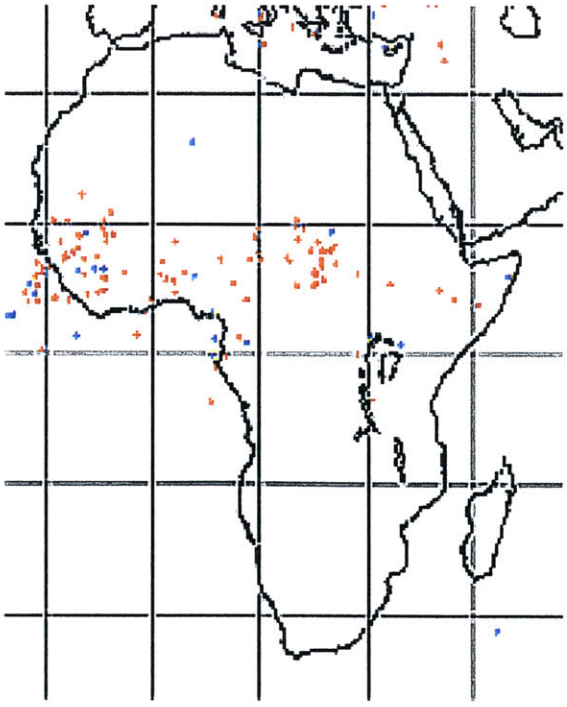

NOAA 0.1 Deg Daily (mm/d) 8 Jun 1998

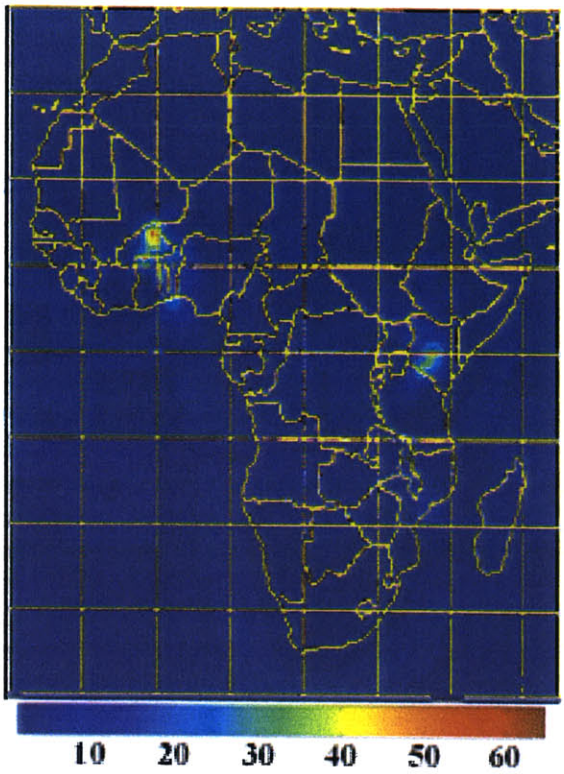

Red = Positive-Stroke
Blue = Negative-Stroke June 8, 1998

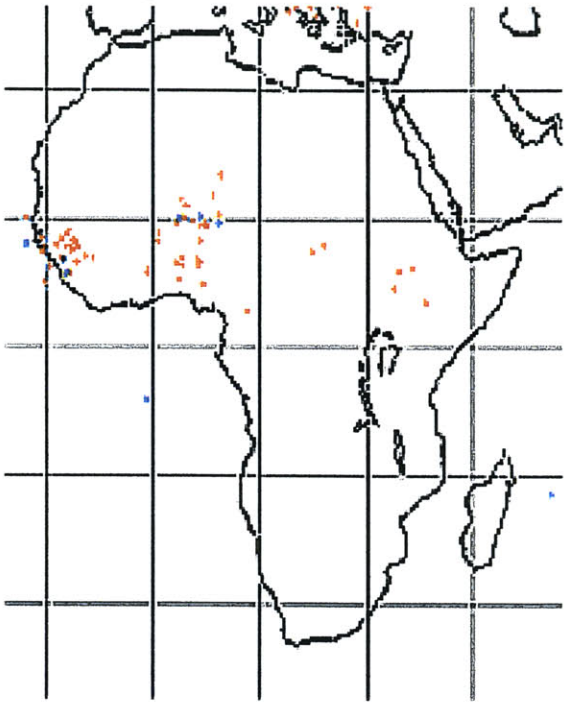

NOAA 0.1 Deg Daily (mm/d) 9 Jun 1998

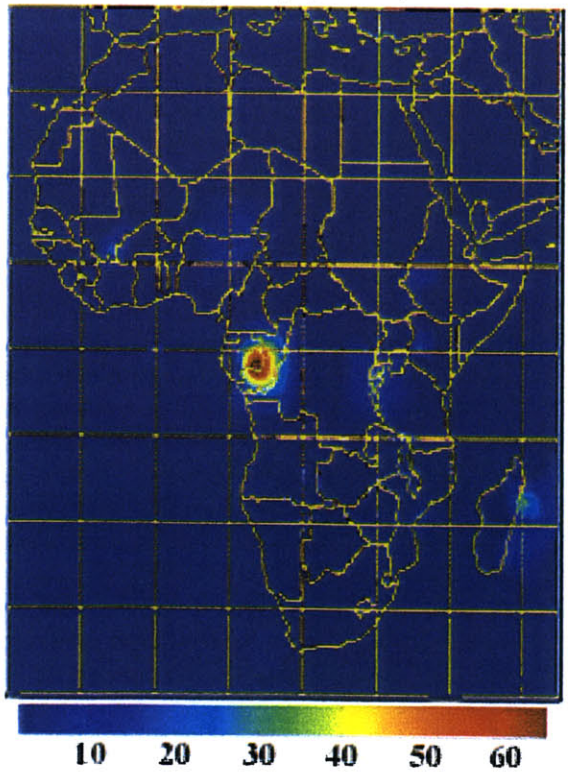

Red = Positive-Stroke
Blue = Negative-Stroke June 9, 1998

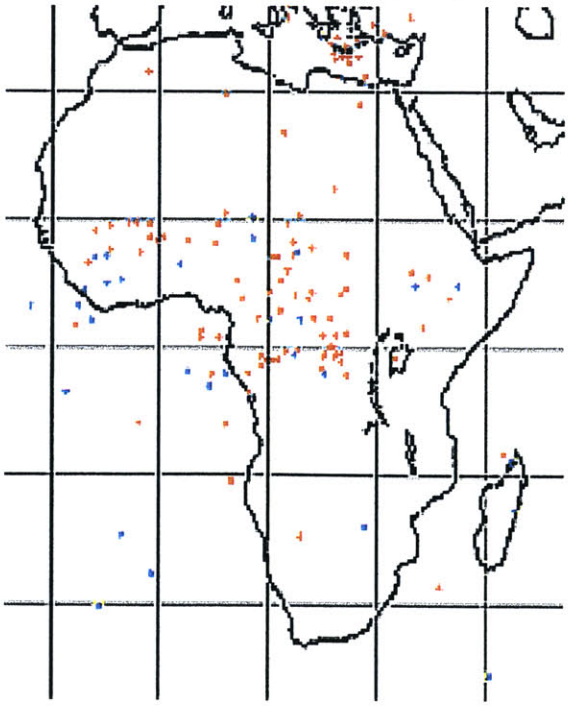

NOAA 0.1 Deg Daily (mm/d) 10 Jun 1998

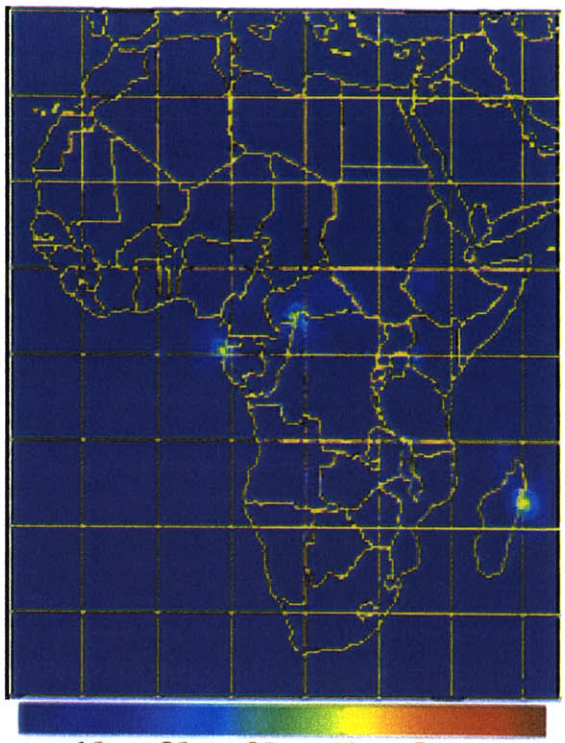

Red = Positive-Stroke
Blue = Negative-Stroke June 10, 1998

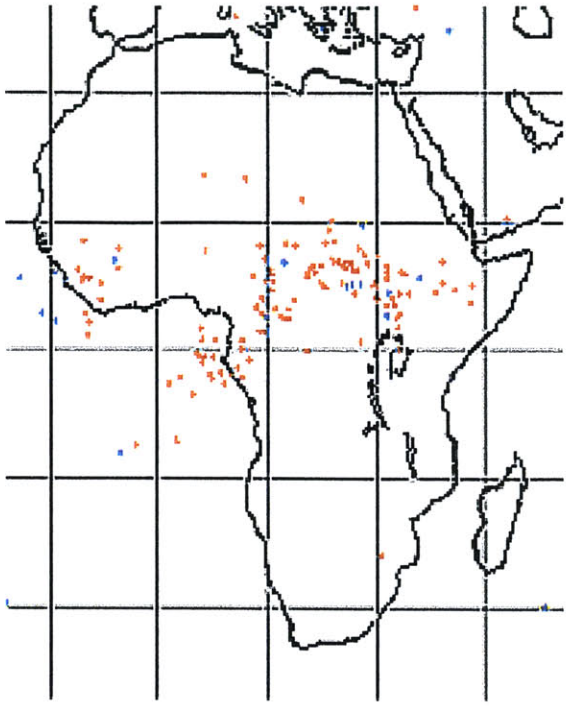

NOAA 0.1 Deg Daily (mm/d) 11 Jun 1998

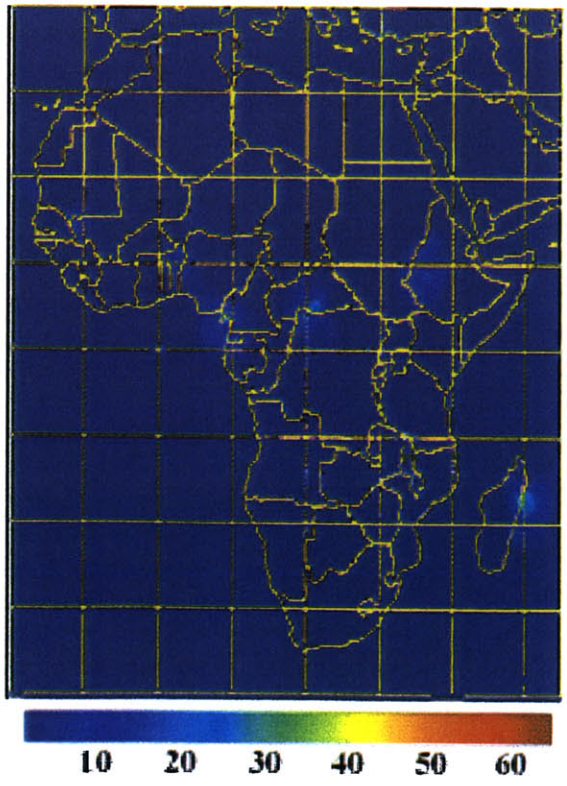

Red = Positive-Stroke
Blue = Negative-Stroke June 11, 1998

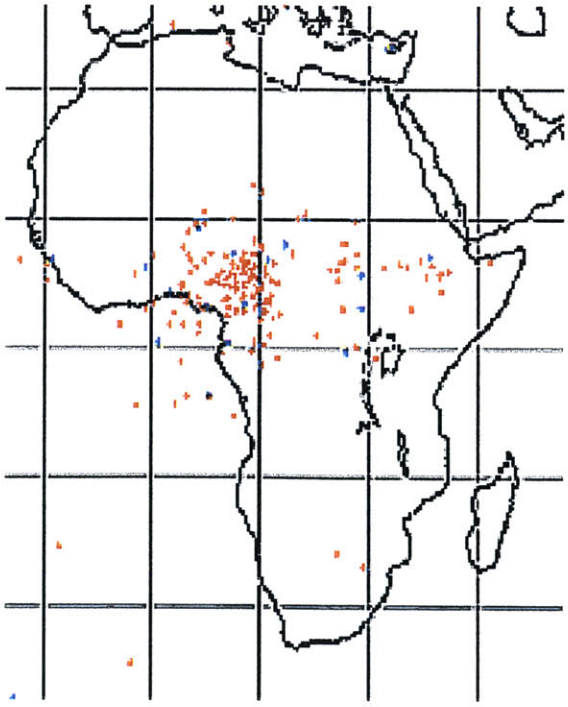

NOAA 0.1 Deg Daily (mm/d) 12 Jun 1998

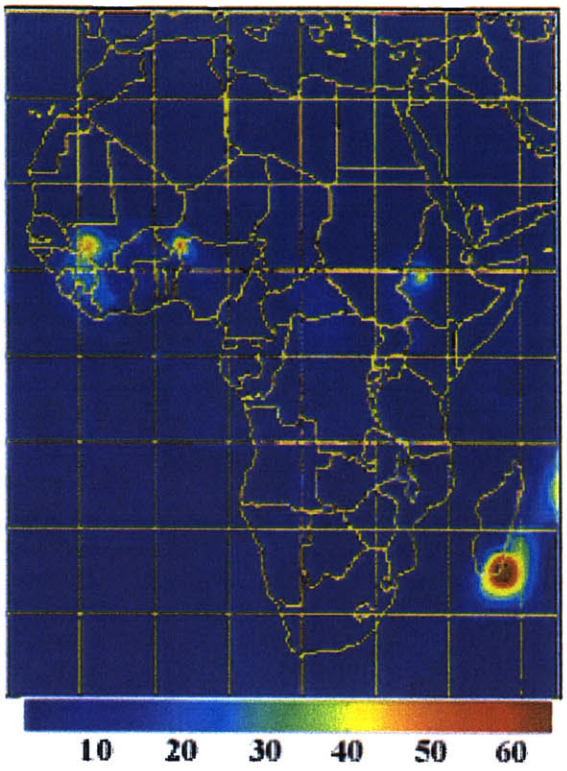

Red = Positive-Stroke
Blue = Negative-Stroke June 12, 1998

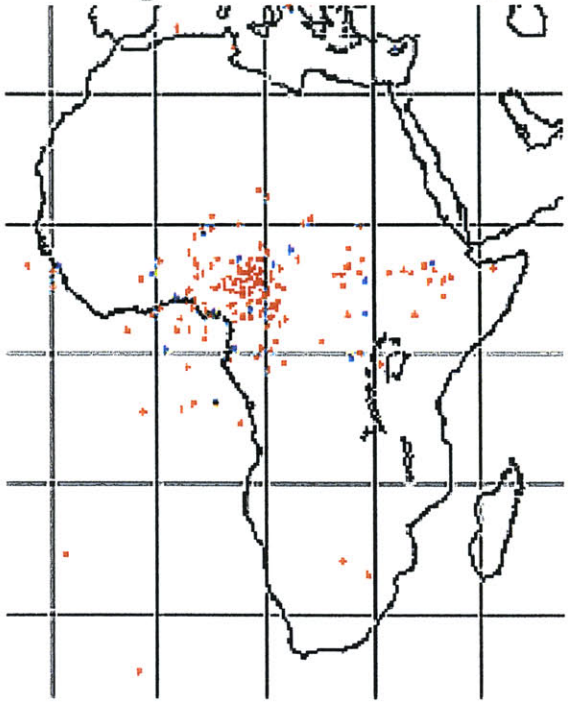

NOAA 0.1 Deg Daily (mm/d) 13 Jun 1998

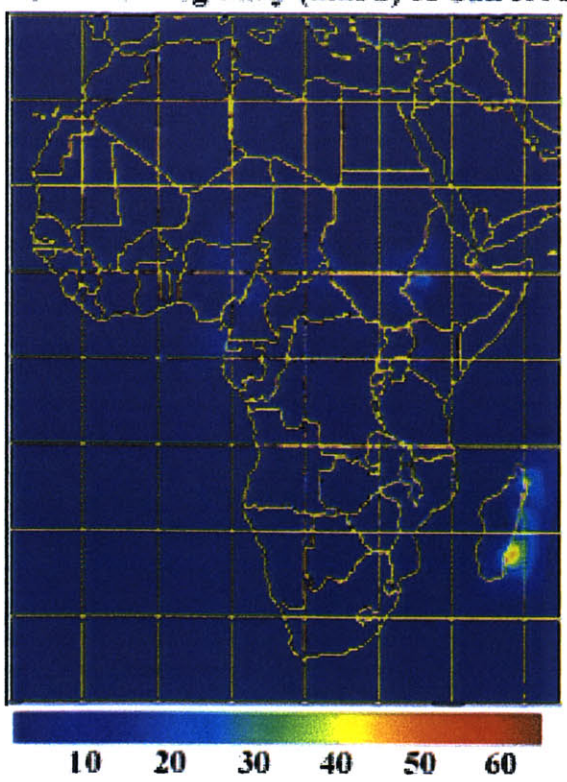

Red = Positive-Stroke
Blue = Negative-Stroke June 13, 1998

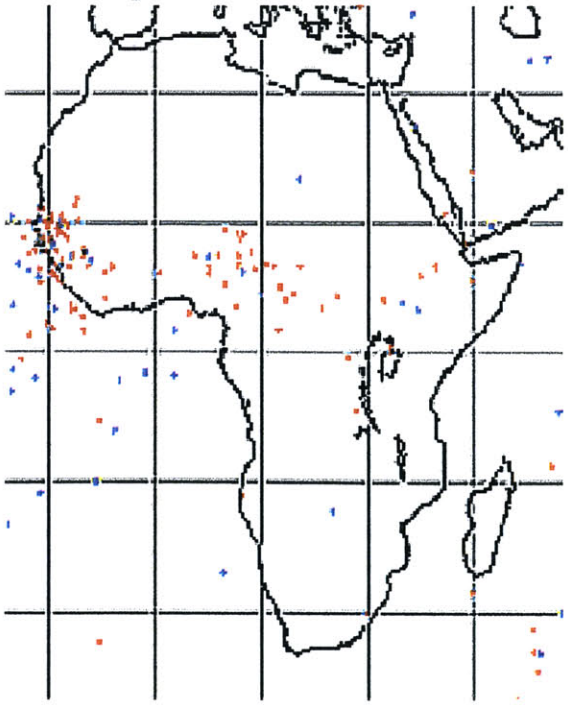

NOAA 0.1 Deg Daily (mm/d) 14 Jun 1998

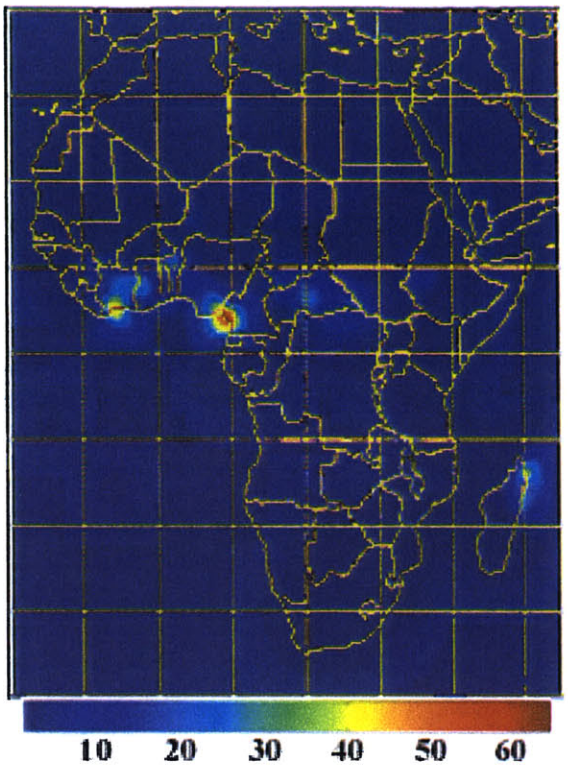

Red = Positive-Stroke
Blue = Negative-Stroke June 14, 1998

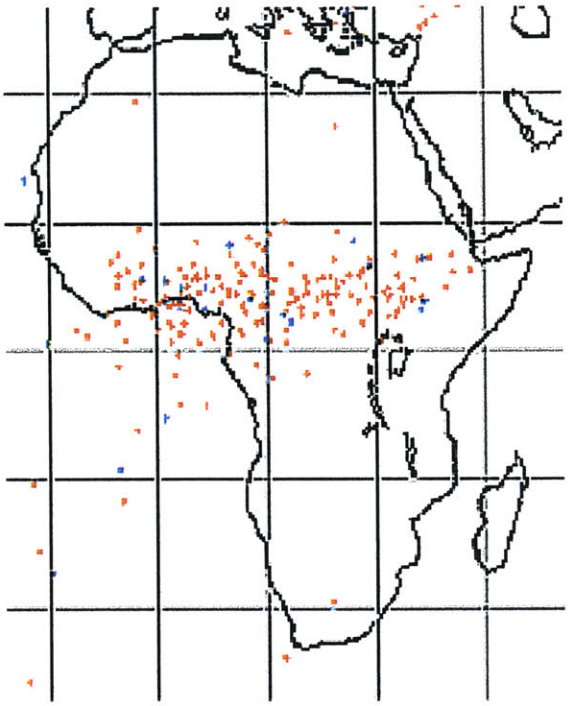

NOAA 0.1 Deg Daily (mm/d) 15 Jun 1998

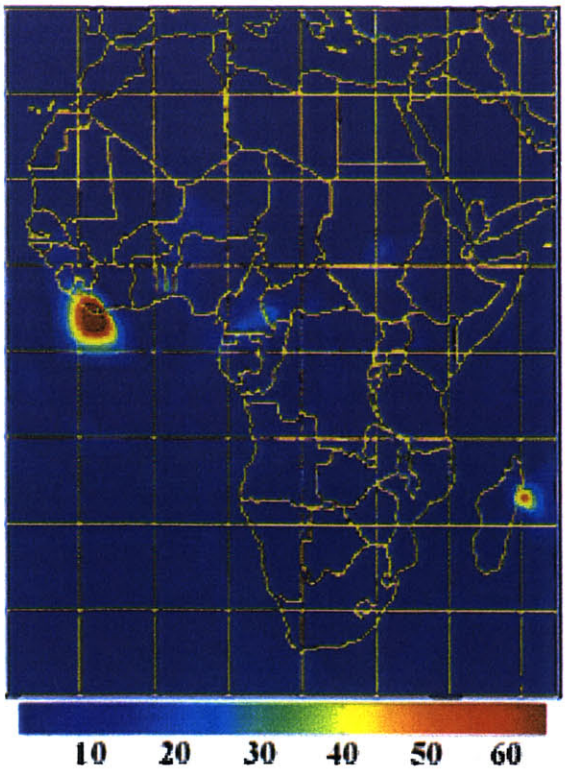

Red = Positive-Stroke
Blue = Negative-Stroke June 15, 1998

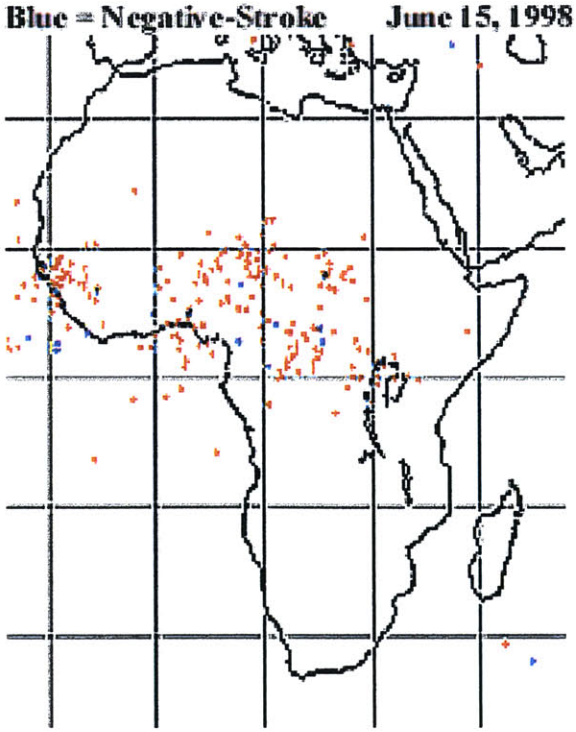

NOAA 0.1 Deg Daily (mm/d) 16 Jun 1998

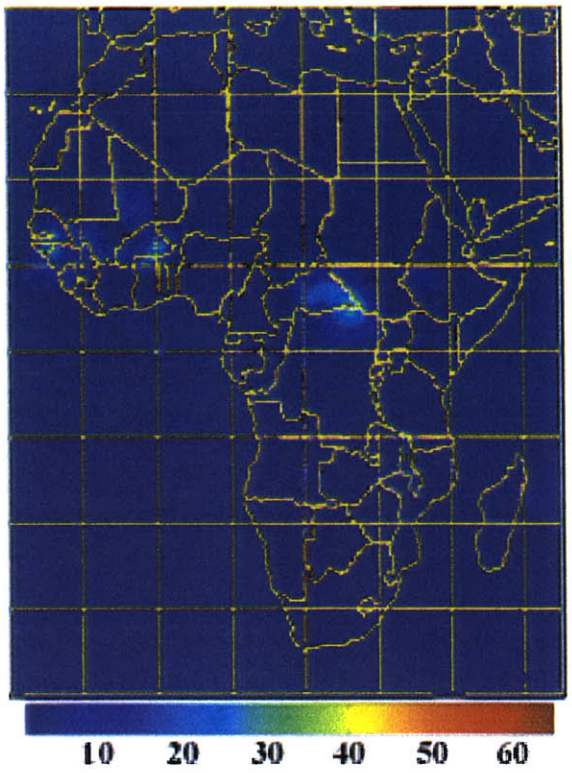

Red = Positive-Stroke
Blue = Negative-Stroke June 16, 1998

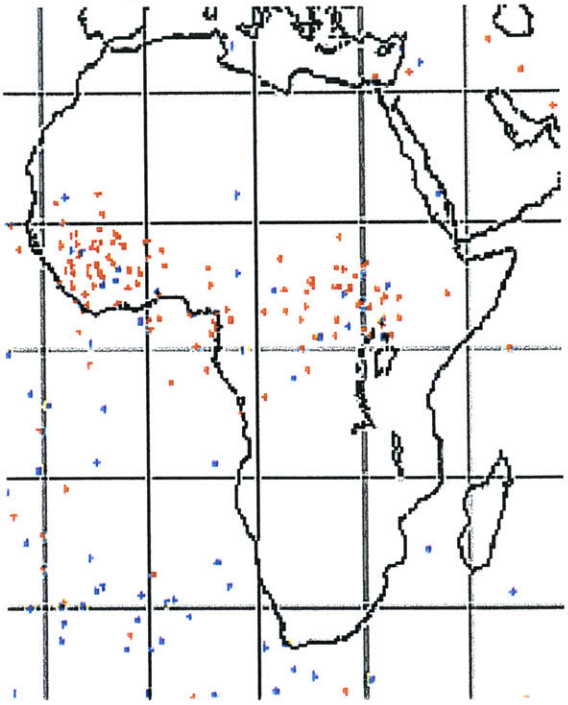

NOAA 0.1 Deg Daily (mm/d) 17 Jun 1998

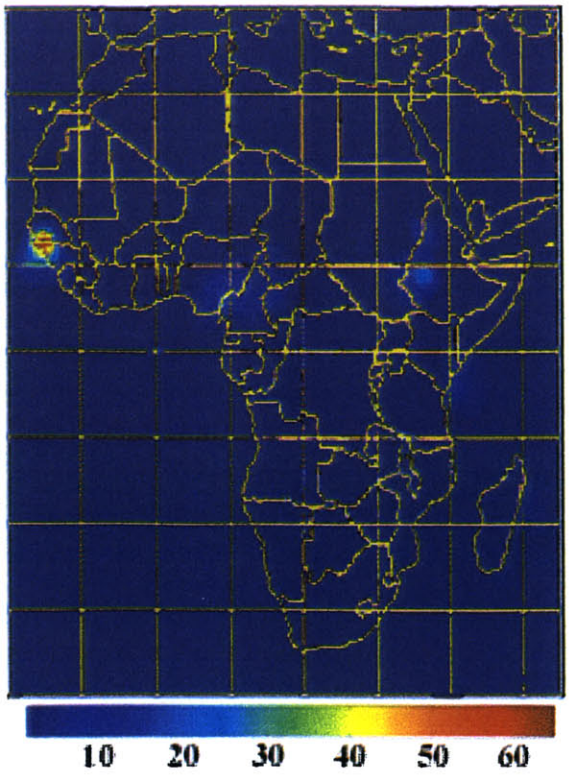

Red = Positive-Stroke
Blue = Negative-Stroke June 17, 1998

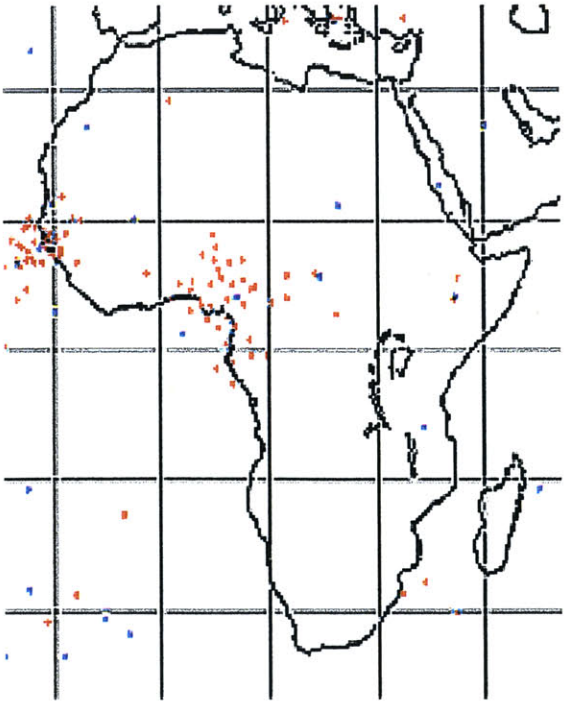

NOAA 0.1 Deg Daily (mm/d) 18 Jun 1998

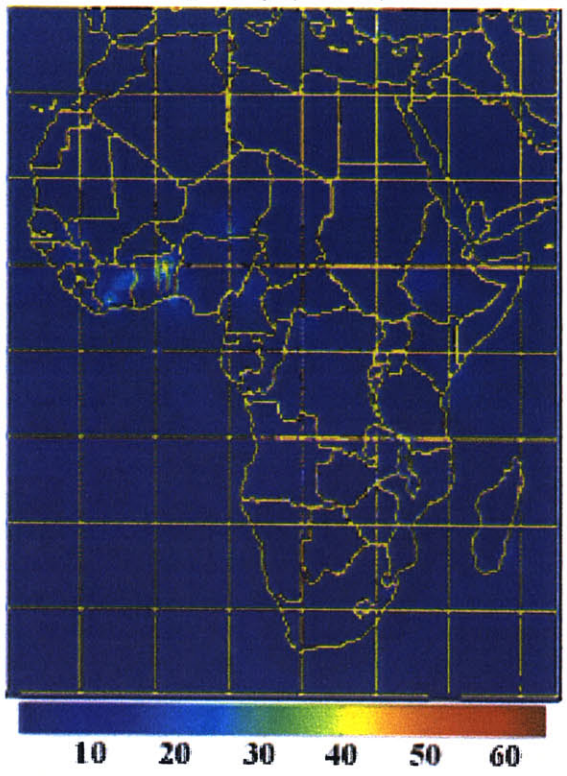

Red = Positive-Stroke
Blue = Negative-Stroke June 18, 1998

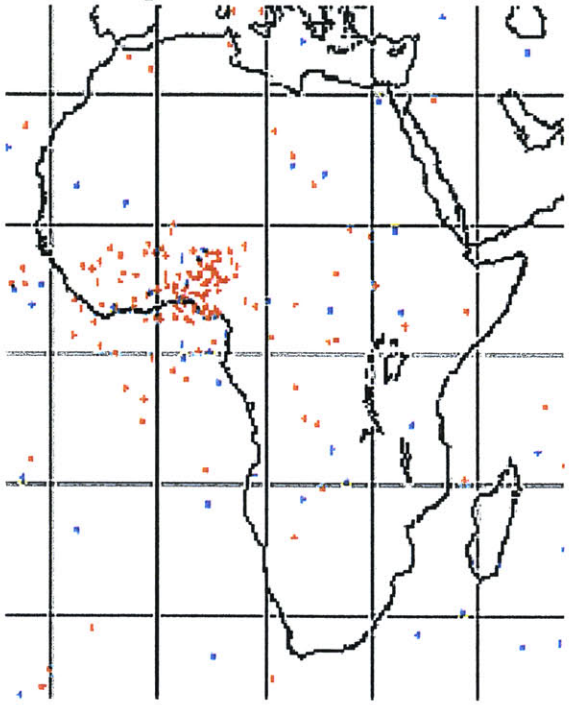

NOAA 0.1 Deg Daily (mm/d) 19 Jun 1998

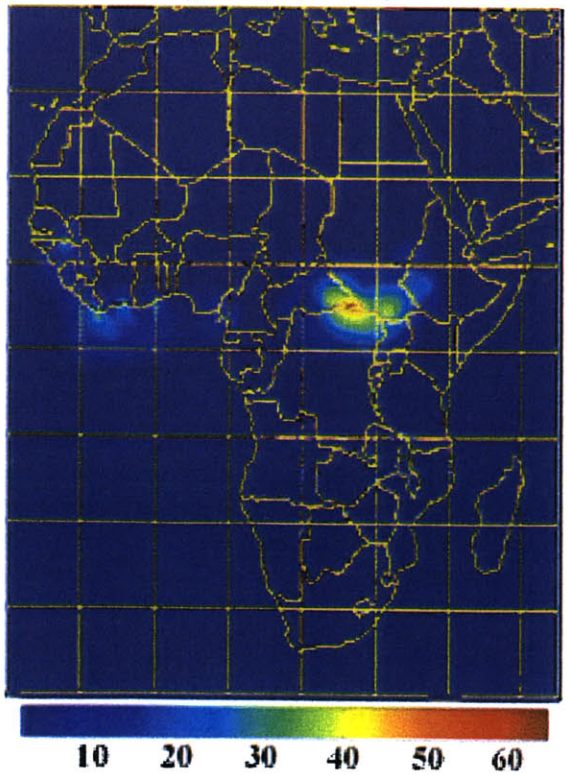

Red = Positive-Stroke
Blue = Negative-Stroke June 19, 1998